



# Design of a suspension system for a formula student race car

by

Ingi Níels Karlsson

Thesis of 60 ECTS credits submitted to the School of Science and Engineering  
at Reykjavík University in partial fulfillment  
of the requirements for the degree of  
**Master of Science (M.Sc.) in Mechanical Engineering**

June 2018

Supervisor:

Indriði Sævar Ríkharðsson, Supervisor  
Assistant Professor, Reykjavík University, Iceland

Examiner:

Dr. Rúnar Unnþórsson, Examiner  
Professor, University of Iceland, Iceland

Copyright  
Ingi Níels Karlsson  
June 2018

# Design of a suspension system for a formula student race car

Ingi Níels Karlsson

June 2018

## **Abstract**

Team Sleipnir formula student team of Reykjavik University is a team of 30 students whose aim is to build a car and compete in the Formula Student competition UK held at Silverstone circuit. Although the team is fairly young and is taking part in its third competition the team finished 15th overall out of 75 teams in last competition.

The aim of this thesis is to design, optimize and build the suspension system for the 2018 car. To be able to design a suspension system background research will be performed to understand the theory behind the suspension geometry and what results should be expected by changing the suspension geometry with the help of MSC Adams Car[4]. Individual components will be designed using Autodesk Inventor and 3D model created of the suspension system. FEA analysis will be used to optimize the parts along with hand calculations. Most suspension components will be manufactured at the university workshop.

# Hönnun fjöðrunarkerfis fyrir formúla stúdent kappakstursbíl

Ingi Níels Karlsson

júní 2018

## Útdráttur

Formúla Stúdent lið Háskólanns í Reykjavík, Sleipnir, samanstendur af 30 nemendum sem hafa það markmið að smíða kappakstursbíl til að taka þátt í Formúla Stúdent keppni haldinni á Silverstone brautinni í Bretlandi. Þó liðið sé ungt og stefni á að taka þátt í sinni þrijuð keppni í sumar þá endaði liðið í 15. sæti af 75 í keppninni í fyrra.

Markmið þessa verkefnis er að hanna og smíða fjöðrunarkerfi fyrir keppnis bíll þessa árs. Til að geta hannað fjöðrunarkerfi þarf að vinna undirbúningsvinnu í að kynna sér fræðina á bakvið fjöðrunarkefi og hvaða eiginleikum sé hægt að reikna með við ákveðnar breitingar auk hermunar með MSC Adams Car[4]. Einstakir hlutar fjöðrunarkerfissins verða hannaðir í Autodesk Inventor og þrívidaðar módel sett saman af heildar fjöðrunarkerfinu. Greiningar á einstökum hlutum fjöðrunarkerfissins verða framkvæmdar og notast við einingaaðferðina við burðarþolsgreiningar auk handrekninga þar sem það á við. Íhlutir fjöðrunarkerfissins verða smíðaðir á verkstæði skólanns.

# Design of a suspension system for a formula student race car

Ingi Níels Karlsson

Thesis of 60 ECTS credits submitted to the School of Science and Engineering  
at Reykjavík University in partial fulfillment of  
the requirements for the degree of  
**Master of Science (M.Sc.) in Mechanical Engineering**

June 2018

Student:

.....  
Ingi Níels Karlsson

Supervisor:

.....  
Indriði Sævar Ríkharðsson

Examiner:

.....  
Dr. Rúnar Unnþórsson



The undersigned hereby grants permission to the Reykjavík University Library to reproduce single copies of this Thesis entitled **Design of a suspension system for a formula student race car** and to lend or sell such copies for private, scholarly or scientific research purposes only.

The author reserves all other publication and other rights in association with the copyright in the Thesis, and except as herein before provided, neither the Thesis nor any substantial portion thereof may be printed or otherwise reproduced in any material form whatsoever without the author's prior written permission.

.....  
date

.....  
Ingi Níels Karlsson  
Master of Science



*This work is dedicated to the memory of my grandfather, Rögnvaldur Ólafsson.*



# Acknowledgements

First I would like to thank my family for providing me with unfailing support and continuous encouragement throughout my years of study and through the process of researching and writing this thesis. I also would especially like to thank Rúnar for his patience while I was working on my thesis. This accomplishment would not have been possible without them. Thank you.

Secondly, I would like to thank my supervisor, Indriði Sævar Ríkharðsson, for his help and knowledge to guide me in the right direction while working on this thesis.

Last but not least I would like to give special thanks to the students that participated in building the car, there will and dedication to the project. Without them, there would not have been a racing team at Reykjavik University.

# Contents

<b>Acknowledgements</b>	<b>xi</b>
<b>Contents</b>	<b>xii</b>
<b>List of Figures</b>	<b>xiv</b>
<b>List of Tables</b>	<b>xvi</b>
<b>List of Abbreviations</b>	<b>xvii</b>
<b>List of Symbols</b>	<b>xix</b>
<b>1 Introduction</b>	<b>1</b>
1.1 Background . . . . .	1
1.2 Design Constraints . . . . .	2
1.3 FS rules . . . . .	3
1.4 Objective . . . . .	3
1.5 Thesis structure . . . . .	4
<b>2 Research</b>	<b>5</b>
2.1 Types of suspension systems . . . . .	5
2.2 Suspension properties . . . . .	5
2.2.1 Kingpin inclination . . . . .	5
2.2.2 Caster . . . . .	5
2.2.3 Camber . . . . .	6
2.2.4 Scrub radius . . . . .	7
2.2.5 Wheel rate . . . . .	7
2.2.6 Roll rate . . . . .	9
<b>3 Design process</b>	<b>11</b>
3.1 Identification of relevant rules . . . . .	12
3.2 Identification of team constraints . . . . .	12
3.3 Preliminary design . . . . .	12
3.3.1 A-arms . . . . .	12
3.3.2 Push rods . . . . .	13
3.3.3 Bell cranks . . . . .	15
3.3.4 Spring and damper . . . . .	15
3.3.5 Anti roll bar . . . . .	15
3.4 Adams . . . . .	18
3.4.1 Introduction . . . . .	18

3.4.2	Adams Car model . . . . .	19
3.4.3	Adams Car simulations . . . . .	20
3.4.4	Results from Adams Car . . . . .	22
3.5	3D modeling . . . . .	25
3.5.1	A-arms . . . . .	25
3.5.2	Pushrods . . . . .	27
3.5.3	Bell cranks . . . . .	28
3.5.4	Anti-roll bar . . . . .	29
<b>4</b>	<b>Manufacturing</b>	<b>31</b>
<b>5</b>	<b>Conclusion</b>	<b>39</b>
<b>6</b>	<b>Future work</b>	<b>41</b>
<b>Bibliography</b>		<b>43</b>
<b>A Datasheets</b>		<b>45</b>
A.1	Aluminum 6061 T6 . . . . .	45
A.2	Aluminum 7075 T6 . . . . .	49
A.3	303 Stainless Steel . . . . .	55
A.4	Structural steel S235 . . . . .	58
A.5	Structural steel S355 . . . . .	61
A.6	Öhlins TTX25 Mk II spring dimensions . . . . .	64
A.7	Öhlins TTX25 Mk II internal schematic . . . . .	66
A.8	Öhlins TTX25 Mk II external dimensions . . . . .	70
A.9	Öhlins TTX25 Mk II dyno plot . . . . .	72
A.10	Fluro spherical bearing . . . . .	76
A.11	Fluro spherical bearing rod end . . . . .	78
A.12	SKF 608-2RSR . . . . .	80
<b>B Drawings</b>		<b>83</b>
<b>C Tables and calculations</b>		<b>127</b>
C.1	Hard point table . . . . .	127
C.2	Results from Adams Car . . . . .	131
C.2.1	Summary of forces . . . . .	131
C.2.2	Pothole simulation . . . . .	133
C.2.3	Plank simulation . . . . .	147
C.2.4	Constant radius cornering simulation . . . . .	161
C.2.5	Tilt simulation . . . . .	175
C.2.6	Front parallel wheel travel simulation . . . . .	189
C.2.7	Rear parallel wheel travel simulation . . . . .	199

# List of Figures

1.1	The 2017 car at Silverstone after the competition . . . . .	2
2.1	Kingpin inclination and caster angles . . . . .	6
2.2	Camber angle . . . . .	6
2.3	Sprung mass and unsprung mass definition. . . . .	8
2.4	The roll center is found by drawing lines between the center of the tire patch to instantaneous centers. . . . .	9
3.1	Design flow chart . . . . .	11
3.2	Proposed A-arm design . . . . .	13
3.3	Push and pull rod suspension [8] . . . . .	13
3.4	Force on the pushrod with 600 N force on the wheel . . . . .	14
3.5	Free body diagram of the forces acting on the pushrod . . . . .	14
3.6	Cutaway model of the Öhlins TTX25 MkII FS damper [9] . . . . .	16
3.7	Öhlins TTX 25 MkII internal schematic [11] . . . . .	16
3.8	Adams Car[4] design flowchart. . . . .	18
3.9	Two body position mechanism [12] . . . . .	19
3.10	Adams Car [4] 3D model of the formula student car . . . . .	20
3.11	Adams Car [4] suspension points table . . . . .	20
3.12	Adams Car [4] part modification window. The preliminary Inventor model was used to define the mass and properties of each part in the Adams model. . . . .	21
3.13	Adams Car [4] part modification window . . . . .	21
3.14	Adams Car [4] parallel wheel travel simulation setup window . . . . .	22
3.15	Adams Car [4] postprocessing window parallel wheel travel simulation camber change results . . . . .	22
3.16	Adams Car [4] constant cornering simulation with wheel forces in red on the picture . . . . .	23
3.17	Adams Car [4] parallel wheel travel simulation of the front suspension system with wheel forces in red on the picture . . . . .	23
3.18	Adams Car [4] parallel wheel travel simulation motion ratio of the spring and damper versus the wheel . . . . .	24
3.19	Inventor [14] hard point 3D model . . . . .	25
3.20	Front upper control arm 3D model from Inventor [14] . . . . .	26
3.21	Front upper control arm FEA results and a free body diagram showing location of whee the force of 3748.9 N is applied . . . . .	26
3.22	Front push rod assembly 3D model from Inventor [14] . . . . .	27
3.23	Buckling end conditions constants [17] . . . . .	27
3.24	Front bell crank 3D model from Inventor [14] . . . . .	28

3.25	Front bell crank FEA results and a free body diagram showing location of where the force of 3748.9 N is applied . . . . .	29
3.26	Front suspension assembly 3D model from Inventor [14] . . . . .	29
4.1	Sleipnir's workspace at the university workshop . . . . .	31
4.2	The university workshop . . . . .	32
4.3	Laser cut brackets for the suspension, first from left is the insert for the rear arm of the A-arms, second from left is the push rod mount bracket for the A-arms, third and fourth from left are mounting brackets for the A-arms to the chassis. . . . .	33
4.4	Spherical bearing seat for the control arms . . . . .	33
4.5	Spherical bearing seat toolpath from Inventor HSM [18] . . . . .	34
4.6	Inserts for spherical rod ends . . . . .	35
4.7	Spacer for spherical rod ends to increase the travel angle of the rod end . . . . .	35
4.8	Spacer for spherical rod ends toolpath from Inventor HSM [18] . . . . .	36
4.9	Inserts welded to A-arm . . . . .	36
4.10	Front A-arms mounted on the chassis . . . . .	37
4.11	Bell crank machined front side . . . . .	38
4.12	Bell crank machined back side . . . . .	38
5.1	Final 3D model of the suspension assembly in Inventor [14] . . . . .	39
C.1	Adams car [4] pothole simulation setup window . . . . .	133
C.2	Adams car [4] plank simulation setup window . . . . .	147
C.3	Adams car [4] constant corner simulation setup window . . . . .	161
C.4	Adams car [4] tilt table simulation setup window . . . . .	175
C.5	Adams car [4] parallel wheel travel simulation setup window . . . . .	189
C.6	Adams car [4] parallel wheel travel simulation setup window . . . . .	199

# List of Tables

3.1	Static setup of the suspension . . . . .	24
3.2	Forces from Adams Car [4] simulations. . . . .	24
5.1	Comparison of weight of left side suspension components between 2017 and 2018 car . . . . .	40

# List of Abbreviations

RU	Reykjavík University
FS	Formula Student
SAE	Society of Automotice Engineers
US	United States
UK	United Kingdom
FSAE	Formula SAE
FSG	Formula Student Germany
IMechE	Institution of Mechanical Engineers
MIRA	Motor Industry Research Association
CNC	Computer numerical control
MDS	Multibody Dynamics Simulation
CoG	Center of Gravity
RC	Roll Center
SF	Safety Factor
CAD	Computer Aided Design
FEA	Finite element analysis



# List of Symbols

Symbol	Description	Value/Units
$K_s$	Spring rate	N m <sup>-1</sup>
$K_T$	Tire spring rate	N m <sup>-1</sup>
$K_w$	Wheel rate	N m <sup>-1</sup>
$M$	Mass	kg
$MR$	Motion ratio	
$F$	Force	N
$f$	Frequency	Hz
$M_s$	Sprung mass	kg
$M_{us}$	Unsprung mass	kg
$l$	Length	m
$\Phi_r/A_y$	Roll gradient	deg/g
$g$	Acceleration	9.81 m s <sup>-2</sup>
$H$	Distance from roll center to CoG	m
$K_{\Phi F}$	Front roll rate	Nm/deg
$K_{\Phi R}$	Rear roll rate	Nm/deg
$t_f$	Front track width	m
$t_r$	Rear track width	m
$K_{LF}$	Left front wheel rate	N/m
$K_{LR}$	Right front wheel rate	N/m
$K_{LR}$	Left rear wheel rate	N/m
$K_{RR}$	Right rear wheel rate	N/m
$K_{\Phi A}$	Total anti roll bar rate needed	Nm/deg
$t_A$	Average track	m
$K_{\Phi des}$	Desired total roll stiffness	Nm/deg
$M_{A-arm}$	Moment around the A-arm mount to the chassis	Nm
$F_{wheel}$	Normal forces on the wheel center	N
$L$	Length	m
$F_N$	Normal force	N
$\theta$	Angle	deg
$F_{pushrod}$	Force acting on the push rod	N
$M_{ARB}$	Torque on the anti roll bar	Nm
$F_{ARB}$	Force on anti roll bar arm	N
$x$	Length	m
$\theta$	Rotation of the anti roll bar	deg
$G$	Modulus of rigidity	GPa
$J_0$	Polar moment of inertia	mm <sup>4</sup>
$F_{ARB}/\theta$	Anti-roll bar torsional stiffness	N/deg

$C$	Buckling end condition	
$E$	Young's modulus	GPa
$D$	outer diameter	m
$d$	inner diameter	m

# Chapter 1

## Introduction

### 1.1 Background

In 1981 the Society of Automotive Engineers (SAE) started the Formula SAE competition in the United States with only four schools taking part in the first competition. In 1982 the competition was hosted by University of Texas and became an official SAE event with the first official FSAE rules introduced and was this the only time that there were no requirements for a suspension system and as a result, many cars that took part were in fact large carts. In 1985 there was a major rule change where the successor to 1000 point system that we have today was introduced and also the maximum engine displacement of  $610 \text{ cm}^3$  and a 23 mm restrictor on the intake of the engine. 1985 was also the first year that the teams had to deliver a cost report and the total project cost could not exceed \$2000. 1997 was the first year that a European team took part in the competition when University of Leeds decided to take part and showed that engineering students everywhere could take part in the competition.[1]

The Formula Student (FS) competition started in the UK in 1998 and the first competition was held at the Motor Industry Research Association (MIRA) proving ground with three US cars and four cars from the UK. With the first UK competition being a success The Institution of Mechanical Engineers in partnership with SAE organized the competition in Europe and the to this day the competition has been held at the end of each academic year since then. [2]

The Formula student team Sleipnir of Reykjavík University (RU) was founded in the autumn of 2015 by the initiative of two students at the school and the team took part in their first competition which was held at the Silverstone circuit in 2016. The first car that the team brought to the competition was rather rough and was manly a proof of concept with limited funds but a great support from the school. Even though it was the first car the team built the car passed scrutineering and was allowed to take part in the dynamic events at the competition and the team finished 74th out of 108 teams. After the first competition, the team determined to use the experience they gained in the previous competition to improve the next car. In 2017 the team returned to Silverstone with a new car that had many great improvements over the first and was lighter, with a more powerful engine and better suspension system. As a result of all of these improvements, the team ended in 15th place out of 75 teams which is a very respectable result for a team with their second car in the competition. This year the team consists of 30 engineering students with different background with the goal of designing a new car which is lighter than the previous car. The background for the project has been to combine theoretical knowledge with practical skills and real problem-solving.

The team manufactures most parts for the car at the RU workshop which is equipped with CNC machines and manual lathes and mills. The team members have to solve how to design each part so it can be manufactured and gaining invaluable experience in design and manufacturing processes as it is no good to design a part that cannot be made.



Figure 1.1: The 2017 car at Silverstone after the competition

The background for this thesis is gain a better knowledge of how race car suspension systems work and with many different types of suspension system what type and setup is best suited to use on this year's car. To find what suspension gives the optimal performance simulations will be done by using MSC Adams Multibody Dynamics Simulation (MDS) software [4]

## 1.2 Design Constraints

Each year IMechE releases a new set of rules that all teams that take part in the competition must use. When the cars go through scrutineering the scrutineers make sure each car complies with the rules provided.

This year there was a significant change in the rules as previous years IMechE had used the FSAE rules in their competition but as most of the team that take part in the competition are European IMechE decided to use the Formula Student Germany (FSG) rules as many other European competitions use these rules so teams that take part in the competition can all follow one set of rules the European competitions.

## 1.3 FS rules

There are certain requirements that the suspension system must fulfill according to the FS rules. The suspension system like other parts of the car must follow the rules set by IMechE for the car to be allowed to take part in the competition. According to the FS rules the suspension must fulfill the following rules: [3]

- Have a fully operational front and rear suspension system with shock absorbers.
- Usable travel of at least 50 mm with 25 mm rebound and 25 mm jounce.
- The minimum static ground clearance of any portion of the vehicle, other than the tires, including a driver, must be a minimum of 30 mm.
- All suspension mounting points must be visible at technical inspection, either by direct view or by removing any covers.
- All moving suspension and steering components and other sharp edges inside the cockpit between the front hoop and a vertical plane 100 mm rearward of the pedals, must be shielded with solid material.
- Covers over suspension and steering components must be removable to allow inspection of the mounting points.
- All spherical rod ends and spherical bearings on the steering or suspension must be in double shear or captured by having a screw/bolt head or washer with an outer diameter that is larger than the spherical bearing housing inner diameter.
- The smaller track of the vehicle (front or rear) must be no less than 75 % of the larger track.
- The track and center of gravity of the vehicle must combine to provide adequate rollover stability.
- The vehicle must have a wheelbase of at least 1525 mm.

In addition to complying to the FS rules, the team has set the goal to reduce the weight of each component on the car by 20% from the previous car and to keep the design as simple and efficient as possible to reduce manufacturing cost and to manufacture as many components as possible in the school.

## 1.4 Objective

The main objective of this thesis is to design and manufacture suspension system for an FS race car that has optimal suspension properties while maintaining a simple design that is easily adjusted and can be manufactured at the RU workshop. The thesis will also pursue to combine theory with real problems to be able to design practical components for the suspension system and then manufacture them. In the thesis Adams Car [4] MDS simulations will be used to find the optimal suspension system setup and do simulations to see what effects changes of camber, caster, and other suspension parameters has on the overall performance of the car. For the design of the suspension system, the data from Adams Car [4] will be used to create a 3D model using Autodesk Inventor [14]. To be able to build the suspension

system as light as possible the data from Adams [4] will also be used to perform a Finite element method (FEM) analysis on major components in the suspension system.

In this thesis the following suspension components will be researched, designed and manufactured:

- A-arms
- Bell cranks
- Springs and dampers
- Anti roll bars

The thesis will look into what effects changes in suspension properties such as camber, caster, wheel rate and other has on the performance of the suspension system.

The suspension system is quite a complex task and has many components that intersect with other components in the car, so it has to be taken into account while designing each component that it does not interfere with other components in the car.

## **1.5 Thesis structure**

The thesis will begin by explaining suspension properties in chapter 2. In chapter 3 the design process will be explained. Chapter 4 will then go into how the suspension system components were manufactured. Chapter 5 will contain conclusion and results following possible future work in chapter 6. Datasheets for materials and parts used in the project will be in appendix A, drawings of the suspension system will be in appendix B and tables, calculations and results from Adams Car in appendix C.

# **Chapter 2**

## **Research**

### **2.1 Types of suspension systems**

There are many different types of suspension systems each having its advantage and draw-back. Most modern race cars use some type of independent suspension system where each wheel can move independently from the other wheels. By having an independent suspension on all wheels where the wheels move after a prescribed path allows for greater control over the wheel travel. Most race cars use so-called double wishbone suspension or sometimes called double A-arm suspension. The main advantage of this type of suspension system is camber gain can easily be adjusted by using an unequal length of A-arms. To reduce unsprung weight the spring and damper are mounted inside the vehicle and connected to the suspension with the bell crank and push rod. This configuration makes the suspension system more responsive as it has to move less weight when it travels.[5]

### **2.2 Suspension properties**

#### **2.2.1 Kingpin inclination**

Kingpin inclination sometimes called "Steering axis inclination" is the angle from vertical to the steering axis of the tire between the upper and lower ball joint viewed from the front as Figure 2.1 shows. Kingpin inclination angle affects the lift of the wheel during cornering. As it lifts the car as it corners and makes the wheels want to steer straight as the weight of the car returns the steering to center. The kingpin inclination angle also affects the camber angle of the wheels as they turn and the wheel will gain positive camber. This can be beneficial to the handling of the car when making tight turns. [5]

#### **2.2.2 Caster**

The angle of the steering axis between the upper and lower ball joints viewed from the side is commonly known as Caster angle. With a positive caster angle as shown in Figure 2.1 the contact point of the tire to the ground called Mechanical trail, is behind the steering axis this creates a torque on the steering axis as the force on this point acts perpendicular to the steering axis and makes the wheel want to steer straight. With a negative caster angle, the contact point of the tire is in front of the steering axis the effects of a negative caster angle are opposite to a positive caster angle as the forces acting on the contact point wants to turn the wheel when cornering making the car unstable. [5]

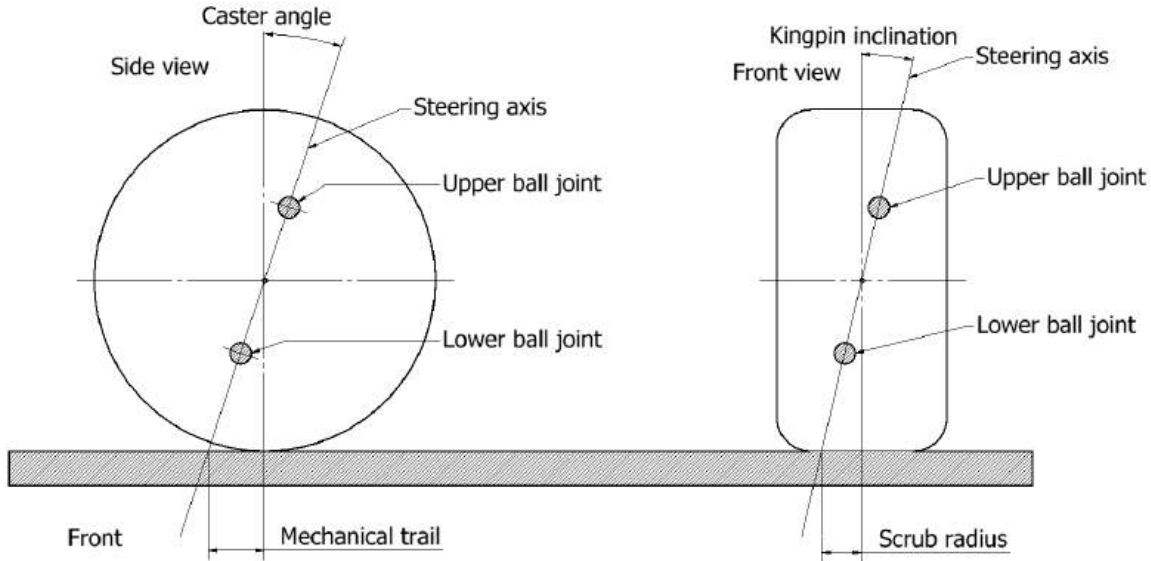


Figure 2.1: Kingpin inclination and caster angles

### 2.2.3 Camber

The angle of the wheel in- or outwards respective to vertical viewed from the front is called a camber angle and will produce lateral force known as camber force. Positive camber is when the top of the wheel is tilted outwards from the vehicle and negative angle when the wheel is tilted in towards the vehicle. Race cars usually have a negative camber to increase high-speed stability and tire grip when cornering as it compensates for the positive camber gain as a result of the Kingpin Inclination angle and maximizes the contact between the tire and the road. [5] Figure 2.2 shows how the camber angle is defined.

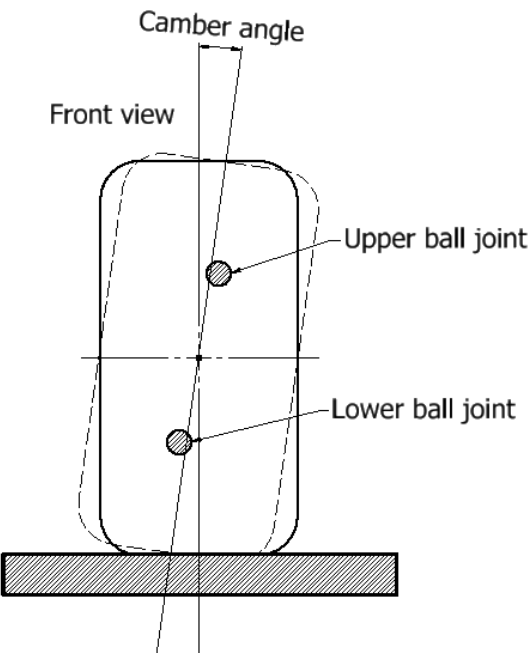


Figure 2.2: Camber angle

### 2.2.4 Scrub radius

Scrub radius is the distance from the steering axis to the center of the contact patch of the tire. The scrub radius creates a lever arm on the steering axis that longitudinal forces act on and depending on the tire grip a net moment can be translated to the steering. Scrub radius is defined as positive and negative depending if it is on the inside or outside of the centerline of the tire. Figure 2.1 shows a negative scrub radius. The scrub radius can affect the toe of the car because of the longitudinal forces that act on the scrub radius arm. [5]

### 2.2.5 Wheel rate

The wheel rate of a car is an important factor in fine tuning suspension properties and a change in wheel rate changes the tire normal force at the ground for each tire and by changing the normal force the lateral force changes to affecting the grip and handling of the car. [5] Wheel rate is the force per unit for vertical displacement of the center of the wheel and is the spring rate measured at the wheel center instead of measuring it at the spring.

The spring rate is calculated by the force required to compress the spring divided by the deflection.

$$K_s = \frac{F}{l} \quad (2.1)$$

Where:

$$\begin{aligned} K_s & \text{ spring ratio (N/m)} \\ F & \text{ the force acting on the spring (N)} \\ l & \text{ spring displacement (m)} \end{aligned}$$

The wheel forces are translated to the suspension spring and damper through the bell crank. The motion ratio of the suspension is therefore defined as the suspension travel divided by the vertical travel.

$$MR = \frac{\text{Spring travel}}{\text{Wheel travel}} \quad (2.2)$$

The wheel rate is found by multiplying the spring rate with the motion ratio squared.

$$K_w = K_s MR^2 \quad (2.3)$$

With a sprung system, it will resonate at its natural frequency with the basic equation for a sprung mass system.

$$f = \frac{1}{2\pi} \sqrt{\frac{K_s}{M}} \quad (2.4)$$

Where:

$$\begin{aligned} f & \text{ frequency (Hz)} \\ K_s & \text{ spring ratio (N/m)} \\ M & \text{ mass (kg)} \end{aligned}$$

By adding to equation 2.4 the spring rate for the tires and wheels we get equation 2.5.

$$f_s = \frac{1}{2\pi} \sqrt{\frac{(K_w K_T)/(K_w + K_T)}{M_s}} \quad (2.5)$$

Where:

- $f_s$  sprung mass natural frequency ( $Hz$ )
- $K_w$  wheel ratio ( $N/m$ )
- $K_T$  tire spring ratio ( $N/m$ )
- $M_s$  sprung mass ( $kg$ )

The recommended sprung mass natural frequency for an FS car is  $2.5 - 3.5\ Hz$  compared to  $1.0 - 2.0\ Hz$  for passenger cars. Higher sprung mass natural frequency results in increased cornering stability as the suspension is stiffer [6]. To find what spring rate gives the recommended sprung mass natural frequency equation 2.5 is solved for the spring rate.

$$K_s = \frac{4M_s\pi^2K_Tf^2}{MR^2(K_T - 4M_s\pi^2f^2)} \quad (2.6)$$

The recommended unsprung mass natural frequency for an FS car is  $15 - 19\ Hz$  while passenger cars have a unsprung mass natural frequency of  $10 - 12\ Hz$ . The higher unsprung mass natural frequency increases the stiffness allowing for lower ride height as suspension travel can be decreased. [6]. The unsprung mass natural frequency is found by adding the spring ratio and tire spring ratio together.

$$f_{us} = \frac{1}{2\pi} \sqrt{\frac{K_w + K_T}{M_{us}}} \quad (2.7)$$

Where:

$$M_{us}$$
 unsprung mass ( $kg$ )

Sprung mass is the chassis, engine, body and everything the suspension has to hold up, unsprung mass on the other hand is the mass of the suspension, brakes, tires and all other components not supported by the suspension. Figure 2.3 shows how the sprung mass and unsprung mass is connected.

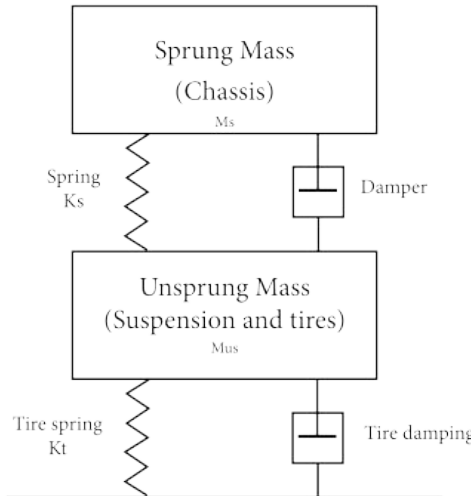


Figure 2.3: Sprung mass and unsprung mass definition.

### 2.2.6 Roll rate

Roll rate is defined as the moment resisting body roll per degree of body roll from the lateral force. The resistance to body roll can be provided by anti-roll bars, track width and suspension setup. [5]. The height of the center of gravity (CoG) and the distance to the roll center affects the roll rate of the car, a car with a high CoG will require stiffer suspension or anti-roll bar to compensate for the higher CoG. To estimate the roll stiffness of the suspension from the springs the roll gradient for the suspension needs to be found.[7]

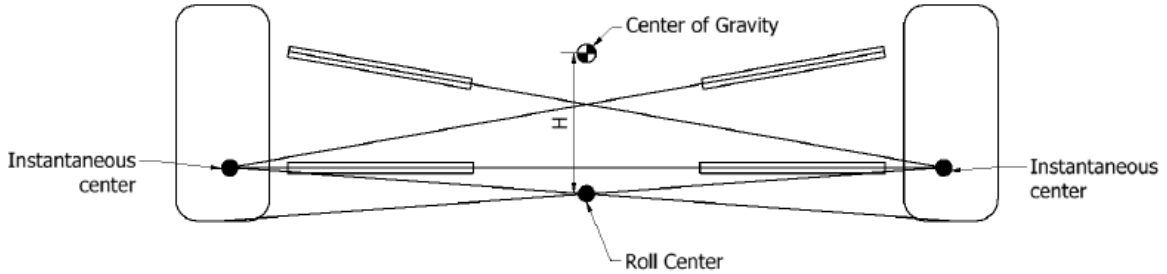


Figure 2.4: The roll center is found by drawing lines between the center of the tire patch to instantaneous centers.

$$\frac{\Phi_r}{A_y} = \frac{M * H}{K_{\Phi F} + K_{\Phi R}} \quad (2.8)$$

Where:

$$\begin{aligned} A_y &\text{ lateral acceleration (g)} \\ H &\text{ distance from roll center to center of gravity (m)} \\ M &\text{ mass of the car (kg)} \\ \frac{\Phi_r}{A_y} &\text{ roll gradient (deg/g)} \\ K_{\Phi F} &\text{ front roll rate (Nm/deg)} \\ K_{\Phi R} &\text{ rear roll rate (Nm/deg)} \end{aligned}$$

$$K_{\Phi F} = \frac{\pi(t_f^2)K_{LF}K_{RF}}{180(K_{LF} + K_{RF})} \quad (2.9)$$

$$K_{\Phi R} = \frac{\pi(t_r^2)K_{LR}K_{RR}}{180(K_{LR} + K_{RR})} \quad (2.10)$$

Where:

$$\begin{aligned} t_f &\text{ front track width (m)} \\ t_r &\text{ rear track width (m)} \\ K_{LF} &\text{ left front wheel rate (N/m)} \\ K_{LR} &\text{ right front wheel rate (N/m)} \\ K_{RL} &\text{ left rear wheel rate (N/m)} \\ K_{RR} &\text{ right rear wheel rate (N/m)} \end{aligned}$$

The desired roll stiffness gradient is the sum of the front and rear roll stiffness and typical values for race cars 0.2 – 0.7 deg/g [7]. If the suspension roll stiffness is not enough anti-roll bars are used to increase roll stiffness. The total anti-roll bar rate needed to increase roll stiffness of the car:

$$K_{\Phi des} = K_{\Phi F} + K_{\Phi R} \quad (2.11)$$

$$K_{\Phi A} = \frac{\pi}{180} \left[ \frac{K_{\Phi des} K_T(t_A^2/2)}{K_T(t_A^2/2)\pi/180 - K_{\Phi des}} \right] - \frac{\pi K_w(t_A^2)}{180} \quad (2.12)$$

Where:

$K_{\Phi A}$  total anti roll bar rate needed ( $Nm/deg$ )

$K_w$  wheel spring rate ( $N/m$ )

$K_t$  tire spring rate ( $N/m$ )

$t_A$  average track ( $m$ )

$K_{\Phi des}$  desired total roll stiffness ( $Nm/deg$ )

Based on the weight distribution of the car the baseline for the front anti-roll bar stiffness is the front weight distribution plus five percent of the total anti-roll bar stiffness needed.

# Chapter 3

## Design process

For the process of designing the suspension system, the suspension of the 2017 car was used as a baseline and books like "Race Car Vehicle Dynamics" by Milliken and Milliken [5] were used to improve the design before simulations were performed in MSC Adams Car. The design process followed the flowchart in Figure 3.1, beginning by identifying relevant

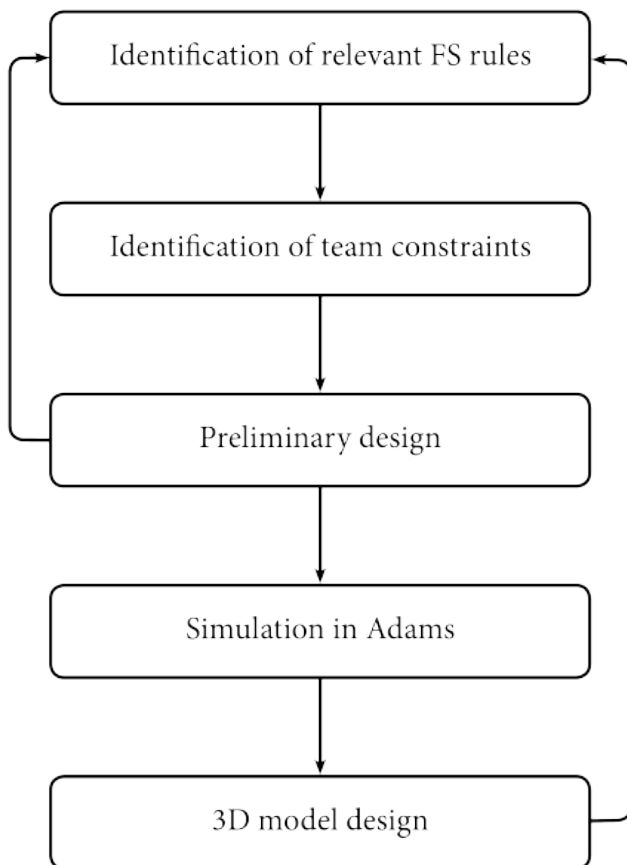


Figure 3.1: Design flow chart

rules in the FS rulebook. The design also has to fulfill constraints set by the team to achieve the goals for making the car lighter and so it does not interfere with other components on the car. A preliminary design was created using Autodesk Inventor 2018 [14] using the constraints mentioned here before. The preliminary design was then used in MSC Adams

Car [4] to simulate the suspension system and necessary improvements made. The results from Adams [4] were then used to update the Inventor 3D model with the parameters from Adams and to design each component of the suspension system and do an FEA on important components of the suspension.

### 3.1 Identification of relevant rules

As mentioned earlier in the thesis it is important that the design follows the rules set by IMechE, so the car is eligible for taking part in the competition.

### 3.2 Identification of team constraints

The team has set the goal that the 2018 car should be 20% lighter than the previous car. To meet those requirements, FEA analysis will reduce the weight of each component as much as possible and to choose a suitable material for the design. The team also has the goal to make as many parts as possible in the university workshop so the manufacturing process has to be taken into account in the design process.

### 3.3 Preliminary design

For the preliminary design, most of the components from the 2017 car will be used as a baseline and adjustment made from that design based on previous design flaws and adjustments needed.

#### 3.3.1 A-arms

Double A-arms or sometimes called wishbones is the most popular suspension setup in Formula Student. The main reasons for its popularity are that this type of suspension system is easy to manufacture and design while giving a great performance. There are mainly two types of double A-arm suspensions, equal and unequal length A-arms. With equal length A-arms, both upper and lower A-arms are equally long. Having equal length A-arms the camber change during suspension movement and is not ideal for cornering as the wheel gains positive camber at suspension jounce. Having unequal length A-arms where the upper A-arm is usually shorter than the lower A-arm the camber change during suspension movement is easier to control, and the suspension gains negative camber at jounce. This improves handling during cornering, especially at the front tires. Because of the design of the chassis on FS cars as the chassis is wider at the top the unequal length A-arm setup fits these cars very well. An a-arm suspension is designed by connecting the uprights to the chassis of the car with a pair of links that resemble the letter A with. At the mounting point to the chassis, the A-arms are connected to the chassis with threaded spherical rod ends that allow for fine tuning of the A-arms. At the mounting point to the upright a single spherical bearing connects the A-arm to the upright providing freedom for the upright to pivot. Figure 3.2 shows proposed A-arm design.

Having threaded rod ends at the mounting point to the chassis allows for fine adjustment by making each arm shorter or longer but by changing the length of the arms, the distance between them changes. To be able to adjust the angle between the A-arm the rear arm is bolted to the plate that holds the spherical bearing as Figure 3.2 shows.

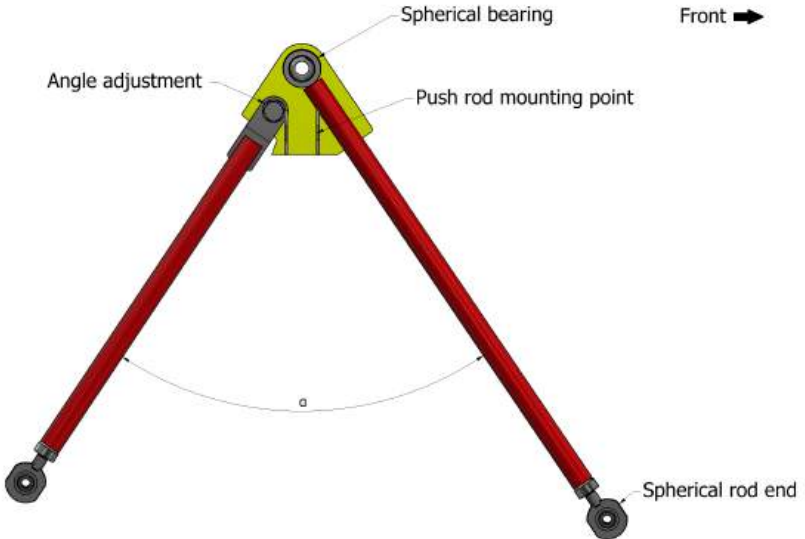


Figure 3.2: Proposed A-arm design

The distance between mounting points to the chassis has been reduced from 490 mm on the 2017 car to 400 mm to make the A-arms more compact and make them lighter. The length of the A-arms also has to be considered as it is one of the factors that control the track of the car.

### 3.3.2 Push rods

In double A-arm suspension systems, the spring and damper can be mounted directly to the lower A-arm end to the chassis to transfer vertical tire forces to the chassis. Race cars with double A-arm suspension system usually use push or pull rod which is mounted to the upper or lower A-arm and the bell crank as Figure 3.3 shows. The advantage of using push or pull rods is that it reduces unsprung weight by moving the spring and damper inboard the vehicle. The main difference between push and pull rods are the forces acting on the push

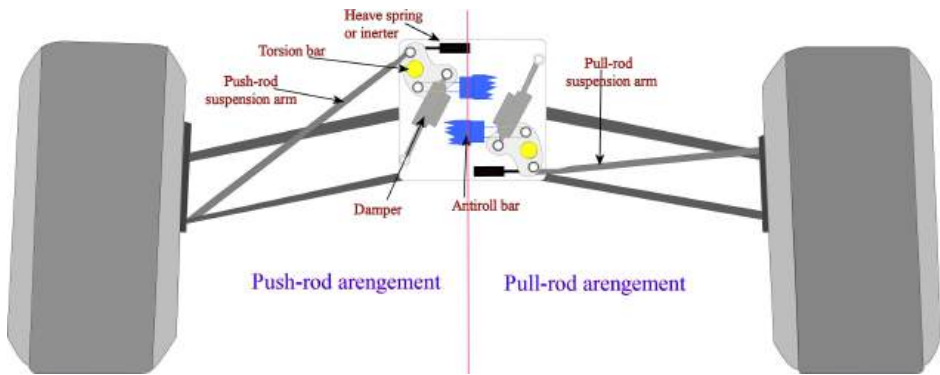


Figure 3.3: Push and pull rod suspension [8]

and pull rod. In a pushrod setup, the push rod is under compression as the vertical wheel force pushes on the push rod as the wheel jounces. In a pull rod setup, the vertical wheel force pulls on the pull rod as the wheel jounces. Each of these setups has its benefits and drawbacks. The center of gravity (CoG) is lower in pull rod suspension while it is harder to access the spring and damper as it sits so low in the car. Push rod setup, on the other hand,

has a higher CoG while making access to the spring and damper much easier as it sits so high in the car. Buckling of the push rod also has to be considered as the load is compressing the push rod there is a risk of it buckling. Even though it has a higher CoG push rod setup was used on the 2017 car with good results so it will be used in the preliminary design for this year's suspension also.

The force on the push rod is a function of the angle of the push rod, as the angle of the push rod from horizontal gets smaller the forces on the push rod gets larger as Figure 3.4.

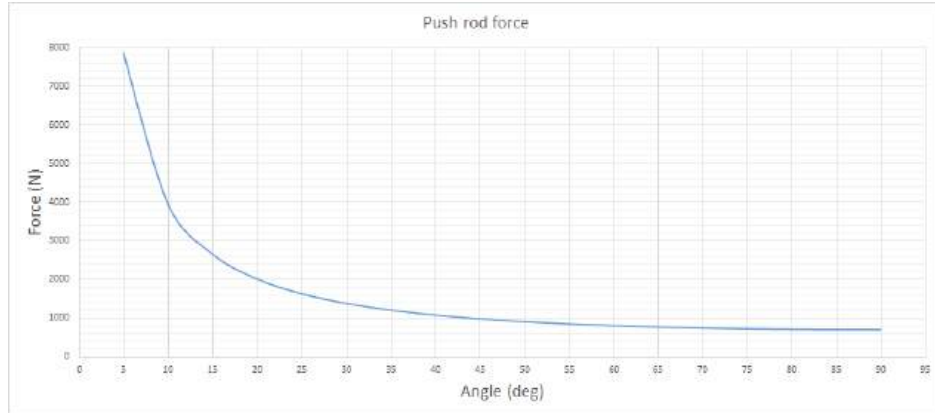


Figure 3.4: Force on the pushrod with 600 N force on the wheel

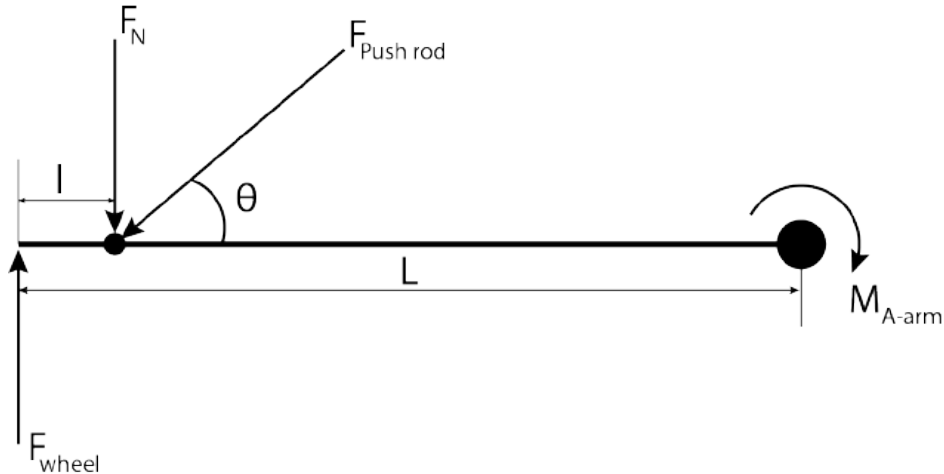


Figure 3.5: Free body diagram of the forces acting on the pushrod

The pushrod forces are found using the wheel load, and the moment it creates on the A-arm around the mounting point to the chassis.

$$M_{A\text{-arm}} = F_{wheel}L \quad (3.1)$$

$$F_N = \frac{M_{A\text{-arm}}}{L - l} \quad (3.2)$$

$$F_{pushrod} = \frac{F_N}{\sin \theta} \quad (3.3)$$

$$F_{pushrod} = \frac{F_{wheel}}{(L - l) \sin \theta} \quad (3.4)$$

Where:

- $M_{A-arm}$  Moment around the A-arm mount to the chassis (Nm)  
 $F_{wheel}$  Normal forces on the wheel center (N)  
 $L$  length of the A-arm (m)  
 $l$  distance between upright mounting and push rod mounting points (m)  
 $F_N$  normal force on the push rod mounting point (N)  
 $\theta$  Angle to the push rod from horizontal ( $^{\circ}$ )  
 $F_{pushrod}$  force acting on the push rod (N)

### 3.3.3 Bell cranks

The bell cranks translate the wheel forces from the push rod and change the angle of the force to the spring and damper that is mounted to the chassis. The motion ratio, how far the spring and damper moves in relation to the vertical motion of the wheel is calculated with Equation 2.2. According to the FS rules the wheels must have at least 50 mm of travel and with a motion ratio of 1:1 the damper must have the same travel.

### 3.3.4 Spring and damper

The spring and damper like mentioned earlier will be mounted to the chassis and connected to the wheel through the bell crank and push rod. This configuration reduces unsprung weight and improves the response of the suspension system. The suspension system uses coil over springs where the springs are mounted to the outside of the damper with an adjustable preload on the spring to adjust the ride height of the car as Figure 3.6 shows.

The dampers proposed for the preliminary design are Öhlins TTX 25 MkII 200 mm long with a 57 mm stroke. These dampers weigh only 394 g without the spring. [10]. The dampers are twin tube with adjustable high and low-speed rebound and compression these settings are important in fine-tuning the suspension. In twin-tube dampers, there are two chambers full of oil in the damper and when the damper is moved the piston moves the oil through the needle valves. The needle valves control the flow of liquid through the orifice in the valve seat restricting the flow of the oil and thus providing controllable flow. The Öhlins TTX MkII has a gas chamber that pressurizes the oil inside the damper with a piston that separates the gas from the oil. By having the oil inside the damper pressurized, improves the performance of the damper and prevents air bubbles forming in the oil and reduces hysteresis [6]. Figure 3.7 shows how the valves and passages inside the damper.

### 3.3.5 Anti roll bar

The anti-roll bars are used to increase the roll stiffness of the car during lateral acceleration and are an important factor in fine-tuning the roll stiffness of the car. The anti-roll bar works by taking the linear motion of the suspension and provide torsional stiffness through a rod or tube. This transfers some of the forces of the vertical forces between the tires during cornering and increases grip. The anti-roll bars are mounted low in the chassis to lower the CoG and have links to the bell cranks. The torsional stiffness of the anti-roll bar is found with Equations 3.5 - 3.8.

$$M_{ARB} = F_{ARB} l \quad (3.5)$$

Where:

- $M_{ARB}$  torque on the anti roll bar (Nm)  
 $F_{ARB}$  force on anti roll bar arm (N)

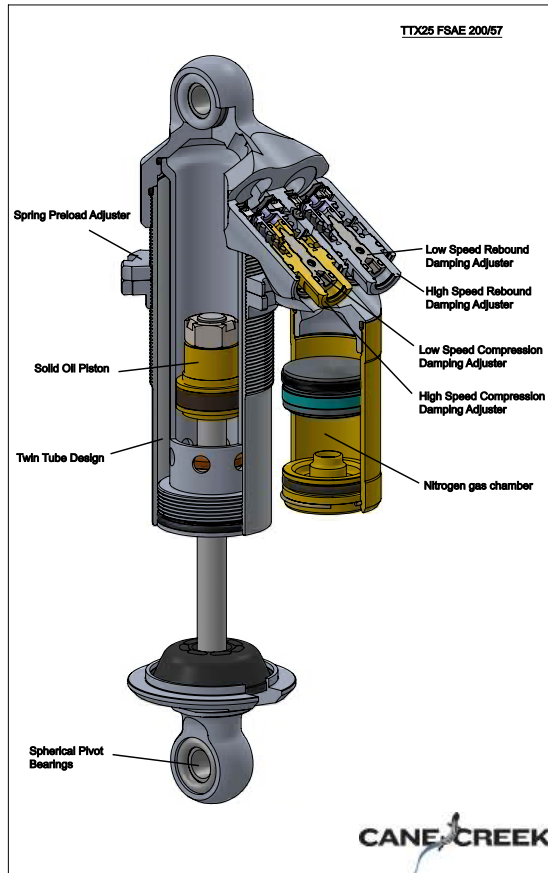


Figure 3.6: Cutaway model of the Öhlins TTX25 MkII FS damper [9]

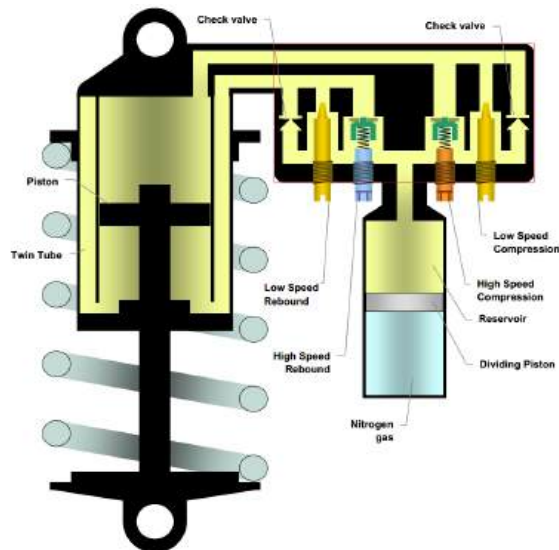


Figure 3.7: Öhlins TTX 25 MkII internal schematic [11]

$x$  distance from anti roll bar center to applied force (m)

$$\theta = \frac{\pi}{180} \frac{L/2M_{ARB}}{GJ_0} \quad (3.6)$$

Where:

$\theta$  rotation of the anti roll bar ( $^{\circ}$ )  
 $l$  length of the anti roll bar (mm)  
 $G$  modulus of rigidity (GPa)  
 $J_0$  polar moment of inertia (mm $^4$ )

$$J_0 = \frac{\pi(D^4 - d^4)}{32} \quad (3.7)$$

Where:

$D$  outside diameter of anti roll bar (mm)  
 $d$  inside diameter of anti roll bar (mm)

$$\frac{F_{ARB}}{\theta} = \frac{G(D^4 - d^4)180}{L/2 l 32} \quad (3.8)$$

Where:

$\frac{F_{ARB}}{\theta}$  is the anti roll bar torsional stiffness (N/deg)

## 3.4 Adams

### 3.4.1 Introduction

Adams Car [4] is one of the most well known multibody dynamics simulation software on the market and is widely used by car manufacturers. By using Adams Car [4], the designer can verify the design immediately and evaluate the results to see potential problems early in the design process. Adams[4] connects mathematical models with computer-aided design (CAD) and multibody systems. As Figure 3.8 shows the workflow in Adams [4] will be to adapt the FSAE 2015 template to the preliminary suspension design, do simulations on the design, analyze the results from the simulations and if needed readjust and optimize the design and simulate again after adjusting the model and see what effect it has on the overall performance of the car. When the design has met the requirements the location of each hardpoint will be exported to Microsoft Excel [15] to be used for the 3D model design in Inventor[14].

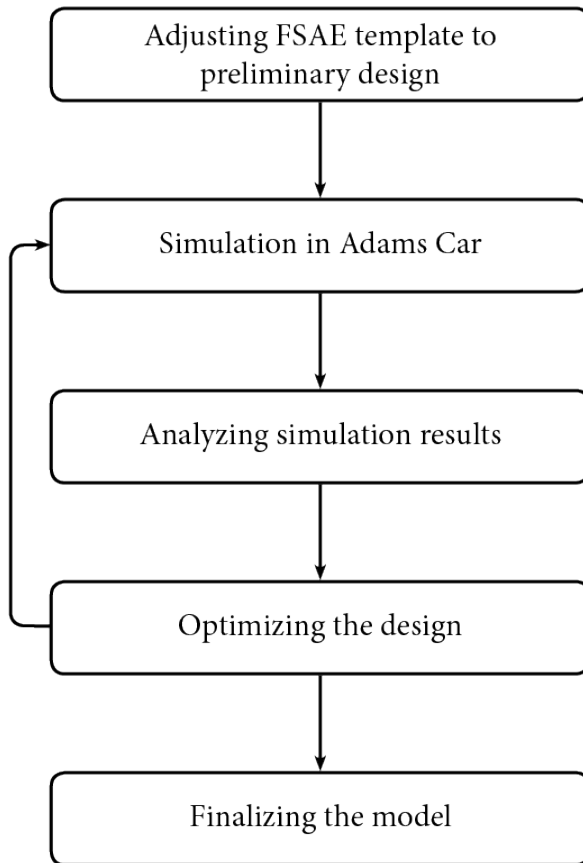


Figure 3.8: Adams Car[4] design flowchart.

A multibody system consist of structural members, or bodies that are connected using ideal joints. These joints can have up to 6 degrees of freedom or be rigid. The position of each body is given in relation to the ground reference point to the centre of mass of the body by a translation vector. Figure 3.9 shows a two body mechanical system where the angles  $\theta_1$  and  $\theta_2$  controls location of the bodies. The vector from point P relative to Q can be located with following equations, [12]

$$r^Q = A(\theta_1)s_1^Q \quad (3.9)$$

$$r^P = r^Q + A(\theta_1 + \theta_2)s_2^{QP} \quad (3.10)$$

Where  $s_2^{QP}$  and  $s_1^Q$  are the vectors to point Q and between Q and P.

$$r^P = \begin{bmatrix} \cos \theta_1 & -\sin \theta_1 \\ \sin \theta_1 & \cos \theta_1 \end{bmatrix} s_1^Q + \begin{bmatrix} \cos(\theta_1 + \theta_2) & -\sin(\theta_1 + \theta_2) \\ \sin(\theta_1 + \theta_2) & \cos(\theta_1 + \theta_2) \end{bmatrix} s_2^{QP} \quad (3.11)$$

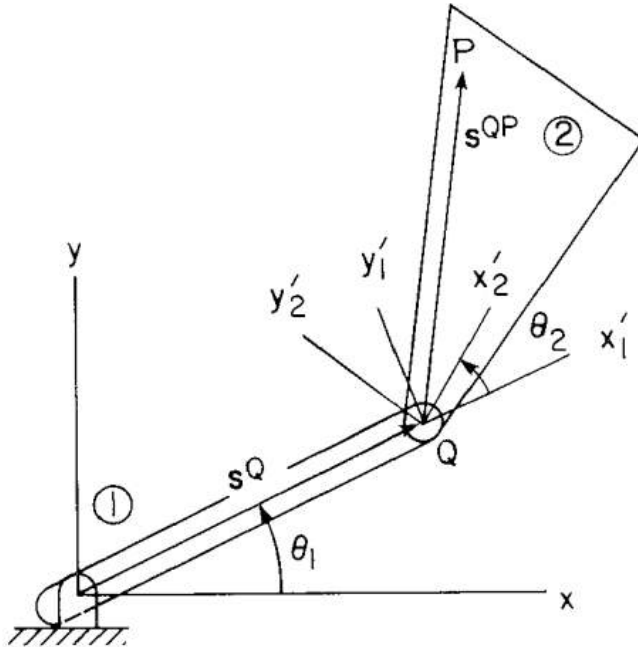


Figure 3.9: Two body position mechanism [12]

### 3.4.2 Adams Car model

In Adams [4] it is possible to create a 3D model by defining hard points in a Cartesian coordinate system, as Figure 3.11 shows, and creating structural members between the hard points. The hard points are all in relation to a fixed ground reference point that is used determine the movement of all bodies in the model. MSC provides the FS teams that are using Adams Car [4] for the design of there cars a template, called FSAE 2015, that has a pre-modeled FS car that can be adjusted to fit the team's needs. The tire properties can be modified in Adams and for the simulations the tire data provided by Hoosier tire manufacturer was used [13]. The mass and material of each structural member can be adjusted in Adams along with its CoG and moment of inertia. Figure 3.12 shows the part properties for the front upper control arm. The preliminary design model hardpoints were used to adapt the FSAE 2015 template to the design.

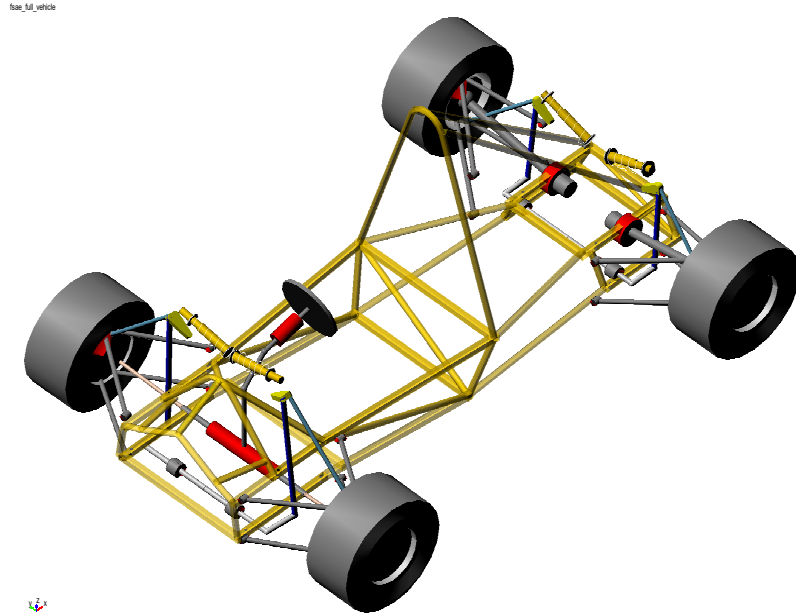


Figure 3.10: Adams Car [4] 3D model of the formula student car

Hardpoint Modification Table				
	loc_x	loc_y	loc_z	remarks
hpl_arb_bushing_mount	500.0	-130.0	80.0	(none)
hpl_arblink_to_bellcrank	592.0	-250.0	590.0	(none)
hpl_bellcrank_pivot	615.0	-190.0	540.0	(none)
hpl_bellcrank_pivot_orient	590.0	-195.0	560.0	(none)
hpl_lca_front	410.0	-260.0	105.0	(none)
hpl_lca_outer	610.0	-590.0	111.0	(none)
hpl_lca_rear	810.0	-285.0	105.0	(none)
hpl_prod_outer	615.0	-526.0	309.0	(none)
hpl_prod_to_bellcrank	615.0	-250.0	590.0	(none)
hpl_shock_to_bellcrank	615.0	-220.0	630.0	(none)
hpl_shock_to_chassis	615.0	-15.0	590.0	(none)
hpl_tierod_inner	670.0	-270.0	125.0	(none)
hpl_tierod_outer	670.0	-560.0	132.0	(none)
hpl_uca_front	410.0	-260.0	280.0	(none)
hpl_uca_outer	620.0	-570.0	297.0	(none)
hpl_uca_rear	810.0	-285.0	280.0	(none)
hpl_wheel_center	615.0	-624.0	201.5	(none)
hps_global	250.0	0.0	-175.0	(none)

Figure 3.11: Adams Car [4] suspension points table

### 3.4.3 Adams Car simulations

In Adams Car [4], it is possible to simulate the suspension system and its subsystems. This can be useful when designing the suspension system to be able to run a simulation only on the front or rear suspension system to get fast results on what effects changes on the suspension system have. Figure 3.13 shows the front suspension and steering subsystem. To analyze the camber change when the suspension jounces and rebounds during parallel or opposite wheel

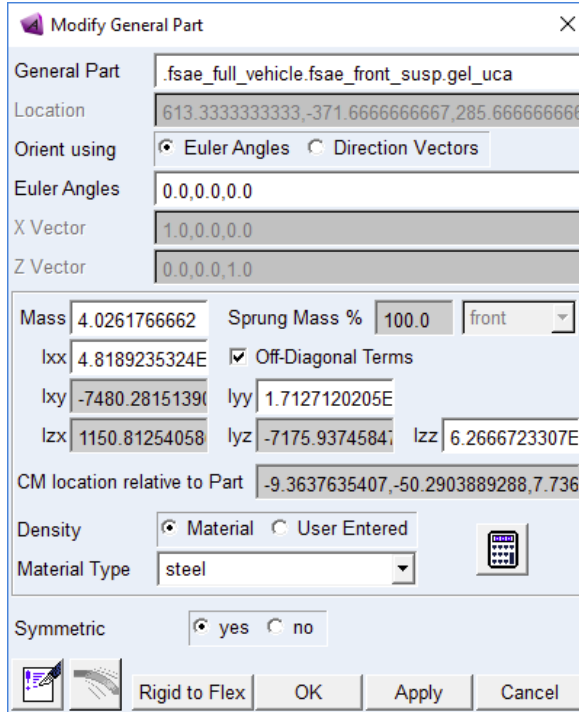


Figure 3.12: Adams Car [4] part modification window. The preliminary Inventor model was used to define the mass and properties of each part in the Adams model.

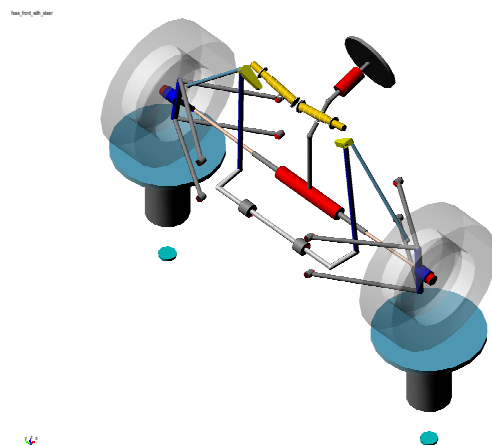


Figure 3.13: Adams Car [4] part modification window

travel. To set up the simulation the jounce and rebound have to be defined and the number of steps in the solution, see Figure 3.14. After running a simulation, the results can be viewed in the postprocessor window in Adams [4]. Figure 3.15 shows the results of a parallel wheel travel simulation and how the camber angle changes as the wheel moves.

The post-processing window allows for detailed analyzation were the location, force, velocity, torque and acceleration for each hard point and joint in the model can be viewed graphically.

In addition to being able to simulate subsystems of the suspension Adams Car [4] can simulate the whole vehicle during driving maneuvers like cornering events and driving around a racetrack. Adams SmartDriver [4] is a simulation where the software simulates how fast the vehicle can drive around a user-defined course. Being able to see what effects changes of the suspension geometry have on the performance of the vehicle is a great advantage of

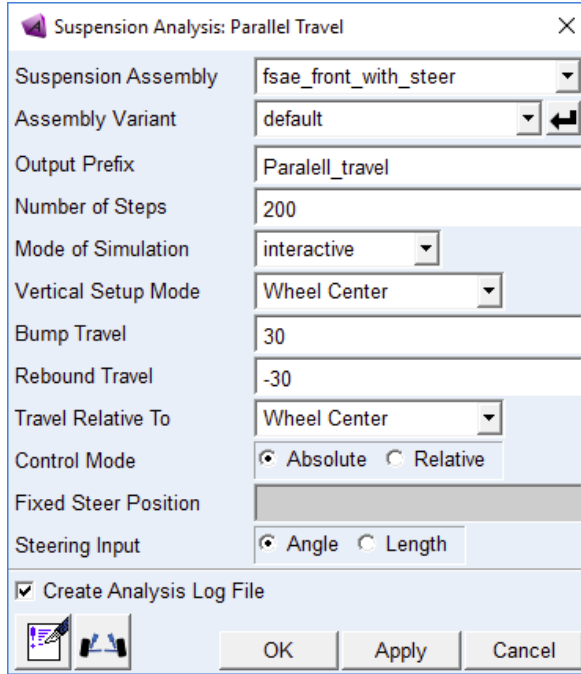


Figure 3.14: Adams Car [4] parallel wheel travel simulation setup window

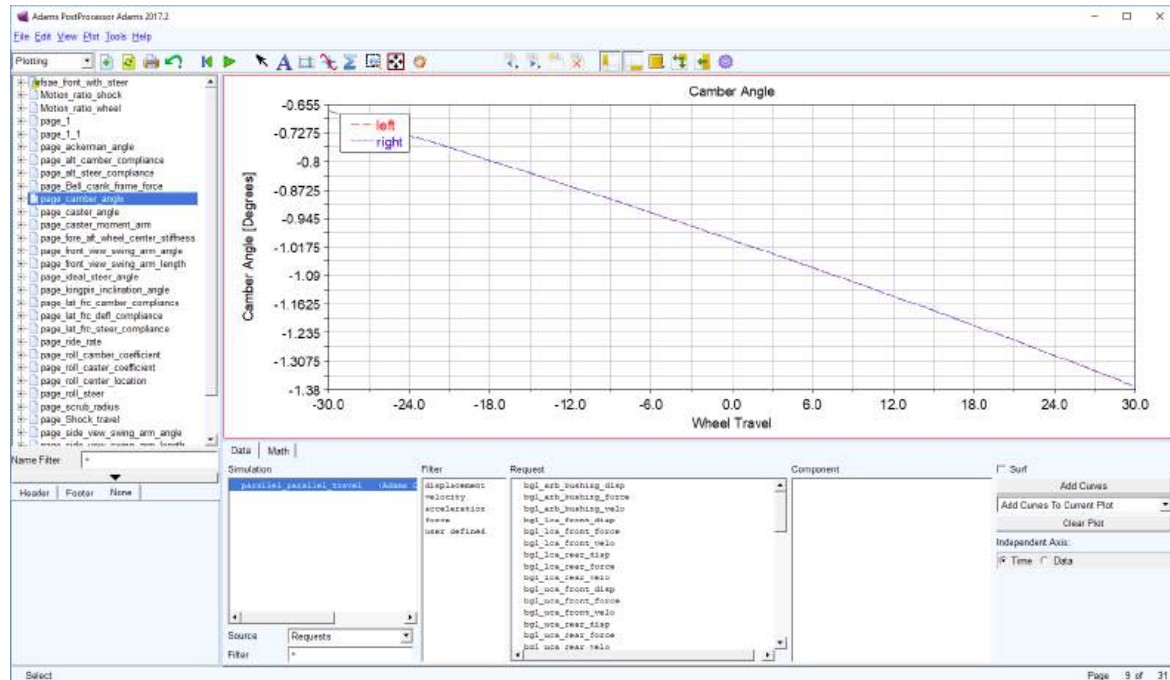


Figure 3.15: Adams Car [4] postprocessing window parallel wheel travel simulation camber change results

using Adams Car [4] simulations and eliminates the need for trial and error testing on the vehicle itself.

### 3.4.4 Results from Adams Car

As mentioned earlier the results from the simulations in Adams Car [4] can be viewed graphically in the built-in postprocessor shown in Figure 3.15 and by an animation of the simulation,

see Figure Figure 3.16, in the animation of the simulation the wheel forces can be displayed in red with an arrow showing the direction of the force as Figure 3.17 shows. A number of

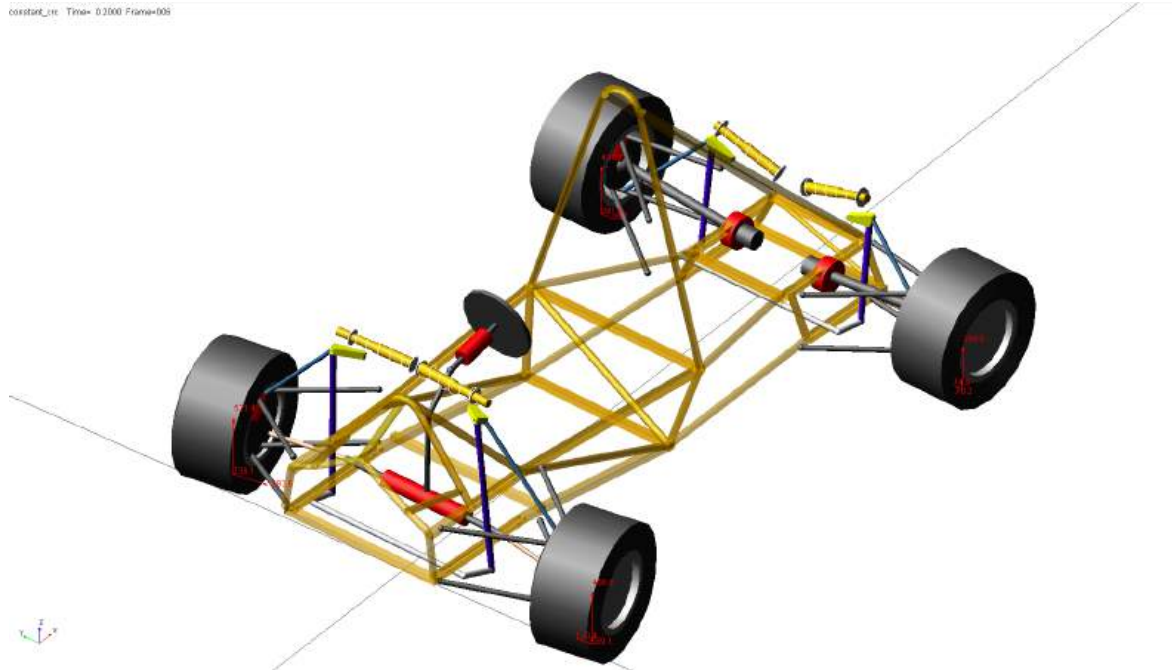


Figure 3.16: Adams Car [4] constant cornering simulation with wheel forces in red on the picture

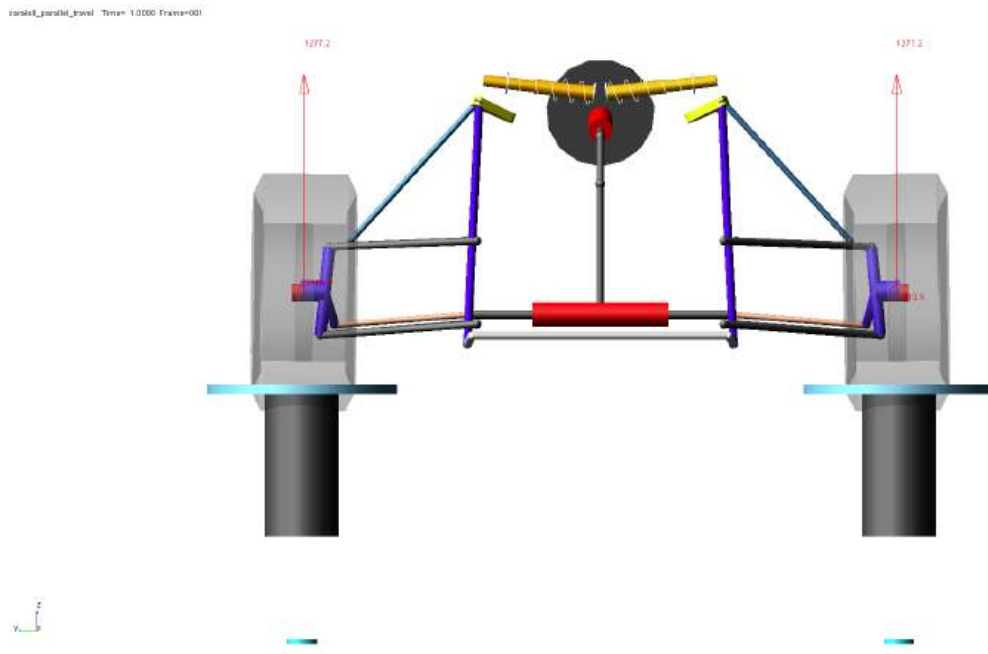


Figure 3.17: Adams Car [4] parallel wheel travel simulation of the front suspension system with wheel forces in red on the picture

simulation were used to optimize the design and the design process started by using parallel and opposite wheel travel simulations for the rear and front subsystems separately to analyze how the wheel angles, camber, caster, and kingpin, changed during wheel movement. After changing the design to acceptable angles gotten from Race Car Vehicle dynamics [5] and

Table 3.1: Static setup of the suspension

Feature	Front	Rear
Camber	-1.0°	0.0°
Caster	3.1°	0.0°
Kingpin inclination	6.1°	7.9°
Scrub radius	26.8 mm	19.9 mm

Table 3.2: Forces from Adams Car [4] simulations.

	Pothole Total (N)	Plank Total (N)	Corner Total (N)	Tilt Total (N)	Parallel Total (N)
Front pushrod to bell crank	1138.9	1915.9	656.9	751.8	4798.9
Front shock mount	1055.6	1794.1	569.8	548.9	1501.6
Front hub	1124.3	1775.4	456.9	760.2	3842.9
Rear pushrod to bell crank	1192.1	2537.2	525.6	605.9	3748.9
Rear shock mount	1131.3	2445.5	637.2	581.3	3164.1
Rear hub	1405.7	1905.8	356.7	560.3	2762.9

experience from the previous year car the static angles can be seen in Table 3.1.

The motion ratio between the spring and damper and the wheel is controlled with the design of the bell crank. By changing the distance from the mounting point of the bell crank to the chassis to the spring and damper and push rod mounting points the motion ratio can be changed. By having the motion ratio increasing it is possible to get a progressive spring rate with linear springs where the spring ratio increases because of the increasing motion ratio. Figure 3.18 shows how the motion ratio of the front suspension changes with wheel travel. Having a progressive spring rate has a beneficial effect on the handling of the car as it reduces the roll rate and increases stability during acceleration and braking.

Based on the results of the simulation in Adams Car [4] the Öhlins TTX25 MK II [10]



Figure 3.18: Adams Car [4] parallel wheel travel simulation motion ratio of the spring and damper versus the wheel

damper was selected for the car because of their lightweight and adjustability.

The forces, seen in Table 3.2, from the simulations in Adams Car will be used in the structural FEA analyzes for the suspension components designed in Autodesk Inventor.

## 3.5 3D modeling

The 3D model for the suspension system was designed in Autodesk Inventor Professional 2018 [14] using parameters for each hard point of the suspension system linked with Microsoft Excel [15] sheet. By having Excel [15] sheet with parameters linked to Inventor [14] changes to the 3D model can be made by exporting the hard point locations from Adams Car [4] and importing them to Excel [15] to update the Inventor [14] 3D model. Figure 3.19 shows the master 3D line model that was used for the design of the suspension system components.

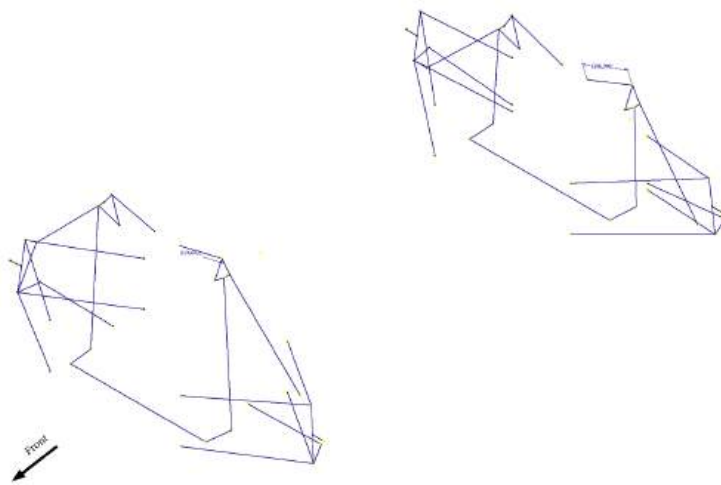


Figure 3.19: Inventor [14] hard point 3D model

### 3.5.1 A-arms

The A-arms are designed to be made as light as possible while keeping the cost as low as possible by using normal steel S235 16x2.0 mm pipes and sheet metal. The A-arm design is based on the design in the 2017 car with a spherical bearing where the A-arm connects to the upright and spherical rod ends where the A-arm mounts to the chassis. By having threaded rod ends where the A-arm mounts to the chassis it is possible to fine-tune the length of each arm of the A-arm but by changing the length of the arms of the A-arm the distance between them changes so to compensate for the change the rear arm is bolted to the connecting plate, see Figure 3.20.

The spherical bearing and rod ends are from Fluro [16] and are specially designed for motorsport applications. To fasten the threaded rod ends inserts made out of steel S355 are welded to the end of the pipes in the A-arms, the inserts are shown in Figure 3.20 in violet. The arms of the A-arm are connected with a plate that holds the spherical bearing seat and mounts for the push rod. The spherical bearing seat is made of S335 steel, and the bearing is fastened with an internal circlip. The length of the A-arms controls the track of the vehicle along with the design of the uprights and wheel hubs. The front and rear track are designed to be 1260 mm but as the rules state the maximum difference in front and rear track is 25% [3]. The wheelbase is designed to be 1585 mm but the minimum wheelbase according to the FS rules is 1525 mm [3].



Figure 3.20: Front upper control arm 3D model from Inventor [14]

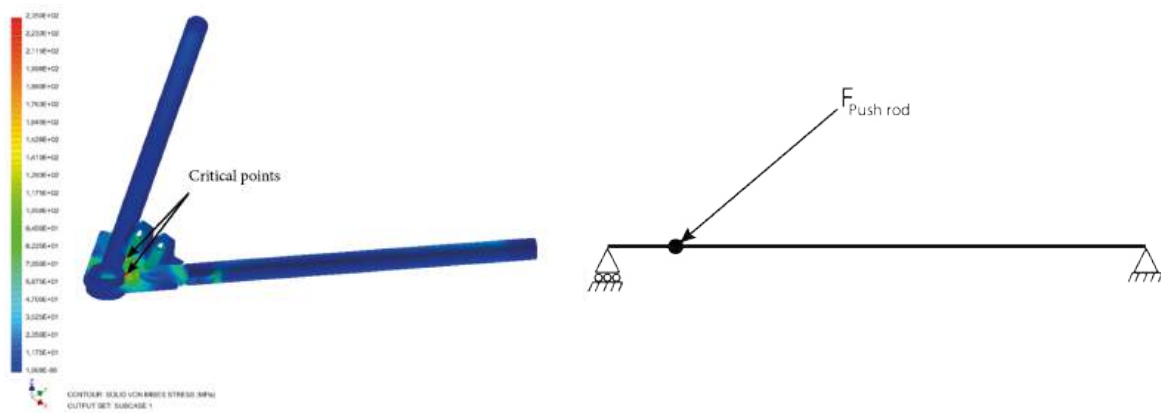


Figure 3.21: Front upper control arm FEA results and a free body diagram showing location of whee the force of 3748.9 N is applied

### 3.5.2 Pushrods

The pushrods are designed to be made out of the same material as the A-arms, 16x2.0 mm S235 pipes and using spherical rod ends on both ends.

One of the factors in designing the push rods is the risk of buckling. The critical buckling



Figure 3.22: Front push rod assembly 3D model from Inventor [14]

load can be found with Equation 3.12.

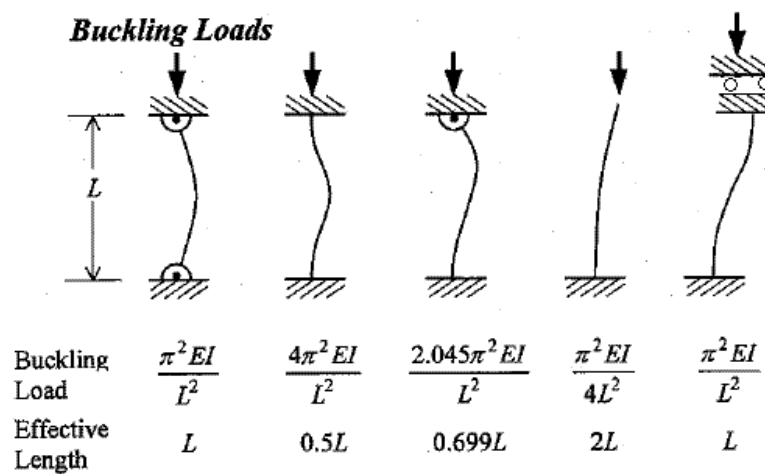


Figure 3.23: Buckling end conditions constants [17]

$$P_{cr} = \frac{\pi^2 EI}{L} \quad (3.12)$$

Where:

$$I = \frac{\pi(D^4 - d^4)}{64} \quad (3.13)$$

$$\begin{aligned}
 C &\text{ end condition} \\
 E &\text{ young's modulus (GPa)} \\
 L &\text{ length of push rod (m)} \\
 D &\text{ outer diameter (m)} \\
 d &\text{ inside diameter (m)}
 \end{aligned}$$

The steel pipes used in the push rods have Young's modulus of 210 GPa, the length of the front push rod is 330 mm and by using equation 3.12 the critical load for the push rod is 42 kN and a buckling safety factor of around 21. The forces from Adams Car [4] were used to run FEA analysis on the A-arms, the highest load was on the front upper control arm due to the forces from the push rod. Figure 3.21 shows the result from the FEA analysis on the front upper control arm.

### 3.5.3 Bell cranks

The bell cranks are designed to be milled out of a solid aluminum block. On the pivot point to the chassis, the bell crank will rotate on two deep groove ball bearings. The bell cranks were designed to be as light as possible and to be made out of 7075-T6 aluminum to have them as strong as possible. Figure 3.24 shows the front bell crank design.

The forces from Adams Car [4] were used to



Figure 3.24: Front bell crank 3D model from Inventor [14]

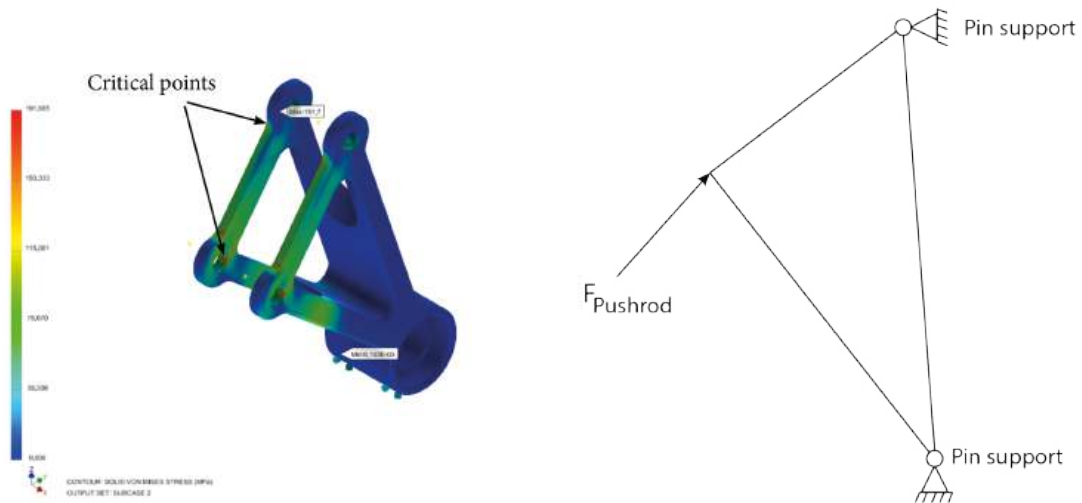


Figure 3.25: Front bell crank FEA results and a free body diagram showing location of where the force of 3748.9 N is applied

### 3.5.4 Anti-roll bar

The anti-roll bar is designed to be mounted as low as possible to keep the CoG as low as possible and use the same steel pipes as the A-arms to simplify the manufacturing process. The anti-roll bar will be mounted to the floor of the vehicle with arms on each side. The anti-roll bar links connect the bell crank, and anti-roll bar as Figure 3.26 shows.



Figure 3.26: Front suspension assembly 3D model from Inventor [14]



# Chapter 4

## Manufacturing

The manufacture of the suspension components took place at the university workshop which the students can use to manufacture parts for their projects. The university workshop is well equipped with most modern tools and equipment and with manual and CNC lathes and mills. The tool paths for the CNC mill and lathe are made using Inventor HSM Ultimate [18] addon in Inventor. The benefit of using a CNC machine for the manufacture is to get consistent parts and be able to quickly machine geometries that would otherwise be hard to manufacture.

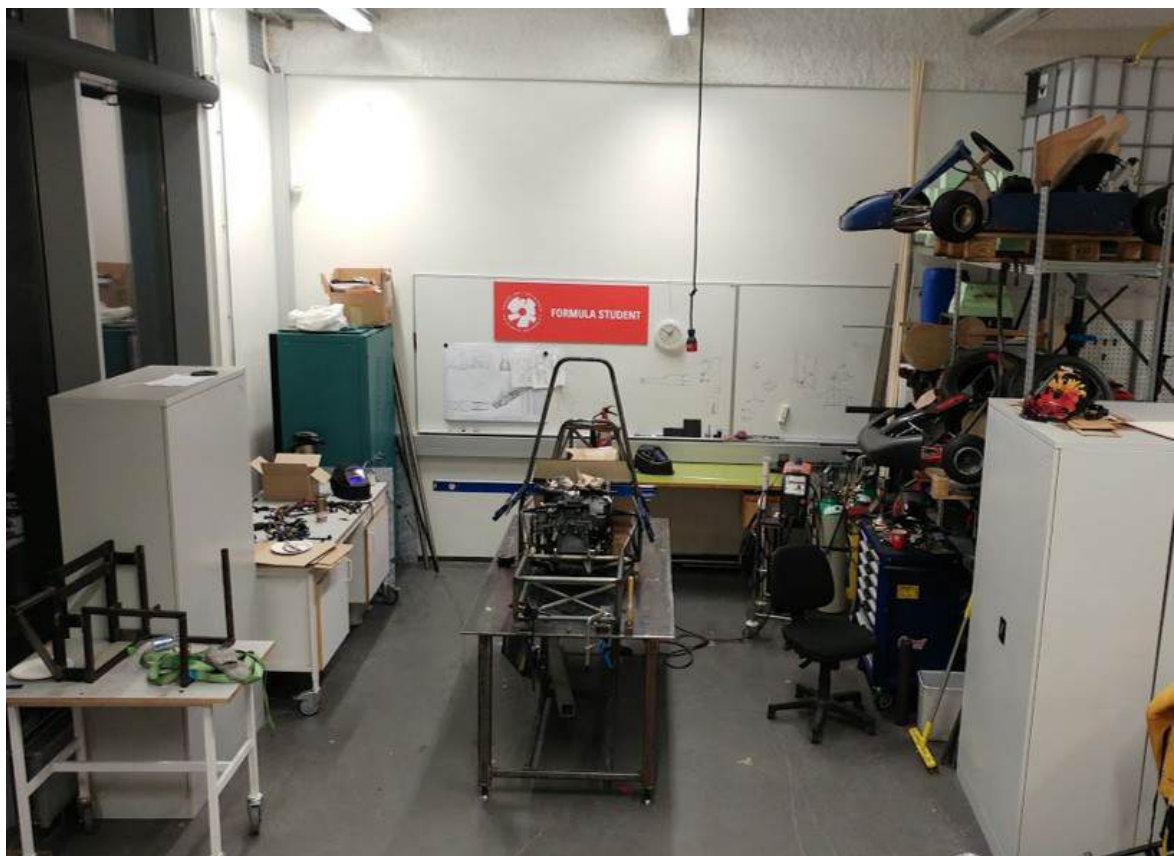


Figure 4.1: Sleipnir's workspace at the university workshop

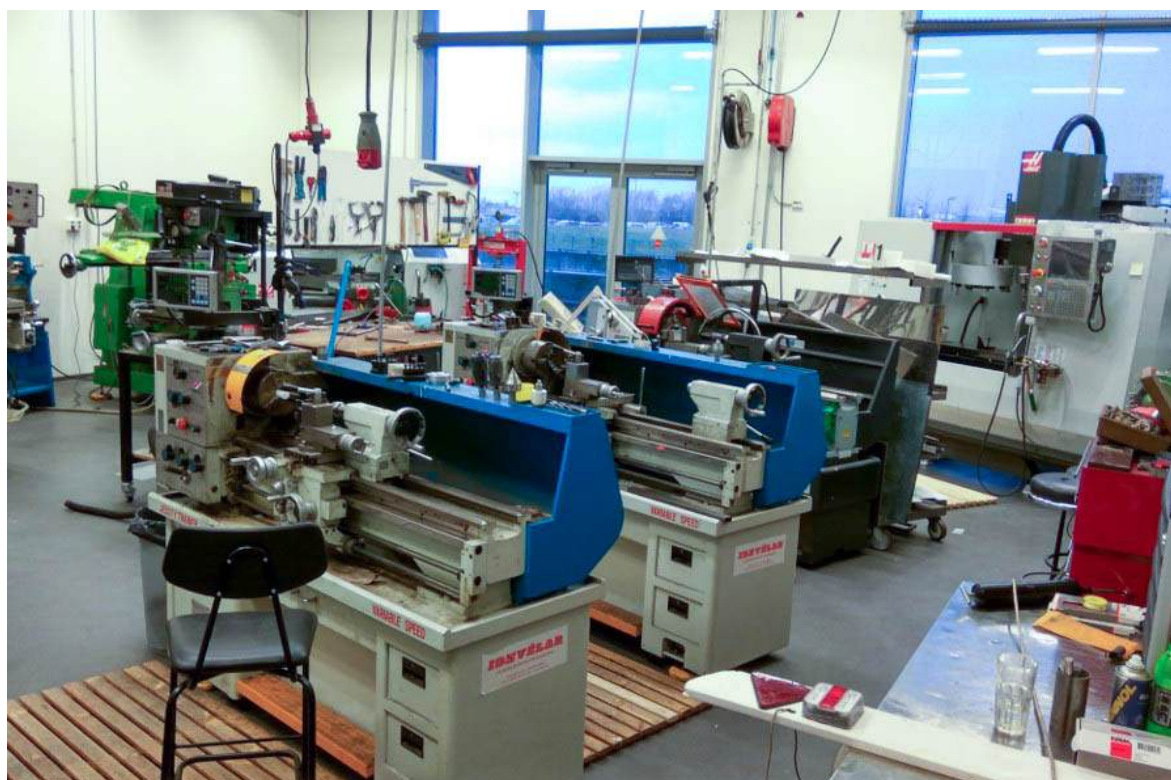


Figure 4.2: The university workshop

The mounting brackets for the suspension and the plates for the A-arms were laser cut out of cold rolled S235 2 mm plate, see Figure 4.3.



Figure 4.3: Laser cut brackets for the suspension, first from left is the insert for the rear arm of the A-arms, second from left is the push rod mount bracket for the A-arms, third and fourth from left are mounting brackets for the A-arms to the chassis.

The spherical bearing seat and the inserts for the spherical rod ends were manufactured using the CNC lathe out of steel S355.

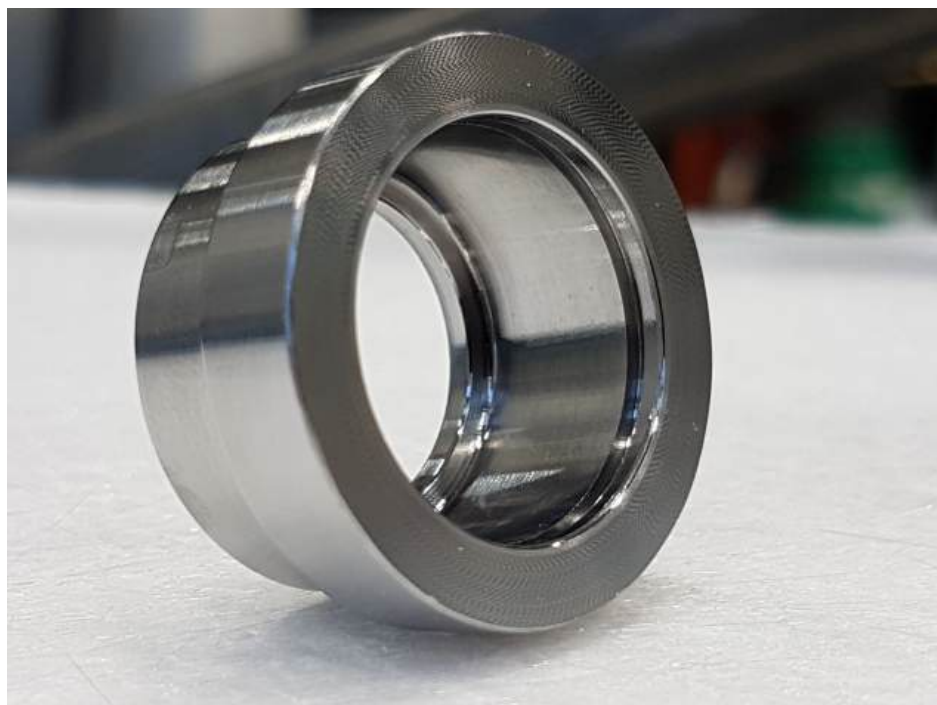


Figure 4.4: Spherical bearing seat for the control arms

The spherical bearing seats were manufactured in a Haas TL-1 lathe [19] in two setups and with the G-code created using Autodesk Inventor HSM Ultimate [18]. In the first setup the outside was machined and the part parted off. In the second setup the inside was machined and the split ring seat machined. Four tools were used for the machining a standard TNMG160404 [20] insert with a step down of 1.0 mm with a cutting speed of 0.2 mm/rev and a surface speed of 90 m/min. The inside was machined using a 14 mm boring bar with a DNMG110404 insert with a step down of 0.5 mm and a cutting speed of 0.15 mm/rev and a surface speed of 100 mm/min. The split ring groove was machined with a boring bar and a 1.1 mm grooving insert with a cutting speed of 0.09 mm/rev and a surface speed of 50 m/min. A 2 mm parting tool was used for parting with a cutting speed of 0.05 mm/rev and a surface speed of 50 m/min. The total machining time was approxemathly 7 minutes. These speeds were used as a baseline for other parts that were machined in the lathe.

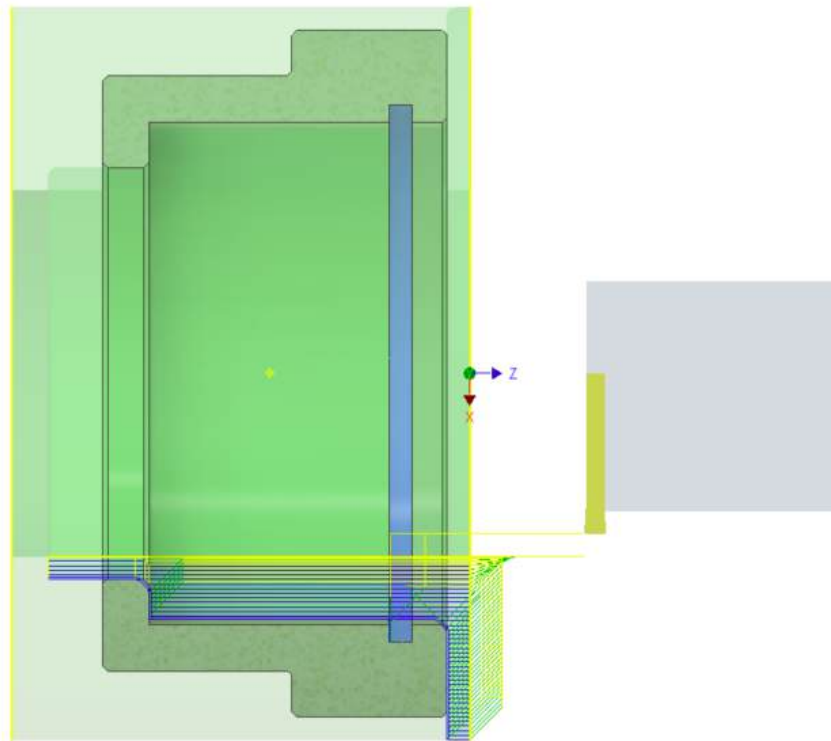


Figure 4.5: Spherical bearing seat toolpath from Inventor HSM [18]



Figure 4.6: Inserts for spherical rod ends

To increase the travel angle of the spherical rod ends spacers were made out of stainless steel 303 using the CNC lathe as shown in Figure 4.7 and Figure 4.8.



Figure 4.7: Spacer for spherical rod ends to increase the travel angle of the rod end

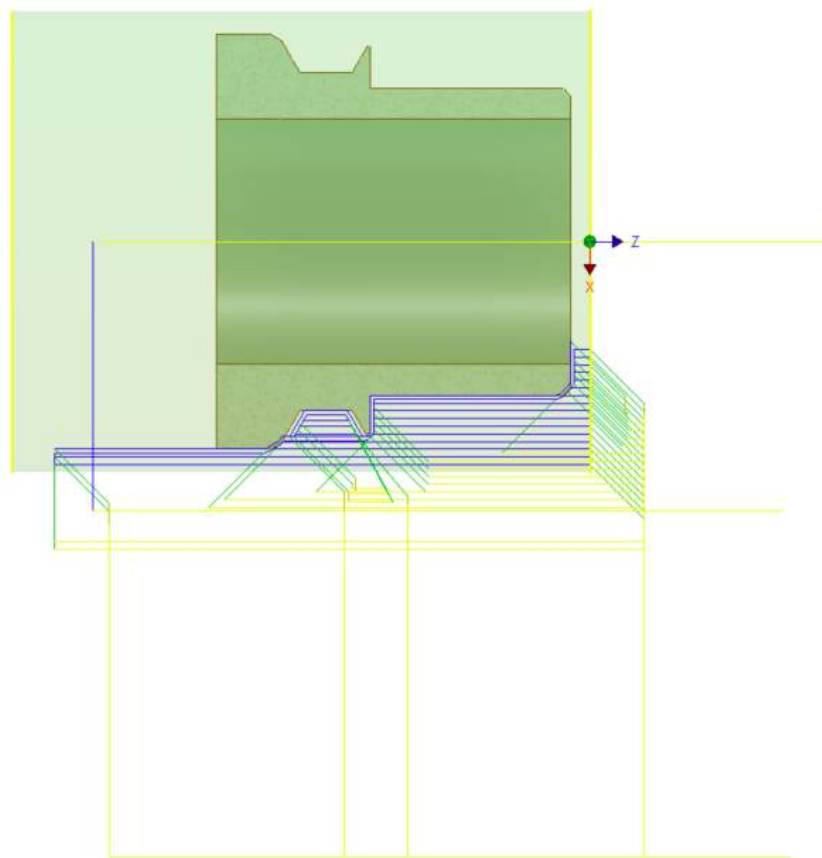


Figure 4.8: Spacer for spherical rod ends toolpath from Inventor HSM [18]

Figure 4.9 shows the front push rod end where the spherical rod end insert has been TIG welded to the pipe and a rod end with a spacer mounted. The mounting brackets were TIG



Figure 4.9: Inserts welded to A-arm

welded to the chassis and A-arms mounted to the frame, see Figure 4.10.



Figure 4.10: Front A-arms mounted on the chassis

The bell cranks were machined out of aluminum 7075-T6 using the CNC mill in three setups, Figure 4.11 shows the front bell crank after the first setup was one side of the bell crank had been machined. Figure 4.12 shows the front bell cranks after both sides of the bell cranks have been machined.

The bell cranks were machined using a Haas TM-1P mill [21]. The bell cranks were roughed with a 16 mm flat end mill and a cutting speed of 1000 mm/min and a spindle speed of 5000 rpm. The finishing on the outside was done with a 10 mm end mill and the same speeds as the 16 mm mill. The pocket inside the bell cranks was machined with a 8 mm flat end mill and a cutting speed of 700 mm/min and a spindle speed of 6000 rpm. The chamfer was machined using a 8 mm 90° spot drill and a cutting speed of 800 mm/min and a spindle speed of 6000 rpm.



Figure 4.11: Bell crank machined front side



Figure 4.12: Bell crank machined back side

# Chapter 5

## Conclusion

As the main objectives of this thesis were to gain a better understanding of how suspension systems work and combine theory and practical knowledge by designing and manufacturing the suspension system. In the thesis suspension properties like camber, caster and kingpin inclination angle was explained and what effects on the overall handling of the car they have. The manufacturing process is also explained and how the design could be as simple as possible without sacrificing performance. After the design of each component of the suspension system, an assembly was created to verify the design and that no interference was between components. Figure 5.1 shows the Inventor [14] 3D model of the final assembly.

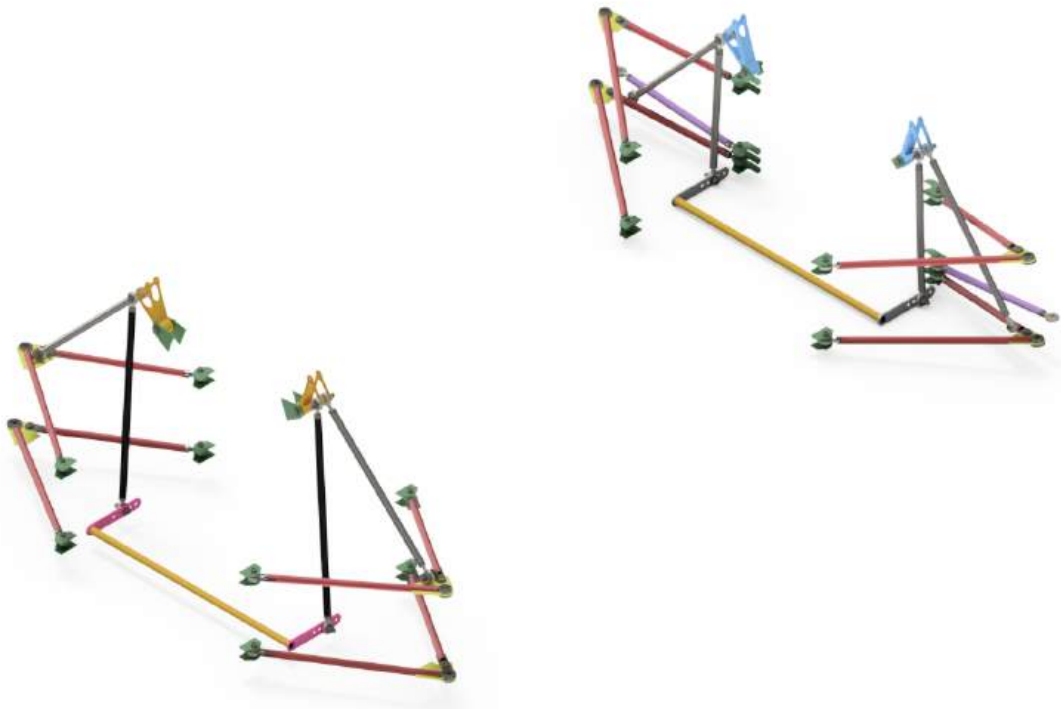


Figure 5.1: Final 3D model of the suspension assembly in Inventor [14]

Table 5.1: Comparison of weight of left side suspension components between 2017 and 2018 car

Weight comparison	2017	2018
Part	Weight [Kg]	Weight [Kg]
Front bell crank	0.218	0.1
Front lower control arm	0.631	0.696
Front upper control arm	0.821	0.700
Front push rod	0.241	0.295
Rear bell crank	0.218	0.128
Rear lower control arm	0.529	0.687
Rear upper control arm	0.674	0.656
Rear push rod	0.207	0.221
Chassis brackets	0.591	0.428
Total weight left	4.13	3.91

One of the goals for the design was to keep each component as light as possible, and the design for the 2018 car is 220 grams lighter than previous design while having the design easier to manufacture than the previous design. The bell cranks on the previous car were made out of aluminum 6061-T6, but to save weight, the 2018 car will have bell cranks made out of aluminum 7075-T6 which has a higher yield strength of 572 MPa [22] versus 276 MPa [23] for 6061-T6 aluminum. The A-arms and pushrods use a similar design as previously except for the A-arms as they use a different method of connecting the arms with the rear arm bolted to the A-arm assembly to solve the problem when the distance between the rod ends changes if the rod ends are adjusted. The design also uses spacers to increase the travel angle of spherical bearing joints and to prevent collision between parts as a result of limited movement in the spherical bearings.

# **Chapter 6**

## **Future work**

As with all design, there is always room for improvement and although the thesis covers extensive analysis of the suspension for the 2018 car further work can be put into lightening the suspension system. There are few potential improvements that can be made to the suspension system such as:

- Looking into the use of composite materials like carbon fiber for components of the suspension system such as A-arms, pushrods and bell cranks
- Analyzing the dampers and fine tune the dampers with simulations in Adams Car [4] and with a test on the car.
- Lowering the CoG by using pull-rod suspension instead of pushrod suspension.
- Designing active suspension system and the possibility of having no anti-roll bar.



# Bibliography

- [1] O. FSAE History, [Online]. Available: <https://www.fsaeonline.com/page.aspx?pageid=c4c5195a-60c0-46aa-acbf-2958ef545b72> (visited on 03/22/2018).
- [2] O. History of Formula Student, [Online]. Available: <https://www.imeche.org/events/formula-student/about-formula-student/history-of-formula-student> (visited on 03/22/2018).
- [3] *FSRules2018*. [Online]. Available: [http://www.imeche.org/docs/default-source/1-oscar/formula-student/fs-rules\\_2018\\_v1-1.pdf?sfvrsn=2](http://www.imeche.org/docs/default-source/1-oscar/formula-student/fs-rules_2018_v1-1.pdf?sfvrsn=2) (visited on 03/26/2018).
- [4] *MSC Adams Car*, version 2017.2, 4675 MacArthur Court, Newport Beach, CA 92660.
- [5] William F. Milliken and Douglas L. Milliken, *Race Car Vehicle Dynamics*. SAE International, ISBN: 978-1-56091-526-3.
- [6] J. Kasprzak, “Understanding Your Dampers: A Guide from Jim Kasprzak”, [Online]. Available: <http://www.kaztechnologies.com/wp-content/uploads/2014/03/A-Guide-To-Your-Dampers-Chapter-from-FSAE-Book-by-Jim-Kasprzak.pdf> (visited on 04/11/2018).
- [7] M. Giaraffa, “Tech Tip: Springs & Dampers, Part Two”, p. 3,
- [8] O. Pushrod-Pullrod, [Online]. Available: [http://www.formula1-dictionary.net/pushrod\\_pullrod.html](http://www.formula1-dictionary.net/pushrod_pullrod.html) (visited on 04/18/2018).
- [9] Öhlins, *TTX25 FSAE 200/57 Cutaway Model*. [Online]. Available: <https://www.ohlinsusa.com/files/TTX25Cutaway2014.pdf>.
- [10] O. Auto Racing Automotive Suspension | TTX25 MkII Shock Absorber | Öhlins USA, [Online]. Available: <https://www.ohlinsusa.com/suspension-products/Auto-motive/Auto+Racing/Shock+Absorber/70/TTX25+MkII> (visited on 04/21/2018).
- [11] ——, *Öhlins TTX25 Mk2 Internal Schematic*. [Online]. Available: <https://www.ohlinsusa.com/files/files/FSAE%20Schematic%202014.pdf>.
- [12] O. ME 451, [Online]. Available: <http://sbel.wisc.edu/Courses/ME451/2009/> (visited on 05/14/2018).
- [13] O. Hoosier Tire | Contingency Awards Program, [Online]. Available: [http://www.hoosiertire.com/contingency\\_rates/fsae/](http://www.hoosiertire.com/contingency_rates/fsae/) (visited on 04/24/2018).
- [14] *Autodesk Inventor Professional 2018*, Autodesk, Inc, 111 McInnis Parkway San Rafael, CA 94903 USA.
- [15] *Microsoft Excel 2016 MSO (16.0.44.56.1003) 64-Bit*, Microsoft Corporation One Microsoft Way Redmond, WA 98052-6399 USA.
- [16] Heinzelmann. O. Motor Sport, [Online]. Available: <http://fluro.de/index.php/en/products/motor-sport> (visited on 04/30/2018).

- [17] (Sep. 25, 2016). Nonlinear buckling with no penetration contact support in 2017, [Online]. Available: <http://blogs.solidworks.com/tech/2016/09/nonlinear-buckling-no-penetration-contact-support-2017.html> (visited on 05/01/2018).
- [18] *Inventor HSM Ultimate, Build 5.3.1.55*, Autodesk, Inc. Attention: General Counsel Legal Department 111 McInnis Parkway San Rafael, CA 94903.
- [19] () . Haas TL-1 | Haas Automation, Inc. | CNC Machine Tools, [Online]. Available: [http://int.haascnc.com/mt\\_spec1.asp?intLanguageCode=1033&id=TL-1&webID=TOOLROOM\\_LATHE](http://int.haascnc.com/mt_spec1.asp?intLanguageCode=1033&id=TL-1&webID=TOOLROOM_LATHE) (visited on 05/14/2018).
- [20] () . Mitsubishi Materials Web Catalogue|Search Result|Turning Inserts, [Online]. Available: [http://www.mitsubishicarbide.net/webcatalog/OMA02F002BLogic.do?ctgr\\_rykshu=turning\\_inserts&mkt\\_rykshu=mhg&gng\\_rykshu=enuk&ybkgu=TNMG160404-MP&zish\\_di\\_bnri\\_id=01](http://www.mitsubishicarbide.net/webcatalog/OMA02F002BLogic.do?ctgr_rykshu=turning_inserts&mkt_rykshu=mhg&gng_rykshu=enuk&ybkgu=TNMG160404-MP&zish_di_bnri_id=01) (visited on 05/14/2018).
- [21] () . Haas TM-1P | Haas Automation, Inc. | CNC Machine Tools, [Online]. Available: [http://int.haascnc.com/mt\\_spec1.asp?intLanguageCode=1033&id=TM-1P&webID=TOOLROOM\\_MILL\\_VMC](http://int.haascnc.com/mt_spec1.asp?intLanguageCode=1033&id=TM-1P&webID=TOOLROOM_MILL_VMC) (visited on 05/14/2018).
- [22] () . Aluminum 7075-T6; 7075-T651, [Online]. Available: [http://www.matweb.com/search/datasheet\\_print.aspx?matguid=4f19a42be94546b686bbf43f79c51b7d](http://www.matweb.com/search/datasheet_print.aspx?matguid=4f19a42be94546b686bbf43f79c51b7d) (visited on 05/03/2018).
- [23] () . Aluminum 6061-T6; 6061-T651, [Online]. Available: <http://www.matweb.com/search/DataSheet.aspx?MatGUID=b8d536e0b9b54bd7b69e4124d8f1d20a> (visited on 05/03/2018).
- [24] () . 303 Stainless Steel, Annealed Bar, [Online]. Available: <http://www.matweb.com/search/datasheet.aspx?matguid=03e319215220463ea920bc7defc6ef87&ckck=1> (visited on 05/04/2018).
- [25] () . S235JR, [Online]. Available: <https://steelnavigator.ovako.com/steel-grades/s235/> (visited on 05/01/2018).
- [26] () . S355JR, [Online]. Available: <https://steelnavigator.ovako.com/steel-grades/s355/> (visited on 05/01/2018).
- [27] Öhlins USA, *Spring Details*. [Online]. Available: [https://www.ohlinsusa.com/files/files/db\\_springs.pdf](https://www.ohlinsusa.com/files/files/db_springs.pdf).
- [28] ——, *Internal Schematic*. [Online]. Available: <https://www.ohlinsusa.com/files/files/FSAE%20Schematic%202014.pdf>.
- [29] ——, *External Dimensions*. [Online]. Available: [https://www.ohlinsusa.com/files/files/DB-FSAE-Outer\\_Dims1.pdf](https://www.ohlinsusa.com/files/files/DB-FSAE-Outer_Dims1.pdf).
- [30] ——, *Dyno Plots TTX25 MkII Metric*. [Online]. Available: [https://www.ohlinsusa.com/files/files/TTX\\_25%20Dyno\\_M.pdf](https://www.ohlinsusa.com/files/files/TTX_25%20Dyno_M.pdf).
- [31] () . Deep Groove Ball Bearings - 608-2RSH, [Online]. Available: <http://www.skf.com/uk/products/bearings-units-housings/ball-bearings/deep-groove-ball-bearings/deep-groove-ball-bearings/index.html?designation=608-2RSH> (visited on 05/03/2018).

# **Appendix A**

## **Datasheets**

### **A.1 Aluminum 6061 T6**

Datasheet from MatWeb [23].

**Aluminum 6061-T6; 6061-T651****Categories:** [Metal](#); [Nonferrous Metal](#); [Aluminum Alloy](#); [6000 Series Aluminum Alloy](#)

**Material Notes:** General 6061 characteristics and uses: Excellent joining characteristics, good acceptance of applied coatings. Combines relatively high strength, good workability, and high resistance to corrosion; widely available. The T8 and T9 tempers offer better chipping characteristics over the T6 temper.

**Applications:** Aircraft fittings, camera lens mounts, couplings, marines fittings and hardware, electrical fittings and connectors, decorative or misc. hardware, hinge pins, magneto parts, brake pistons, hydraulic pistons, appliance fittings, valves and valve parts; bike frames.

Data points with the AA note have been provided by the Aluminum Association, Inc. and are NOT FOR DESIGN.

**Composition Notes:**

Composition information provided by the Aluminum Association and is not for design.

**Key Words:** al6061, UNS A96061; ISO AIMg1SiCu; Aluminium 6061-T6, AD-33 (Russia); AA6061-T6; 6061T6, ISO AIMg1SiCu; Aluminium 6061-T651, AD-33 (Russia); AA6061-T651

**Vendors:** [Click here to view all available suppliers for this material.](#)

Please [click here](#) if you are a supplier and would like information on how to add your listing to this material.

Physical Properties	Metric	English	Comments
Density	2.70 g/cc	0.0975 lb/in <sup>3</sup>	AA; Typical
Mechanical Properties	Metric	English	Comments
Hardness, Brinell	95	95	AA; Typical; 500 g load; 10 mm ball
Hardness, Knoop	120	120	Converted from Brinell Hardness Value
Hardness, Rockwell A	40	40	Converted from Brinell Hardness Value
Hardness, Rockwell B	60	60	Converted from Brinell Hardness Value
Hardness, Vickers	107	107	Converted from Brinell Hardness Value
Tensile Strength, Ultimate	310 MPa	45000 psi	AA; Typical
	24.0 MPa @Temperature 371 °C	3480 psi @Temperature 700 °F	
	32.0 MPa @Temperature 316 °C	4640 psi @Temperature 601 °F	
	51.0 MPa @Temperature 260 °C	7400 psi @Temperature 500 °F	
	131 MPa @Temperature 204 °C	19000 psi @Temperature 399 °F	
	234 MPa @Temperature 149 °C	33900 psi @Temperature 300 °F	
	290 MPa @Temperature 100 °C	42100 psi @Temperature 212 °F	
	310 MPa @Temperature 24.0 °C	45000 psi @Temperature 75.2 °F	
	324 MPa @Temperature -28.0 °C	47000 psi @Temperature -18.4 °F	
	338 MPa @Temperature -80.0 °C	49000 psi @Temperature -112 °F	
	414 MPa @Temperature -196 °C	60000 psi @Temperature -321 °F	
Tensile Strength, Yield	276 MPa	40000 psi	AA; Typical
	12.0 MPa @Strain 0.200 %, Temperature 371 °C	1740 psi @Strain 0.200 %, Temperature 700 °F	
	19.0 MPa @Strain 0.200 %, Temperature 316 °C	2760 psi @Strain 0.200 %, Temperature 601 °F	
	34.0 MPa	4930 psi	

	@Strain 0.200 %, Temperature 260 °C	@Strain 0.200 %, Temperature 500 °F	
	103 MPa @Strain 0.200 %, Temperature 204 °C	14900 psi @Strain 0.200 %, Temperature 399 °F	
	214 MPa @Strain 0.200 %, Temperature 149 °C	31000 psi @Strain 0.200 %, Temperature 300 °F	
	262 MPa @Strain 0.200 %, Temperature 100 °C	38000 psi @Strain 0.200 %, Temperature 212 °F	
	276 MPa @Strain 0.200 %, Temperature 24.0 °C	40000 psi @Strain 0.200 %, Temperature 75.2 °F	
	283 MPa @Strain 0.200 %, Temperature -28.0 °C	41000 psi @Strain 0.200 %, Temperature -18.4 °F	
	290 MPa @Strain 0.200 %, Temperature -80.0 °C	42100 psi @Strain 0.200 %, Temperature -112 °F	
	324 MPa @Strain 0.200 %, Temperature -196 °C	47000 psi @Strain 0.200 %, Temperature -321 °F	
Elongation at Break	17 % @Temperature -28.0 °C	17 % @Temperature -18.4 °F	
	17 % @Temperature 24.0 °C	17 % @Temperature 75.2 °F	
	18 % @Temperature -80.0 °C	18 % @Temperature -112 °F	
	18 % @Temperature 100 °C	18 % @Temperature 212 °F	
	20 % @Temperature 149 °C	20 % @Temperature 300 °F	
	22 % @Temperature -196 °C	22 % @Temperature -321 °F	
	28 % @Temperature 204 °C	28 % @Temperature 399 °F	
	60 % @Temperature 260 °C	60 % @Temperature 500 °F	
	85 % @Temperature 316 °C	85 % @Temperature 601 °F	
	95 % @Temperature 371 °C	95 % @Temperature 700 °F	
	12 % @Thickness 1.59 mm	12 % @Thickness 0.0625 in	AA; Typical
	17 % @Diameter 12.7 mm	17 % @Diameter 0.500 in	AA; Typical
Modulus of Elasticity	68.9 GPa	10000 ksi	AA; Typical; Average of tension and compression. Compression modulus is about 2% greater than tensile modulus.
Notched Tensile Strength	324 MPa	47000 psi	2.5 cm width x 0.16 cm thick side-notched specimen, $K_t = 17$ .
Ultimate Bearing Strength	607 MPa	88000 psi	Edge distance/pin diameter = 2.0
Bearing Yield Strength	386 MPa	56000 psi	Edge distance/pin diameter = 2.0
Poissons Ratio	0.33	0.33	Estimated from trends in similar Al alloys.
Fatigue Strength	96.5 MPa @# of Cycles 5.00e+8	14000 psi @# of Cycles 5.00e+8	completely reversed stress; RR Moore machine/specimen
Fracture Toughness	29.0 MPa-m <sup>1/2</sup>	26.4 ksi-in <sup>1/2</sup>	$K_{IC}$ ; TL orientation.
Machinability	50 %	50 %	0-100 Scale of Aluminum Alloys
Shear Modulus	26.0 GPa	3770 ksi	Estimated from similar Al alloys.
Shear Strength	207 MPa	30000 psi	AA; Typical
Electrical Properties	Metric	English	Comments
Electrical Resistivity	0.00000399 ohm-cm @Temperature 20.0 °C	0.00000399 ohm-cm @Temperature 68.0 °F	AA; Typical

Thermal Properties	Metric	English	Comments
CTE, linear 	23.6 $\mu\text{m}/\text{m}\cdot^\circ\text{C}$ @Temperature 20.0 - 100 $^\circ\text{C}$	13.1 $\mu\text{in}/\text{in}\cdot^\circ\text{F}$ @Temperature 68.0 - 212 $^\circ\text{F}$	AA; Typical; average over range
	25.2 $\mu\text{m}/\text{m}\cdot^\circ\text{C}$ @Temperature 20.0 - 300 $^\circ\text{C}$	14.0 $\mu\text{in}/\text{in}\cdot^\circ\text{F}$ @Temperature 68.0 - 572 $^\circ\text{F}$	
Specific Heat Capacity	0.896 J/g- $^\circ\text{C}$	0.214 BTU/lb- $^\circ\text{F}$	
Thermal Conductivity	167 W/m-K	1160 BTU-in/hr-ft <sup>2</sup> - $^\circ\text{F}$	AA; Typical at 77°F
Melting Point	582 - 651.7 $^\circ\text{C}$	1080 - 1205 $^\circ\text{F}$	AA; Typical range based on typical composition for wrought products 1/4 inch thickness or greater; Eutectic melting can be completely eliminated by homogenization.
Solidus	582 $^\circ\text{C}$	1080 $^\circ\text{F}$	AA; Typical
Liquidus	651.7 $^\circ\text{C}$	1205 $^\circ\text{F}$	AA; Typical
Processing Properties	Metric	English	Comments
Solution Temperature	529 $^\circ\text{C}$	985 $^\circ\text{F}$	
Aging Temperature	160 $^\circ\text{C}$	320 $^\circ\text{F}$	Rolled or drawn products; hold at temperature for 18 hr
	177 $^\circ\text{C}$	350 $^\circ\text{F}$	Extrusions or forgings; hold at temperature for 8 hr
Component Elements Properties	Metric	English	Comments
Aluminum, Al	95.8 - 98.6 %	95.8 - 98.6 %	As remainder
Chromium, Cr	0.04 - 0.35 %	0.04 - 0.35 %	
Copper, Cu	0.15 - 0.40 %	0.15 - 0.40 %	
Iron, Fe	<= 0.70 %	<= 0.70 %	
Magnesium, Mg	0.80 - 1.2 %	0.80 - 1.2 %	
Manganese, Mn	<= 0.15 %	<= 0.15 %	
Other, each	<= 0.05 %	<= 0.05 %	
Other, total	<= 0.15 %	<= 0.15 %	
Silicon, Si	0.40 - 0.80 %	0.40 - 0.80 %	
Titanium, Ti	<= 0.15 %	<= 0.15 %	
Zinc, Zn	<= 0.25 %	<= 0.25 %	

[References](#) for this datasheet.

Some of the values displayed above may have been converted from their original units and/or rounded in order to display the information in a consistent format. Users requiring more precise data for scientific or engineering calculations can click on the property value to see the original value as well as raw conversions to equivalent units. We advise that you only use the original value or one of its raw conversions in your calculations to minimize rounding error. We also ask that you refer to MatWeb's [terms of use](#) regarding this information. [Click here](#) to view all the property values for this datasheet as they were originally entered into MatWeb.

## **A.2 Aluminum 7075 T6**

Datasheet from MatWeb [22].

## Aluminum 7075-T6; 7075-T651

Categories: [Metal](#); [Nonferrous Metal](#); [Aluminum Alloy](#); [7000 Series Aluminum Alloy](#)

**Material Notes:** General 7075 characteristics and uses (from Alcoa): Very high strength material used for highly stressed structural parts. The T7351 temper offers improved stress-corrosion cracking resistance.

**Applications:** Aircraft fittings, gears and shafts, fuse parts, meter shafts and gears, missile parts, regulating valve parts, worm gears, keys, aircraft, aerospace and defense applications; bike frames, all terrain vehicle (ATV) sprockets.

Data points with the AA note have been provided by the Aluminum Association, Inc. and are NOT FOR DESIGN.

**Composition Notes:**

A Zr + Ti limit of 0.25 percent maximum may be used with this alloy designation for extruded and forged products only, but only when the supplier and the purchaser have mutually agreed. Composition information provided by the Aluminum Association and is not for design.

**Key Words:** Aluminium 7075-T6; Aluminium 7075-T651, UNS A97075; ISO AlZn5.5MgCu; Aluminium 7075-T6; Aluminium 7075-T651; AA7075-T6

**Vendors:** [Click here to view all available suppliers for this material.](#)

Please [click here](#) if you are a supplier and would like information on how to add your listing to this material.

Physical Properties	Metric	English	Comments
Density	2.81 g/cc	0.102 lb/in <sup>3</sup>	AA; Typical
Mechanical Properties	Metric	English	Comments
Hardness, Brinell	150	150	AA; Typical; 500 g load; 10 mm ball
Hardness, Knoop	191	191	Converted from Brinell Hardness Value
Hardness, Rockwell A	53.5	53.5	Converted from Brinell Hardness Value
Hardness, Rockwell B	87	87	Converted from Brinell Hardness Value
Hardness, Vickers	175	175	Converted from Brinell Hardness Value
Tensile Strength, Ultimate	572 MPa	83000 psi	AA; Typical
	41.0 MPa @Temperature 371 °C	5950 psi @Temperature 700 °F	
	55.0 MPa @Temperature 316 °C	7980 psi @Temperature 601 °F	
	76.0 MPa @Temperature 260 °C	11000 psi @Temperature 500 °F	
	110 MPa @Temperature 204 °C	16000 psi @Temperature 399 °F	
	214 MPa @Temperature 149 °C	31000 psi @Temperature 300 °F	
	483 MPa @Temperature 100 °C	70100 psi @Temperature 212 °F	
	572 MPa @Temperature 24.0 °C	83000 psi @Temperature 75.2 °F	
	593 MPa @Temperature -28.0 °C	86000 psi @Temperature -18.4 °F	
	621 MPa	90100 psi	

	@Temperature -80.0 °C 703 MPa @Temperature -196 °C >= 462 MPa @Thickness 88.93 - 102 mm >= 490 MPa @Thickness 76.23 - 88.9 mm >= 496 MPa @Thickness 63.53 - 76.2 mm >= 510 MPa @Thickness 0.203 - 0.279 mm >= 524 MPa @Thickness 0.305 - 0.991 mm >= 524 MPa @Thickness 50.83 - 63.5 mm >= 531 MPa @Thickness 25.43 - 50.8 mm >= 538 MPa @Thickness 1.02 - 3.17 mm >= 538 MPa @Thickness 3.20 - 6.32 mm >= 538 MPa @Thickness 6.35 - 12.7 mm >= 538 MPa @Thickness 12.7 - 25.4 mm	@Temperature -112 °F 102000 psi @Temperature -321 °F >= 67000 psi @Thickness 3.501 - 4.00 in >= 71100 psi @Thickness 3.001 - 3.50 in >= 71900 psi @Thickness 2.501 - 3.00 in >= 74000 psi @Thickness 0.00800 - 0.0110 in >= 76000 psi @Thickness 0.0120 - 0.0390 in >= 76000 psi @Thickness 2.001 - 2.50 in >= 77000 psi @Thickness 1.001 - 2.00 in >= 78000 psi @Thickness 0.0400 - 0.125 in >= 78000 psi @Thickness 0.126 - 0.249 in >= 78000 psi @Thickness 0.250 - 0.499 in >= 78000 psi @Thickness 0.500 - 1.00 in	Plate; T62, T651 Plate; T62, T651 Plate; T62, T651 Sheet Sheet Plate; T62, T651 Plate; T62, T651 Sheet Sheet Plate; T62, T651 Plate; T62, T651 Plate; T62, T651 AA; Typical
Tensile Strength, Yield	503 MPa	73000 psi	
	= 372 MPa @Thickness 88.93 - 102 mm >= 400 MPa @Thickness 76.23 - 88.9 mm >= 421 MPa @Thickness 63.53 - 76.2 mm >= 434 MPa @Thickness 0.203 - 0.279 mm >= 441 MPa @Thickness 50.83 - 63.5 mm >= 462 MPa @Thickness 0.305 - 0.991 mm >= 462 MPa @Thickness 6.35 - 12.7 mm >= 462 MPa @Thickness 25.43 - 50.8 mm >= 469 MPa @Thickness 1.02 - 3.17 mm >= 469 MPa @Thickness 12.7 - 25.4 mm >= 476 MPa @Thickness 3.20 - 6.32 mm	= 54000 psi @Thickness 3.501 - 4.00 in >= 58000 psi @Thickness 3.001 - 3.50 in >= 61100 psi @Thickness 2.501 - 3.00 in >= 62900 psi @Thickness 0.00800 - 0.0110 in >= 64000 psi @Thickness 2.001 - 2.50 in >= 67000 psi @Thickness 0.0120 - 0.0390 in >= 67000 psi @Thickness 0.250 - 0.499 in >= 67000 psi @Thickness 1.001 - 2.00 in >= 68000 psi @Thickness 0.0400 - 0.125 in >= 68000 psi @Thickness 0.500 - 1.00 in >= 69000 psi @Thickness 0.126 - 0.249 in	Plate; T62, T651 Plate; T62, T651 Plate; T62, T651 Sheet Plate; T62, T651 Sheet Plate; T62, T651 Plate; T62, T651 Plate; T62, T651 Sheet Plate; T62, T651 Plate; T62, T651 Plate; T62, T651 Sheet Plate; T62, T651 Sheet
	32.0 MPa @Strain 0.200 %, Temperature 271 °C 45.0 MPa @Strain 0.200 %, Temperature 316 °C 62.0 MPa @Strain 0.200 %, Temperature 260 °C 87.0 MPa @Strain 0.200 %, Temperature 204 °C 186 MPa @Strain 0.200 %, Temperature 149 °C 448 MPa @Strain 0.200 %, Temperature 100 °C	4640 psi @Strain 0.200 %, Temperature 520 °F 6530 psi @Strain 0.200 %, Temperature 601 °F 8990 psi @Strain 0.200 %, Temperature 500 °F 12600 psi @Strain 0.200 %, Temperature 399 °F 27000 psi @Strain 0.200 %, Temperature 300 °F 65000 psi @Strain 0.200 %, Temperature 212 °F	

	503 MPa @Strain 0.200 %, Temperature 24.0 °C	73000 psi @Strain 0.200 %, Temperature 75.2 °F	
	517 MPa @Strain 0.200 %, Temperature -28.0 °C	75000 psi @Strain 0.200 %, Temperature -18.4 °F	
	545 MPa @Strain 0.200 %, Temperature -80.0 °C	79000 psi @Strain 0.200 %, Temperature -112 °F	
	634 MPa @Strain 0.200 %, Temperature -196 °C	92000 psi @Strain 0.200 %, Temperature -321 °F	
Elongation at Break 	9.0 % @Temperature -196 °C	9.0 % @Temperature -321 °F	
	11 % @Temperature -80.0 °C	11 % @Temperature -112 °F	
	11 % @Temperature -28.0 °C	11 % @Temperature -18.4 °F	
	11 % @Temperature 24.0 °C	11 % @Temperature 75.2 °F	
	14 % @Temperature 100 °C	14 % @Temperature 212 °F	
	30 % @Temperature 149 °C	30 % @Temperature 300 °F	
	55 % @Temperature 204 °C	55 % @Temperature 399 °F	
	65 % @Temperature 260 °C	65 % @Temperature 500 °F	
	70 % @Temperature 316 °C	70 % @Temperature 601 °F	
	70 % @Temperature 371 °C	70 % @Temperature 700 °F	
	>= 3.0 % @Thickness 88.93 - 102 mm	>= 3.0 % @Thickness 3.501 - 4.00 in	Plate; T62, T651
	>= 5.0 % @Thickness 0.203 - 0.279 mm	>= 5.0 % @Thickness 0.00800 - 0.0110 in	Sheet
	>= 5.0 % @Thickness 50.83 - 63.5 mm	>= 5.0 % @Thickness 2.001 - 2.50 in	Plate; T62, T651
	>= 5.0 % @Thickness 63.53 - 76.2 mm	>= 5.0 % @Thickness 2.501 - 3.00 in	Plate; T62, T651
	>= 5.0 % @Thickness 76.23 - 88.9 mm	>= 5.0 % @Thickness 3.001 - 3.50 in	Plate; T62, T651
	>= 6.0 % @Thickness 25.43 - 50.8 mm	>= 6.0 % @Thickness 1.001 - 2.00 in	Plate; T62, T651
	>= 7.0 % @Thickness 0.305 - 0.991 mm	>= 7.0 % @Thickness 0.0120 - 0.0390 in	Sheet
	>= 7.0 % @Thickness 12.7 - 25.4 mm	>= 7.0 % @Thickness 0.500 - 1.00 in	Plate; T62, T651
	>= 8.0 % @Thickness 1.02 - 3.17 mm	>= 8.0 % @Thickness 0.0400 - 0.125 in	Sheet
	>= 8.0 % @Thickness 3.20 - 6.32 mm	>= 8.0 % @Thickness 0.126 - 0.249 in	Sheet
	>= 9.0 % @Thickness 6.35 - 12.7 mm	>= 9.0 % @Thickness 0.250 - 0.499 in	Plate; T62, T651
	11 % @Thickness 1.59 mm	11 % @Thickness 0.0625 in	AA; Typical
	11 % @Diameter 12.7 mm	11 % @Diameter 0.500 in	AA; Typical
Modulus of Elasticity	71.7 GPa	10400 ksi	AA; Typical; Average of tension and compression. Compression modulus is about 2% greater than tensile modulus.
Poissons Ratio	0.33	0.33	
Fatigue Strength	159 MPa @# of Cycles 5.00e+8	23000 psi @# of Cycles 5.00e+8	completely reversed stress; RR Moore machine/specimen
Fracture Toughness	17.6 MPa-m <sup>1/2</sup>	16.0 ksi-in <sup>1/2</sup>	T651; Plate; S-L; average

16.5 - 19.8 MPa-m <sup>1/2</sup>	15.0 - 18.0 ksi-in <sup>1/2</sup>	T651; Plate; S-L
18.7 MPa-m <sup>1/2</sup>	17.0 ksi-in <sup>1/2</sup>	T651; forgings; S-L
20.0 MPa-m <sup>1/2</sup>	18.2 ksi-in <sup>1/2</sup>	K(IC) in S-L Direction
22.0 - 25.3 MPa-m <sup>1/2</sup>	20.0 - 23.0 ksi-in <sup>1/2</sup>	T651; Plate; T-L
24.2 MPa-m <sup>1/2</sup>	22.0 ksi-in <sup>1/2</sup>	T651; Plate; T-L; average
25.0 MPa-m <sup>1/2</sup>	22.8 ksi-in <sup>1/2</sup>	K(IC) in T-L Direction
28.6 MPa-m <sup>1/2</sup>	26.0 ksi-in <sup>1/2</sup>	T651; Plate; L-T; average
27.5 - 29.7 MPa-m <sup>1/2</sup>	25.0 - 27.0 ksi-in <sup>1/2</sup>	T651; Plate; L-T
29.0 MPa-m <sup>1/2</sup>	26.4 ksi-in <sup>1/2</sup>	K(IC) in L-T Direction
Machinability	70 %	0-100 Scale of Aluminum Alloys
Shear Modulus	26.9 GPa	3900 ksi
Shear Strength	331 MPa	48000 psi
		AA; Typical

Electrical Properties	Metric	English	Comments
Electrical Resistivity	0.00000515 ohm-cm @Temperature 20.0 °C	0.00000515 ohm-cm @Temperature 68.0 °F	AA; Typical

Thermal Properties	Metric	English	Comments
CTE, linear 	21.6 µm/m-°C @Temperature -50.0 - 20.0 °C	12.0 µin/in-°F @Temperature -58.0 - 68.0 °F	
	23.4 µm/m-°C @Temperature 20.0 - 100 °C	13.0 µin/in-°F @Temperature 68.0 - 212 °F	
	23.6 µm/m-°C @Temperature 20.0 - 100 °C	13.1 µin/in-°F @Temperature 68.0 - 212 °F	AA; Typical; average over range
	24.3 µm/m-°C @Temperature 20.0 - 200 °C	13.5 µin/in-°F @Temperature 68.0 - 392 °F	
	25.2 µm/m-°C @Temperature 20.0 - 300 °C	14.0 µin/in-°F @Temperature 68.0 - 572 °F	

Specific Heat Capacity	0.960 J/g-°C	0.229 BTU/lb-°F	
Thermal Conductivity	130 W/m-K	900 BTU-in/hr-ft <sup>2</sup> -°F	AA; Typical at 77°F
Melting Point	477 - 635.0 °C	890 - 1175 °F	AA; Typical range based on typical composition for wrought products 1/4 inch thickness or greater. Homogenization may raise eutectic melting temperature 20-40°F but usually does not eliminate eutectic melting.
Solidus	477 °C	890 °F	AA; Typical
Liquidus	635.0 °C	1175 °F	AA; Typical

Processing Properties	Metric	English	Comments
Annealing Temperature	413 °C	775 °F	
Solution Temperature	466 - 482 °C	870 - 900 °F	
Aging Temperature	121 °C	250 °F	

Component Elements Properties	Metric	English	Comments
Aluminum, Al	87.1 - 91.4 %	87.1 - 91.4 %	As remainder
Chromium, Cr	0.18 - 0.28 %	0.18 - 0.28 %	
Copper, Cu	1.2 - 2.0 %	1.2 - 2.0 %	
Iron, Fe	<= 0.50 %	<= 0.50 %	
Magnesium, Mg	2.1 - 2.9 %	2.1 - 2.9 %	

Manganese, Mn	<= 0.30 %	<= 0.30 %
Other, each	<= 0.05 %	<= 0.05 %
Other, total	<= 0.15 %	<= 0.15 %
Silicon, Si	<= 0.40 %	<= 0.40 %
Titanium, Ti	<= 0.20 %	<= 0.20 %
Zinc, Zn	5.1 - 6.1 %	5.1 - 6.1 %

[References](#) for this datasheet.

Some of the values displayed above may have been converted from their original units and/or rounded in order to display the information in a consistent format. Users requiring more precise data for scientific or engineering calculations can click on the property value to see the original value as well as raw conversions to equivalent units. We advise that you only use the original value or one of its raw conversions in your calculations to minimize rounding error. We also ask that you refer to MatWeb's [terms of use](#) regarding this information. [Click here](#) to view all the property values for this datasheet as they were originally entered into MatWeb.

## **A.3 303 Stainless Steel**

Datasheet from MatWeb [24].

**303 Stainless Steel, annealed bar****Categories:** [Metal](#); [Ferrous Metal](#); [Heat Resisting](#); [Stainless Steel](#); [T 300 Series Stainless Steel](#)

**Key Words:** T303, T 303, 303SS, 303 SS, AFNOR Z 10 CNF 18.09 (Fr), UNI X 10 CrNiS 18 09, SUS 303, SS14 2346 (Sweden), B.S. 303 S 21, UNS S30300, AMS 5640 (1), ASME SA194, ASME SA320, ASTM A194, ASTM A314, ASTM A320, ASTM A320, ASTM A473, ASTM A581, ASTM A582, MIL SPEC MIL-S-862, SAE J405 (30303), DIN 1.4305, X12CrNiS188, EN 58M, austenitic, ISO 683/13 17, 18-8

**Vendors:** [Click here to view all available suppliers for this material.](#)

Please [click here](#) if you are a supplier and would like information on how to add your listing to this material.

Physical Properties	Metric	English	Comments
Density	8.00 g/cc	0.289 lb/in <sup>3</sup>	
Mechanical Properties	Metric	English	Comments
Hardness, Brinell	160	160	
Hardness, Knoop	180	180	Converted from Brinell hardness.
Hardness, Rockwell B	83	83	Converted from Brinell hardness.
Hardness, Vickers	167	167	Converted from Brinell hardness.
Tensile Strength, Ultimate	620 MPa	89900 psi	
Tensile Strength, Yield	240 MPa @Strain 0.200 %	34800 psi @Strain 0.200 %	
Elongation at Break	50 %	50 %	in 50 mm
Tensile Modulus	193 GPa	28000 ksi	
Poissons Ratio	0.25	0.25	Calculated
Fatigue Strength	240 MPa	34800 psi	annealed
	330 MPa	47900 psi	25% hardened
Shear Modulus	77.2 GPa	11200 ksi	
Electrical Properties	Metric	English	Comments
Electrical Resistivity	0.0000720 ohm-cm	0.0000720 ohm-cm	
Magnetic Permeability	1.008	1.008	at RT
Thermal Properties	Metric	English	Comments
CTE, linear 	17.2 µm/m-°C @Temperature 0.000 - 100 °C	9.56 µin/in-°F @Temperature 32.0 - 212 °F	
	17.8 µm/m-°C @Temperature 0.000 - 315 °C	9.89 µin/in-°F @Temperature 32.0 - 599 °F	
	18.4 µm/m-°C @Temperature 0.000 - 540 °C	10.2 µin/in-°F @Temperature 32.0 - 1000 °F	
	18.7 µm/m-°C @Temperature 0.000 - 650 °C	10.4 µin/in-°F @Temperature 32.0 - 1200 °F	
Specific Heat Capacity	0.500 J/g-°C @Temperature 0.000 - 100 °C	0.120 BTU/lb-°F @Temperature 32.0 - 212 °F	
Thermal Conductivity 	16.2 W/m-K @Temperature 100 °C	112 BTU-in/hr-ft <sup>2</sup> -°F @Temperature 212 °F	
	21.5 W/m-K @Temperature 500 °C	149 BTU-in/hr-ft <sup>2</sup> -°F @Temperature 932 °F	
Melting Point	1400 - 1420 °C	2550 - 2590 °F	
Solidus	1400 °C	2550 °F	
Liquidus	1420 °C	2590 °F	

Component Elements Properties	Metric	English	Comments
Carbon, C	<= 0.15 %	<= 0.15 %	
Chromium, Cr	18 %	18 %	
Iron, Fe	69 %	69 %	
Manganese, Mn	<= 2.0 %	<= 2.0 %	
Molybdenum, Mo	<= 0.60 %	<= 0.60 %	
Nickel, Ni	9.0 %	9.0 %	
Phosphorous, P	<= 0.20 %	<= 0.20 %	
Silicon, Si	<= 1.0 %	<= 1.0 %	
Sulfur, S	>= 0.15 %	>= 0.15 %	

[References](#) for this datasheet.

Some of the values displayed above may have been converted from their original units and/or rounded in order to display the information in a consistent format. Users requiring more precise data for scientific or engineering calculations can click on the property value to see the original value as well as raw conversions to equivalent units. We advise that you only use the original value or one of its raw conversions in your calculations to minimize rounding error. We also ask that you refer to MatWeb's [terms of use](#) regarding this information. [Click here](#) to view all the property values for this datasheet as they were originally entered into MatWeb.

## A.4 Structural steel S235

Datasheet from Ovako AB [25].

Material data sheet  
**Steel grade**

**SB1312  
IM2191**

Last revised: Tue, 31 Jan 2017 13:56:17 GMT



## S235JR All

### General Information

Soft structural steel easy to weld and bend.

Variants suitability for hot dip zinc coating according the classification in Table 1 EN 10025-2:2004: Class 1: Si max 0,030% and Si + 2,5 P max 0,090%. Class 2: Si max 0,035%. Class 3 Si 0,14...0,25% and P max 0,035%.

### Similar designations

SS 1312, S235JR, 1.0038, Fe 360 BFN, RSt37-2, 40 B

### Chemical composition

Variant	Cast	Weldability		C %	Mn %	P %	S %	Cu %	N %
S235JR EN10025-2 (ref)	Std	CEV 0.35 <sub>max</sub>	Mn	-	-	-	-	-	-
		Pcm 0.25 <sub>max</sub>	Max	0.17	1.40	0.035	0.035	0.55	0.0120

S235JR: C max 0,20 % for sizes over 40 mm. Only CEV required in standard

SS 1312: Not binding recommendation for Mn (0,4 - 0,7) % in standard

### Mechanical Properties

Variant	Condition	Format	Dimension [mm]	Yield strength min [MPa]	Tensile strength [MPa]	Elongation A <sub>5</sub> [%]	Impact (ISO-V) strength <sub>min</sub>
S235JR EN10025-2 (ref)	+AR	All formats	< 16	235*	360-510	26	20 °C 27 J (long)
		All formats	16.1 < 40	225*	360-510	26	20 °C 27 J (long)
		All formats	40.1 < 63	215*	360-510	25	20 °C 27 J (long)
		All formats	63.1 < 100	215*	360-510	24	20 °C 27 J (long)
		All formats	100.1 < 150	195*	350-500	22	20 °C 27 J (long)
		All formats	150.1 < 200	185*	340-490	21	20 °C 27 J (long)

Rp0.2 \* Reh, \*\* Rel

### Transformation temperatures

	Temperature °C
MS	485
AC1	725
AC3	863

### Other properties (typical values)

Youngs module (GPa)	Poisson's ratio (-)	Shear module (GPa)	Density (kg/m <sup>3</sup> )
210	0.3	80	7800
Average CTE 20-300°C (μm/m°K)	Specific heat capacity 50/100°C (J/kg°K)	Thermal conductivity Ambient temperature (W/m°K)	Electrical resistivityAmbient temperature (μΩm)
12	460 - 480	40 - 45	0.20 - 0.25

### Contact us

Would you like to know more about our offers? Don't hesitate to contact us:

Via e-mail: [info@ovako.com](mailto:info@ovako.com)

Via telephone: +46 8 622 1300

For more detailed information please visit <http://www.ovako.com/en/Contact-Ovako/>

**Disclaimer**

*The information in this document is for illustrative purposes only. The data and examples are only general recommendations and not a warranty or a guarantee. The suitability of a product for a specific application can be confirmed only by Ovako once given the actual conditions. The purchaser of an Ovako product has the responsibility to ascertain and control the applicability of the products before using them. Continuous development may necessitate changes in technical data without notice. This document is only valid for Ovako material. Other material, covering the same international specifications, does not necessarily comply with the properties presented in this document.*

## **A.5 Structural steel S355**

Datasheet from Ovako AB [26].

## S355JR All

### General Information

S355 is a structural micro-alloyed grade used for a great variety of applications. It is standardized with a specified impact strength of 27 J at a few different temperatures, but EN10027 gives guidelines how to extend the designation.

### Similar designations

S355K2 - 15Mn4, S355JR - C16, S355J2 - C16

### Chemical composition

Variant	Cast	Weldability	C %	Si %	Mn %	P %	S %	Cu %	N %
S355JR	CC	CEV0.52 <sub>max</sub>	Mn	-	-	-	-	-	-
		Pcm 0.35 <sub>max</sub>	Max	0.24	0.55	1.60	0.040	0.040	0.40
S355JR EN10025-2:2004	CC	CEV0.52 <sub>max</sub>	Mn	-	-	-	-	-	-
		Pcm 0.35 <sub>max</sub>	Max	0.24	0.55	1.60	0.035	0.035	0.55

### Mechanical Properties

Variant	Condition	Format	Dimension [mm]	Yield strength min [MPa]	Tensile strength [MPa]	Elongation A <sub>5</sub> [%]	Hardness	Impact (ISO-V) strength <sub>min</sub>
S355JR +AR		Flat bar	< 16	355**	470-630	22	140-190 HB	20 °C 27 J (long)
		Flat bar	16 < 40	345**	470-630	22	140-190 HB	20 °C 27 J (long)
		Flat bar	40 < 63	335**	470-630	21	140-190 HB	20 °C 27 J (long)
		Flat bar	63 < 80	325**	470-630	20	140-190 HB	20 °C 27 J (long)
		Flat bar	80 < 100	315**	470-630	20	140-190 HB	20 °C 27 J (long)

Rp<sub>0.2</sub>\* Rel, \*\* Rel

### Transformation temperatures

	Temperature °C
MS	540
AC1	720
AC3	790

### Other properties (typical values)

Youngs module (GPa)	Poisson's ratio (-)	Shear module (GPa)	Density (kg/m <sup>3</sup> )
210	0.3	80	7800
Average CTE 20-300°C (μm/m°K)	Specific heat capacity 50/100°C (J/kg°K)	Thermal conductivity Ambient temperature (W/m°K)	Electrical resistivityAmbient temperature (μΩm)
12	460 - 480	40 - 45	0.20 - 0.25

### Contact us

Would you like to know more about our offers? Don't hesitate to contact us:

Via e-mail: [info@ovako.com](mailto:info@ovako.com)

Via telephone: +46 8 622 1300

For more detailed information please visit <http://www.ovako.com/en/Contact-Ovako/>

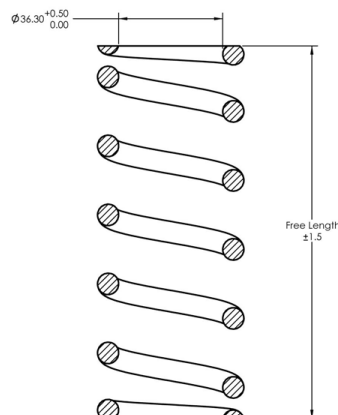
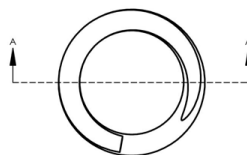
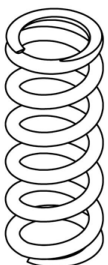
**Disclaimer**

*The information in this document is for illustrative purposes only. The data and examples are only general recommendations and not a warranty or a guarantee. The suitability of a product for a specific application can be confirmed only by Ovako once given the actual conditions. The purchaser of an Ovako product has the responsibility to ascertain and control the applicability of the products before using them. Continuous development may necessitate changes in technical data without notice. This document is only valid for Ovako material. Other material, covering the same international specifications, does not necessarily comply with the properties presented in this document.*

## A.6 Öhlins TTX25 Mk II spring dimensions

Datasheet from Öhlins USA [27].

REV.	DESCRIPTION	ENGR	DATE
A	Production release	TR	10/11/2005



Part No.	Spring Rate lb/in	Spring Rate kg/mm	Free Length mm	Material	Finish
DBB2.25/250	250	4.46	122	SRS60 Steel	Black Enamel
DBB2.25/300	300	5.36	122	SRS60 Steel	Black Enamel
DBB2.25/350	350	6.25	123	SRS60 Steel	Black Enamel
DBB2.25/400	400	7.14	124	SRS60 Steel	Black Enamel
DBB2.25/450	450	8.04	125	SRS60 Steel	Black Enamel
DBB2.25/500	500	8.93	125	SRS60 Steel	Black Enamel
DBB2.25/550	550	9.82	126	SRS60 Steel	Black Enamel
DBB2.25/600	600	10.71	130	SRS60 Steel	Black Enamel
DBB2.25/650	650	11.61	134	SRS60 Steel	Black Enamel
DBB2.25/700	700	12.50	136	SRS60 Steel	Black Enamel
DBB2.25/750	750	13.39	140	SRS60 Steel	Black Enamel

**Notes:**  
 1. Material: Per part number table  
 2. Finish: Per part number table  
 3. Treatment: Heat treated, shot peened, and pressurized.  
 4. End turns closed and ground (min. 75% of end plane must be flat).  
 5. Spring rate tolerance ±5%  
 6. Stroke tolerance ±0.05".  
 7. Right hand winding.  
 8. Marking: "Spring rate X Stroke" in 4mm text height placed on third coil. Text is white.  
 Example: **300 x 2.25**

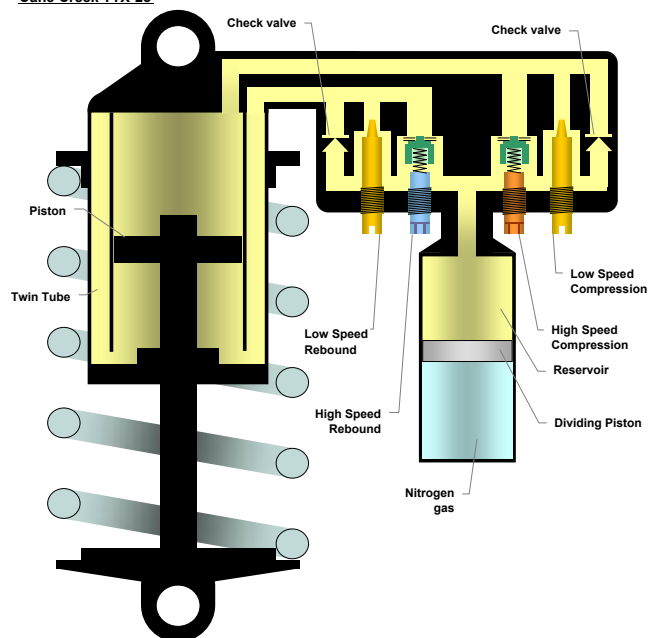
SECTION A-A

mm Dimensions: A = 3.630 A ± 0.2 A = 90.000 A ± 0.050	This drawing and all information contained herein are the property of Cane Creek Cycling Components and its Subsidiaries. They may not be made public or copied without the expressed written consent of Cane Creek. This drawing is not to be used for any other purpose than that for which it is submitted to Cane Creek and its Subsidiaries.
Printed Angle Property Line	Material See Table
Material See Table	Print No. <b>B</b>
Printed Materials by part number	See Table
Finish: See Table	Color See Table
	SCALE: 1:1   SHEET 1 OF 1

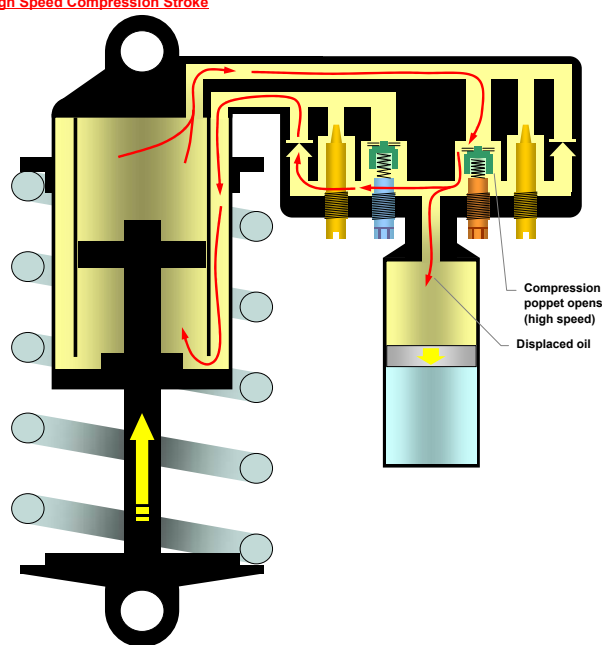
## A.7 Öhlins TTX25 Mk II internal schematic

Datasheet from Öhlins USA [28].

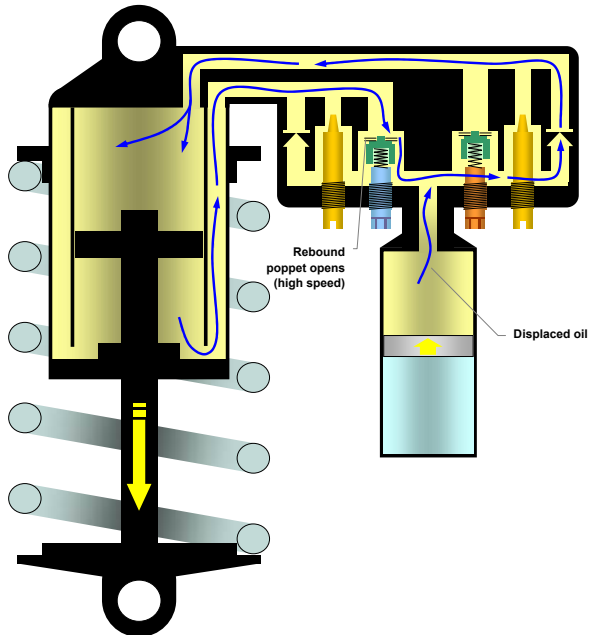
Cane Creek TTX-25



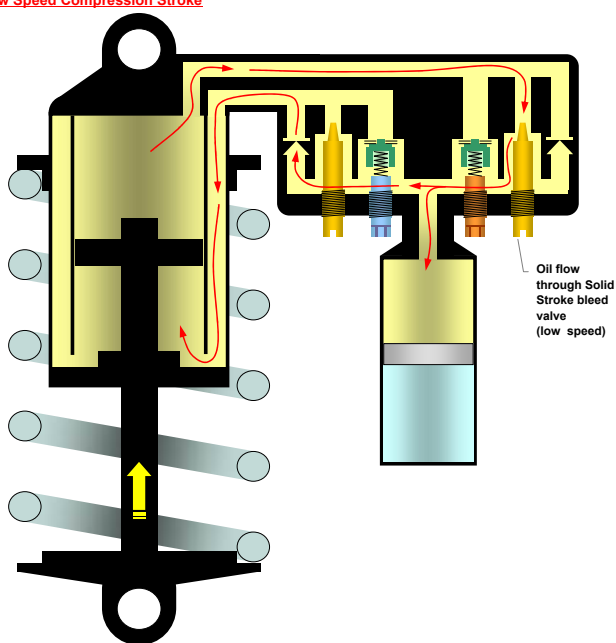
High Speed Compression Stroke



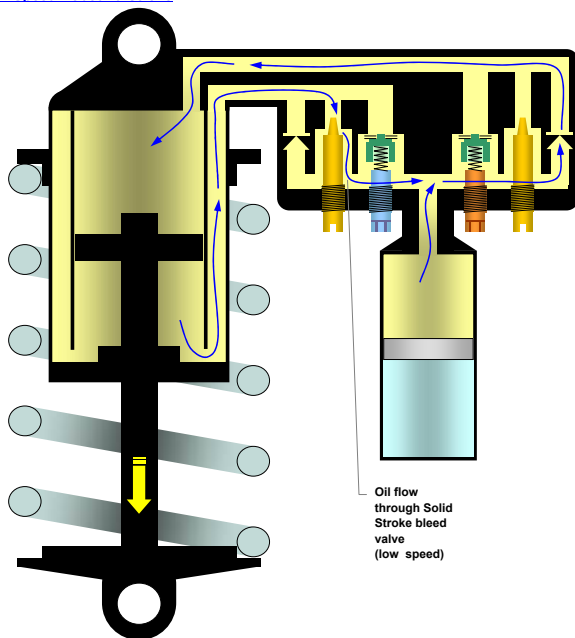
High Speed Rebound Stroke



Low Speed Compression Stroke

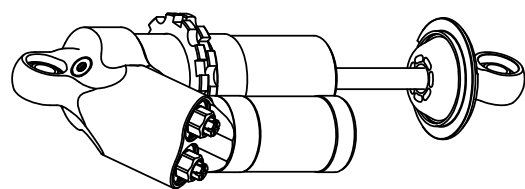
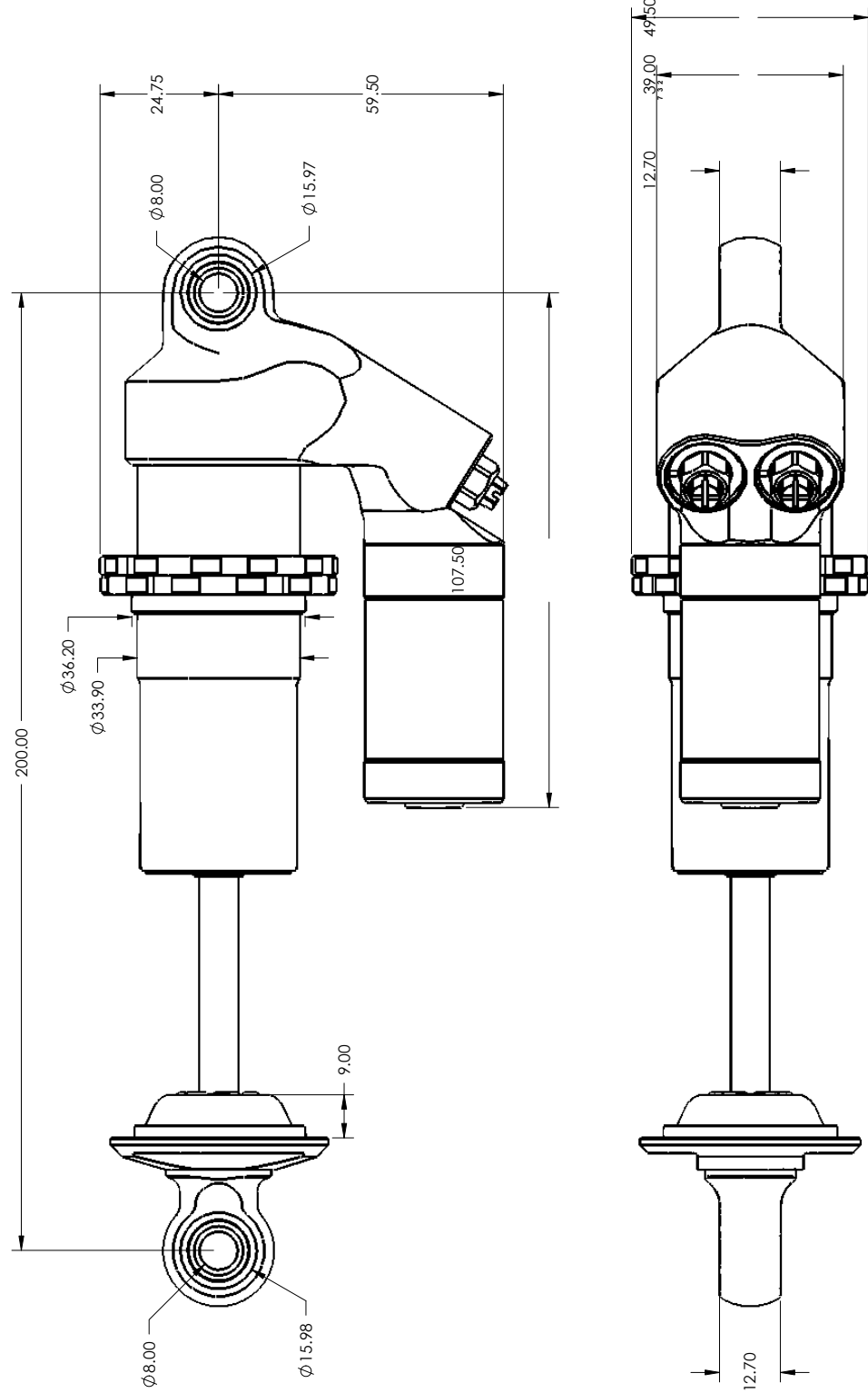


Low Speed Rebound Stroke



## A.8 Öhlins TTX25 Mk II external dimensions

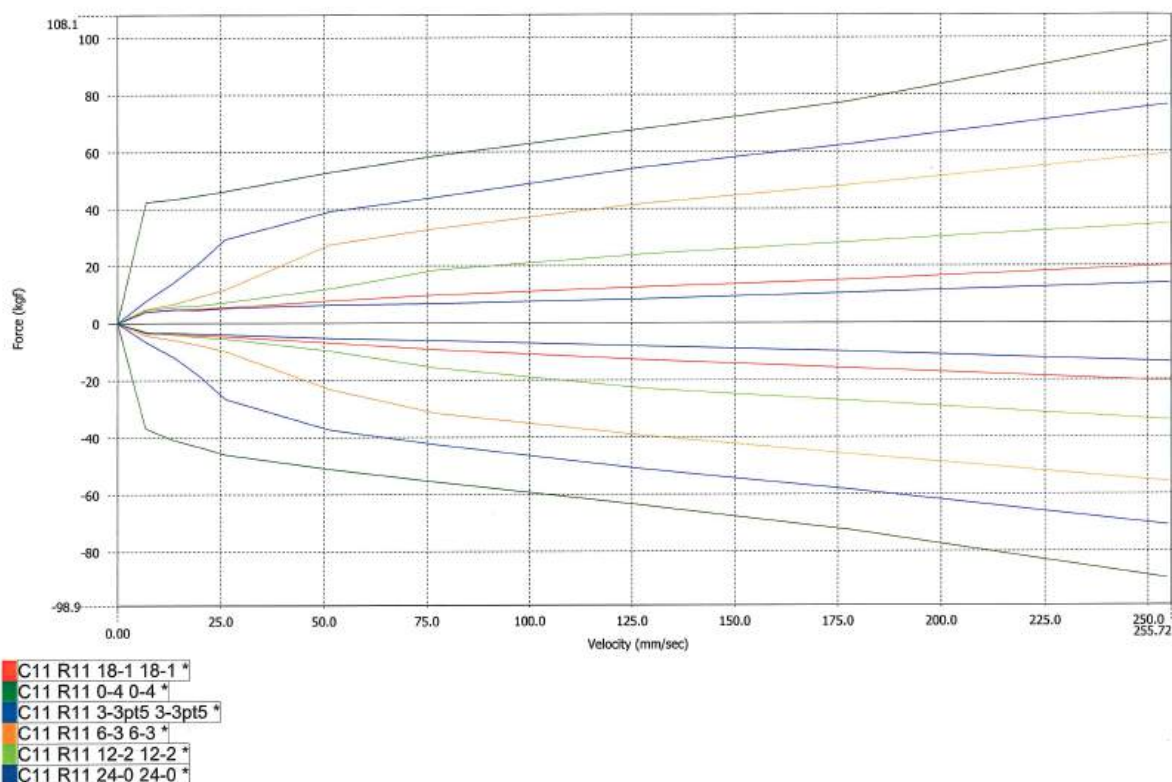
Datasheet from Öhlins USA [29].



## A.9 Öhlins TTX25 Mk II dyno plot

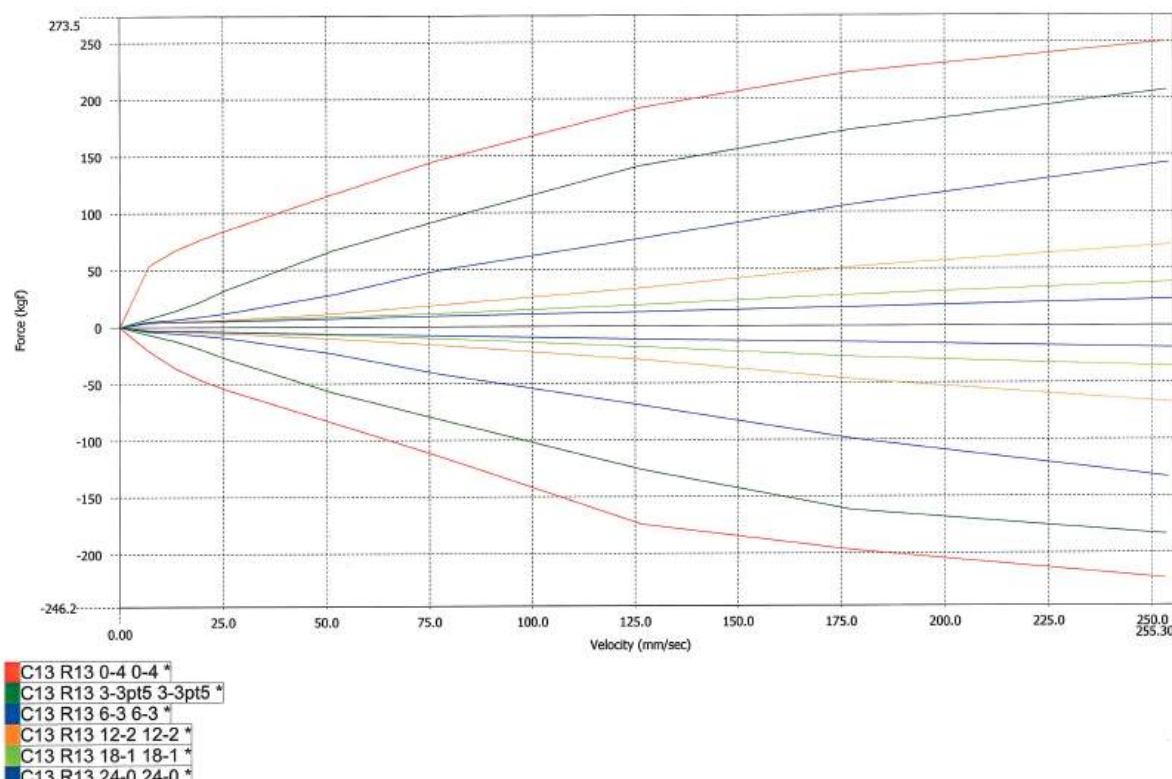
Datasheet from Öhlins USA [30].

Force Vs. Absolute Velocity



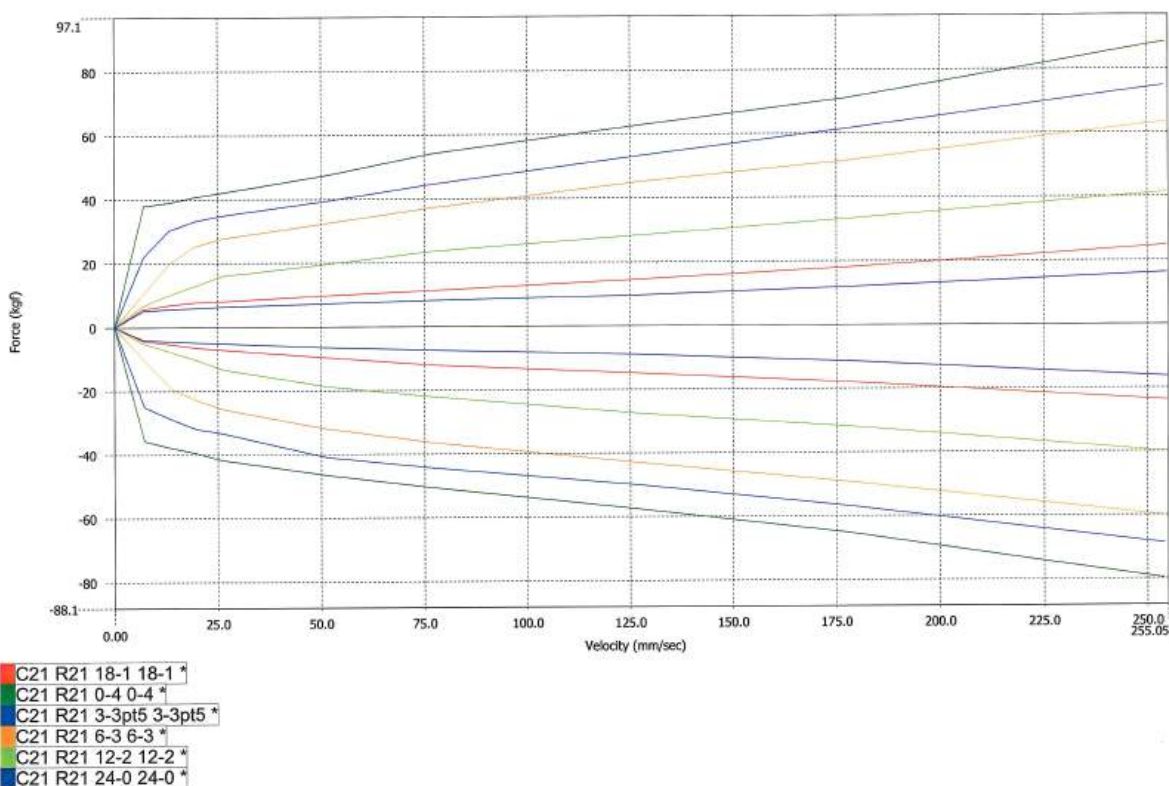
TTX 25 FSAE - (LSC-HSC LSR-HSR) Low speed clicks counted from fully closed (clockwise), High speed turns counted from fully open (counter clockwise)

Force Vs. Absolute Velocity

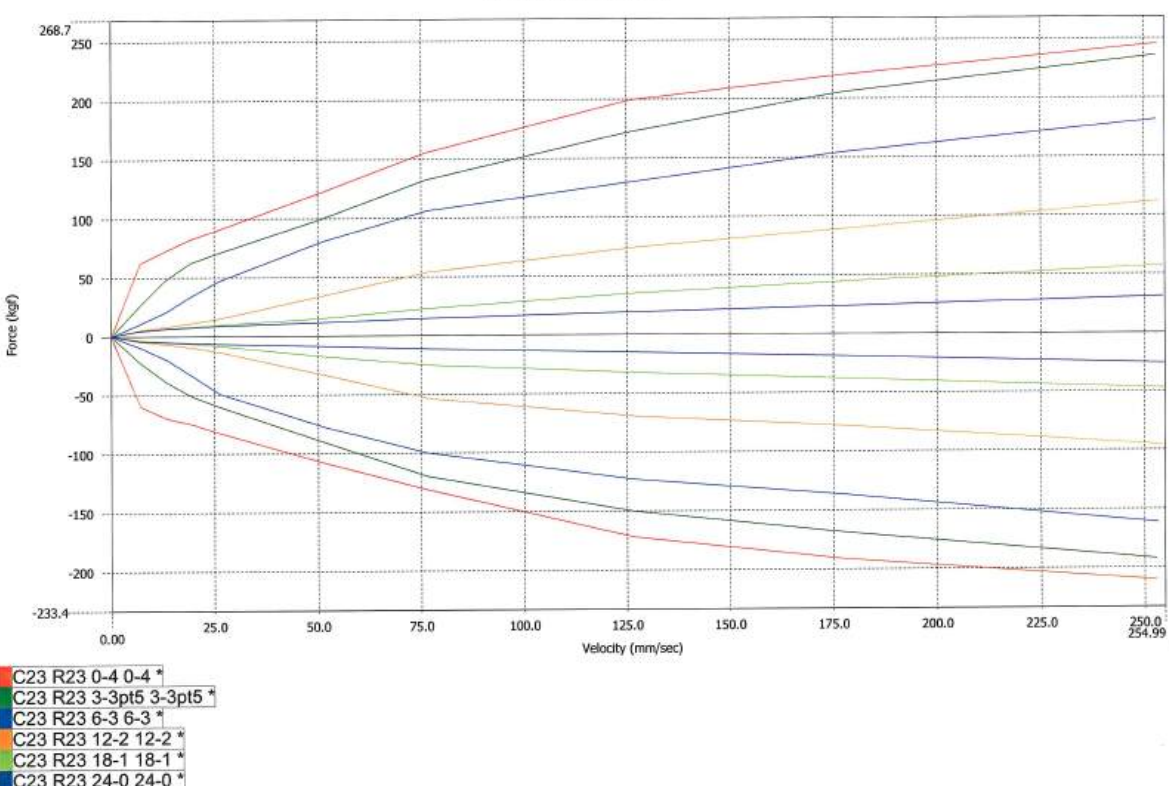


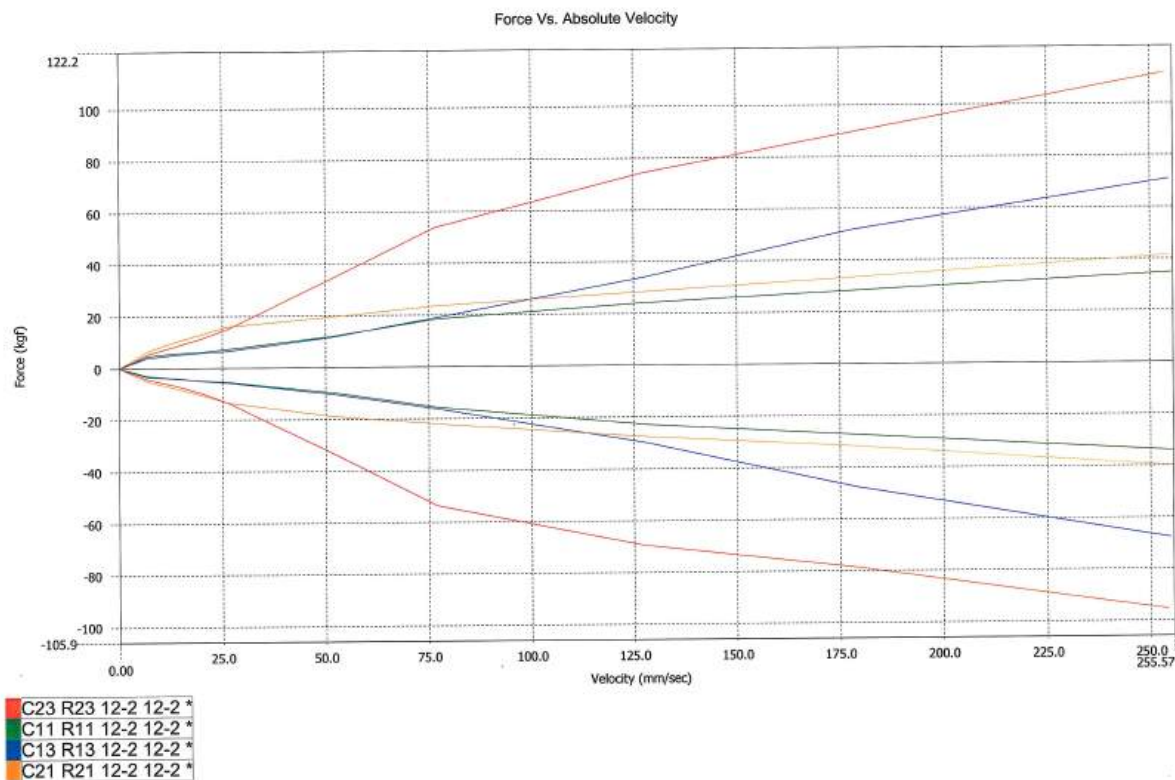
TTX 25 FSAE - (LSC-HSC LSR-HSR) Low speed clicks counted from fully closed (clockwise), High speed turns counted from fully open (counter clockwise)

Force Vs. Absolute Velocity



Force Vs. Absolute Velocity

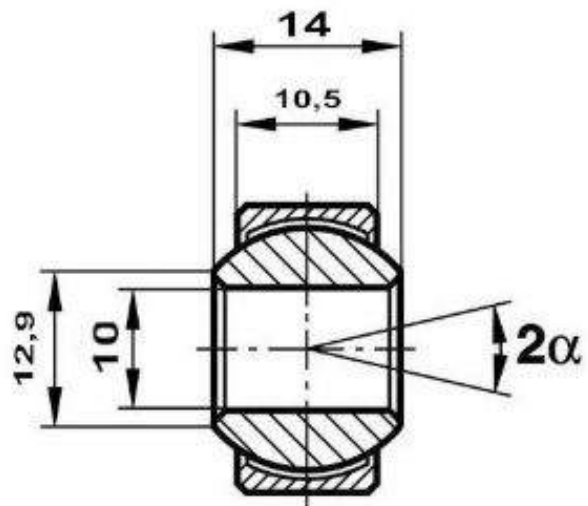
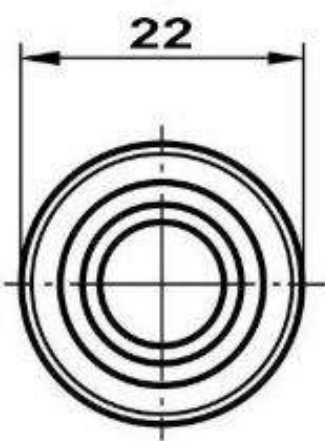




TTX 25 FSAE - Valving options (stock valving = C11 R11)  
 (LSC-HSC LSR-HSR) Low speed clicks counted from fully closed (clockwise), High speed turns counted from fully open (counter clockwise)

## A.10 Fluro spherical bearing

Datasheet from FLURO-Gelenklager GmbH [16].

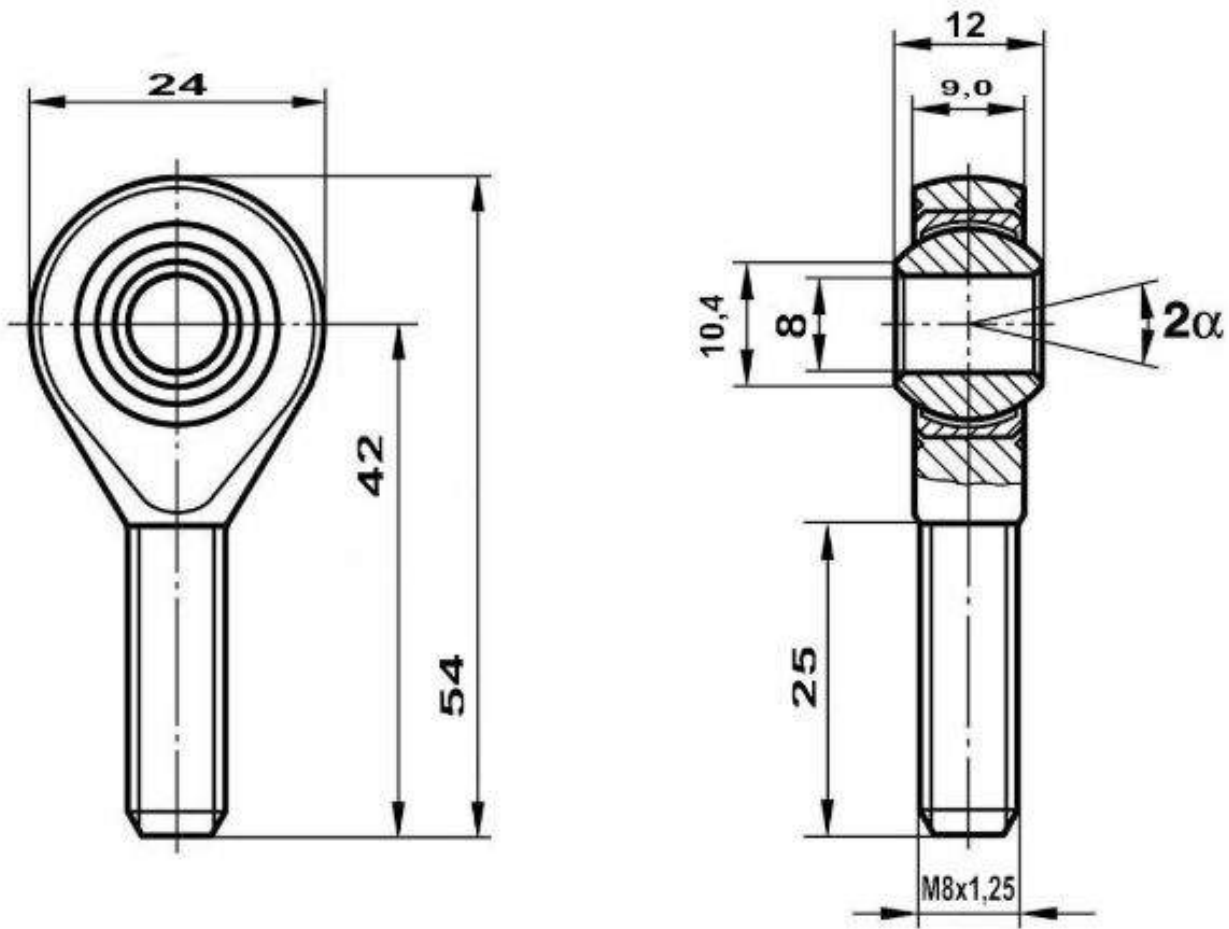


FLURO-No. GXSW 10.22 MS

statische radiale Tragzahl C <sub>0</sub> kN static radial load C <sub>0</sub> kN	dynamische radiale Tragzahl C kN dynamic radial load Torque Nm	Drehmoment N/dm Torque Nm	$\alpha$	Stückgewicht gr. / lb. part weight gr. / lb.
39,0	28,1	2-14	13°	26 / 0,057

## A.11 Fluro spherical bearing rod end

Datasheet from FLURO-Gelenklager GmbH [16].



FLURO-No. GAXSW 08 MS

statische radiale Tragzahl $C_0$ kN static radial load $C_0$ kN	dynamische radiale Tragzahl C kN dynamic radial load C kN	Drehmoment N/dm Torque Nm	Kippwinkel $\alpha$ pivoting angle	Stückgewicht gr. / lb. Part weight gr. / lb.
19,5	19,5	4-12	14°	33 / 0,073

## A.12 SKF 608-2RSH

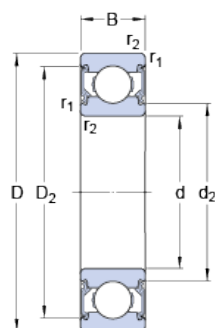
Datasheet from SKF [31].



## 608-2RSH

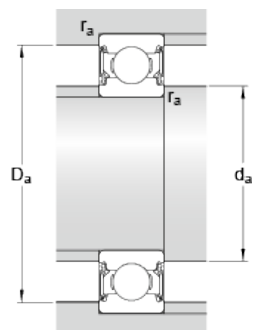
Popular item  
SKF Explorer

### Dimensions



d	8	mm
D	22	mm
B	7	mm
$d_2$	$\approx$ 10.55	mm
$D_2$	$\approx$ 19.2	mm

### Abutment dimensions



$d_a$	min.	10	mm
$d_a$	max.	10.5	mm
$D_a$	max.	20	mm
$r_a$	max.	0.3	mm

### Calculation data

Basic dynamic load rating	C	3.45	kN
Basic static load rating	$C_0$	1.37	kN
Fatigue load limit	$P_u$	0.057	kN
Limiting speed		22000	r/min
Calculation factor	$k_r$	0.025	
Calculation factor	$f_0$	12	

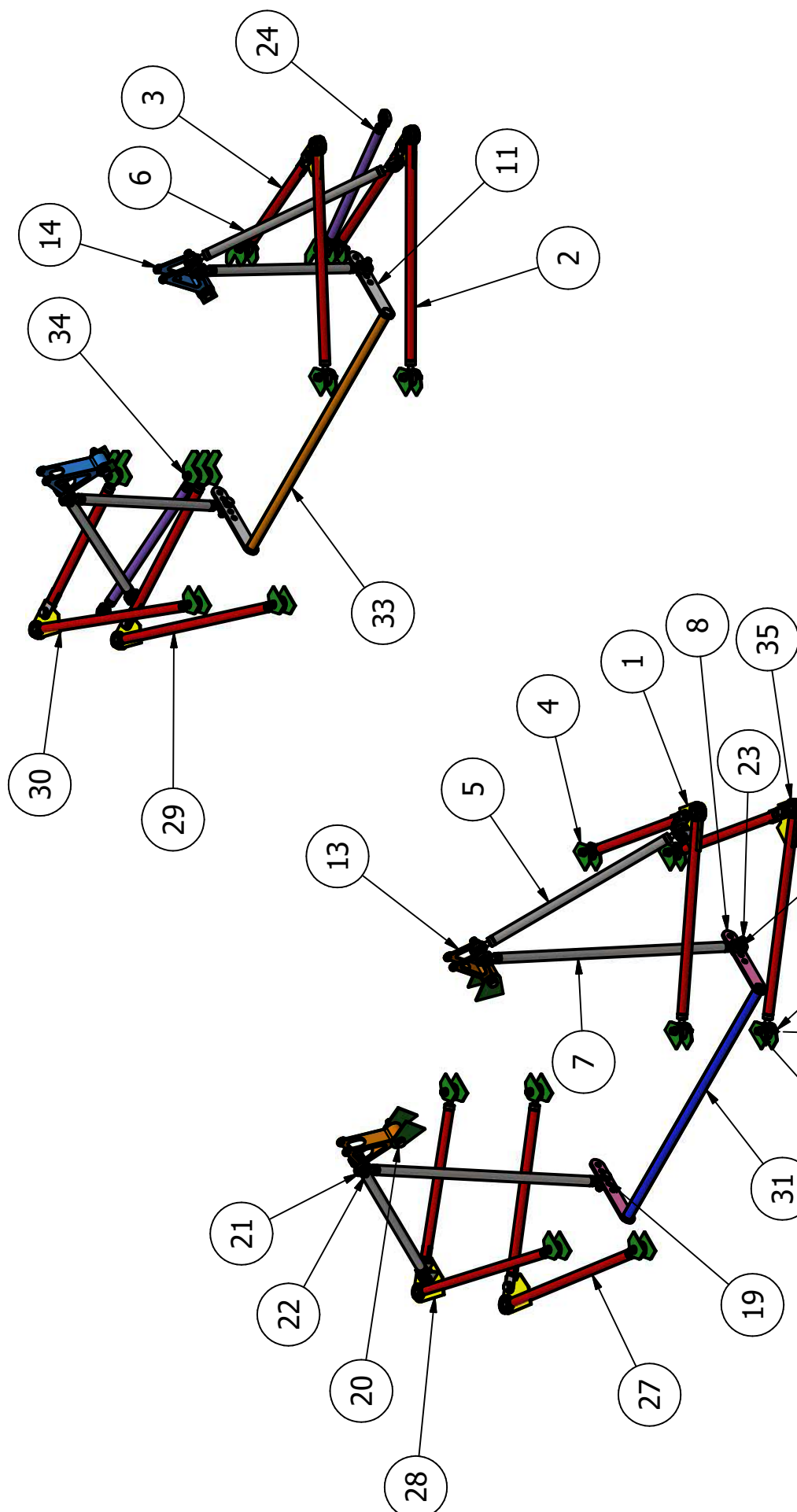
### Mass

Mass bearing	0.012	kg
--------------	-------	----



## **Appendix B**

### **Drawings**



Suspension assembly		
Designed by Ingi Þórhallur Karlsson	Checked by None	Material None
Date 25.4.2018		Scale 1:10
Suspension.iam	Suspension.ipt	Sheet 1 / 42

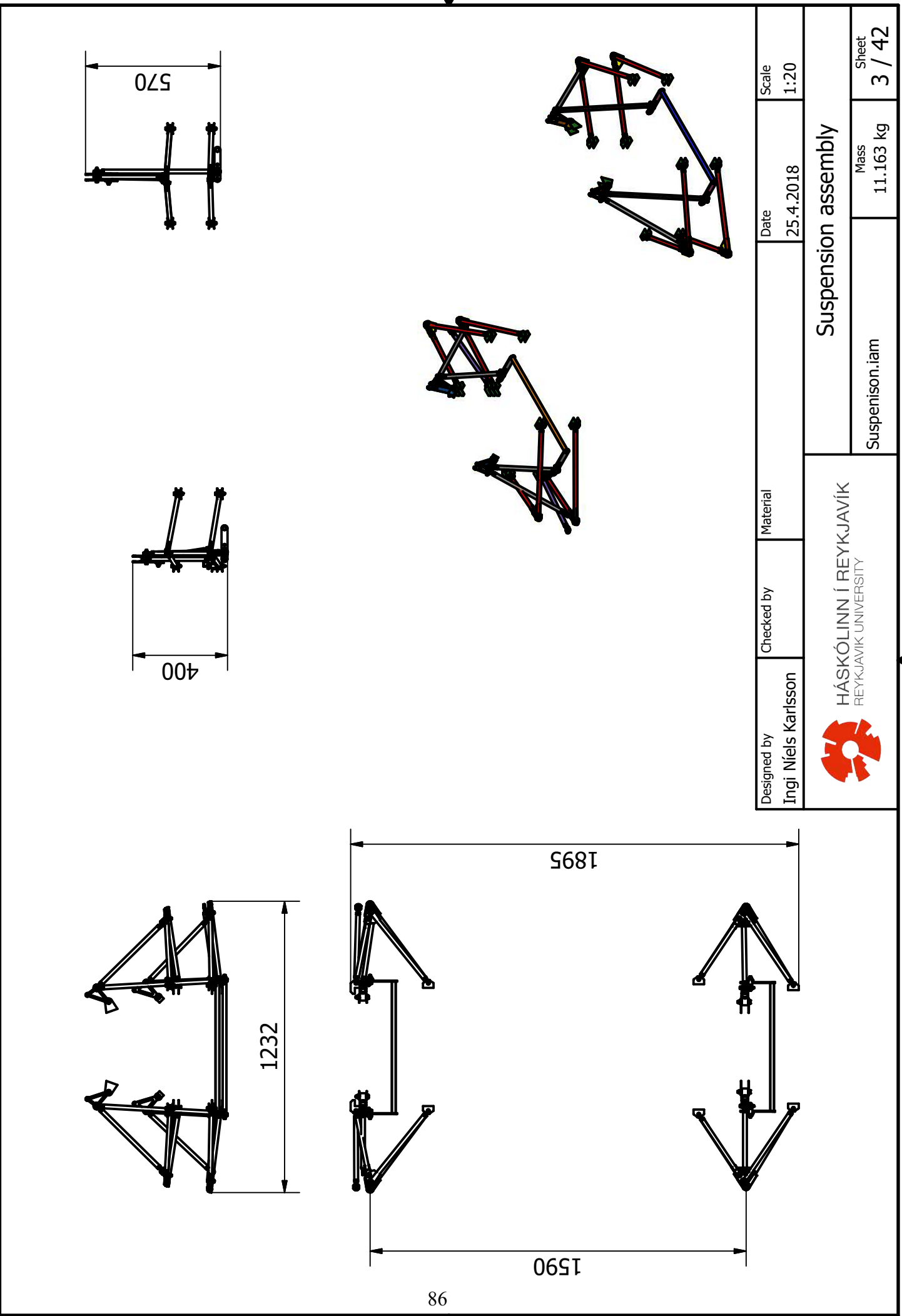
HÁSKÓLÍNN Í REYKJAVÍK  
REYKJAVÍK UNIVERSITY

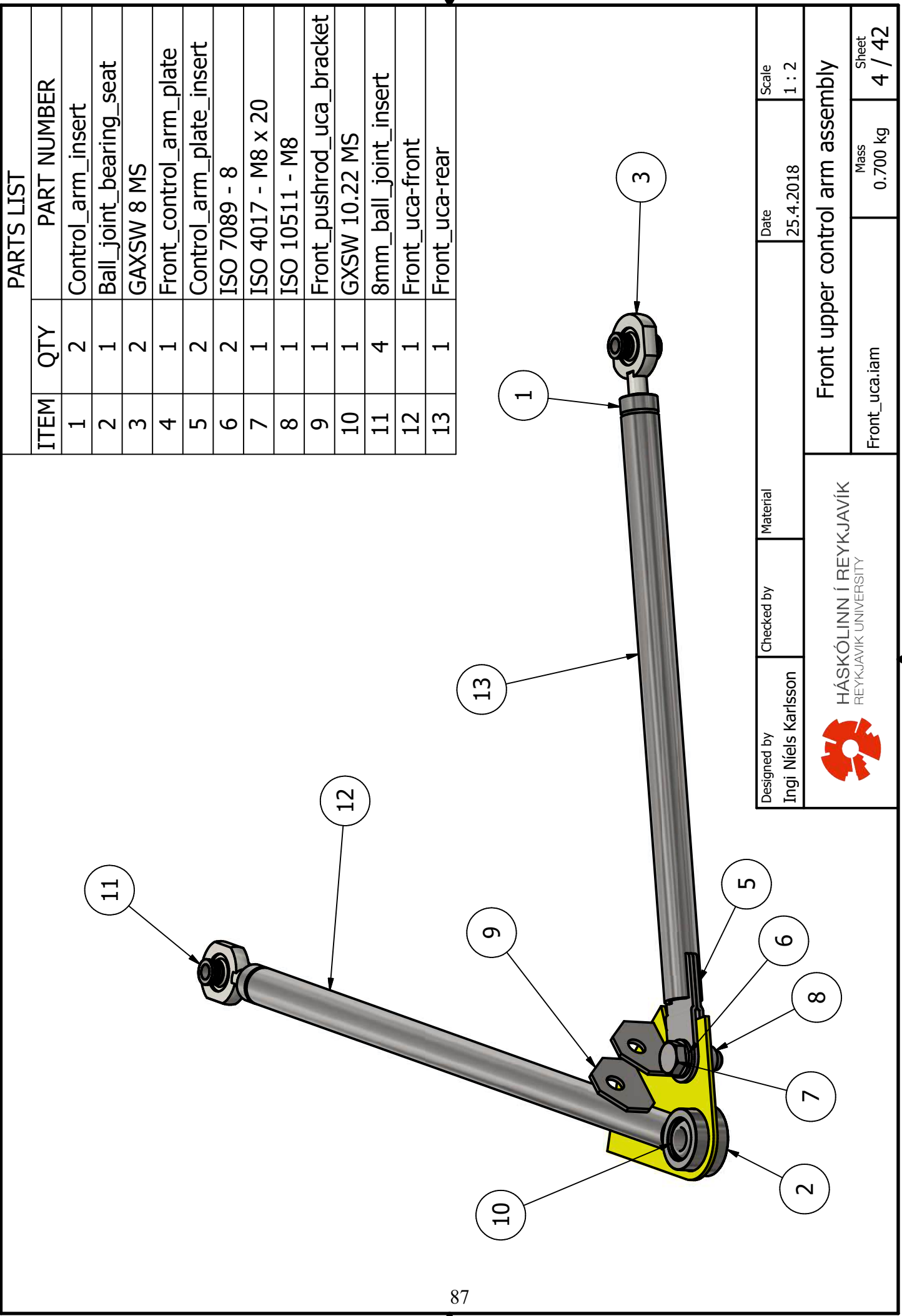


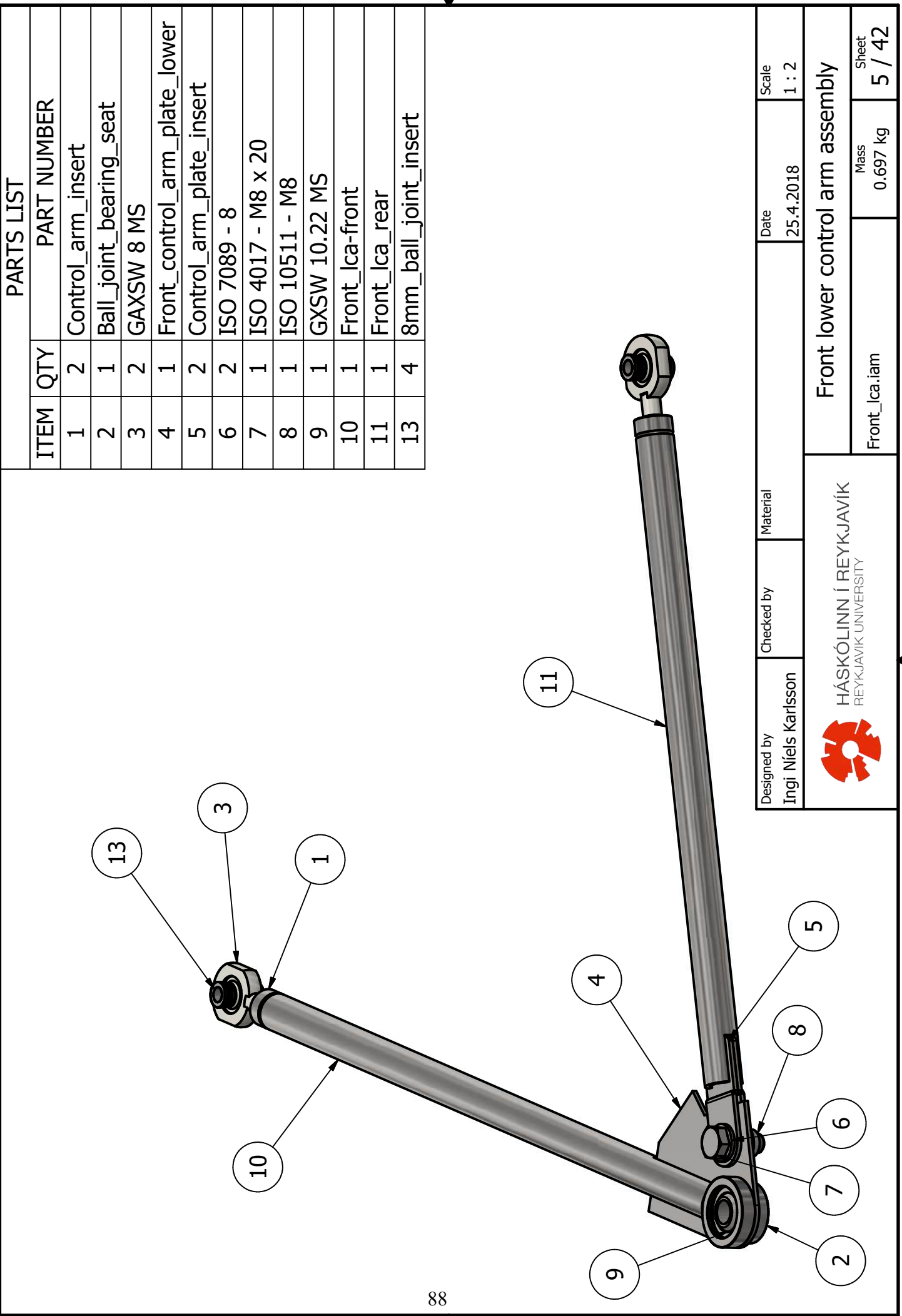
## PARTS LIST

ITEM	QTY	PART NUMBER
1	1	Front_ uca
2	1	Rear_ lca
3	1	Rear_ uca
4	1	Suspension_fasteners
5	2	Front_pushrod_assembly
6	2	Rear_pushrod_assembly
7	2	Front_antiroll_bar_link
8	2	front_antiroll_bar_arm
9	1	Front_antiroll_bar
10	2	rear_antiroll_bar_link
11	2	rear_antiroll_bar_arm
12	1	rear_antiroll_bar
13	2	Front_bc_solid
14	2	Rear_bc
15	40	DIN 125 - A 6,4
16	16	DIN 912 - M6 x 35
17	22	DIN 985 - M6
18	8	DIN 985 - M8
19	24	DIN 125 - A 8,4
20	4	ISO 4017 - M8 x 50
21	4	DIN 9021 - 6,4
22	4	DIN 912 - M6 x 55
23	4	ISO 4017 - M8 x 30
24	2	rear_tierod
25	8	DIN 625 SKF - SKF 608-2RSR
26	2	spacer_bc
27	1	Right_Front_lca
28	1	Right_Front_uca
29	1	Right_Rear_lca1
30	1	Right_Rear_uca1
31	1	Right_Front_antiroll_bar1
32	2	Right_spacer_bc1
33	1	Right_rear_antiroll_bar1
34	2	DIN 912 - M6 x 60
35	1	Front_lca

Designed by Ingi Níels Karlsson	Checked by	Material	Date 25.4.2018	Scale
	HÁSKÓLINN Í REYKJAVÍK REYKJAVÍK UNIVERSITY		Suspension assembly part list	
85		Mass	Sheet 2 / 42	







PARTS LIST			
ITEM	QTY	PART NUMBER	
1	2	Control_arm_insert	
2	2	GAXSW 8 MS	
3	1	Rear_control_arm_plate	
4	2	Control_arm_plate_insert	
5	2	ISO 7092 - ST 8 - 140 HV	
6	1	ISO 4017 - M8 x 20	
7	1	ISO 10511 - M8	
8	1	Ball_joint_bearing_seat	
9	1	GXSW 10.22 MS	
10	1	Rear_uca_Front	
11	1	Rear_uca_rear	
12	4	8mm_ball_joint_insert	

89

Designed by  
Ingi Níels Karlsson

Date  
25.4.2018

Scale  
1 : 2

Rear upper control arm assembly

HÁSKÓLINN Í REYKJAVÍK  
REYKJAVÍK UNIVERSITY



Mass 0.656 kg	Sheet 6 / 42
------------------	-----------------

PARTS LIST		
ITEM	QTY	PART NUMBER
1	2	Control_arm_insert
2	1	Ball_joint_bearing_seat
3	2	SA 8 E
4	1	Rear_control_arm_plate
5	2	Control_arm_plate_insert
6	2	ISO 7089 - 8
7	1	ISO 4017 - M8 x 20
8	1	ISO 10511 - M8
9	1	veitilega
10	4	8mm_ball_joint_insert
11	1	Rear_lca_front
12	1	Rear_lca_rear

90

Designed by  
Ingi Níels Karlsson

Date  
25.4.2018

Scale  
1 : 2

Rear\_lower\_control\_arm\_assembly

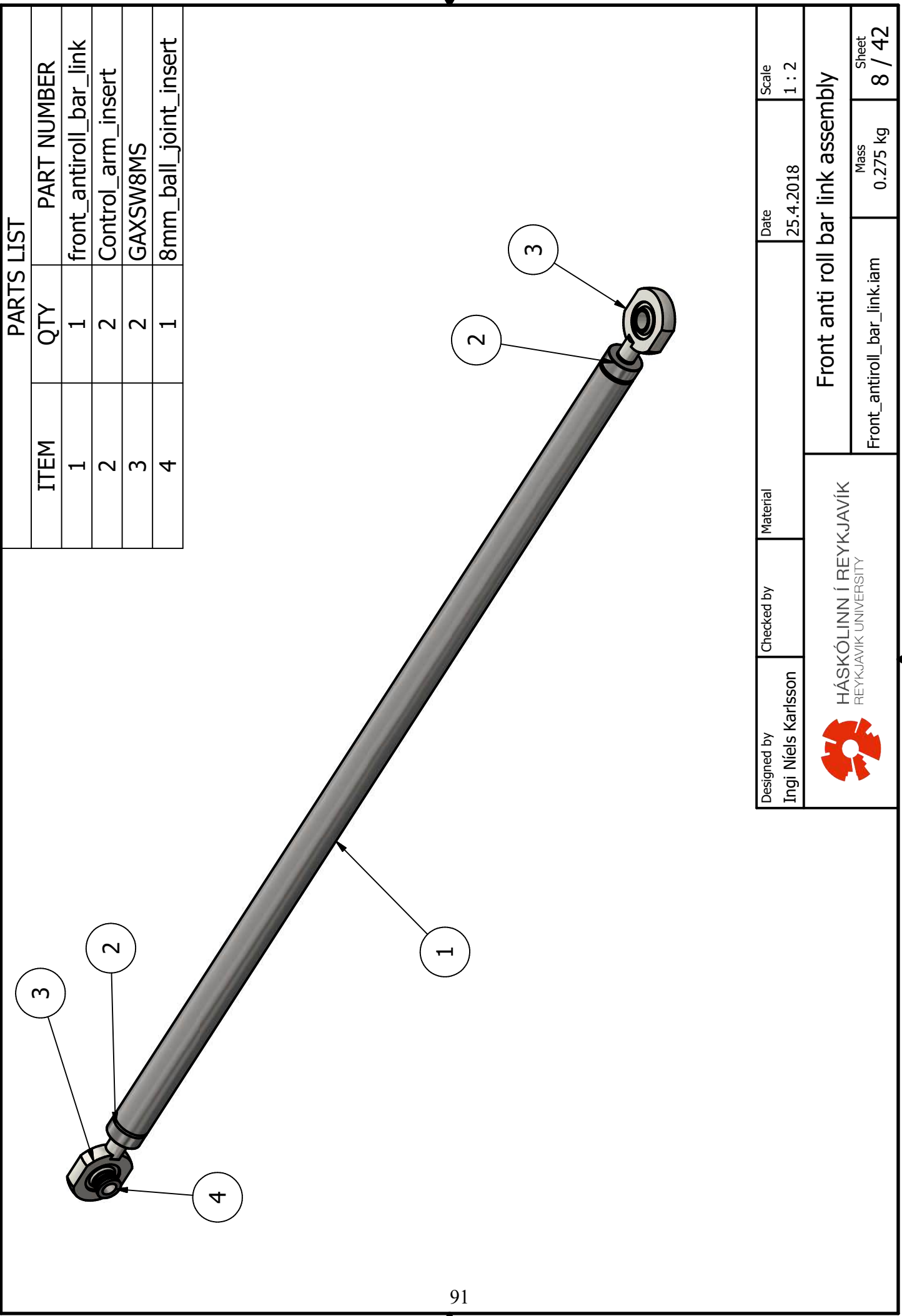
Rear\_lca.iam

HÁSKÓLINN Í REYKJAVÍK  
REYKJAVÍK UNIVERSITY



Mass  
0.687 kg

Sheet  
7 / 42



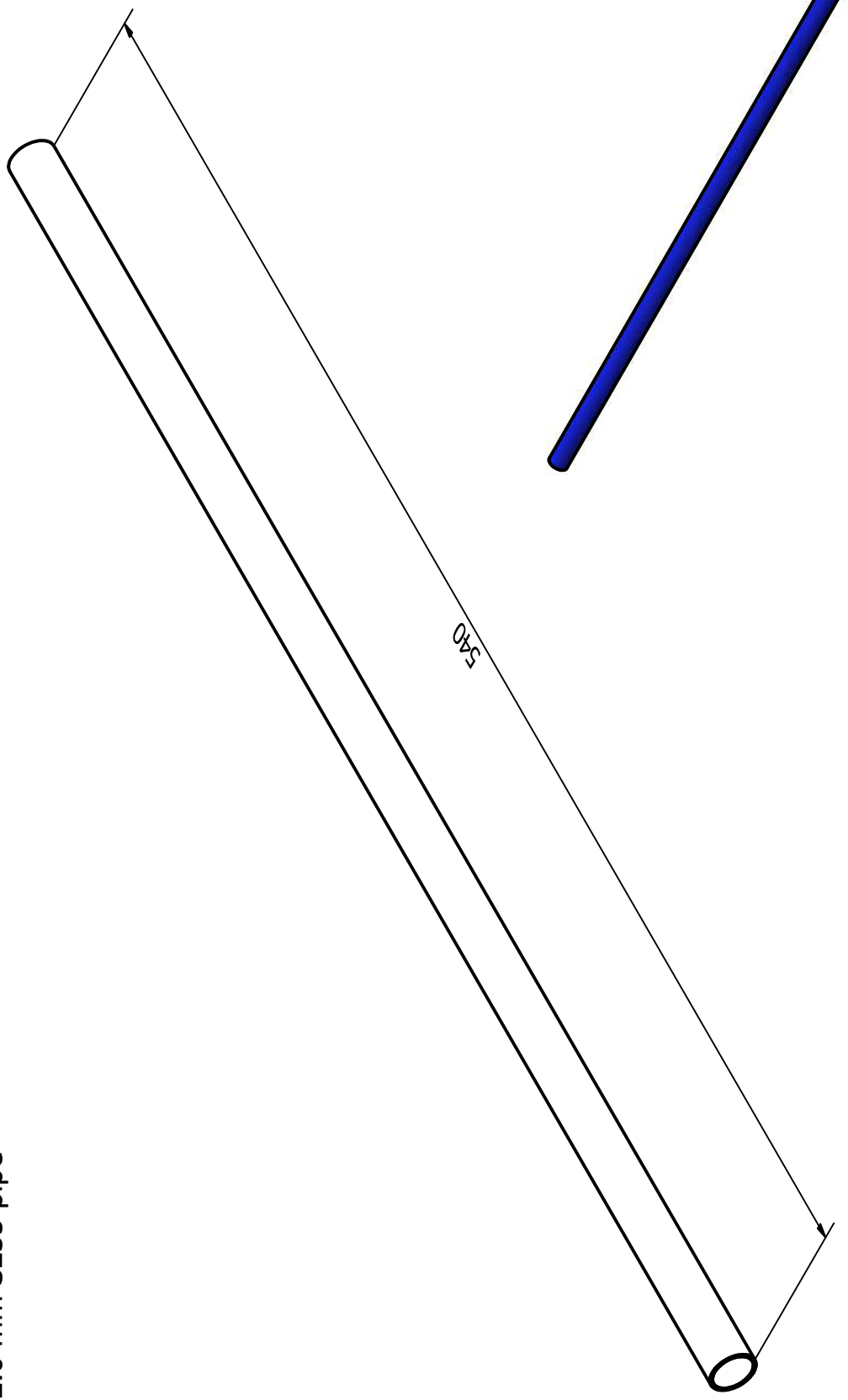


92

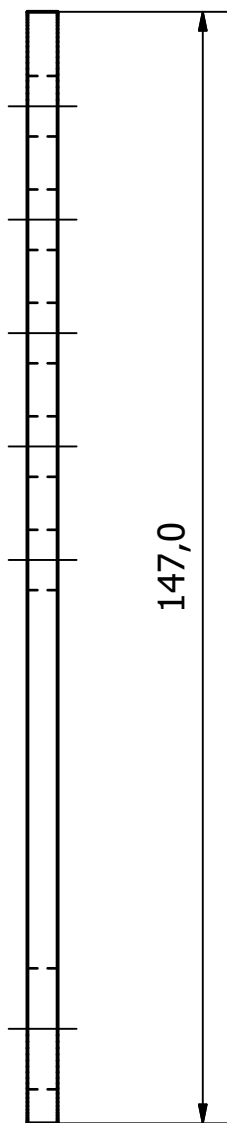
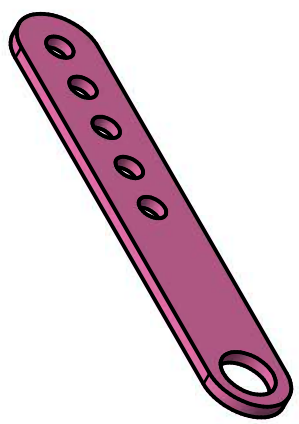
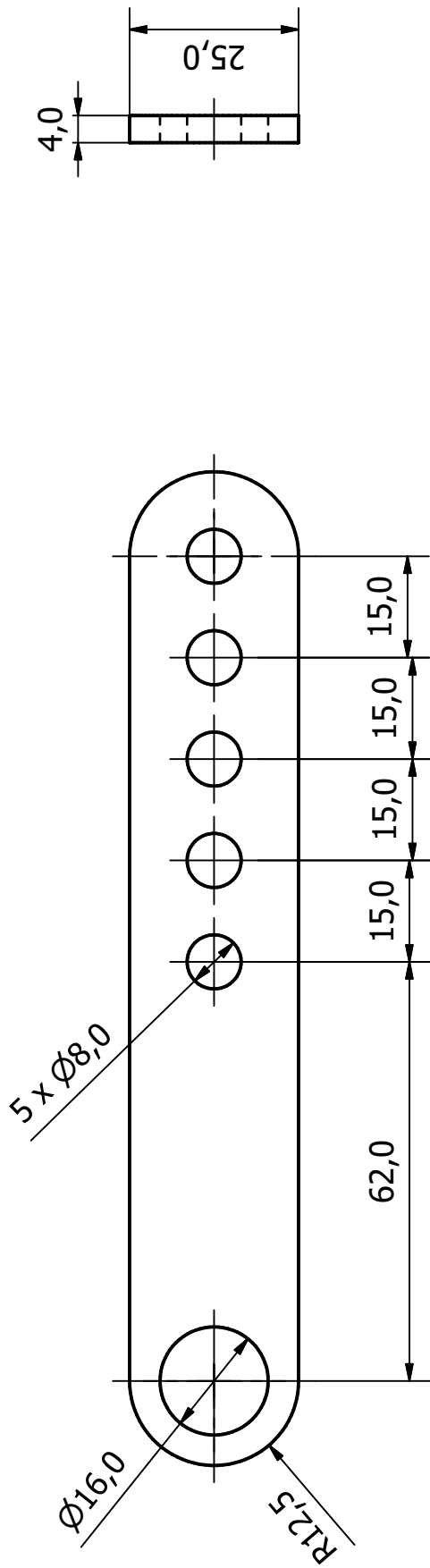
Designed by Ingi Níels Karlsson	Checked by	Material	Date 25.4.2018	Scale 1 : 2
<b>Front anti roll bar link assembly</b>				
Front_antiroll_bar_link.iam	Mass 0.275 kg	Sheet 9 / 42		



$\phi 16 \times 2.0$  mm S235 pipe



Designed by Ingí Níels Karlsson	Checked by	Material Steel, Mild	Date 25.4.2018	Scale 1 : 5
Front anti roll bar link				
HÁSKÓLINN Í REYKJAVÍK REYKJAVÍK UNIVERSITY	Front_antiroll_bar.ipt	Mass 0.200 kg	Sheet 10 / 42	4

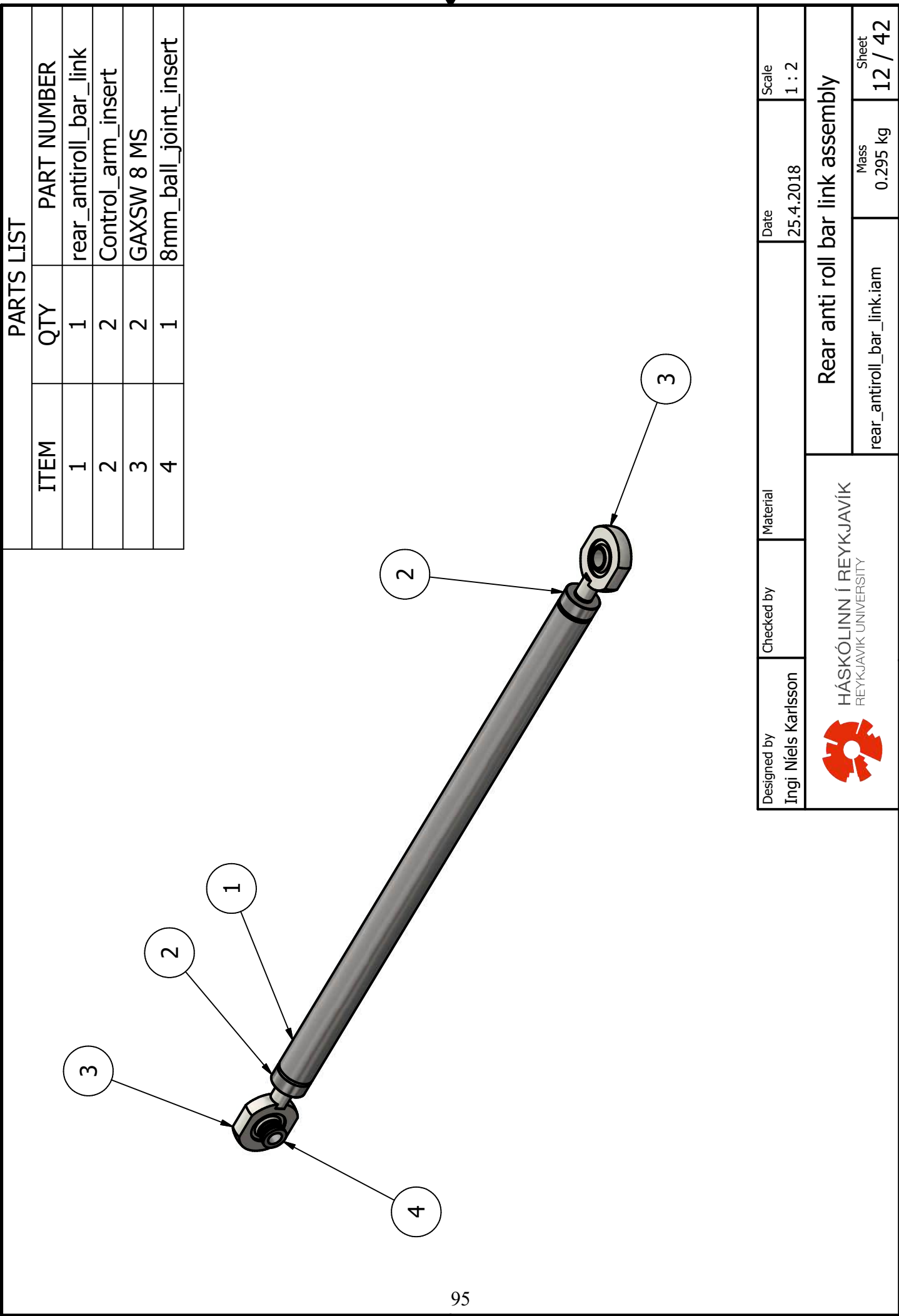


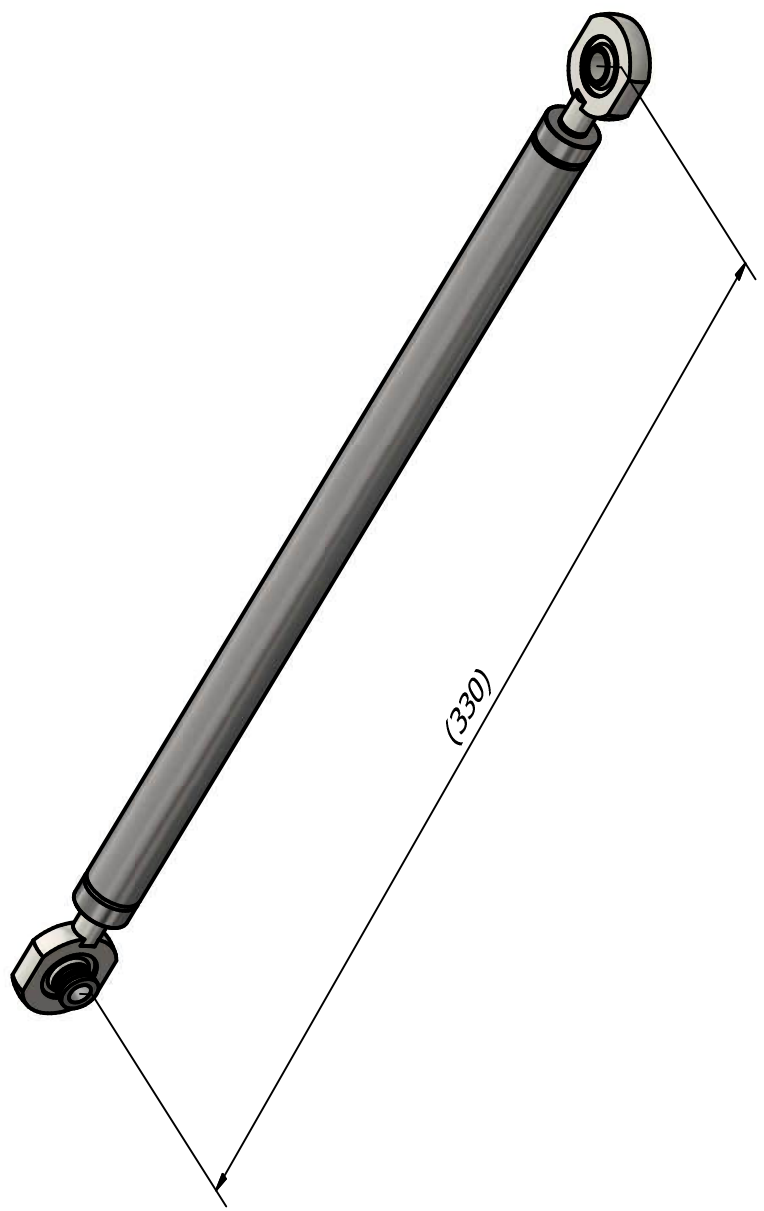
94

Designed by Ingi Þórhallur Karlsson	Checked by	Material Steel, Mild	Date 25.4.2018	Scale 1 : 1
Front anti roll bar arm				
front_antiroll_bar_arm.ipt		Mass 0.097 kg	Sheet 11 / 42	



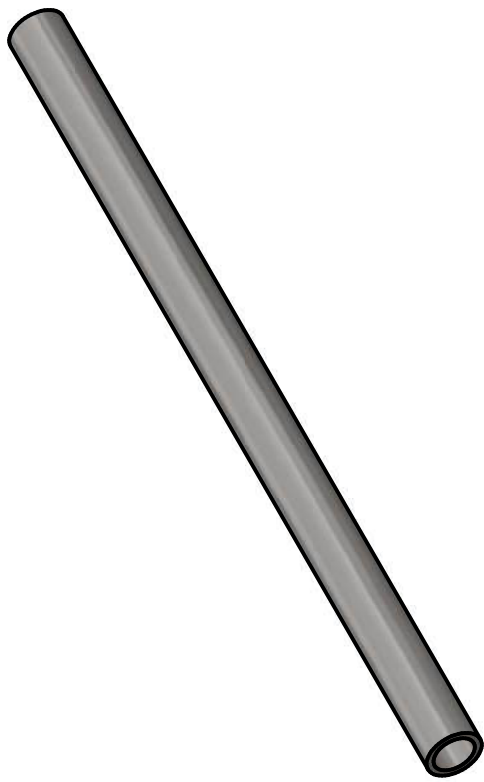
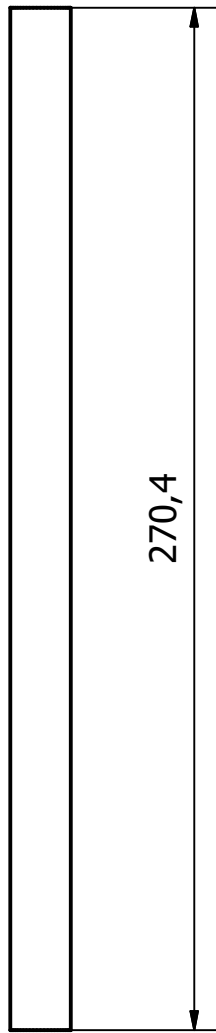
HÁSKÓLINN Í REYKJAVÍK  
REYKJAVÍK UNIVERSITY



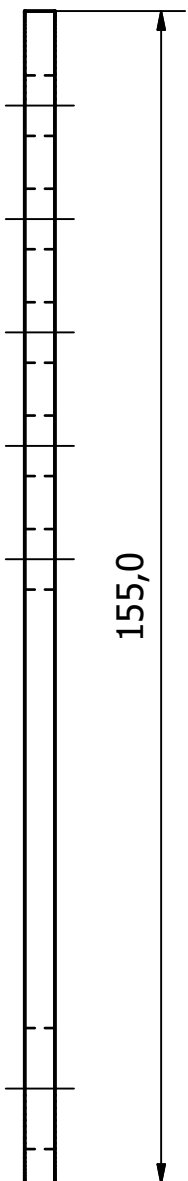
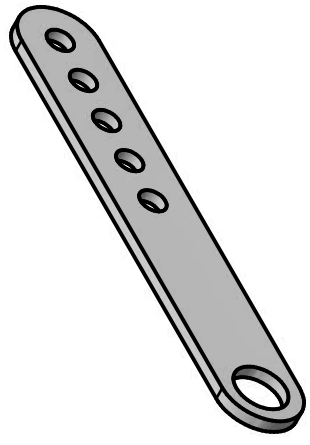
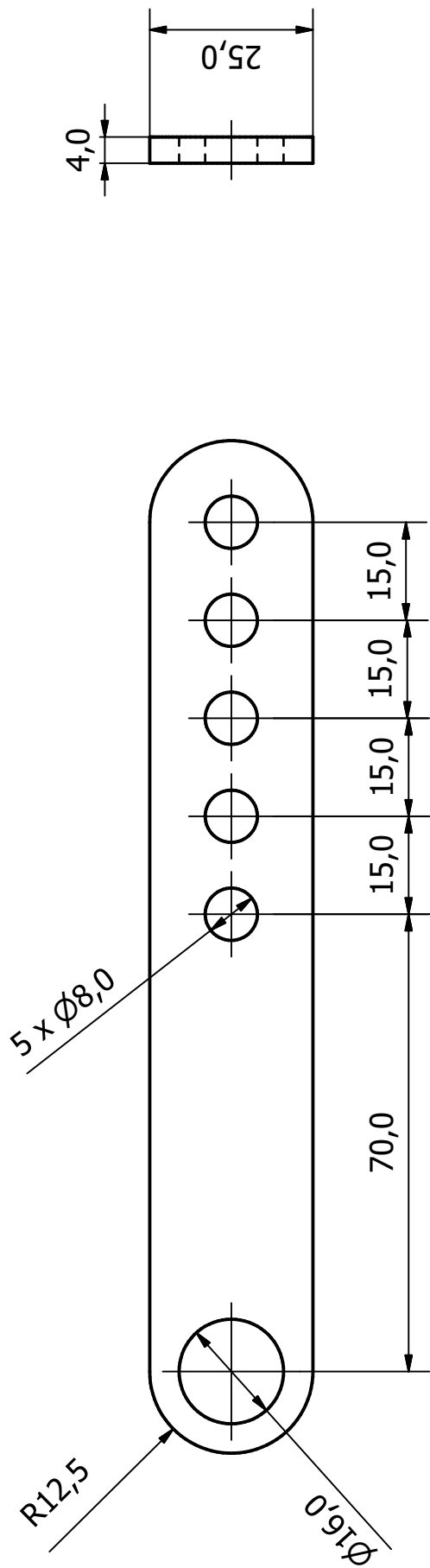


Designed by Ingi Þórhallur Karlsson	Checked by	Material	Date 25.4.2018	Scale 1 : 2
<b>Rear anti roll bar link assembly</b>				
rear_antiroll_bar_link.iam	Mass 0.295 kg	Sheet 13 / 42		

$\varnothing 16 \times 2.0$  mm S235 pipe

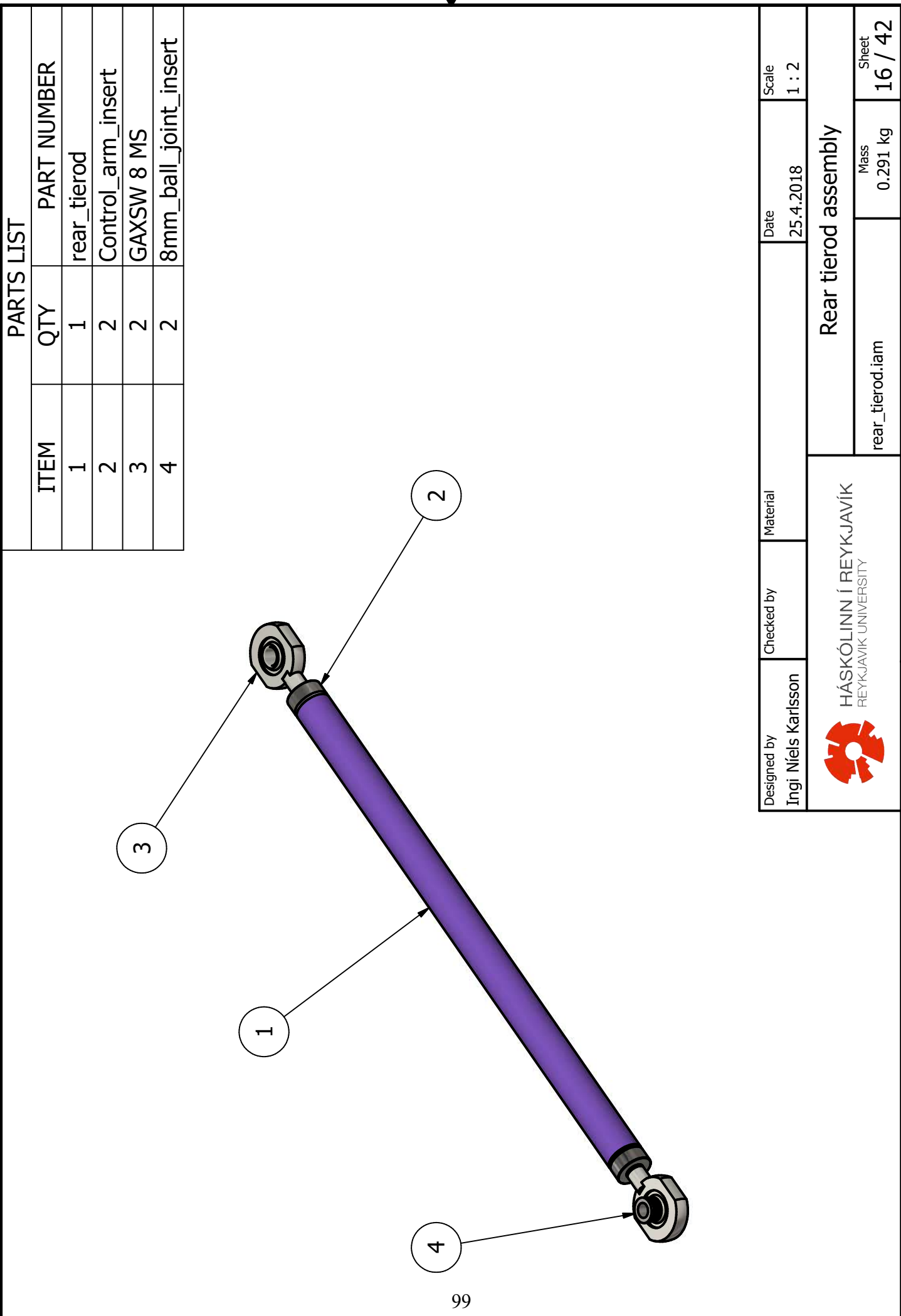


Designed by Ingi Níels Karlsson	Checked by	Material Steel, Mild	Date 25.4.2018	Scale 1 : 2
HÁSKÓLINN Í REYKJAVÍK REYKJAVÍK UNIVERSITY				Rear anti roll bar link
rear_antiroll_bar_link.ipt			Mass 0.187 kg	Sheet 14 / 42

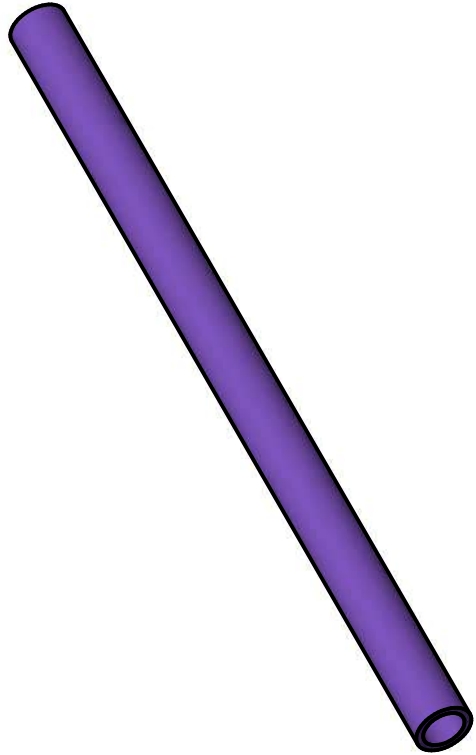
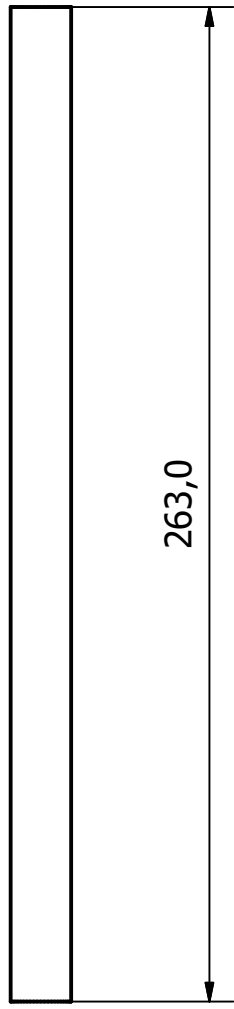


Designed by Ingi Níels Karlsson	Checked by	Material Aluminum 6061	Date 25.4.2018	Scale 1 : 1
Rear anti roll bar arm				
rear_antiroll_bar_arm.ipt		Mass 0,036 kg	Sheet 15 / 42	

HÁSKÓLÍNN Í REYKJAVÍK  
REYKJAVÍK UNIVERSITY



$\phi 16 \times 2.0$  mm S235 pipe



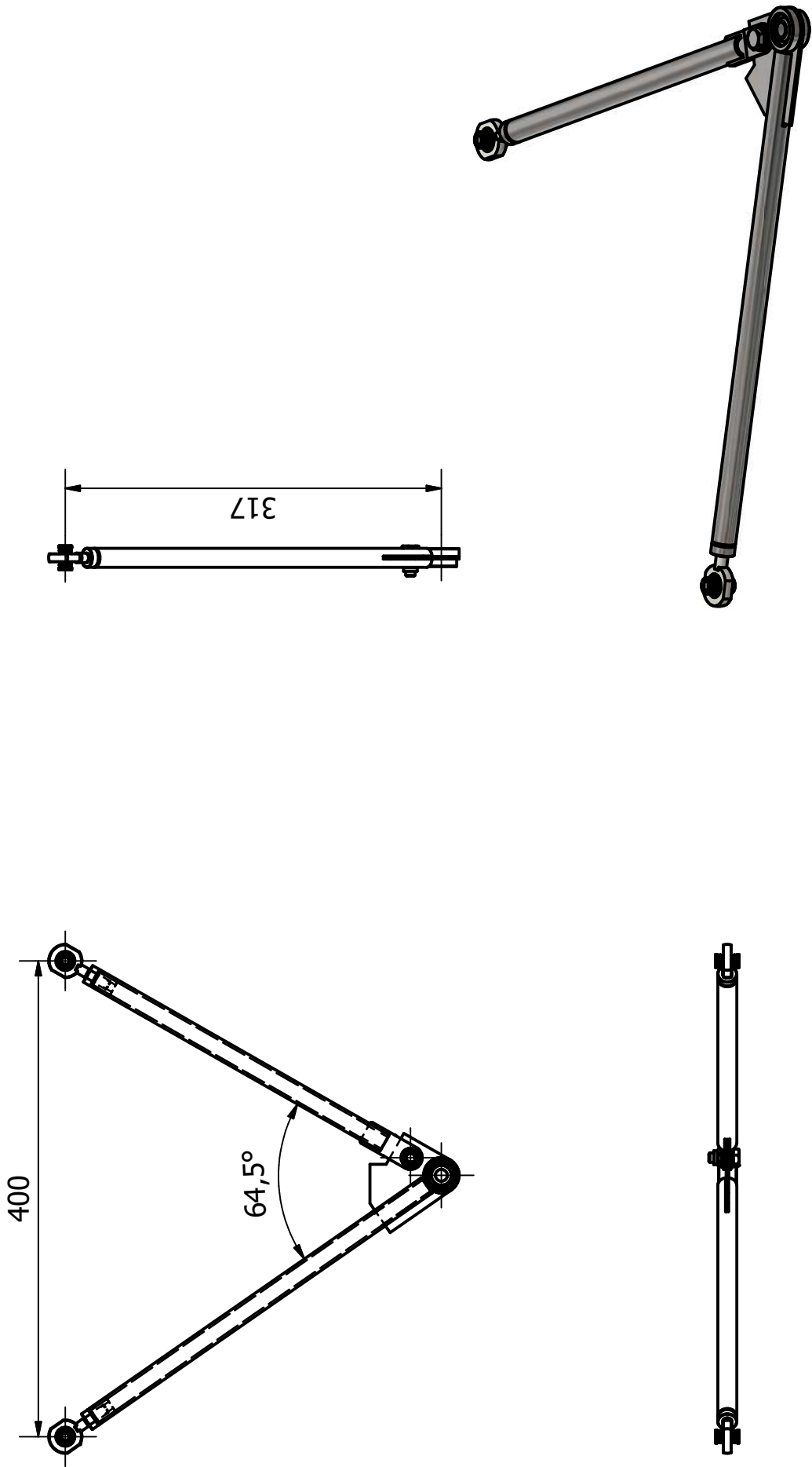
100

Designed by Ingi Níels Karlsson	Checked by	Material Steel, Mild	Date 25.4.2018	Scale 1 : 2
Rear tierod				
rear_tierod.ipt				Mass 0.182 kg

HÁSKÓLINN Í REYKJAVÍK  
REYKJAVÍK UNIVERSITY

The logo of the University of Iceland (Háskólinn í Reykjavík) is located in the bottom right corner of the table. It features a red circular emblem with a stylized white design resembling a sun or a wheel.

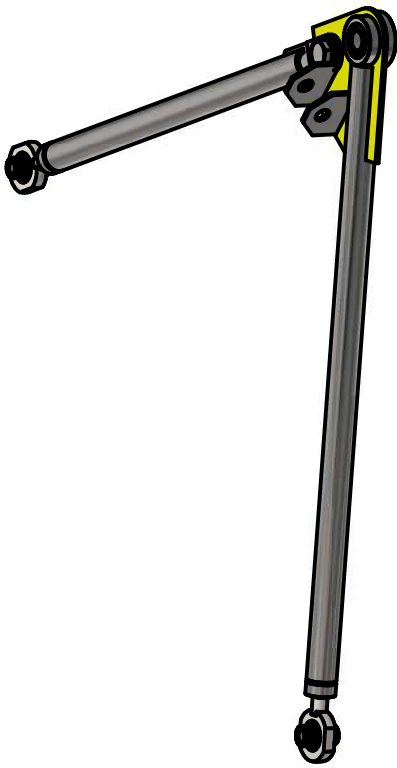
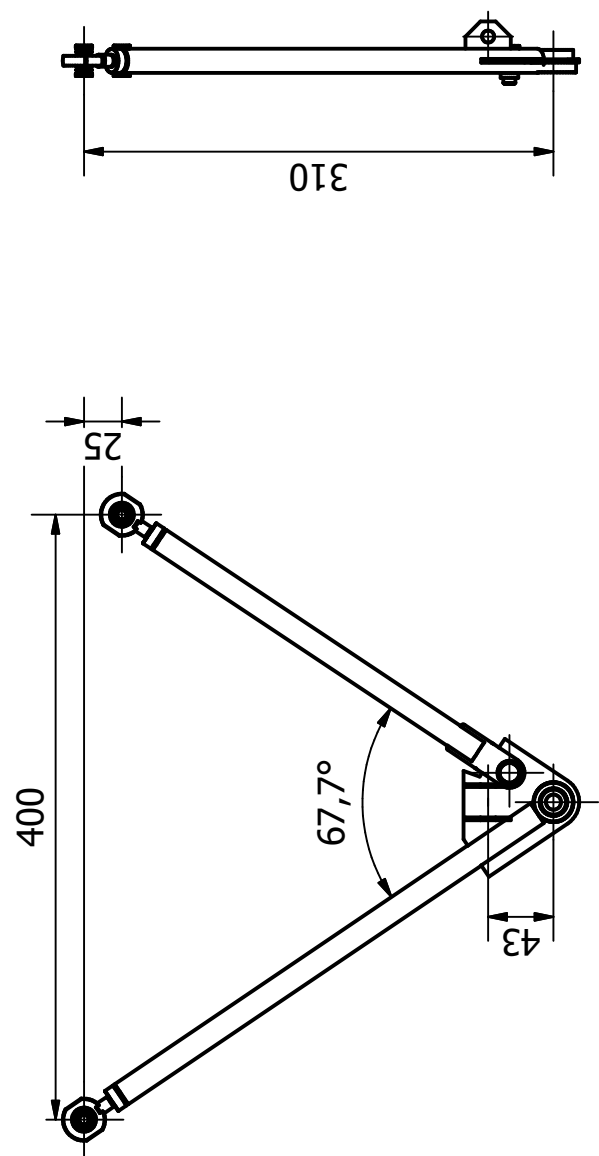
4



Designed by Ingi Níels Karlsson	Checked by	Material	Date 25.4.2018	Scale 1 : 5
Front_lca.iam				Front lower control arm assembly
Front_lca.iam	Mass 0.697 kg	Sheet 18 / 42		



HÁSKÓLINN Í REYKJAVÍK  
REYKJAVÍK UNIVERSITY

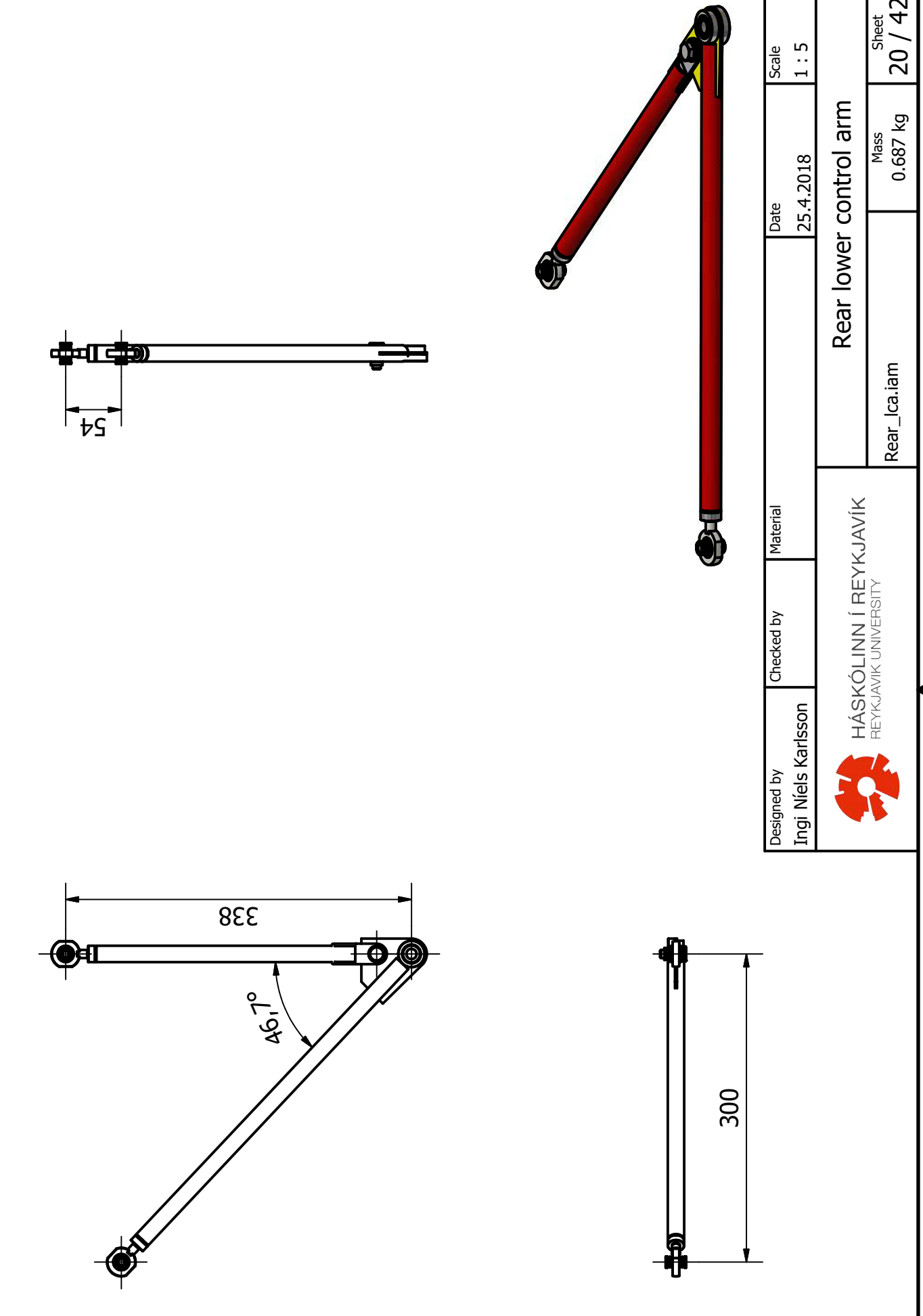


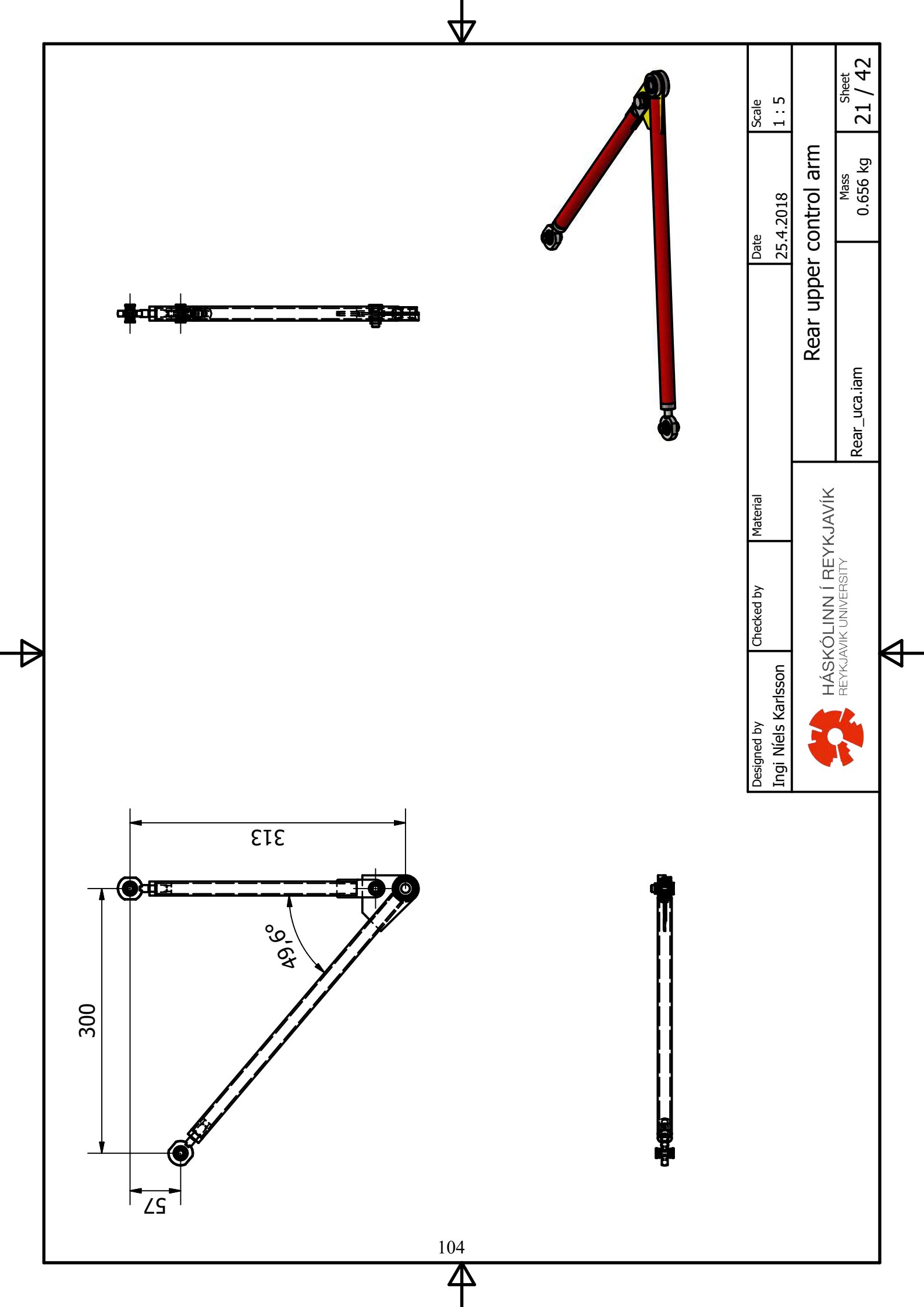
102

Designed by Ingi Níels Karlsson	Checked by	Material	Date 25.4.2018	Scale 1 : 5
Front upper control arm assembly				
Front_uca.iam	Mass 0.700 kg	Sheet 19 / 42		

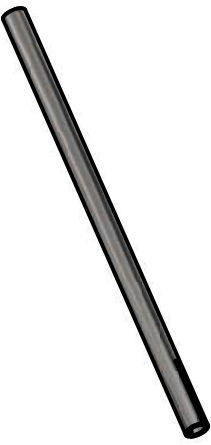
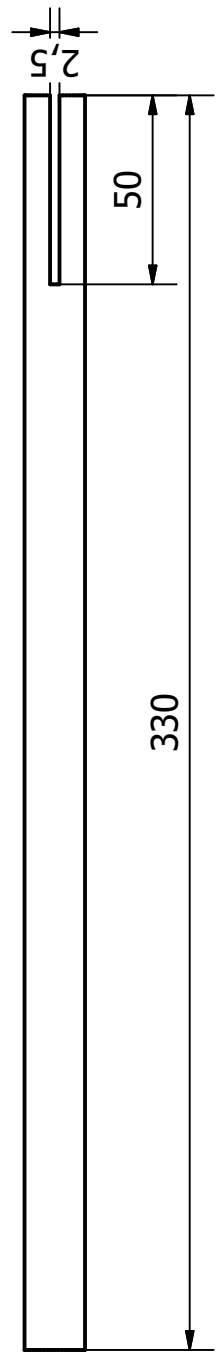


HÁSKÓLINN Í REYKJAVÍK  
REYKJAVÍK UNIVERSITY





$\phi 16 \times 2.0$  mm S235 pipe



105

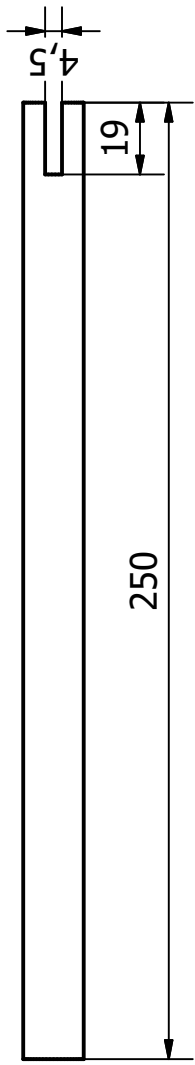
Designed by Ingi Níels Karlsson	Checked by	Material Steel, High Strength, Low Alloy	Date 25.4.2018	Scale 1 : 2
Front upper control arm front				
Front_uca-front.ckpt	Mass 0,225 kg	Sheet 22 / 42		



HÁSKÓLINN Í REYKJAVÍK  
REYKJAVÍK UNIVERSITY

4

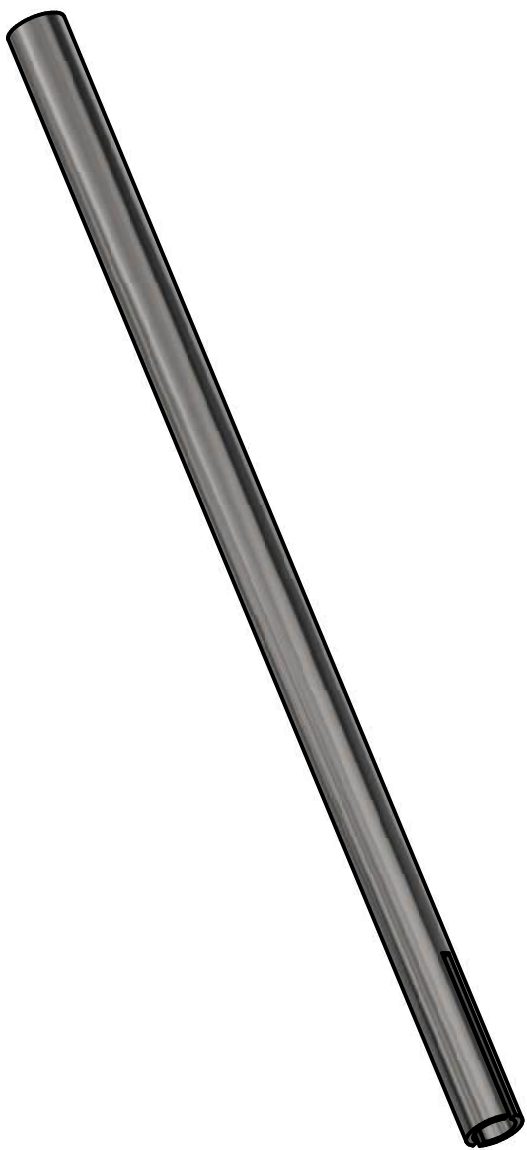
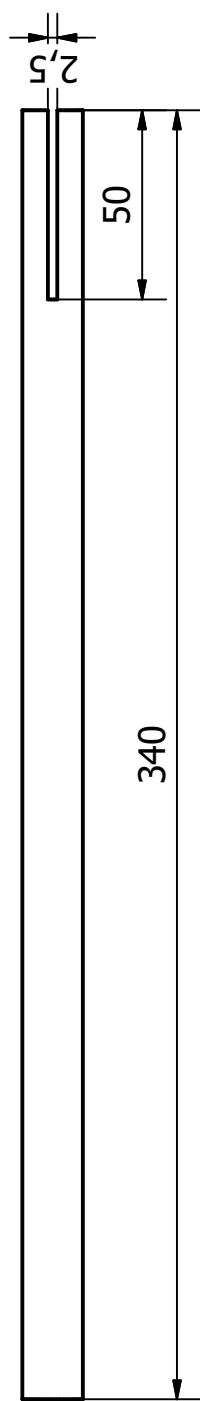
$\varnothing 16 \times 2.0$  mm S235 pipe



106

Designed by Ingi Þórhallur Karlsson	Checked by	Material Steel, High Strength, Low Alloy	Date 25.4.2018	Scale 1 : 2
<b>Front upper control arm rear</b>				
Front_uca-rear.ipt	Front_uca-rear.ipt	Mass 0,172 kg	Sheet 23 / 42	4

$\varnothing 16 \times 2.0$  mm S235 pipe



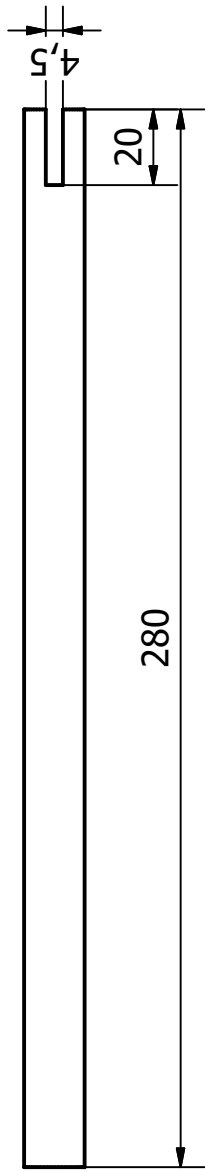
107

Designed by Ingi Níels Karlsson	Checked by	Material Steel, High Strength, Low Alloy	Date 25.4.2018	Scale 1 : 2
Front_lower control arm front				
Front_lca_front.ipt	Mass 0,231 kg	Sheet 24 / 42		



4

$\varnothing 16 \times 2.0$  mm S235 pipe



108

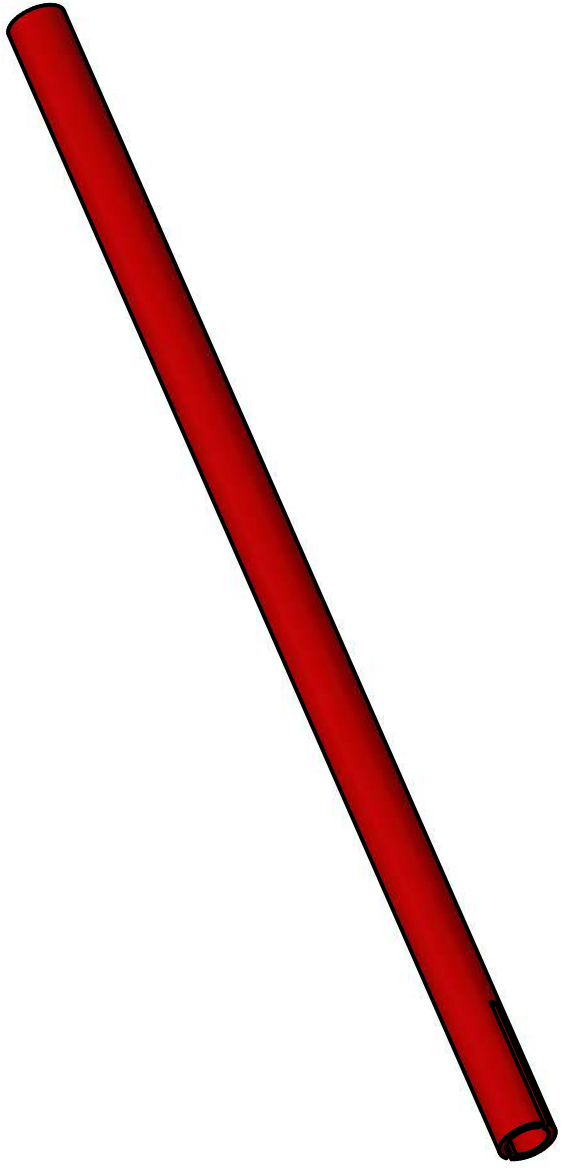
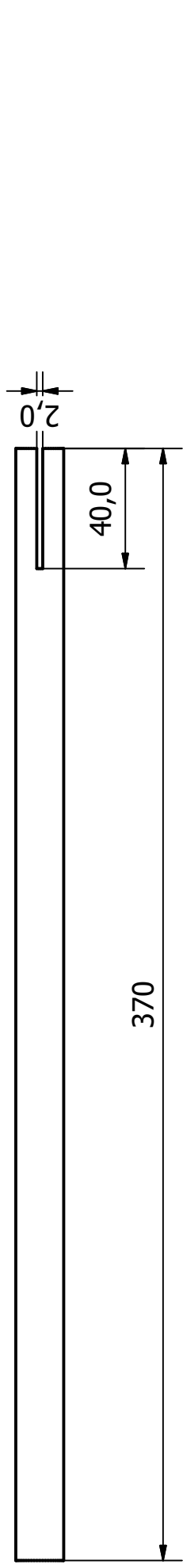
Designed by Ingi Níels Karlsson	Checked by	Material Steel, High Strength, Low Alloy	Date 25.4.2018	Scale 1 : 2
Front lower control arm rear				
Front_lca_rear.ipt	Mass 0,190 kg	Sheet 25 / 42		



HÁSKÓLINN Í REYKJAVÍK  
REYKJAVÍK UNIVERSITY

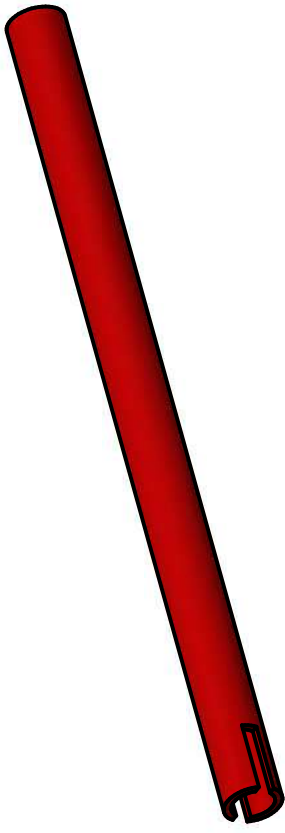
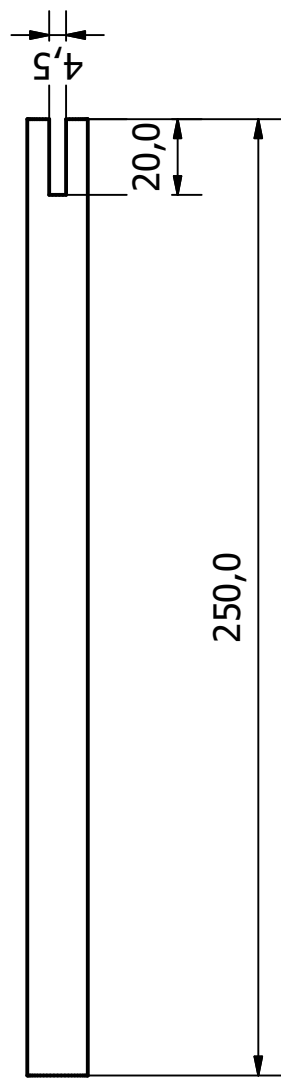
4

$\phi 16 \times 2.0$  mm S235 pipe



Designed by Ingi Níels Karlsson	Checked by	Material Steel, High Strength, Low Alloy	Date 25.4.2018	Scale 1 : 2
Rear_lca_front				Rear lower control arm front
Rear_lca_front.ipt	Mass 0.253 kg	Sheet 26 / 42		

$\phi 16 \times 2.0$  mm S235 pipe



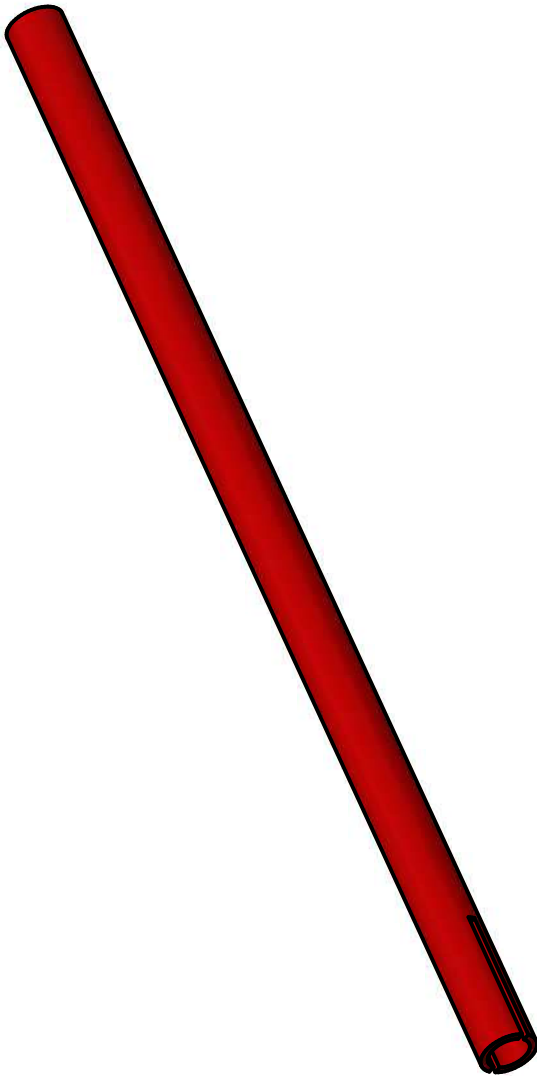
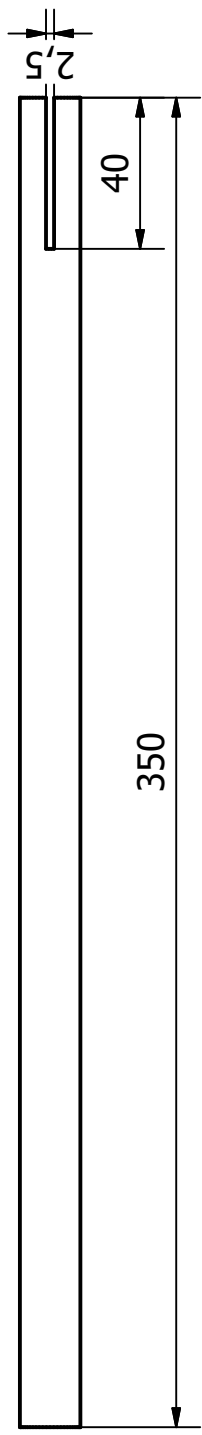
110

Designed by Ingi Níels Karlsson	Checked by	Material Steel, High Strength, Low Alloy	Date 25.4.2018	Scale 1 : 2
Rear lower control arm rear				
Rear_lca_rear.ipt	Mass 0.172 kg	Sheet 27 / 42		



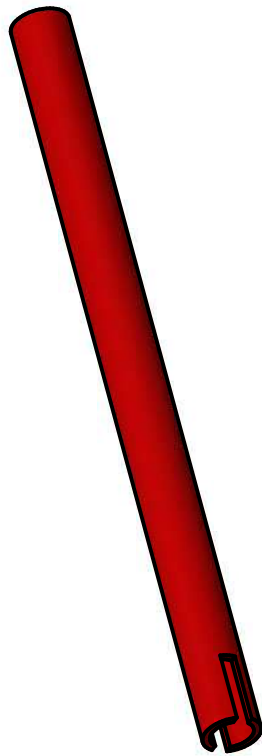
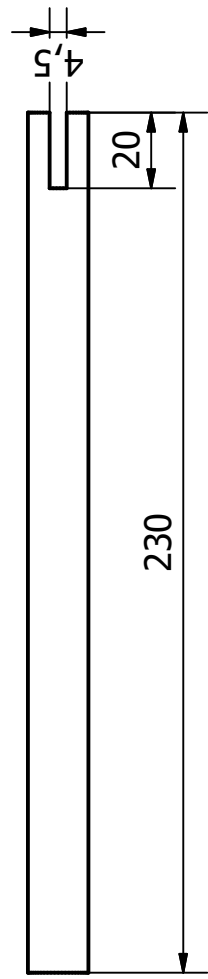
4

$\phi 16 \times 2.0$  mm S235 pipe



Designed by Ingi Níels Karlsson	Checked by	Material Steel, High Strength, Low Alloy	Date 25.4.2018	Scale 1 : 2
Rear upper control arm front				
Rear_uca_Front.ipt	Mass 0,240 kg	Sheet 28 / 42		

$\phi 16 \times 2.0$  mm S235 pipe

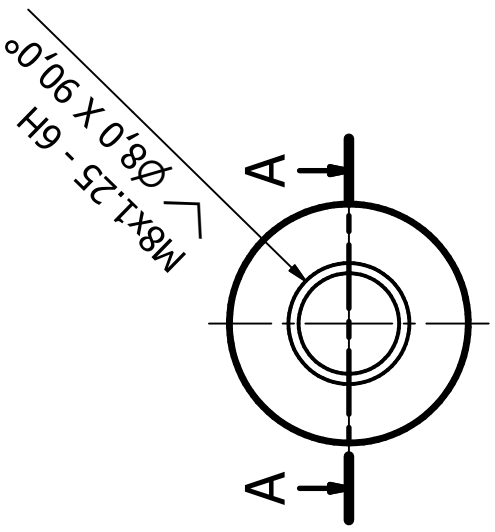
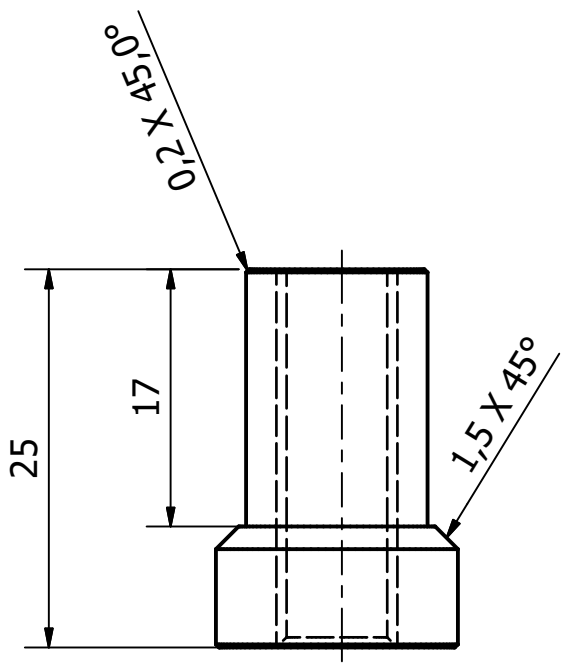


112

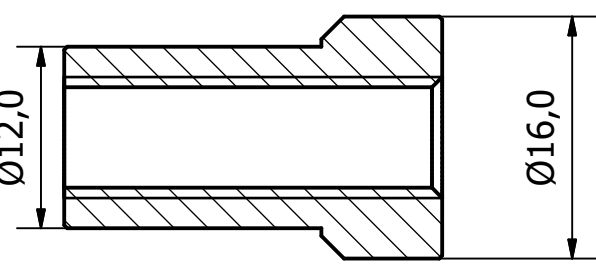
Designed by Ingi Níels Karlsson	Checked by	Material Steel, High Strength, Low Alloy	Date 25.4.2018	Scale 1 : 2
Rear upper control arm rear				
Rear_uca_rear.ipt	Mass 0,154 kg	Sheet 29 / 42		



4



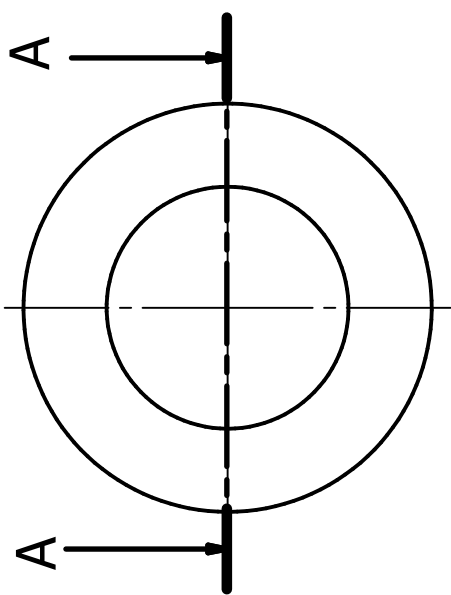
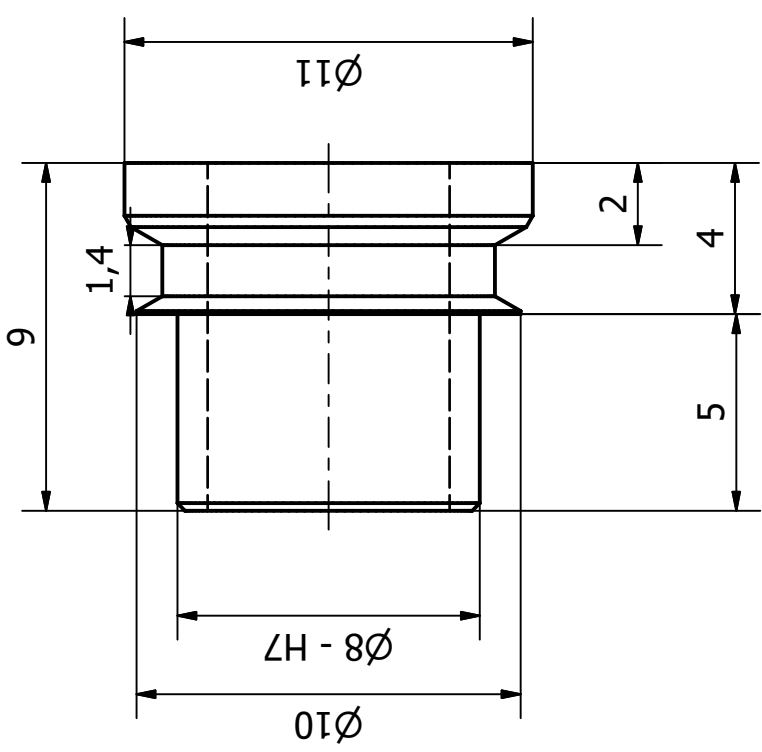
A-A ( 2 : 1 )



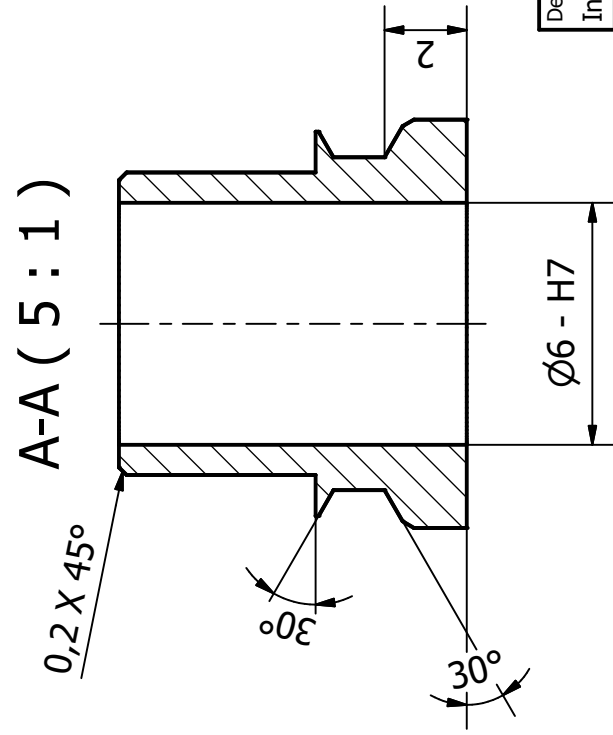
Designed by Ingi Þórhallur Karlsson	Checked by	Material Steel, High Strength, Low Alloy	Date 25.4.2018	Scale 2 : 1
Control arm M8 insert				
Control_arm_insert.ipt	Mass 0.020 kg	Sheet 30 / 42		



HÁSKÓLINN Í REYKJAVÍK  
REYKJAVÍK UNIVERSITY



A-A ( 5 : 1 )



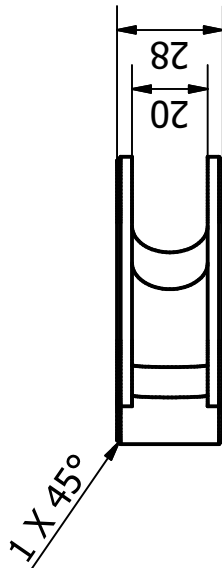
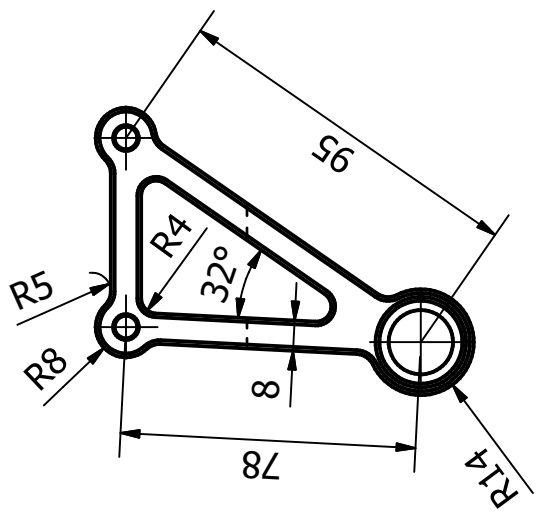
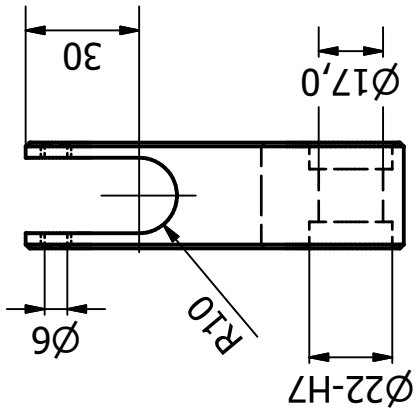
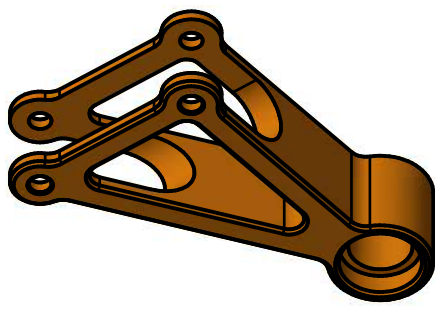
114

Designed by Ingi Níels Karlsson	Checked by	Material Titanium	Date 25.4.2018	Scale 5 : 1
Spherical bearing insert 8 mm				
8mm_ball_joint_insert.ipt				Mass 0.001 kg



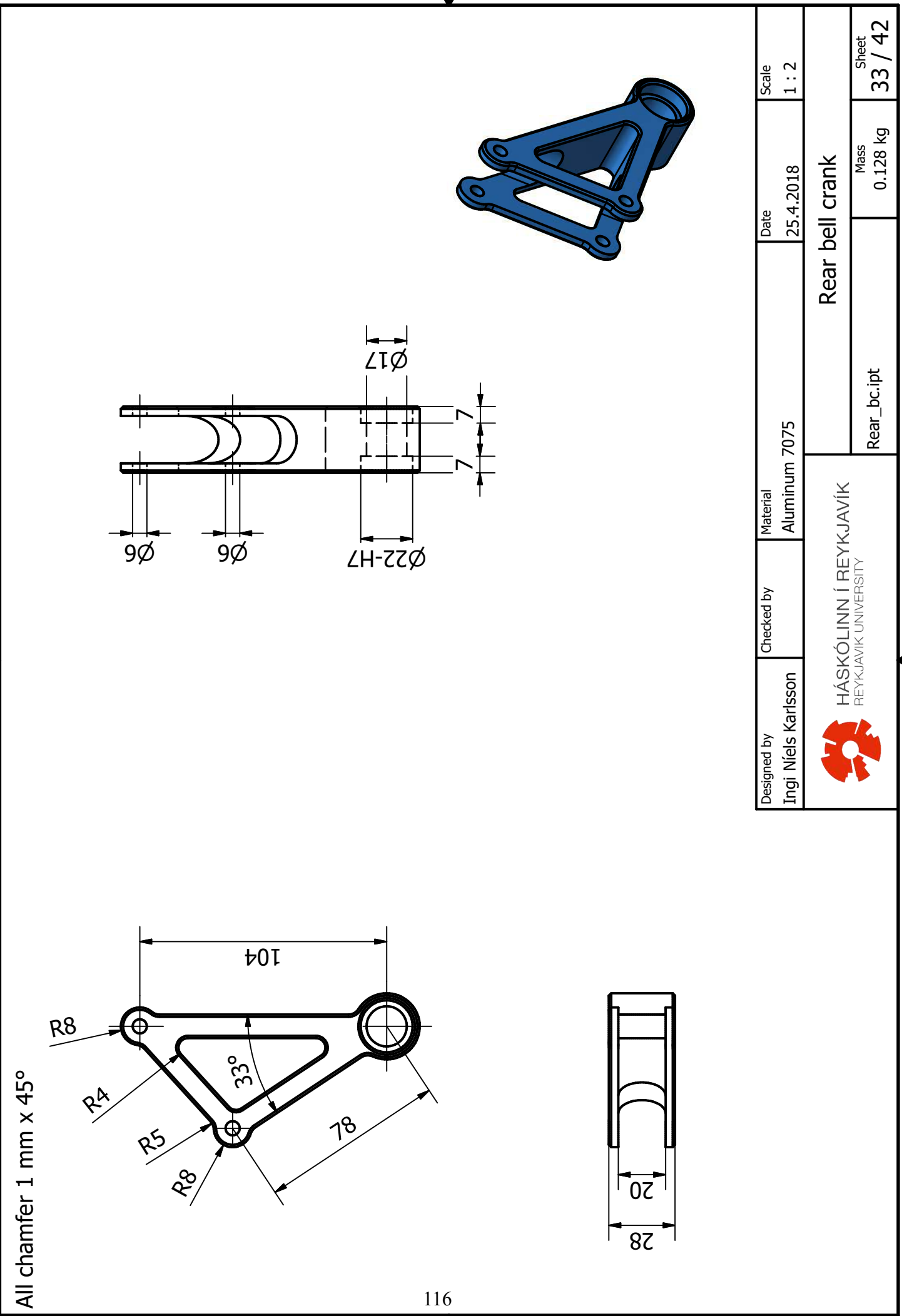
HÁSKÓLINN Í REYKJAVÍK  
REYKJAVÍK UNIVERSITY

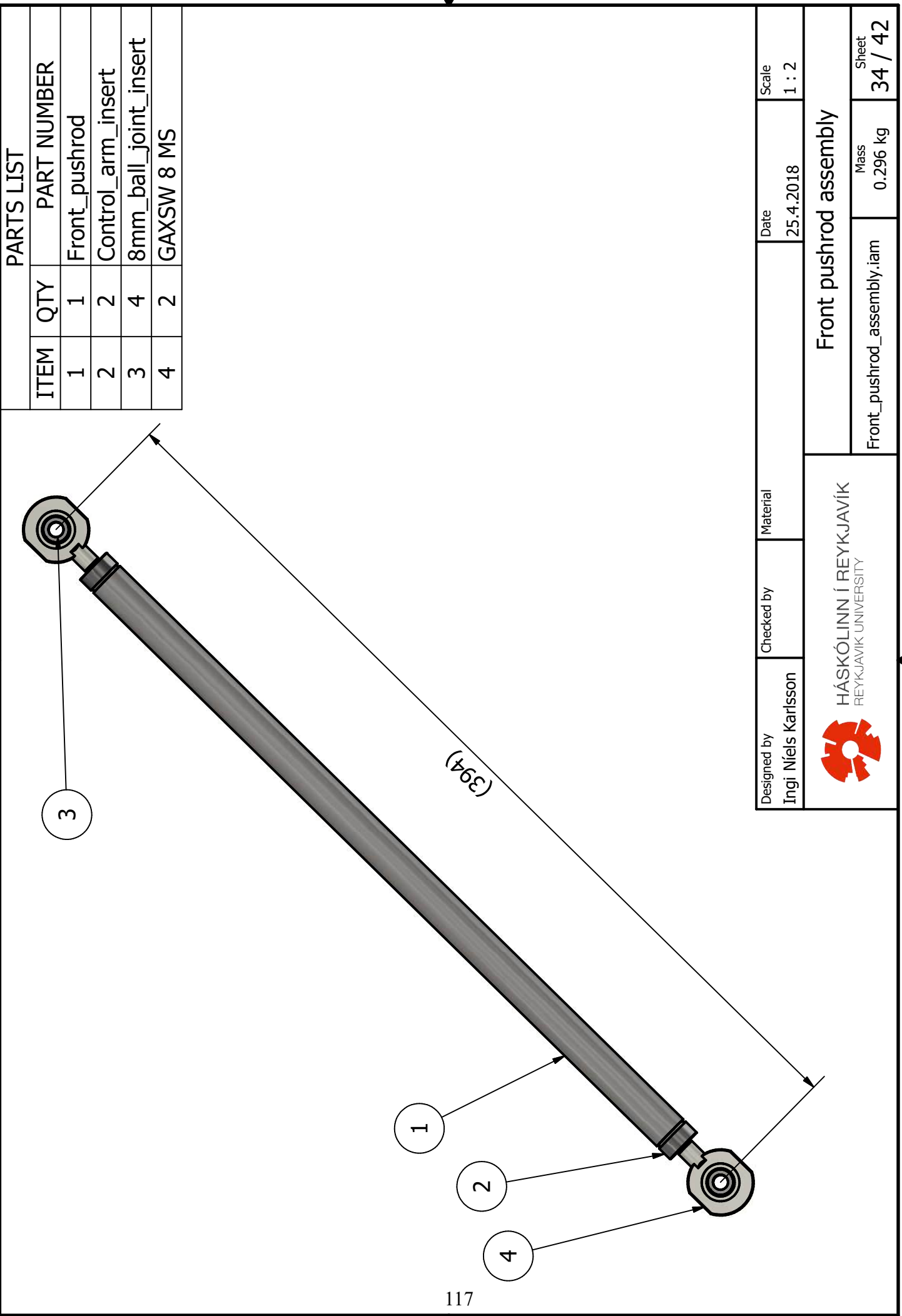
Sheet  
31 / 42



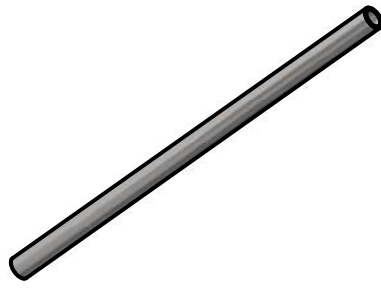
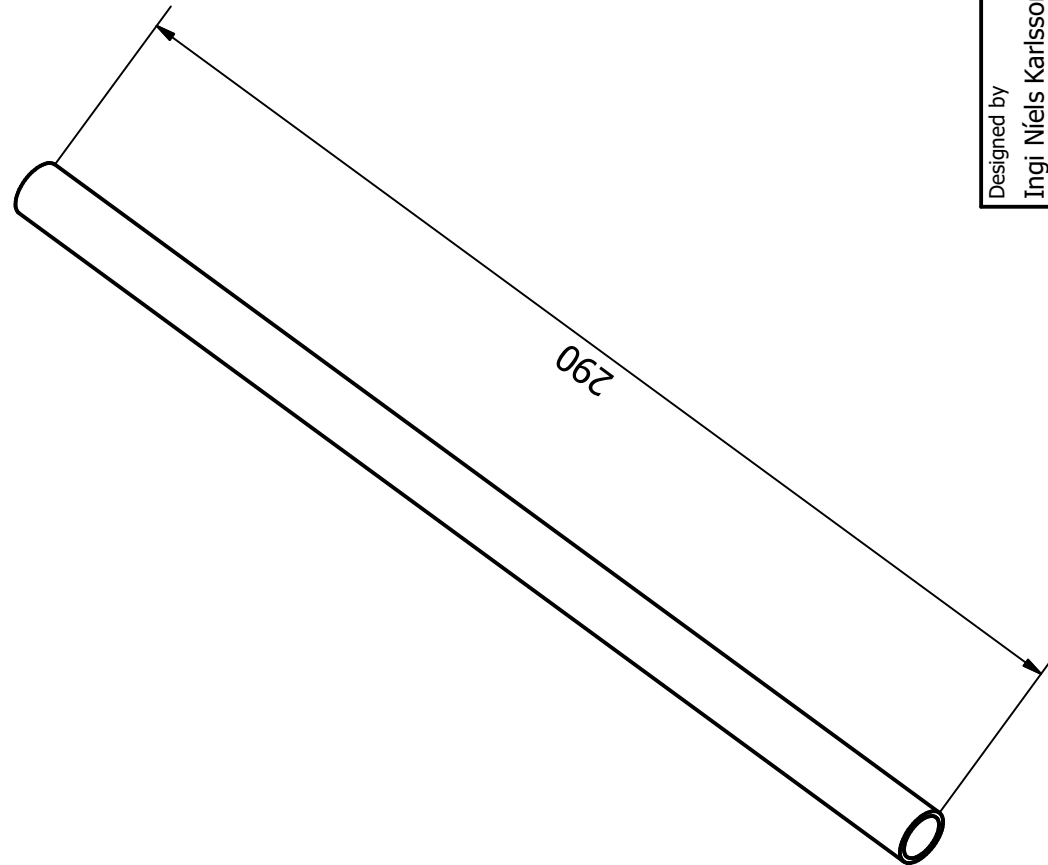
Designed by Ingi Níels Karlsson	Checked by	Material Aluminum 7075	Date 25.4.2018	Scale 1 : 2
<b>Front bell crank</b>				
Front_bc_solid.ipt	Mass 0.100 kg	Sheet 32 / 42		

HÁSKÓLINN Í REYKJAVÍK  
REYKJAVÍK UNIVERSITY





$\phi 16 \times 2.0$  mm S235 pipe



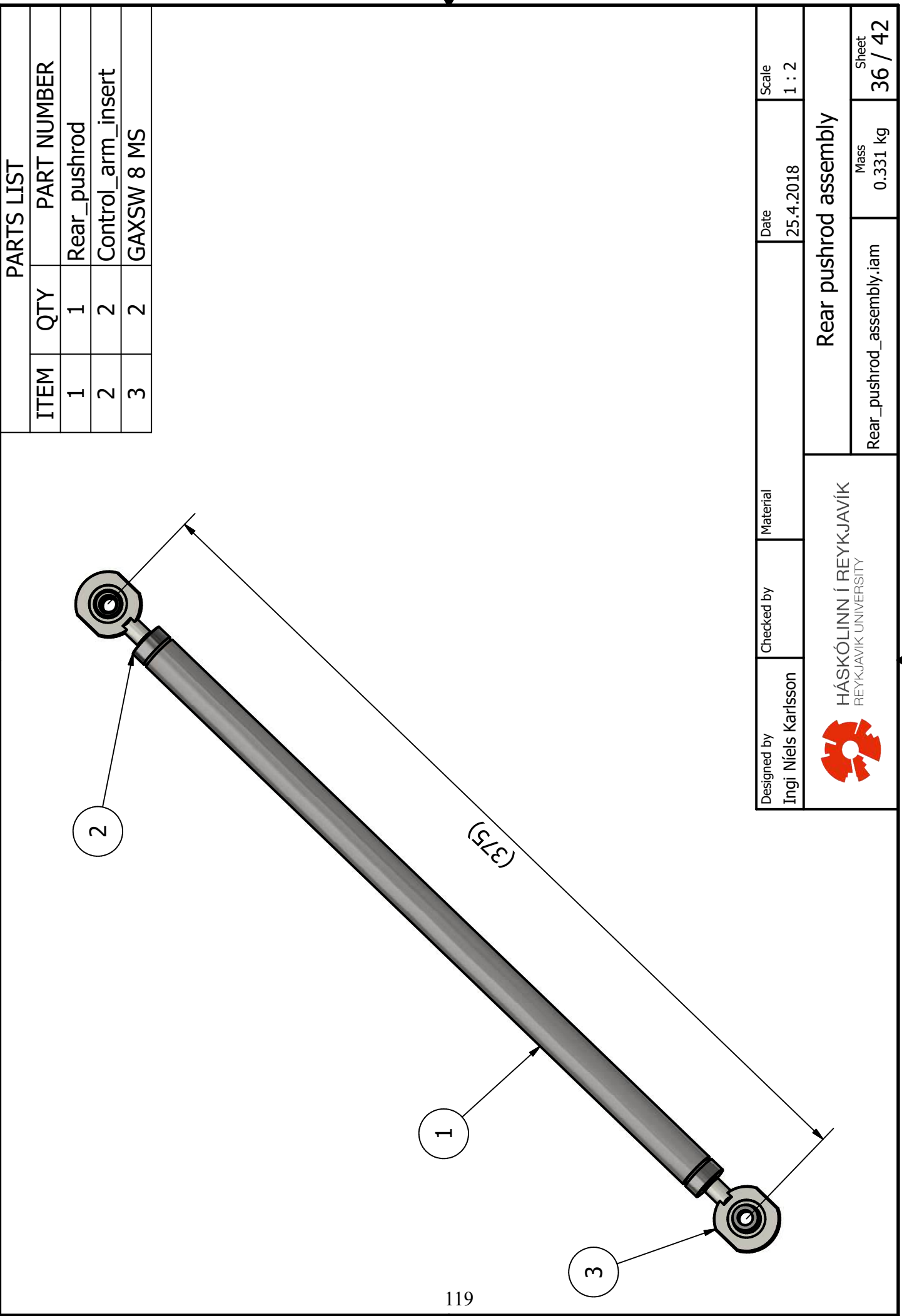
118

290

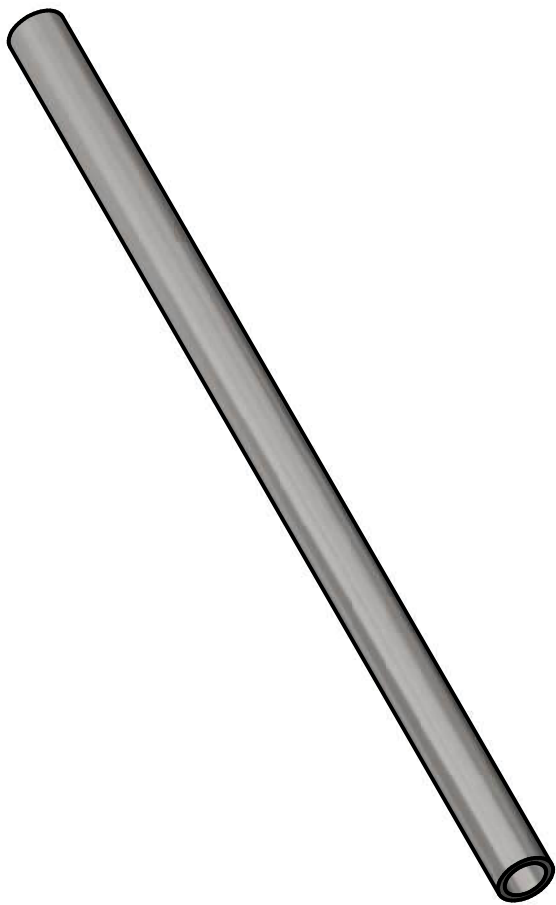
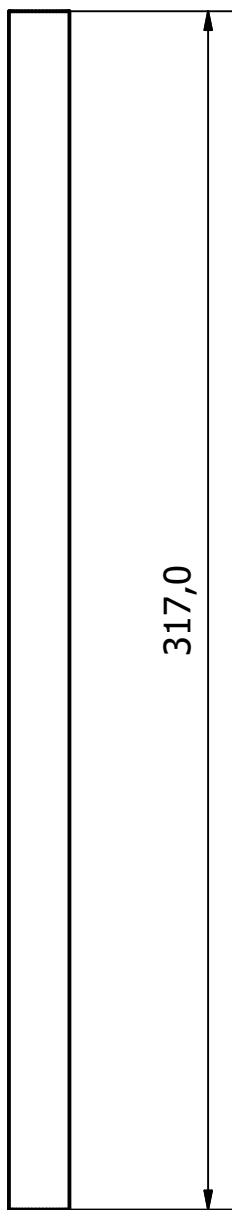
Designed by Ingi Níels Karlsson	Checked by	Material Steel, Mild	Date 25.4.2018	Scale 1 : 2
HÁSKÓLINN Í REYKJAVÍK REYKJAVÍK UNIVERSITY				Front push rod
Front_pushrod.ipt		Mass 0.179 kg	Sheet 35 / 42	



4



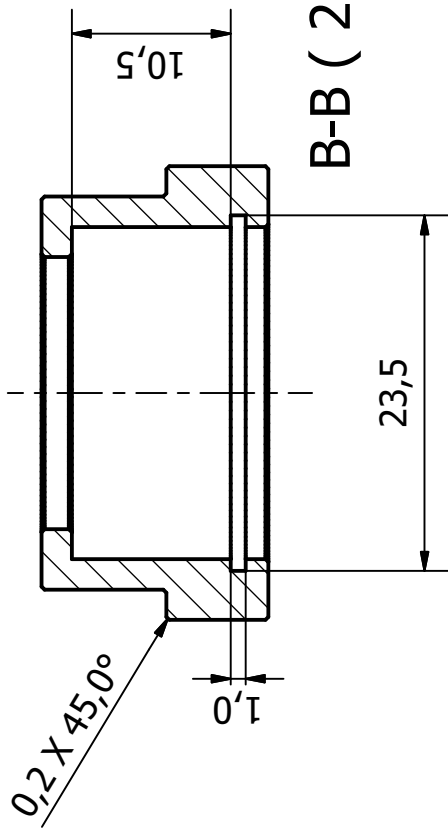
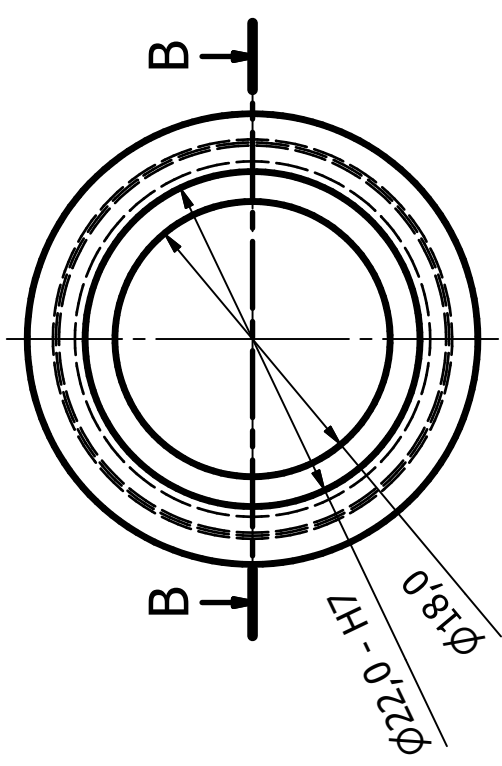
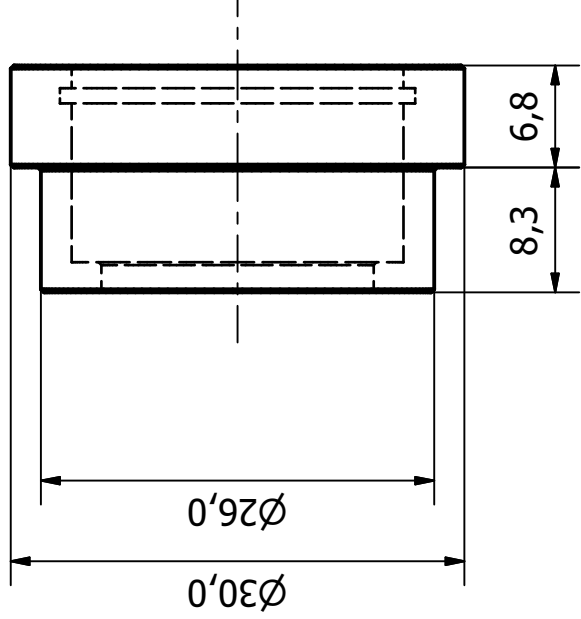
$\varnothing 16 \times 2.0$  mm S235 pipe



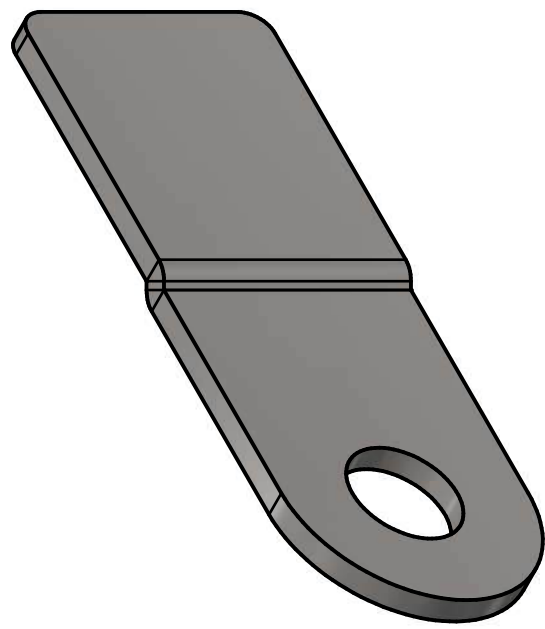
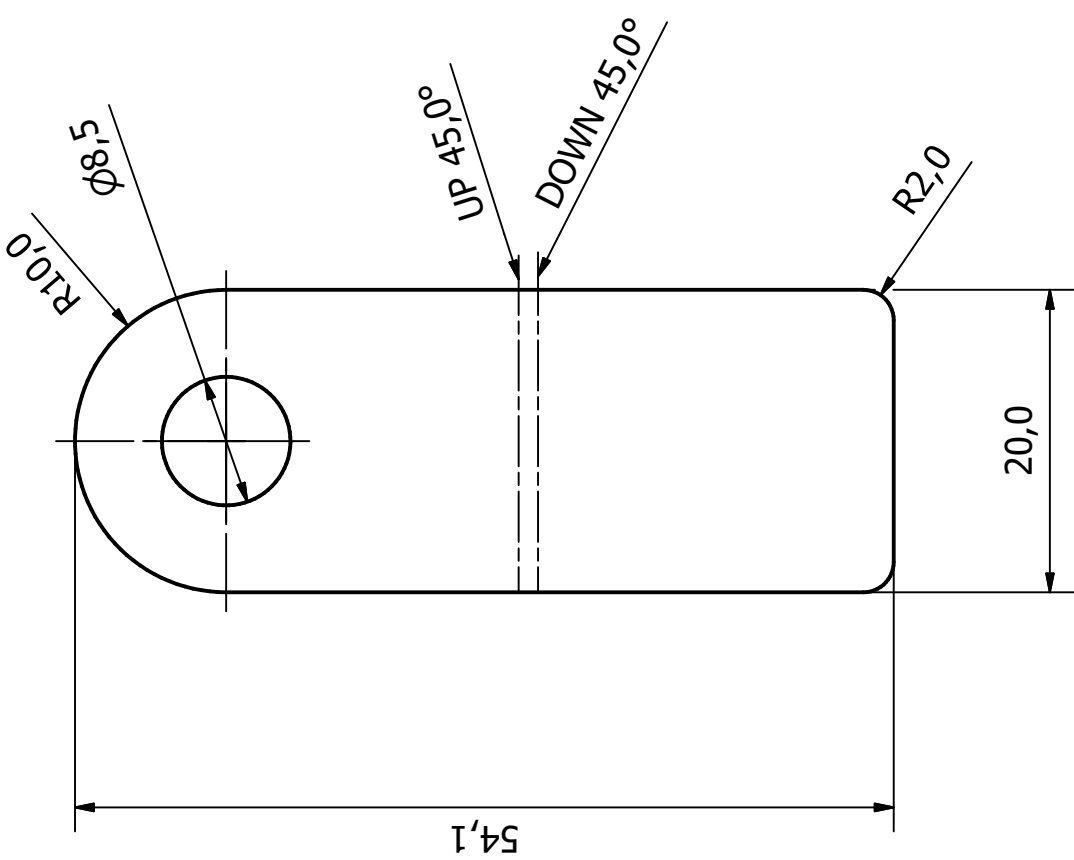
120

Designed by Ingi Níels Karlsson	Checked by	Material Steel, Mild	Date 25.4.2018	Scale 1 : 2
Rear pushrod				
HÁSKÓLINN Í REYKJAVÍK REYKJAVÍK UNIVERSITY	Rear_pushrod.ipt	Mass 0,219 kg	Sheet 37 / 42	

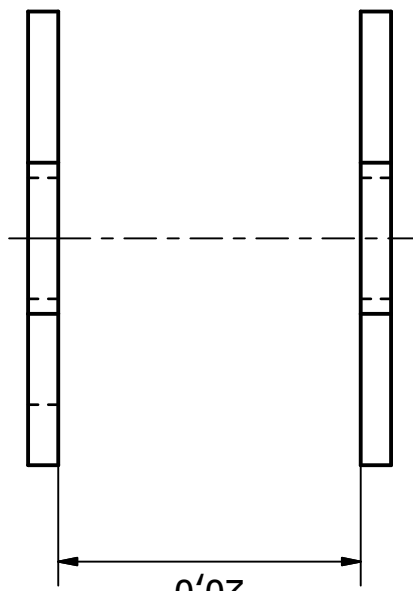
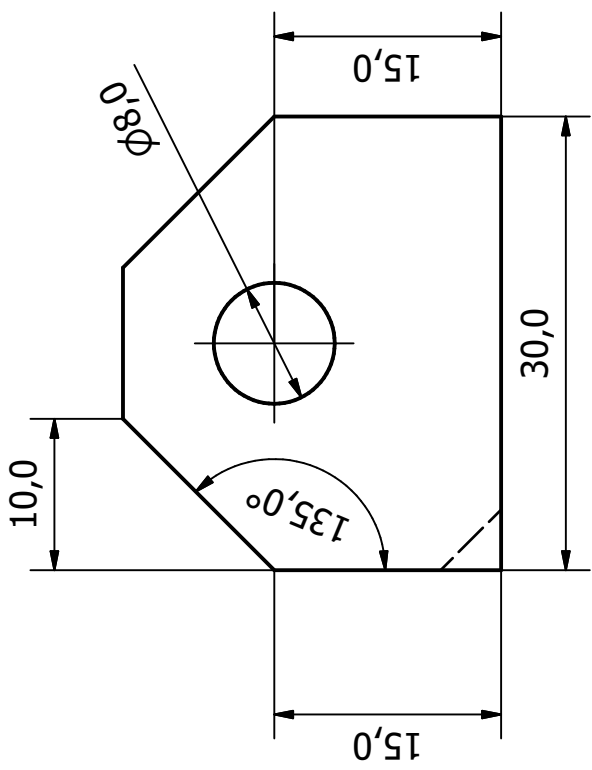
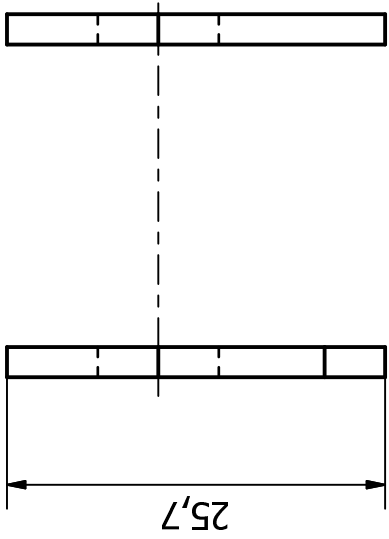
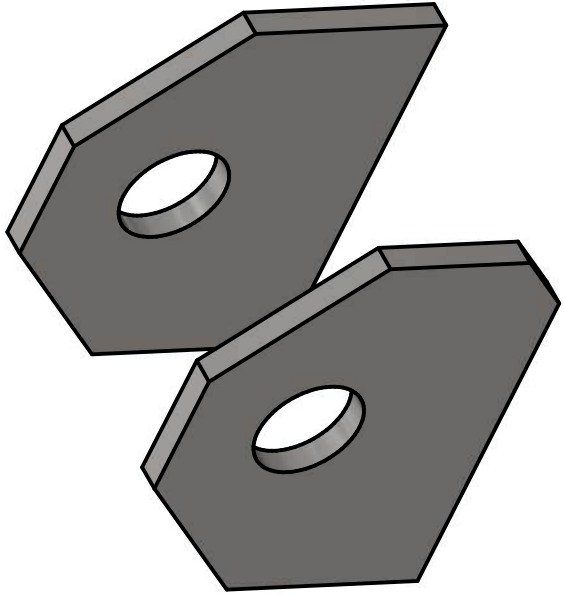
4



Designed by Ingi Níels Karlsson	Checked by	Material Steel, High Strength, Low Alloy	Date 25.4.2018	Scale 2 : 1
<b>Spherical bearing seat</b>				
Ball_joint_bearing_seat.ipt	Mass 0,029 kg	Sheet 38 / 42		



Designed by Ingi Níels Karlsson	Checked by	Material Steel, Mild	Date 25.4.2018	Scale 2 : 1
Control arm link plate				HÁSKÓLINN Í REYKJAVÍK REYKJAVÍK UNIVERSITY
Control_arm_plate_insert.ckpt	Mass 0,015 kg	Sheet 39 / 42		



123

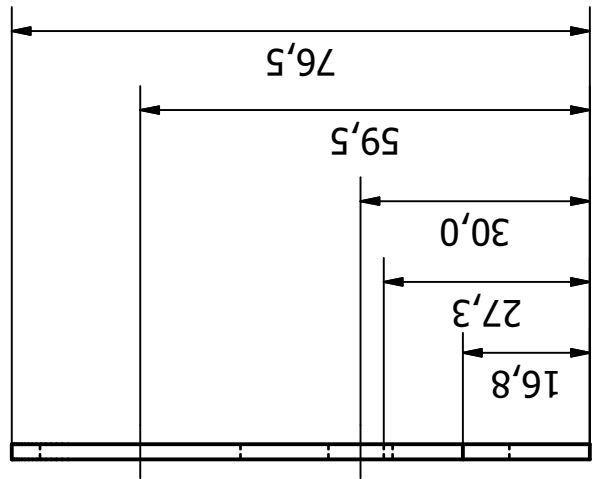
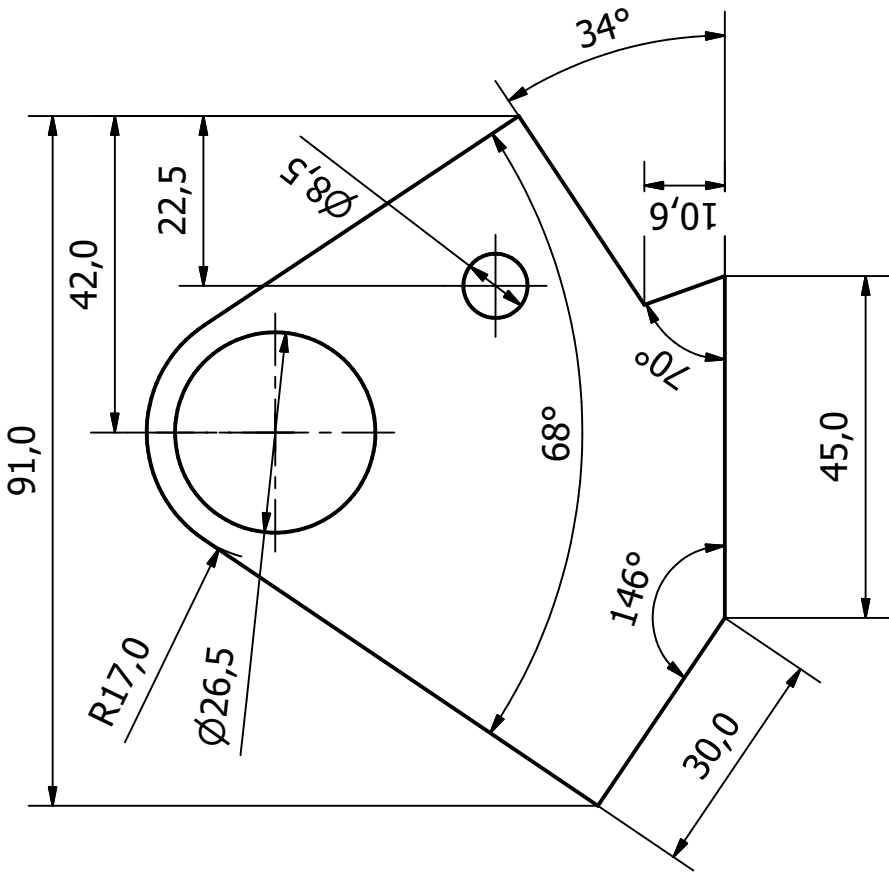
Designed by Ingi Níels Karlsson	Checked by	Material Steel, Mild	Date 25.4.2018	Scale 2 : 1
<b>Push rod bracket</b>				
Front_pushrod_uca_bracket.ipt				Mass 0.019 kg

HÁSKÓLINN Í REYKJAVÍK  
REYKJAVÍK UNIVERSITY



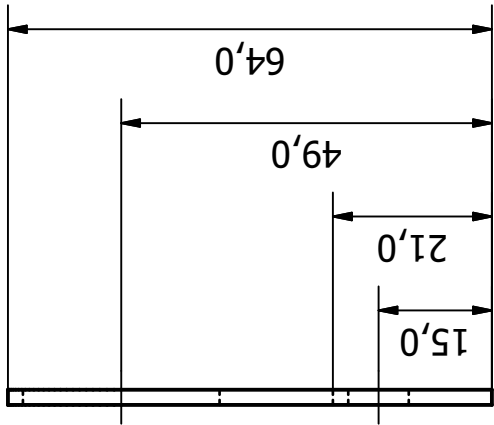
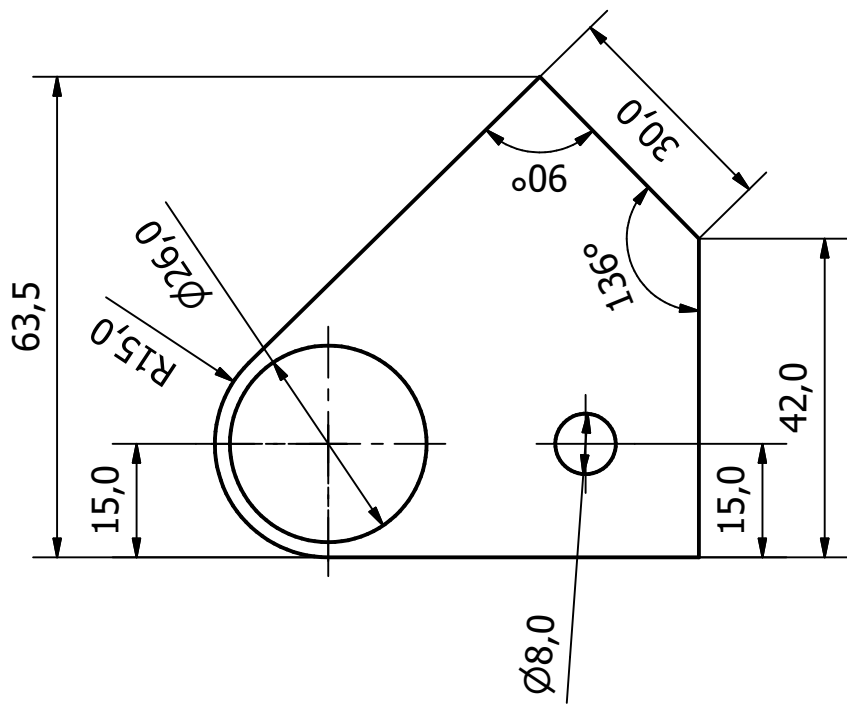
Sheet  
40 / 42

2 mm cold rolled steel S235



Designed by Ingi Níels Karlsson	Checked by	Material Steel, Mild	Date 25.4.2018	Scale 1 : 1
Front control arm plate				HÁSKÓLINN Í REYKJAVÍK REYKJAVÍK UNIVERSITY
Front_control_arm_plate.ckpt	Mass 0.058 kg	Sheet 41 / 42		

2 mm cold rolled steel S235



Designed by Ingi Níels Karlsson	Checked by	Material Steel, Mild	Date 25.4.2018	Scale 1 : 1
<b>Rear control arm plate</b>				
Rear_control_arm_plate.ipt	Mass 0.036 kg	Sheet 42 / 42		



HÁSKÓLINN Í REYKJAVÍK  
REYKJAVÍK UNIVERSITY



# **Appendix C**

## **Tables and calculations**

### **C.1 Hard point table**

front_lca_front_x	410	mm
front_lca_front_y	-260	mm
front_lca_front_z	105	mm
front_lca_rear_x	810	mm
front_lca_rear_y	-285	mm
front_lca_rear_z	105	mm
front_lca_bj_x	610	mm
front_lca_bj_y	-590	mm
front_lca_bj_z	111	mm
front_uca_front_x	410	mm
front_uca_front_y	-260	mm
front_uca_front_z	280	mm
front_uca_rear_x	810	mm
front_uca_rear_y	-285	mm
front_uca_rear_z	280	mm
front_uca_bj_x	620	mm
front_uca_bj_y	-570	mm
front_uca_bj_z	297	mm
front_damper_chassis_x	615	mm
front_damper_chassis_y	-50	mm
front_damper_cassis_z	590	mm
front_bc_chassis_x	615	mm
front_bc_chassis_y	-190	mm
front_bc_chassis_z	540	mm
front_pushrod_outer_x	620	mm
front_pushrod_outer_y	-526	mm
front_pushrod_outer_z	309	mm
front_pushrod_inner_x	615	mm
front_pushrod_inner_y	-250	mm
front_pushrod_inner_z	590	mm
front_tierod_outer_x	670	mm
front_tierod_outer_y	-560	mm
front_tierod_outer_z	132	mm
front_tierod_inner_x	670	mm
front_tierod_inner_y	-270	mm
front_tierod_inner_z	125	mm
front_damper_bc_x	615	mm
front_damper_bc_y	-220	mm
front_damper_bc_z	630	mm
front_wheel_center_x	615	mm
front_wheel_center_y	-624	mm
front_wheel_center_z	201.5	mm
front_anti_roll_bar_bell_crank_x	592	mm
front_anti_roll_bar_bell_crank_y	-250	mm
front_anti_roll_bar_bell_crank_z	590	mm
front_anti_roll_bar_pushrod_x	592	mm
front_anti_roll_bar_pushrod_y	-280	mm
front_anti_roll_bar_pushrod_z	80	mm
front_anti_roll_bar_arm_to_anti_rollbar_x	500	mm
front_anti_roll_bar_arm_to_anti_rollbar_y	-270	mm

front_anti_roll_bar_arm_to_anti_rollbar_z	80	mm
rear_lca_front_x	1954	mm
rear_lca_front_y	-270	mm
rear_lca_front_z	70	mm
rear_lca_rear_x	2260	mm
rear_lca_rear_y	-270	mm
rear_lca_rear_z	70	mm
rear_lca_bj_x	2200	mm
rear_lca_bj_y	-600	mm
rear_lca_bj_z	111	mm
rear_uca_front_x	1954	mm
rear_uca_front_y	-270	mm
rear_uca_front_z	245	mm
rear_uca_rear_x	2260	mm
rear_uca_rear_y	-270	mm
rear_uca_rear_z	255	mm
rear_uca_bj_x	2200	mm
rear_uca_bj_y	-575	mm
rear_uca_bj_z	292	mm
rear_damper_chassis_x	2240	mm
rear_damper_chassis_y	-50	mm
rear_damper_cassis_z	350	mm
rear_bc_chassis_x	2230	mm
rear_bc_chassis_y	-210	mm
rear_bc_chassis_z	330	mm
rear_pushrod_outer_x	2190	mm
rear_pushrod_outer_y	-540	mm
rear_pushrod_outer_z	120	mm
rear_pushrod_inner_x	2230	mm
rear_pushrod_inner_y	-270	mm
rear_pushrod_inner_z	380	mm
rear_tierod_outer_x	2250	mm
rear_tierod_outer_y	-590	mm
rear_tierod_outer_z	135	mm
rear_tierod_inner_x	2260	mm
rear_tierod_inner_y	-270	mm
rear_tierod_inner_z	92	mm
rear_damper_bc_x	2230	mm
rear_damper_bc_y	-240	mm
rear_damper_bc_z	430	mm
rear_wheel_center_x	2200	mm
rear_wheel_center_y	-631.5	mm
rear_wheel_center_z	201.5	mm
rear_anti_roll_bar_bell_crank_x	2207	mm
rear_anti_roll_bar_bell_crank_y	-270	mm
rear_anti_roll_bar_bell_crank_z	380	mm
rear_anti_roll_bar_pushrod_x	2200	mm
rear_anti_roll_bar_pushrod_y	-285	mm
rear_anti_roll_bar_pushrod_z	50	mm
rear_anti_roll_bar_arm_to_anti_rollbar_x	2100	mm

rear_anti_roll_bar_arm_to_anti_rollbar_y	-280	mm
rear_anti_roll_bar_arm_to_anti_rollbar_z	50	mm

## C.2 Results from Adams Car

### C.2.1 Summary of forces

	Pothole simulation			
	x (N)	y (N)	z (N)	Total (N)
Front push rod to bell crank	74.5	-773.6	-832.5	<b>1138.9</b>
Front shock mount	-31.6	-1045.8	139.5	<b>1055.6</b>
Front hub	-949.9	-592.6	103.4	<b>1124.3</b>
Rear push rod to bell crank	-158.8	-857.2	-813.2	<b>1192.1</b>
Rear shock mount	-38.2	-1038.8	446.5	<b>1131.3</b>
Rear hub	1040.5	-112.2	-938.4	<b>1405.7</b>

	Plank simulation			
	x (N)	y (N)	z (N)	Total (N)
Front push rod to bell crank	188.5	-1307.9	-1387.3	<b>1915.9</b>
Front shock mount	-42.1	-1771.9	278.5	<b>1794.1</b>
Front hub	178.6	-930.8	-1501.3	<b>1775.4</b>
Rear push rod to bell crank	-337.4	-1818.2	-1737.1	<b>2537.2</b>
Rear shock mount	-80.0	-2253.2	947.1	<b>2445.5</b>
Rear hub	621.4	199.6	-1790.6	<b>1905.8</b>

	Corner simulation			
	x (N)	y (N)	z (N)	Total (N)
Front push rod to bell crank	361.5	-372.3	-403.0	<b>657.0</b>
Front shock mount	395.7	-409.8	12.3	<b>569.8</b>
Front hub	-419.4	-145.2	108.9	<b>457.0</b>
Rear push rod to bell crank	298.4	-305.7	-306.2	<b>525.6</b>
Rear shock mount	434.2	-444.7	140.5	<b>637.2</b>
Rear hub	-100.3	91.8	-329.8	<b>356.7</b>

	Tilt simulation			
	x (N)	y (N)	z (N)	Total (N)
Front push rod to bell crank	44.2	-409.9	-628.7	<b>751.8</b>
Front shock mount	-30.8	-478.9	-266.7	<b>549.0</b>
Front hub	-745.6	-148.1	0.0	<b>760.2</b>
Rear push rod to bell crank	-59.1	-319.0	-511.8	<b>606.0</b>
Rear shock mount	-20.5	-555.1	-171.2	<b>581.3</b>
Rear hub	-0.1	-136.4	-543.4	<b>560.3</b>

	Parallel wheel travel simulation			
	x (N)	y (N)	z (N)	Total (N)
Front push rod to bell crank	-101.1	-3533.8	-3245.2	<b>4798.9</b>
Front shock mount	-41.2	-1044.5	1078.0	<b>1501.6</b>
Front hub	0.0	0.0	-3843.0	<b>3843.0</b>
Rear push rod to bell crank	-398.5	-2781.9	-2481.3	<b>3748.9</b>
Rear shock mount	-172.5	-2804.2	1455.4	<b>3164.1</b>
Rear hub	0.0	0.0	-2762.9	<b>2762.9</b>

### C.2.2 Pothole simulation

Full vehicle simulation driving in a 150 mm pothole during acceleration.

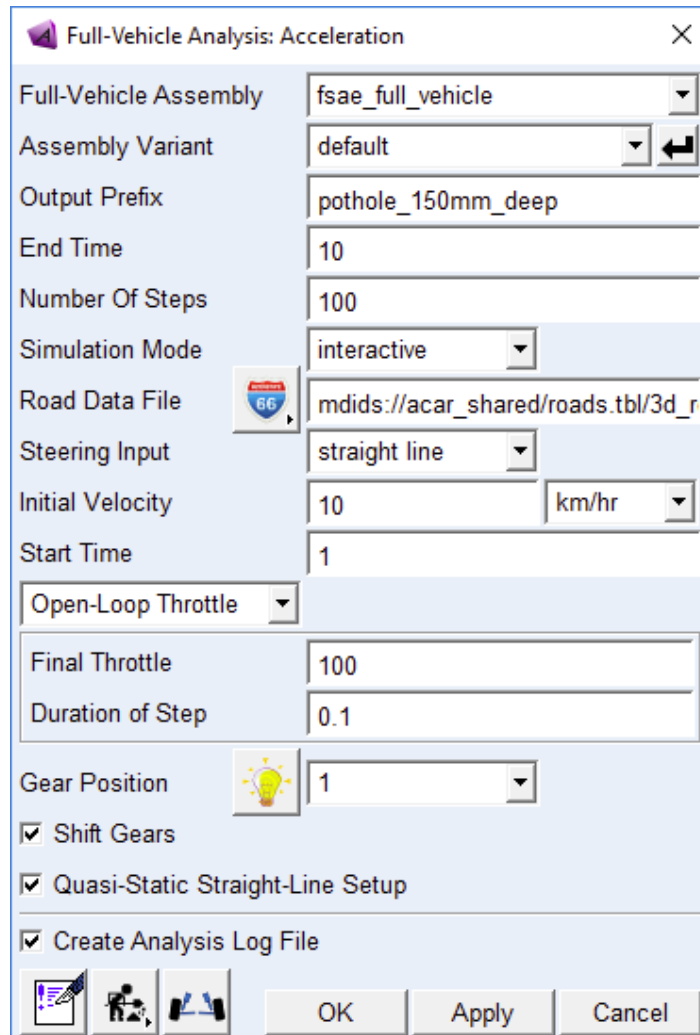
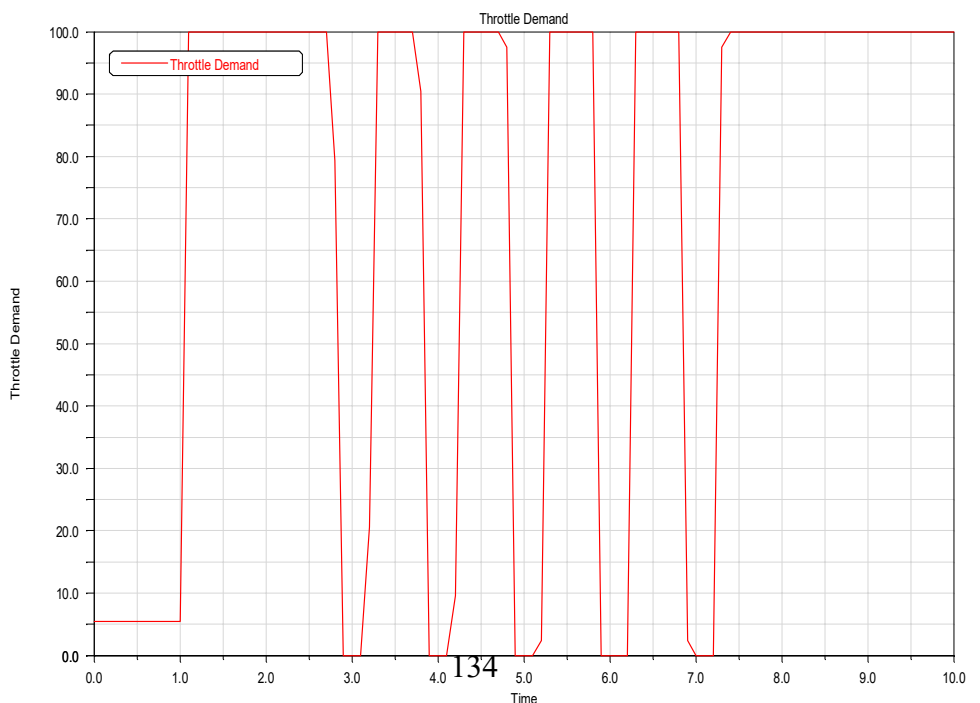
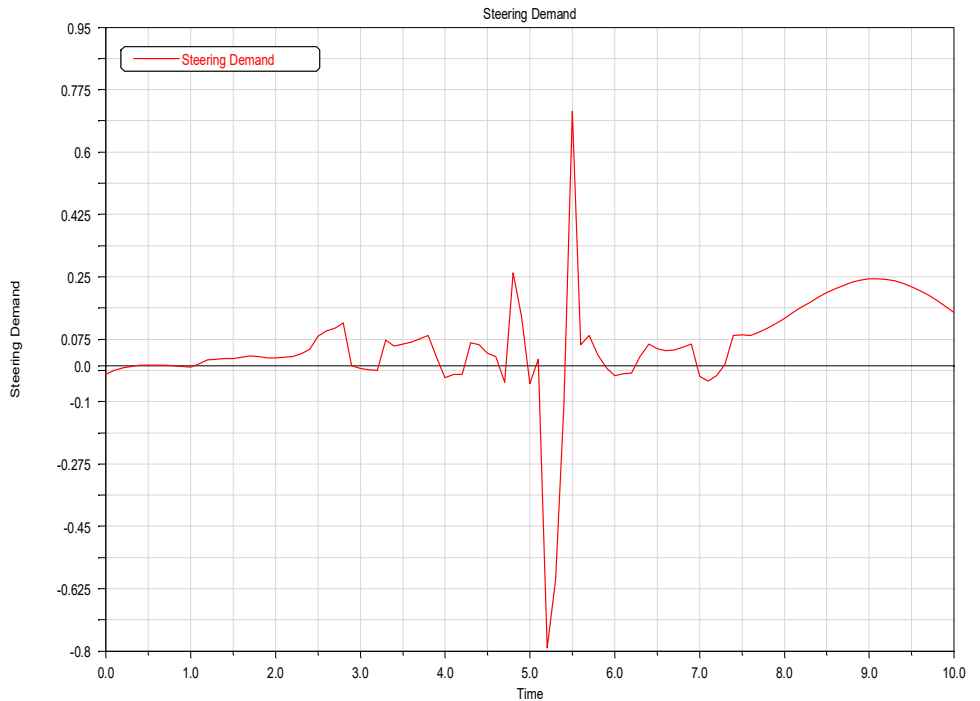
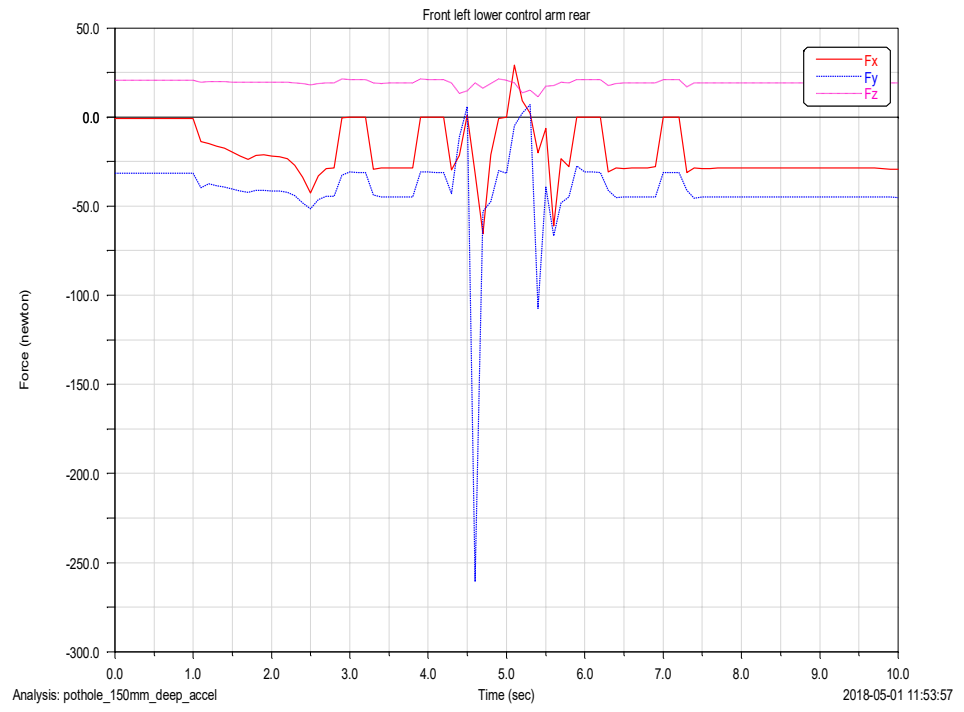
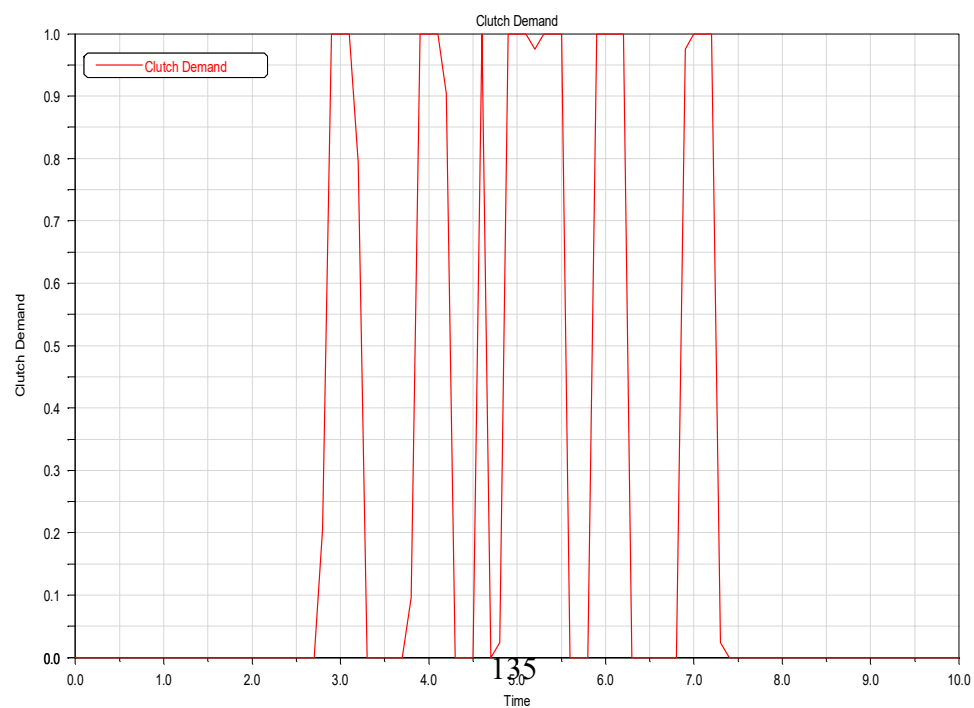
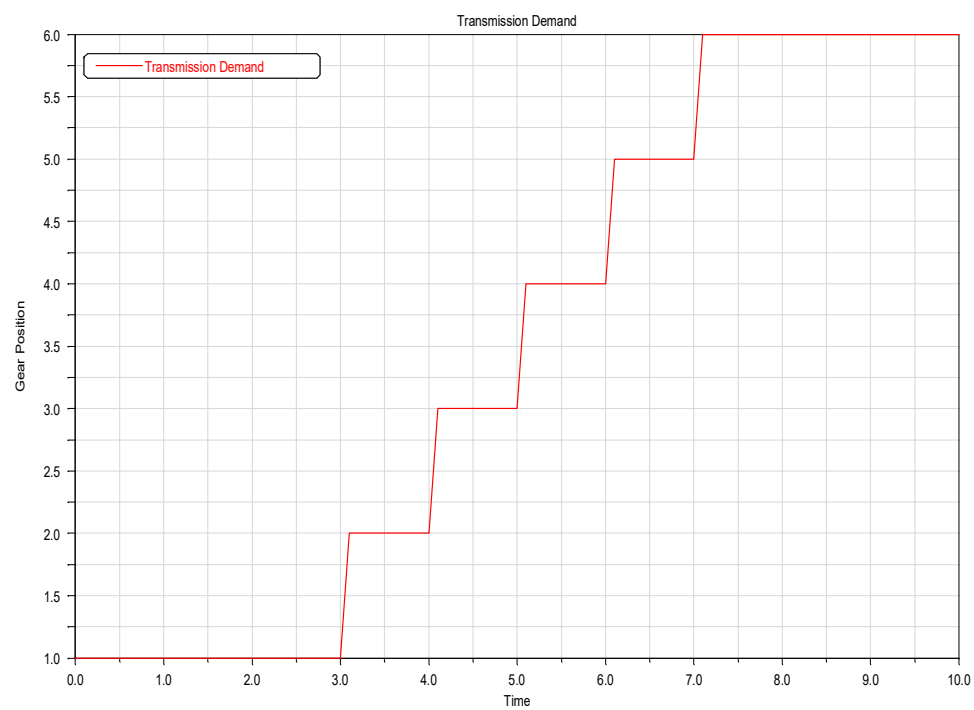
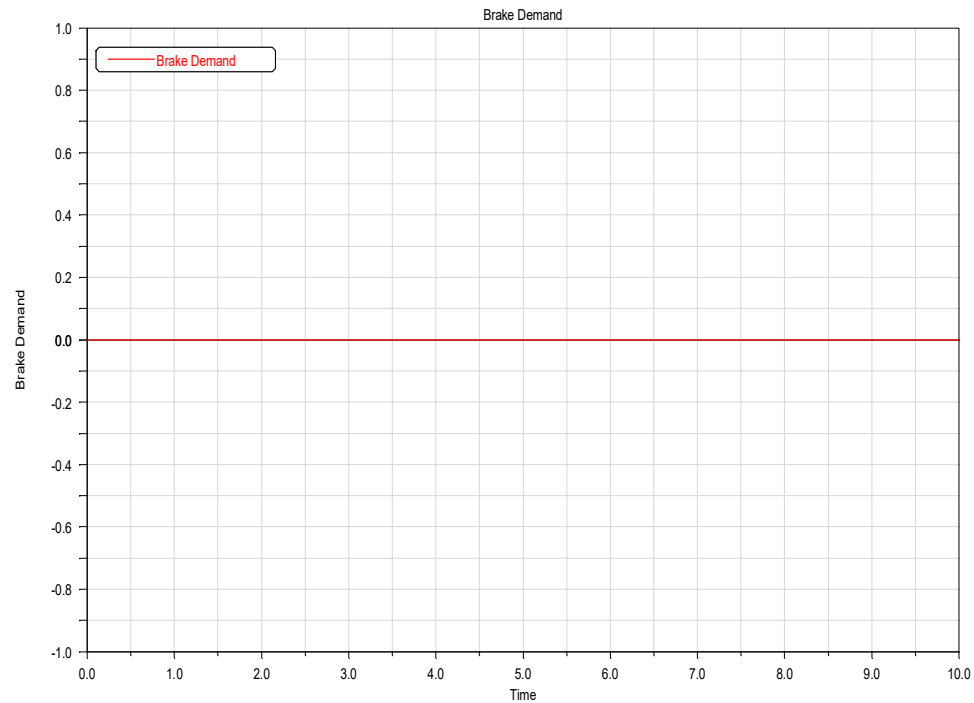
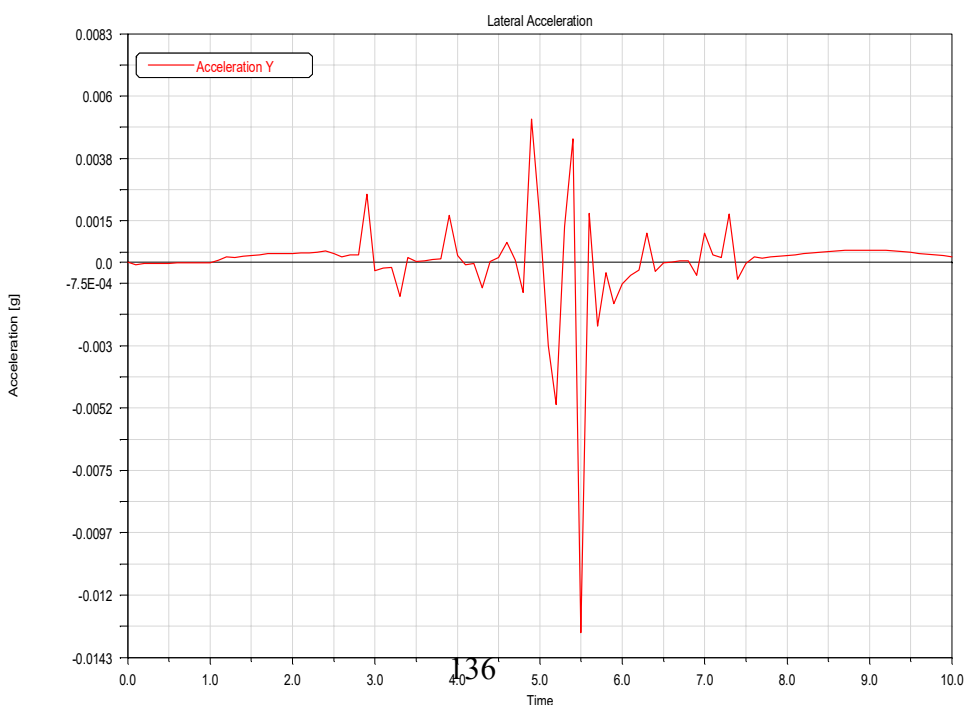
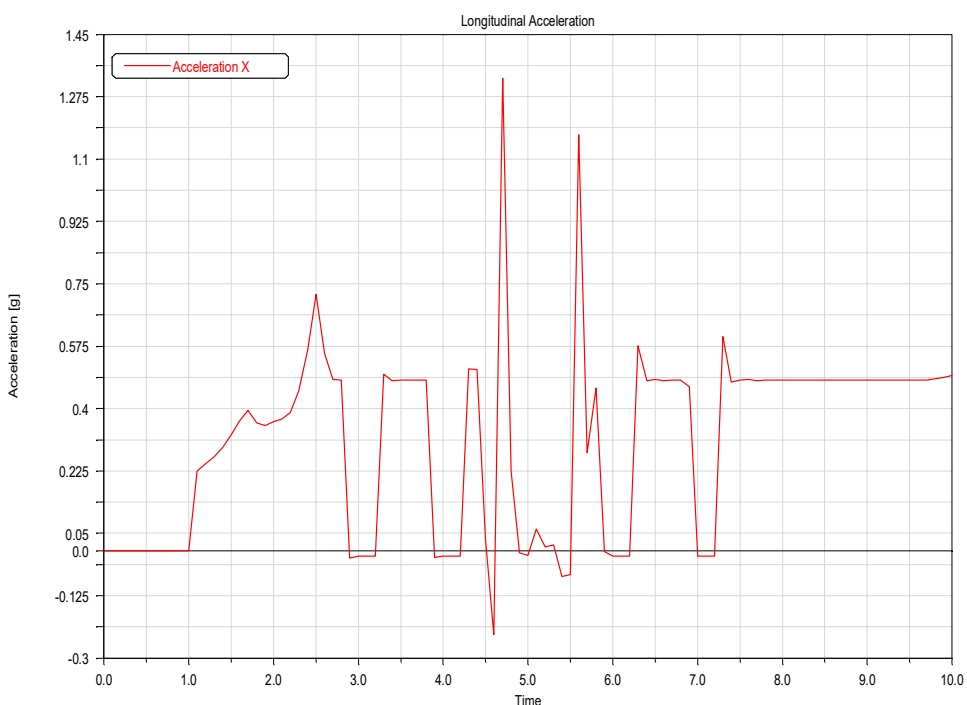
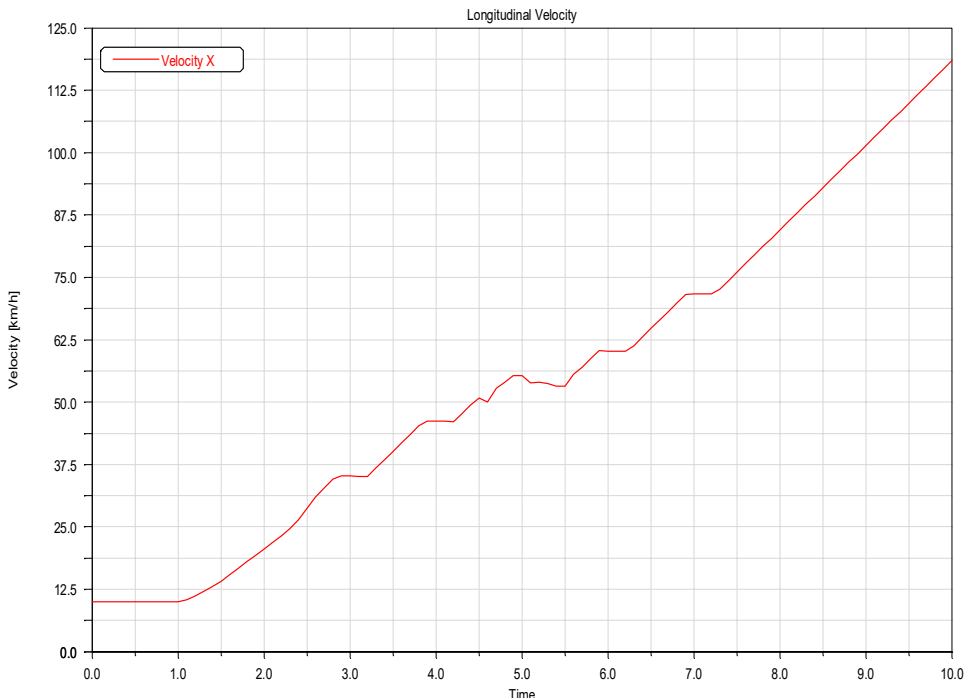
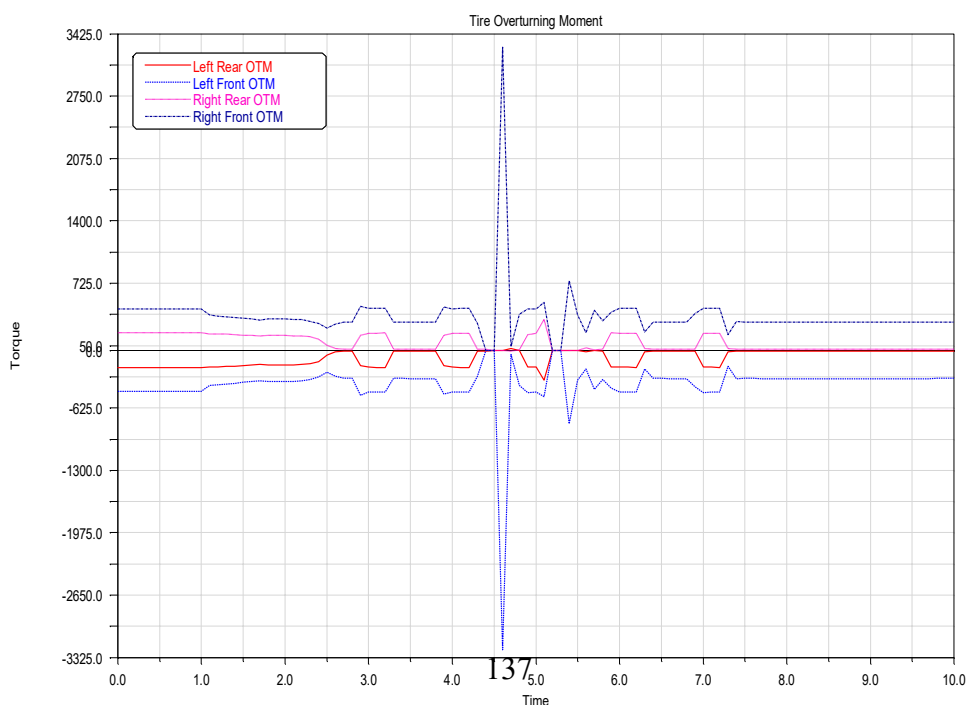
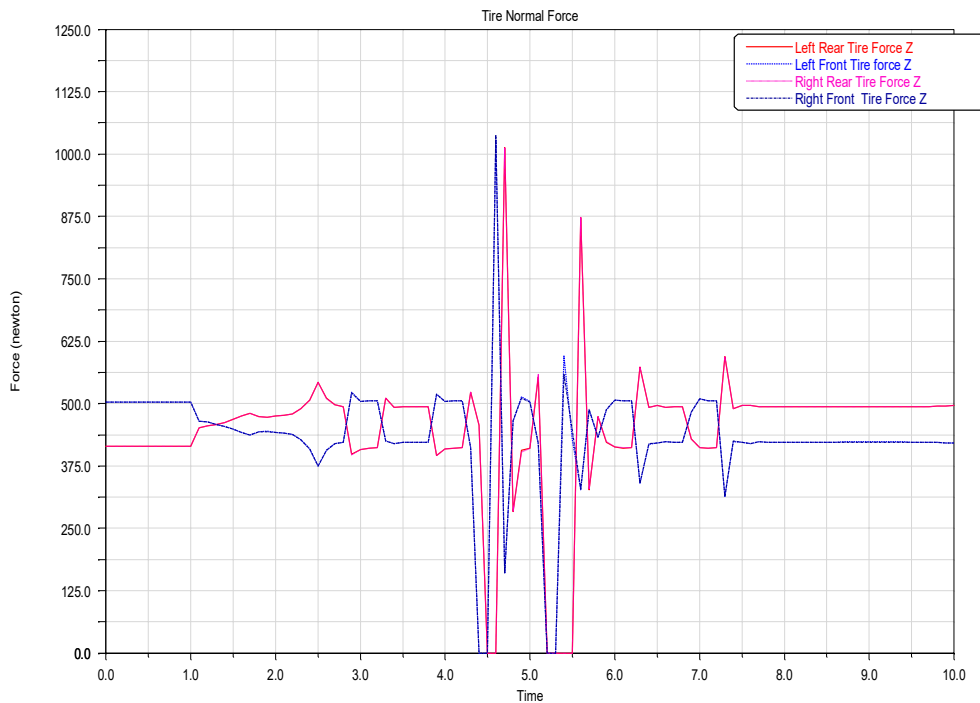
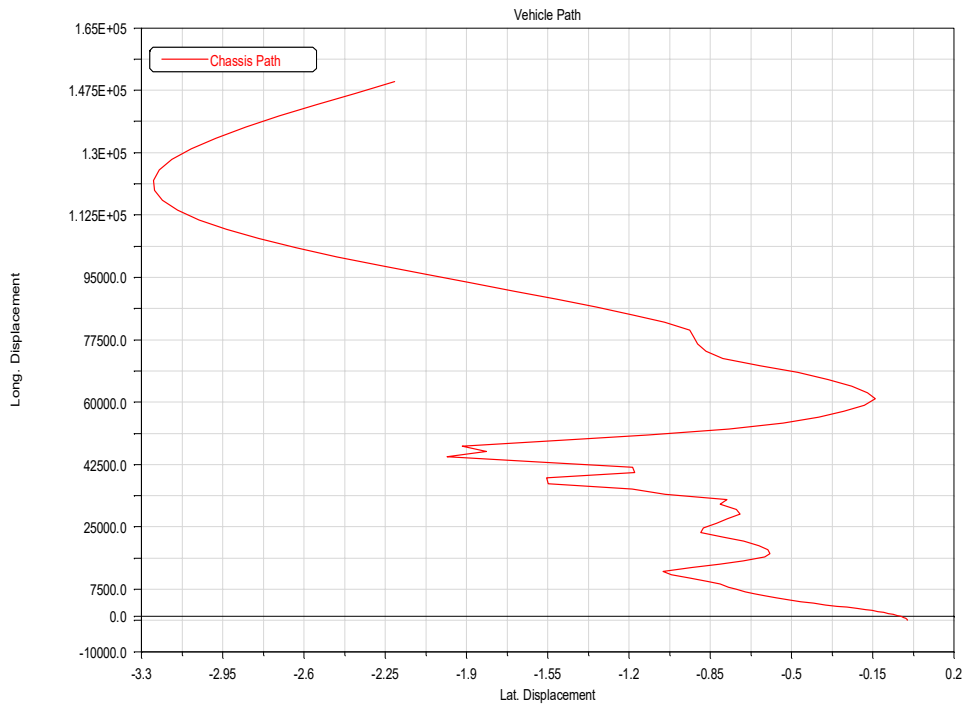


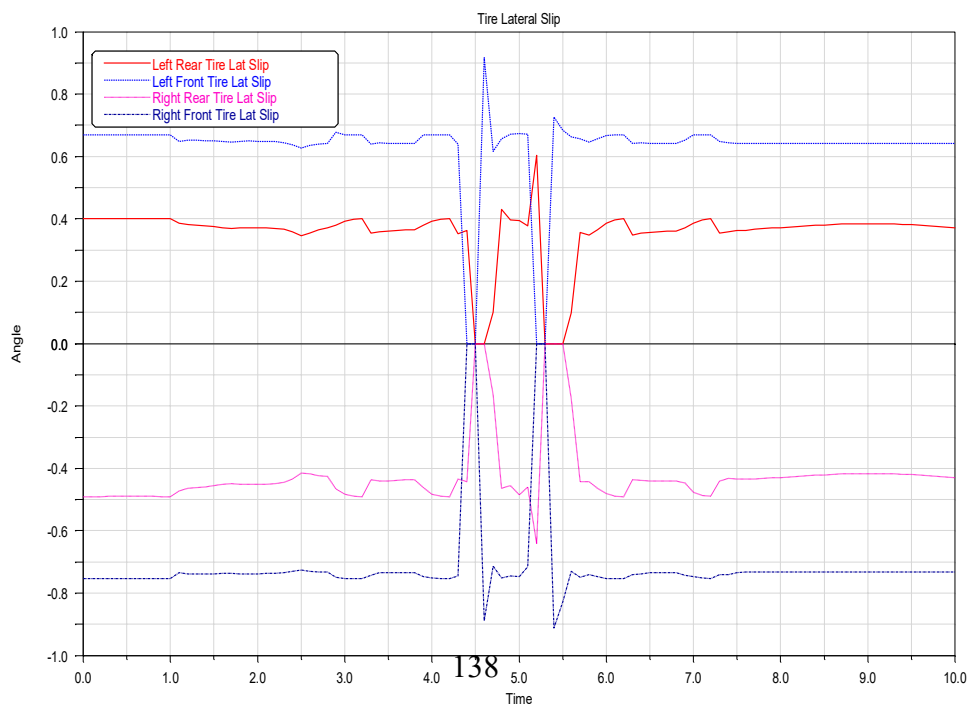
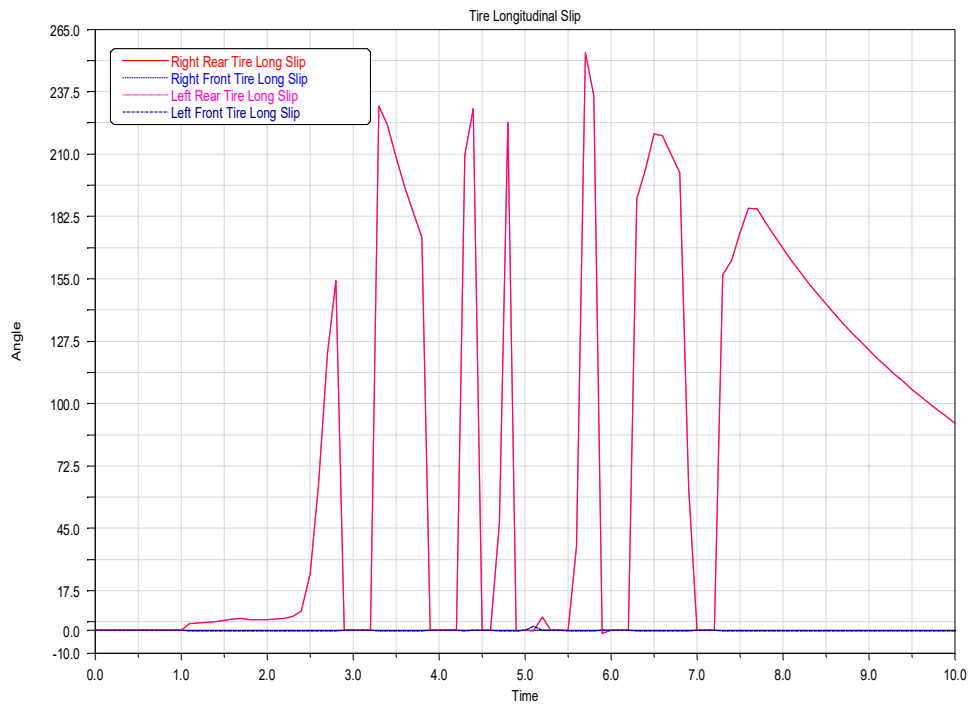
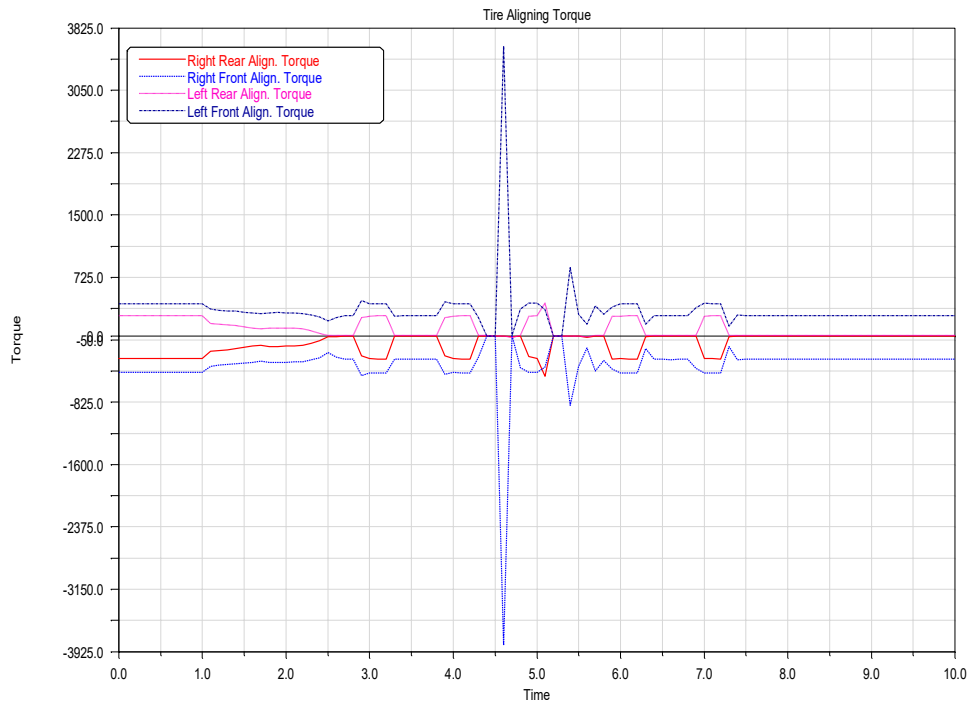
Figure C.1: Adams car [4] pothole simulation setup window

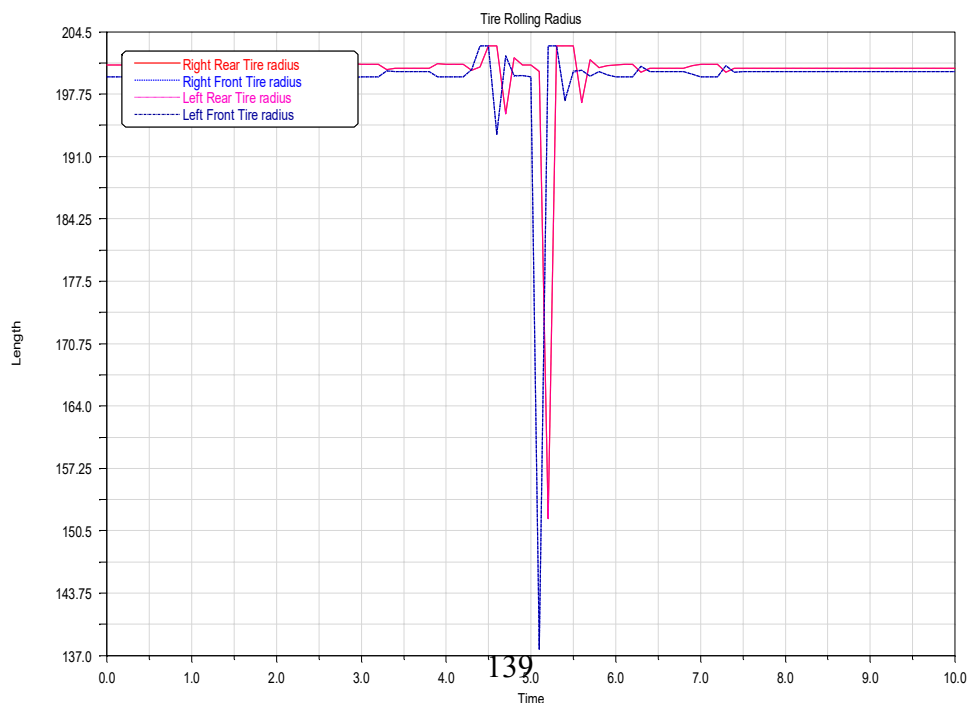
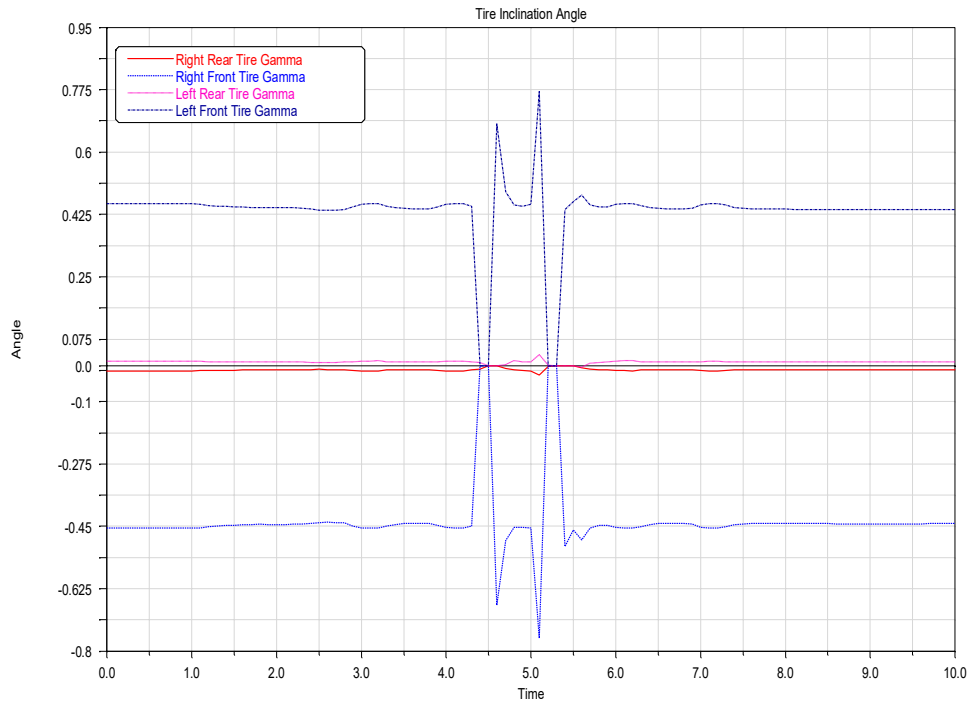
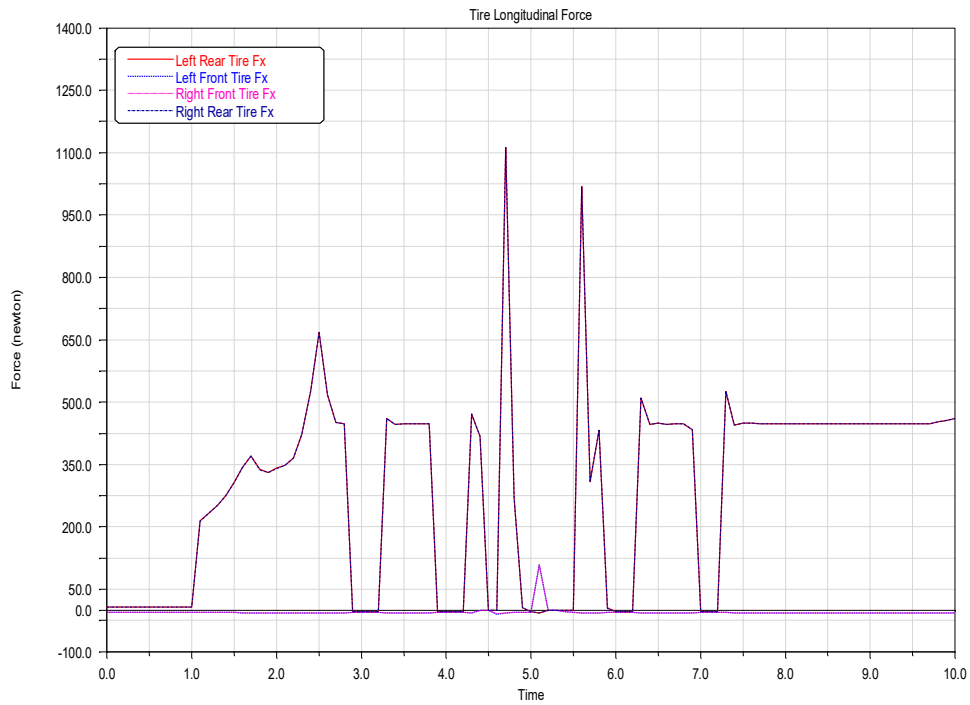


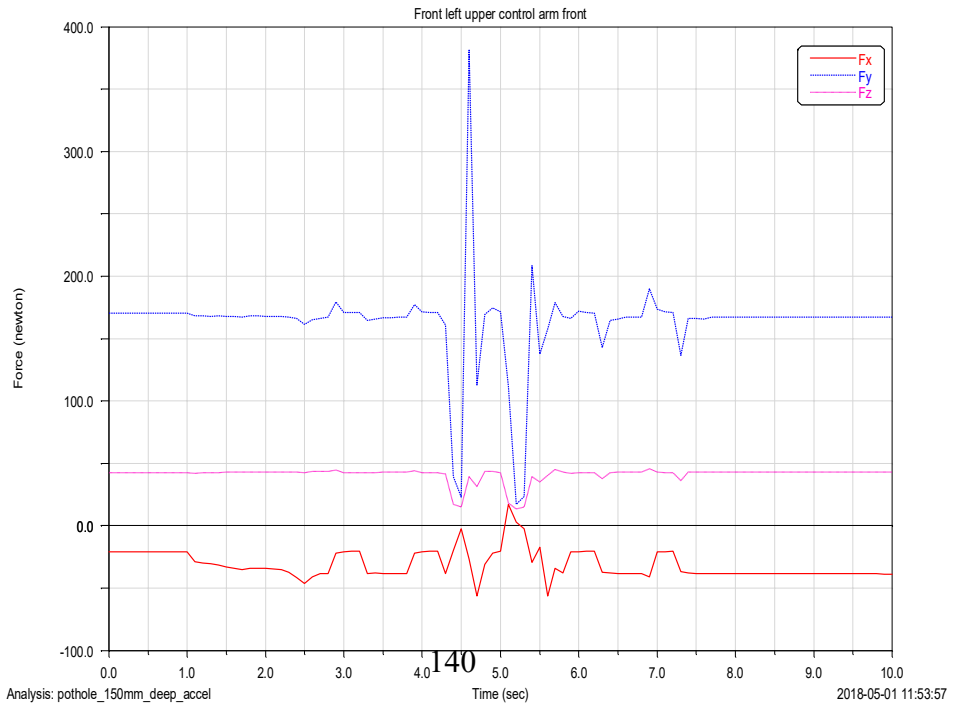
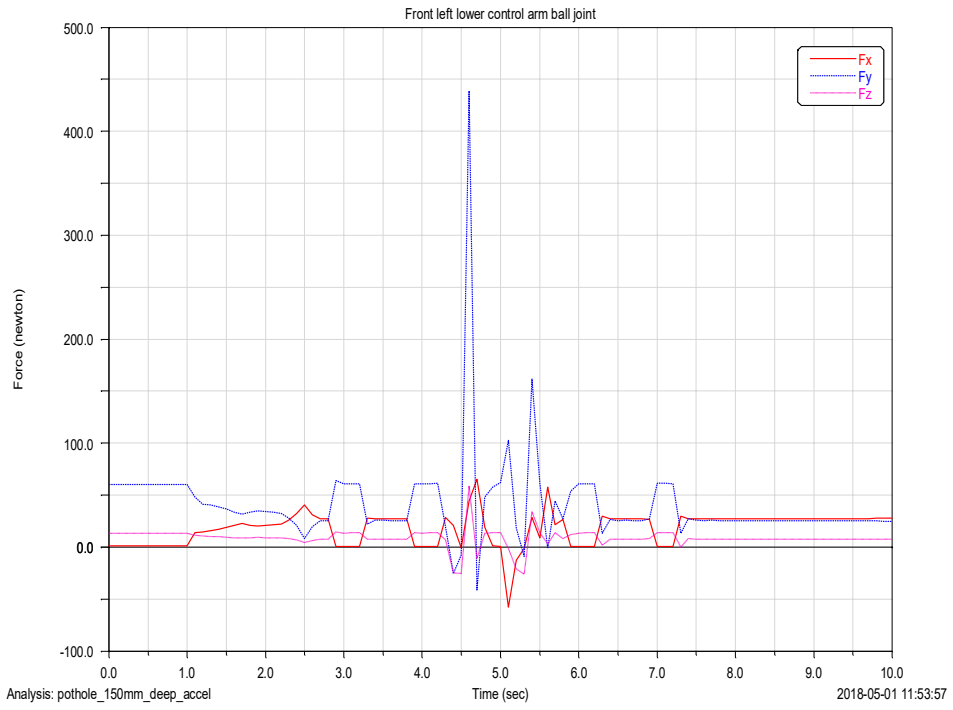
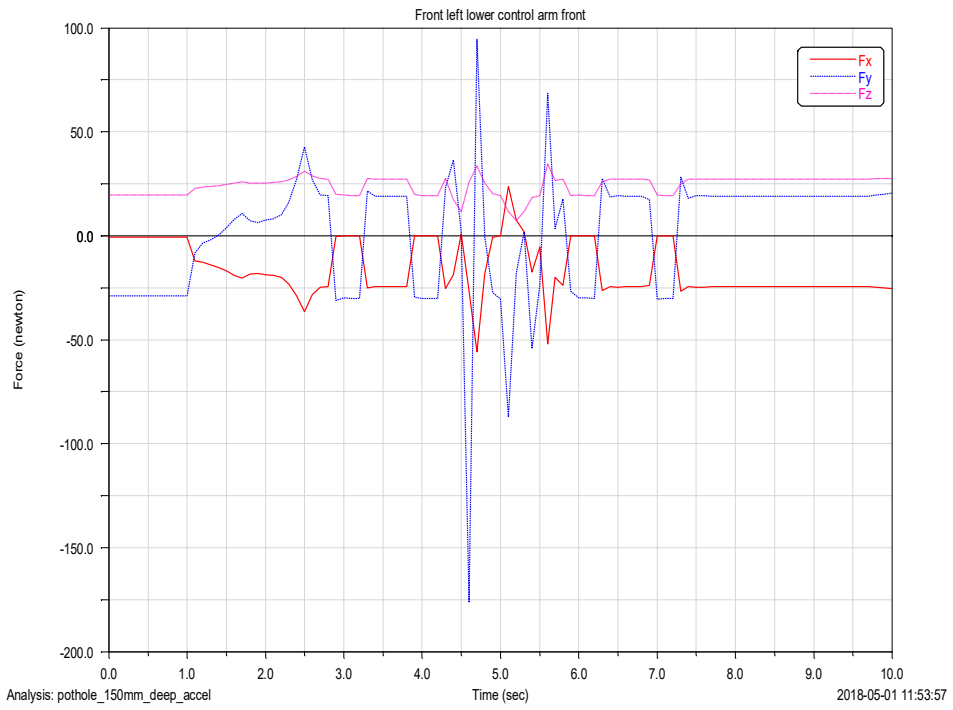


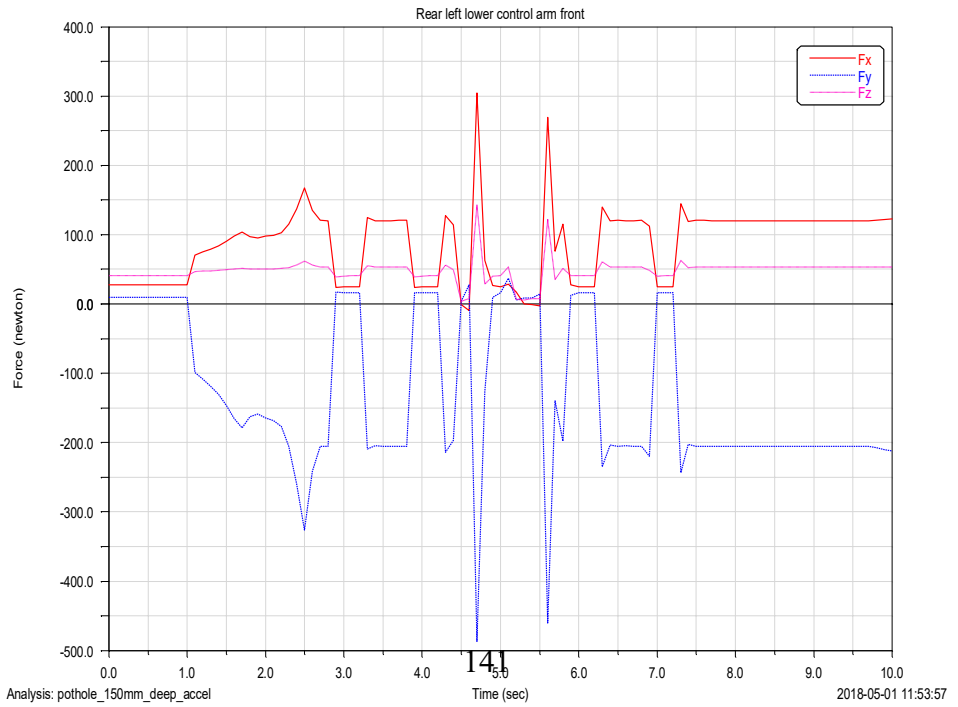
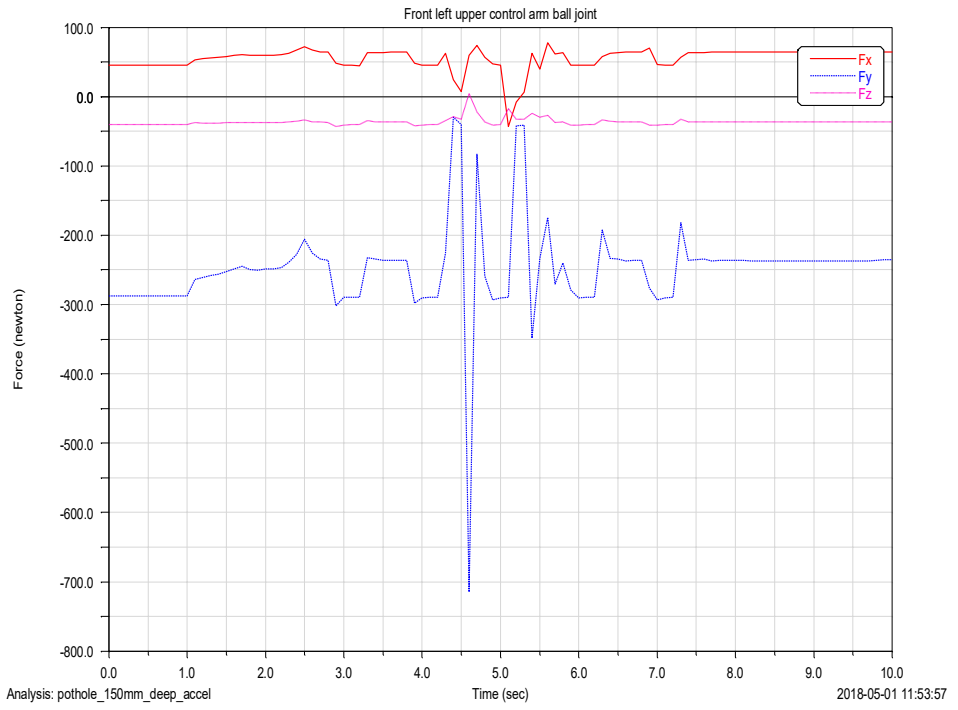
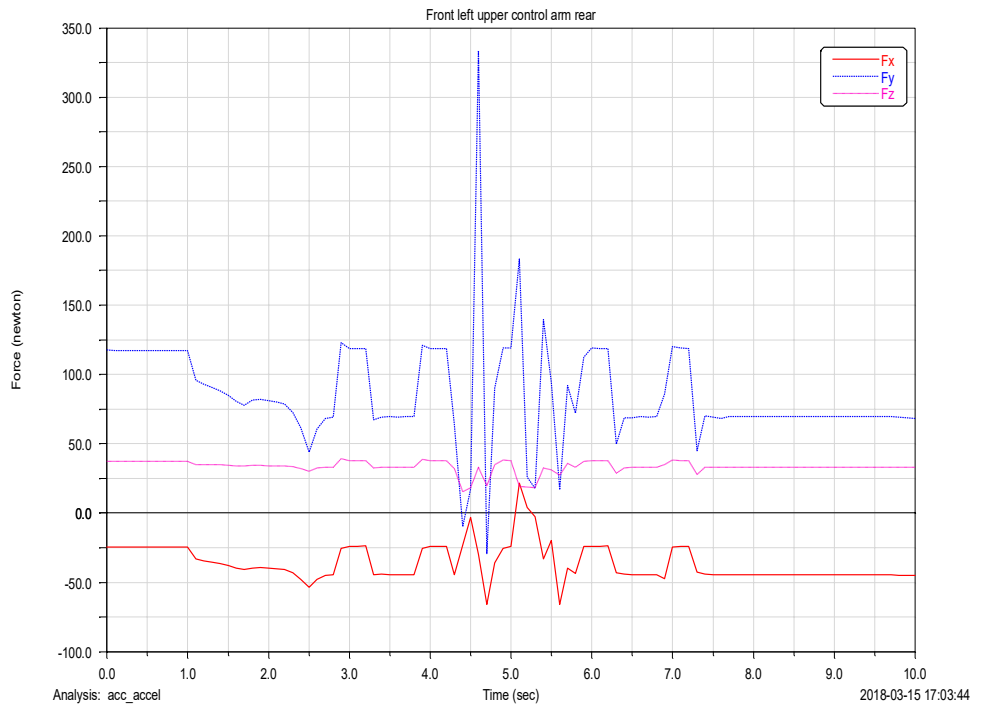


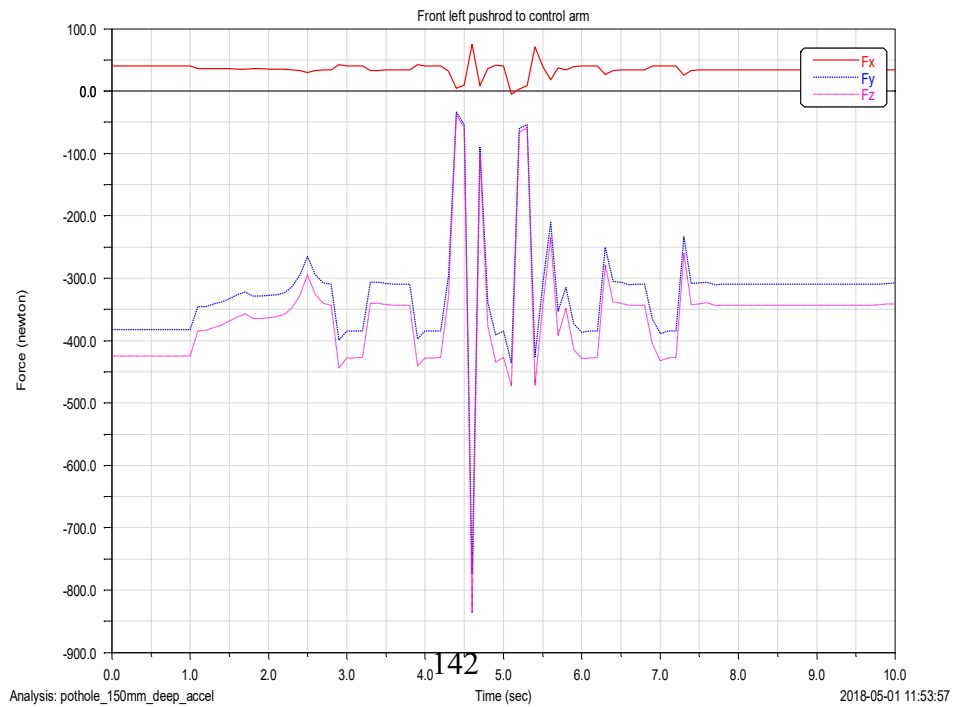
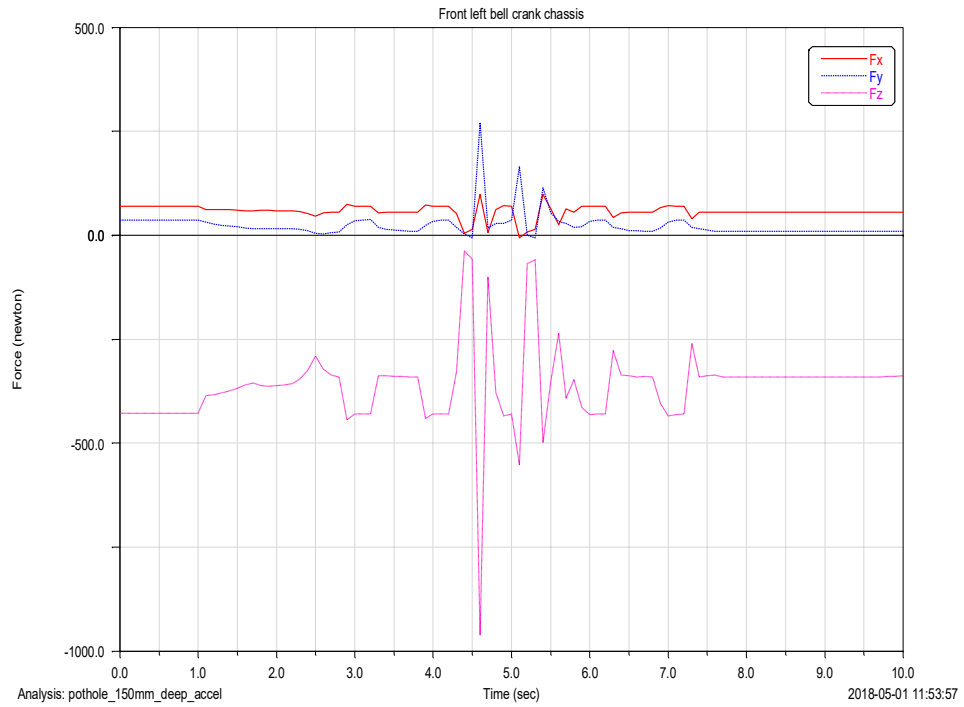
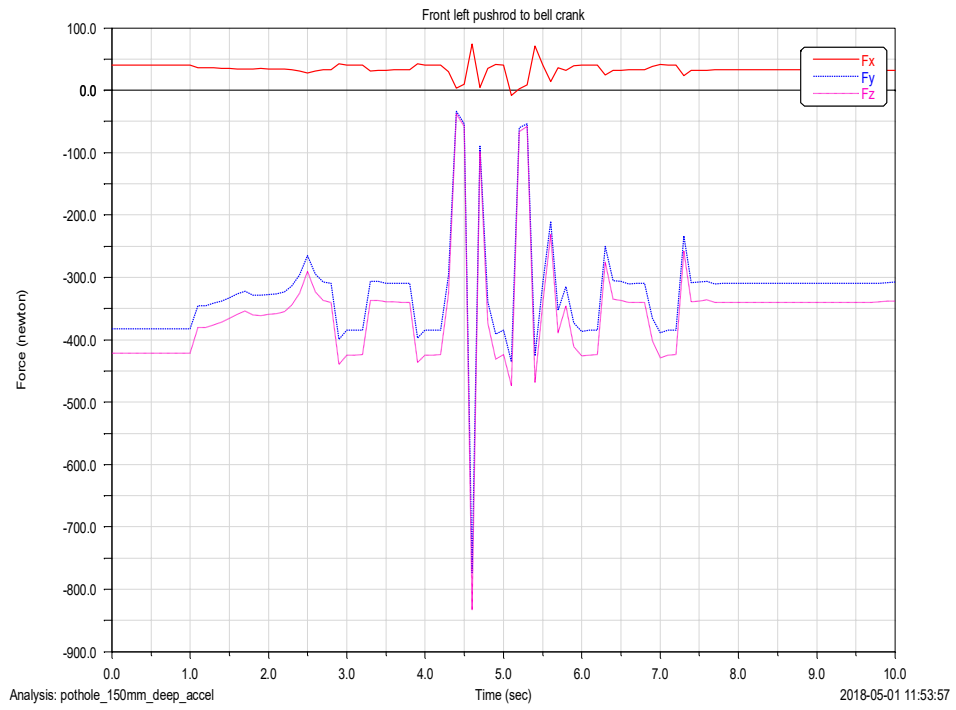


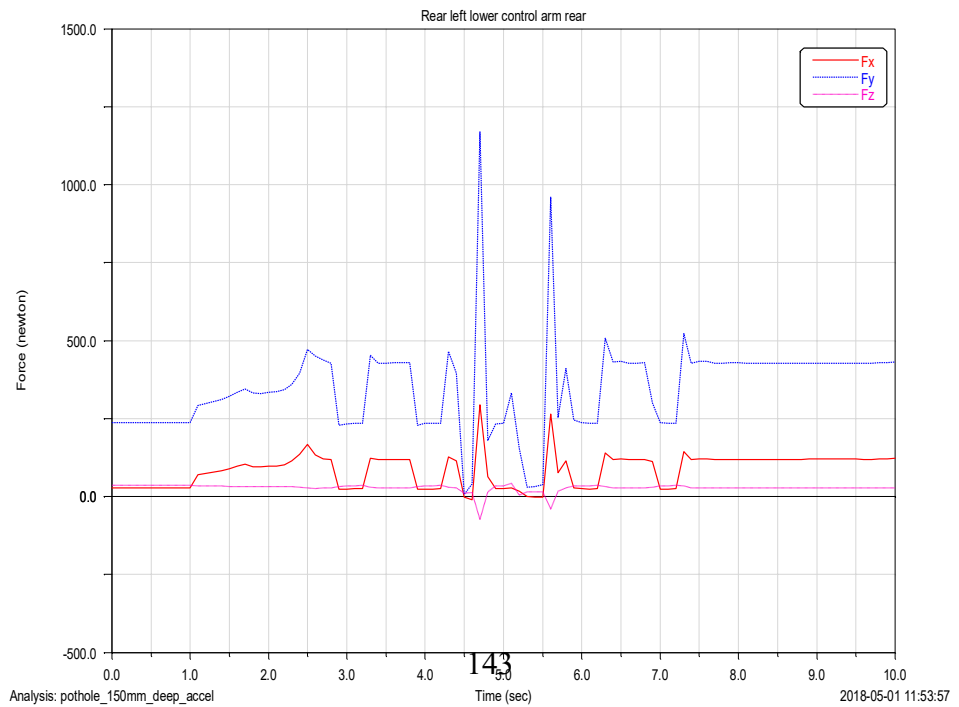
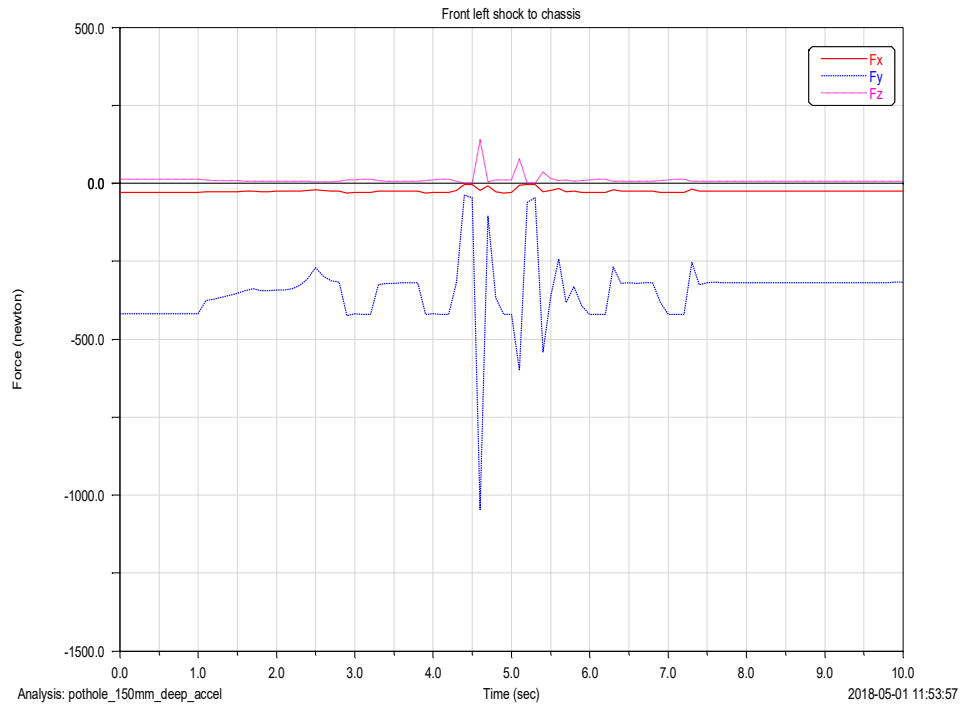
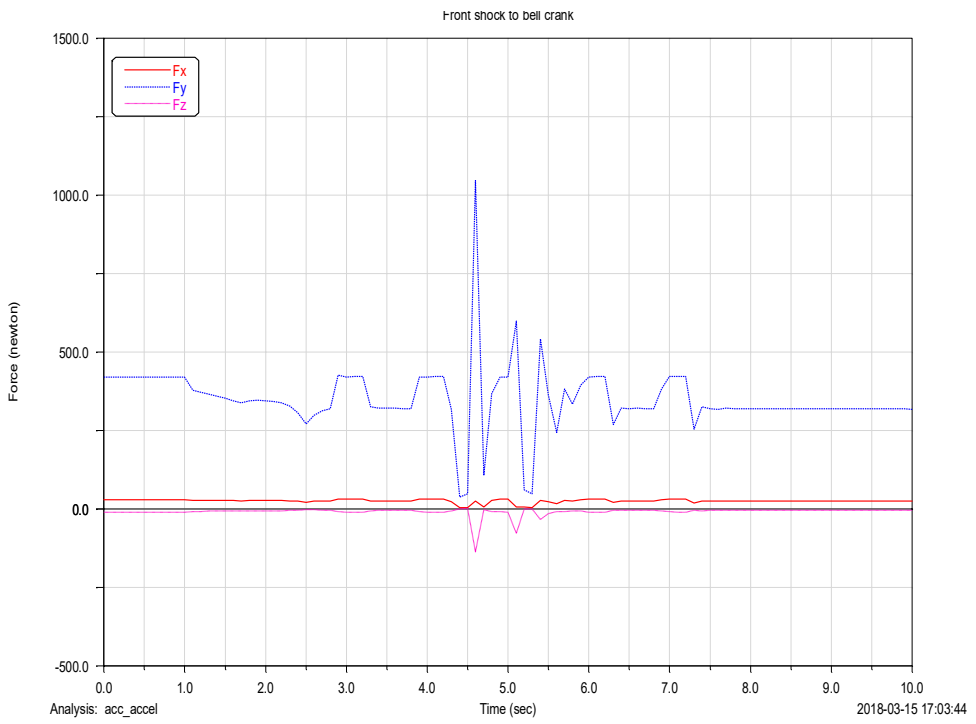


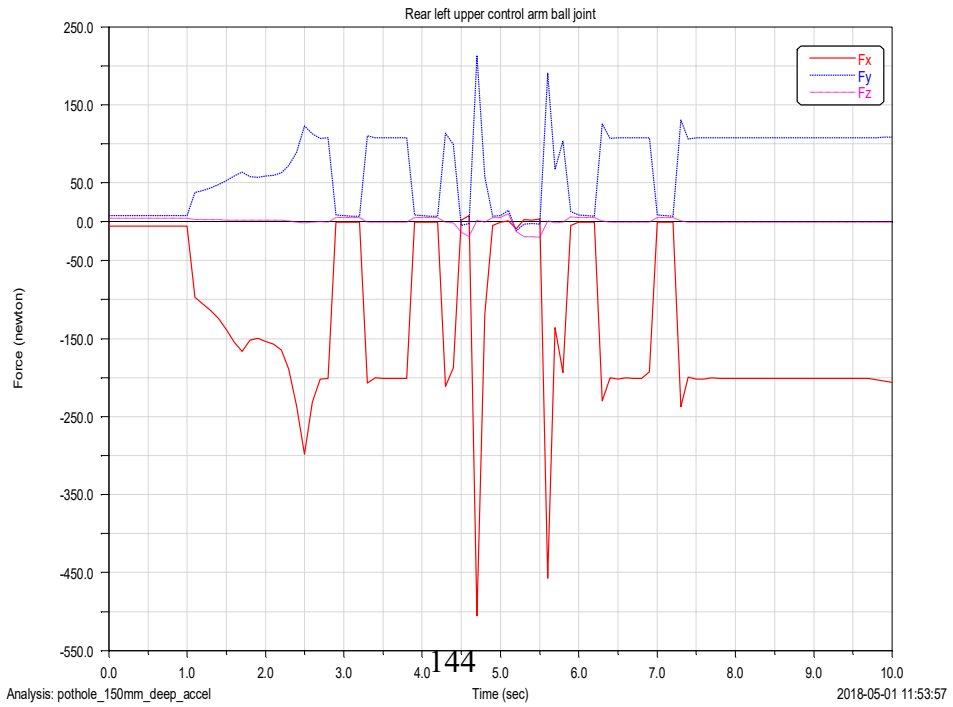
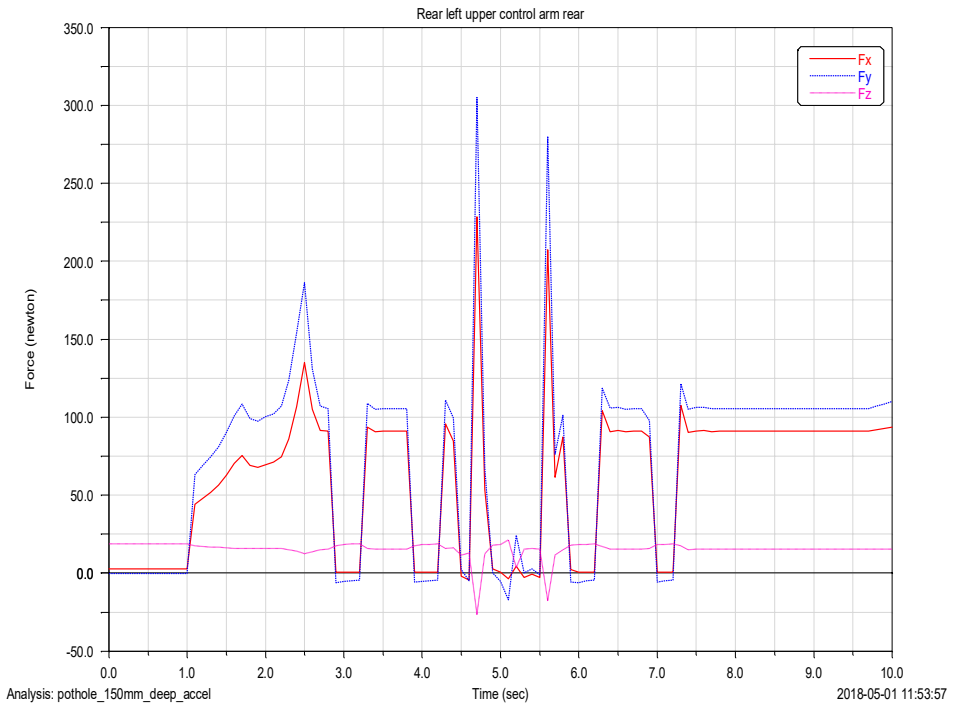
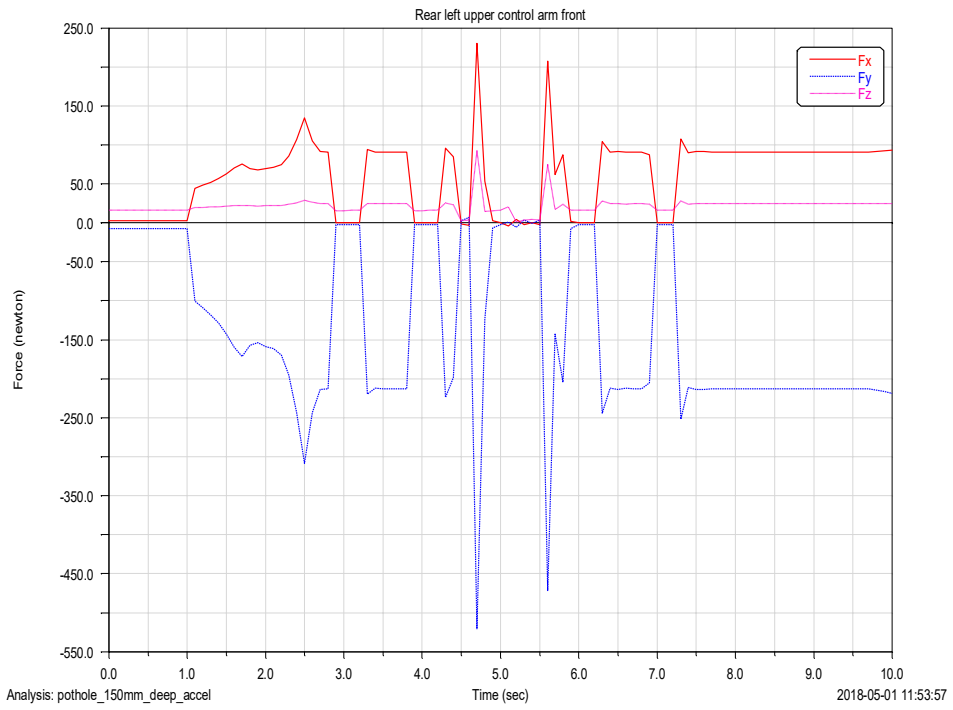


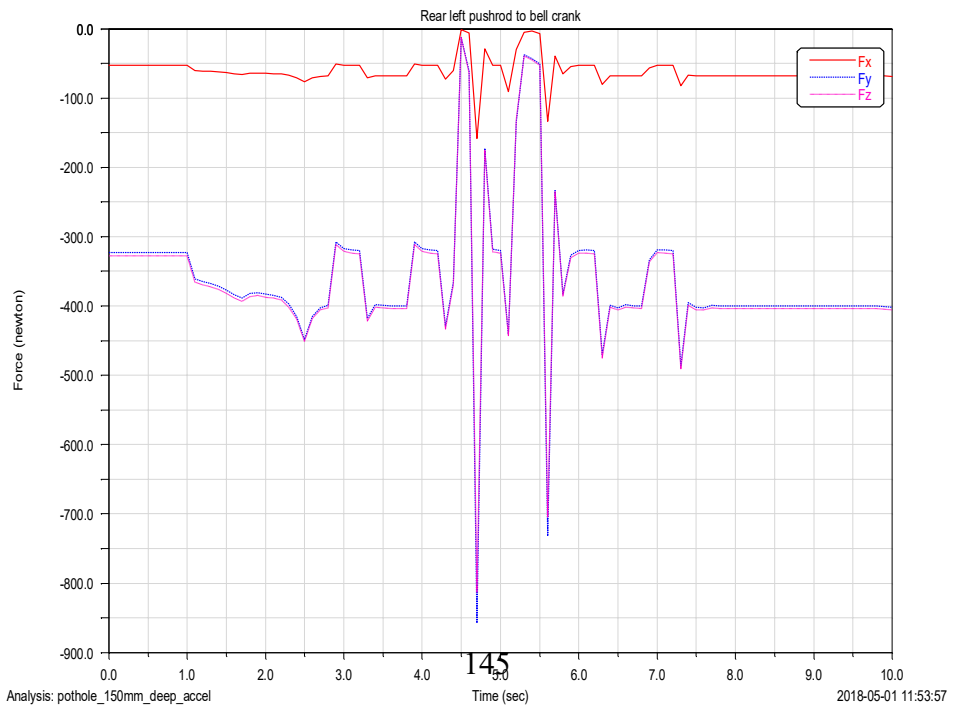
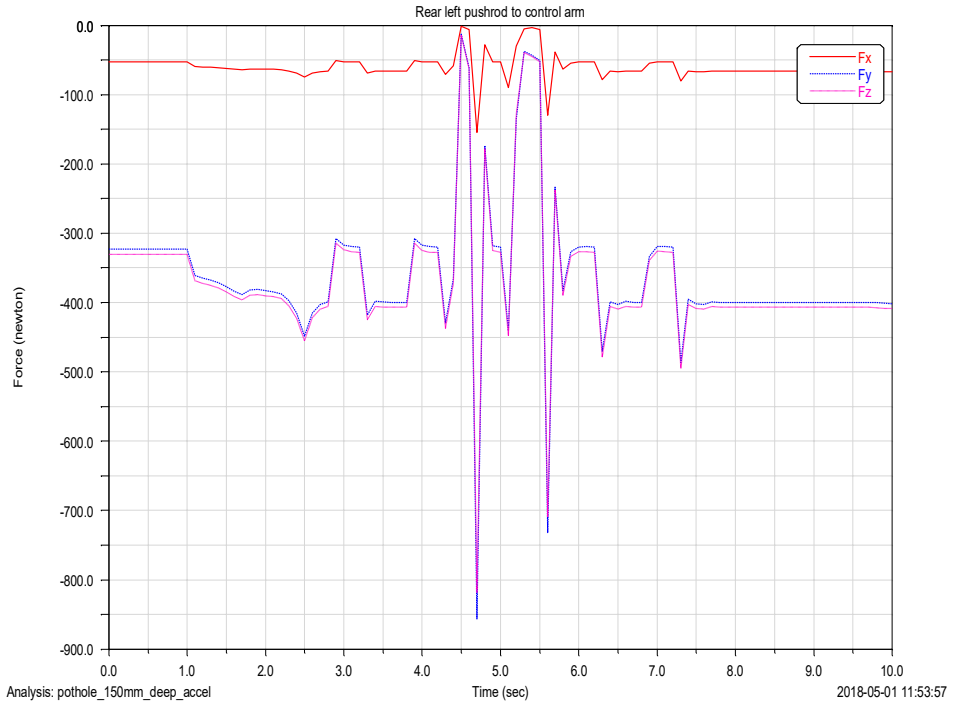
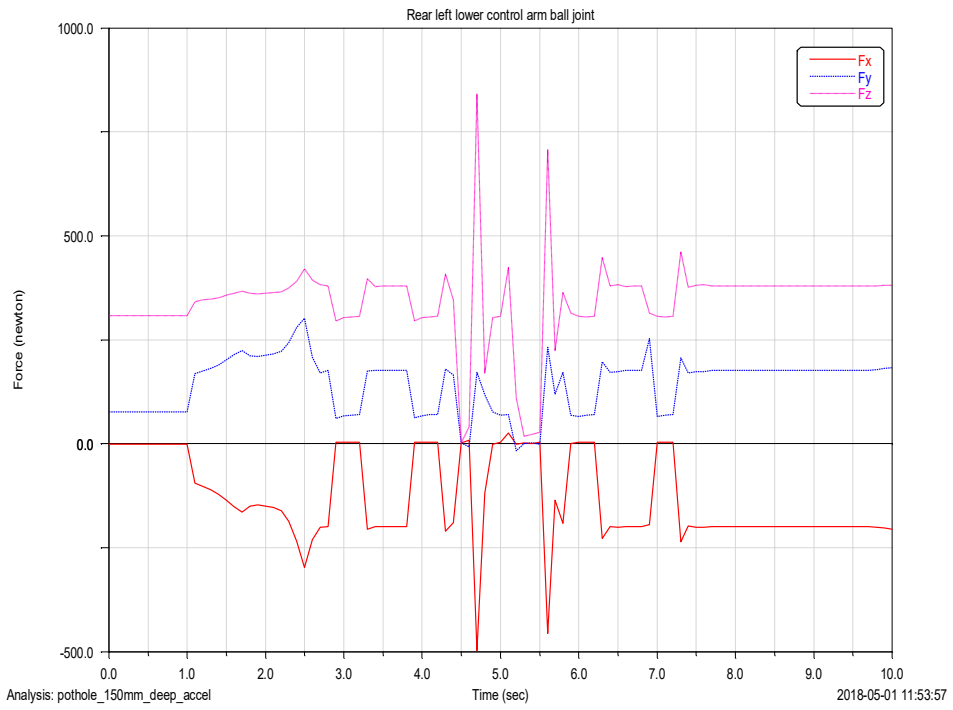


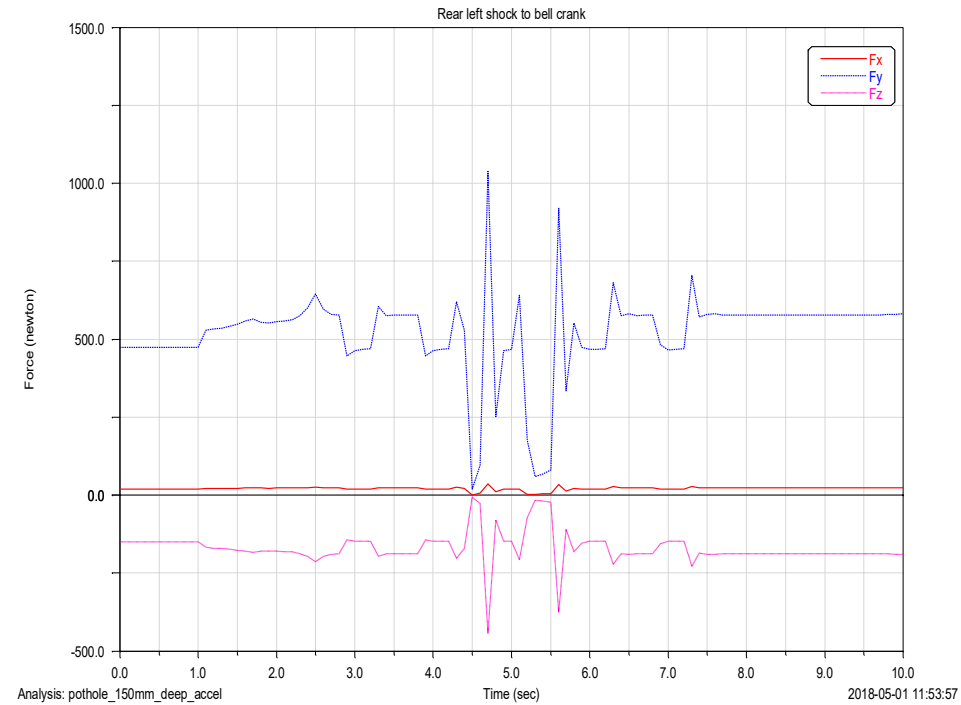
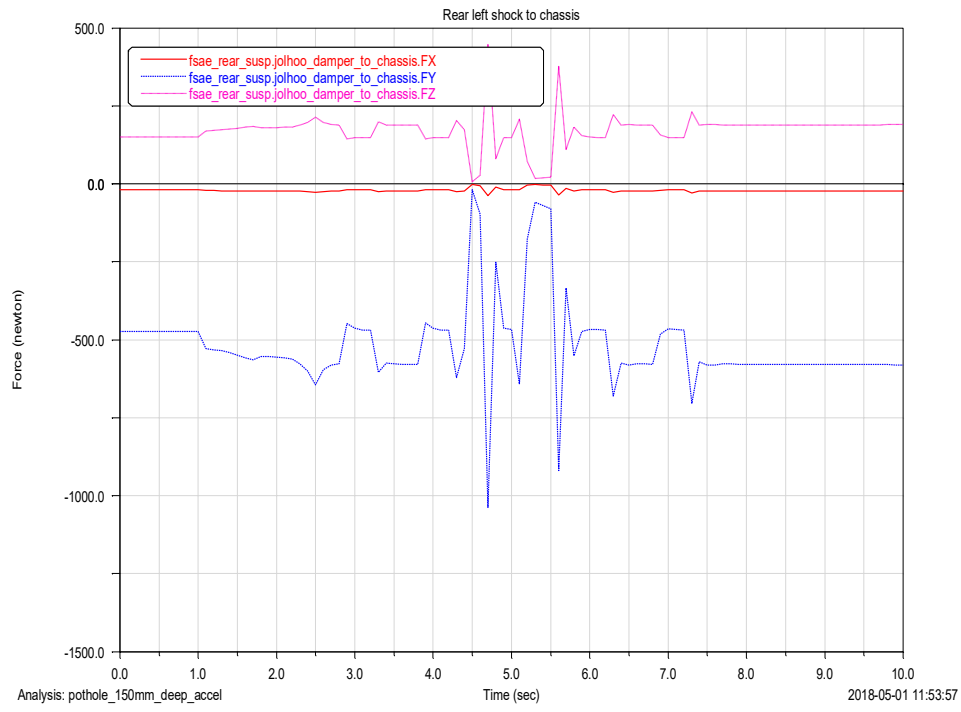












### C.2.3 Plank simulation

Full vehicle simulation driving in over a 150 mm plank during acceleration.

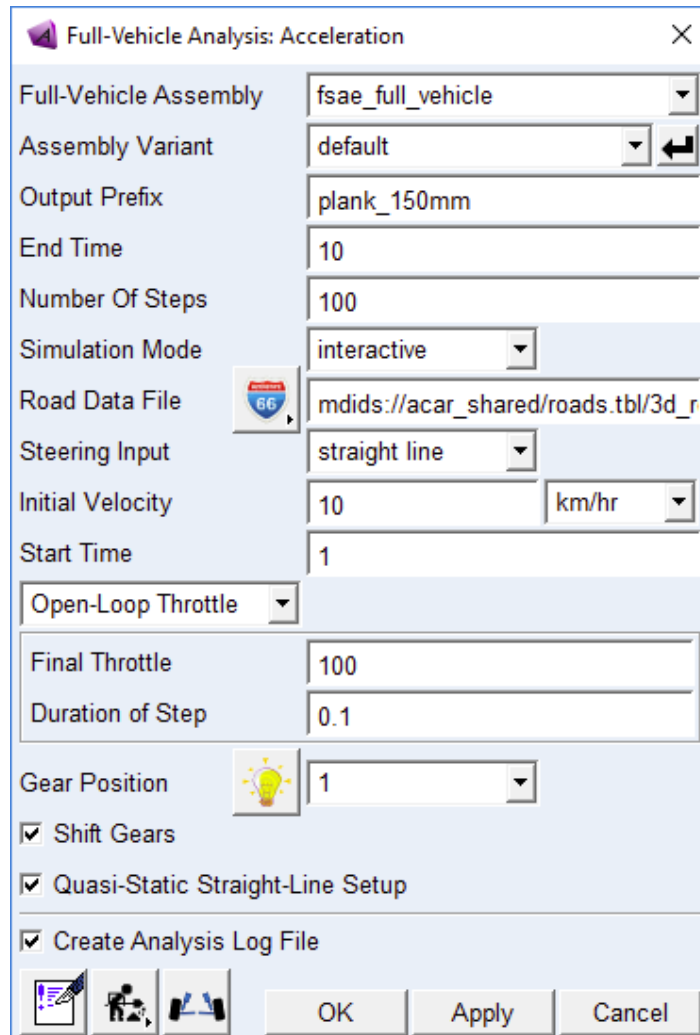
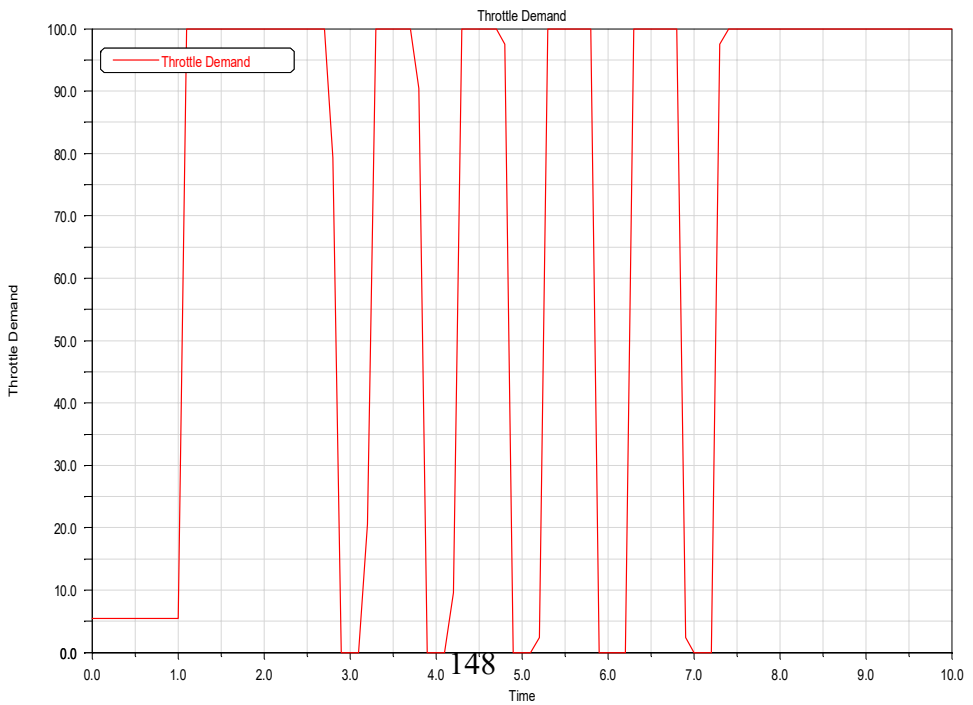
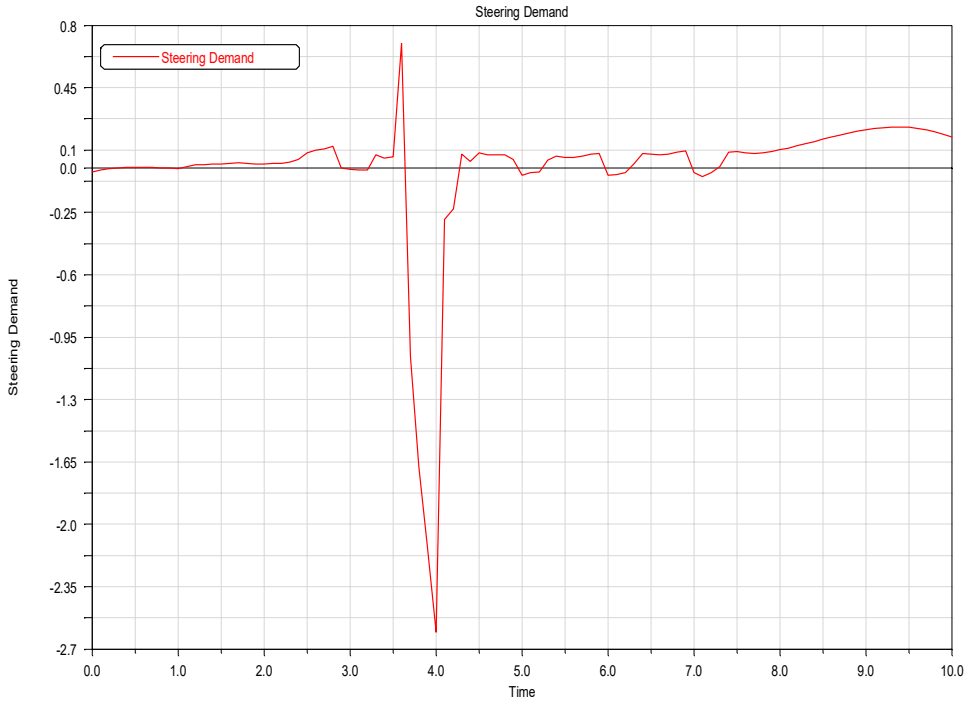
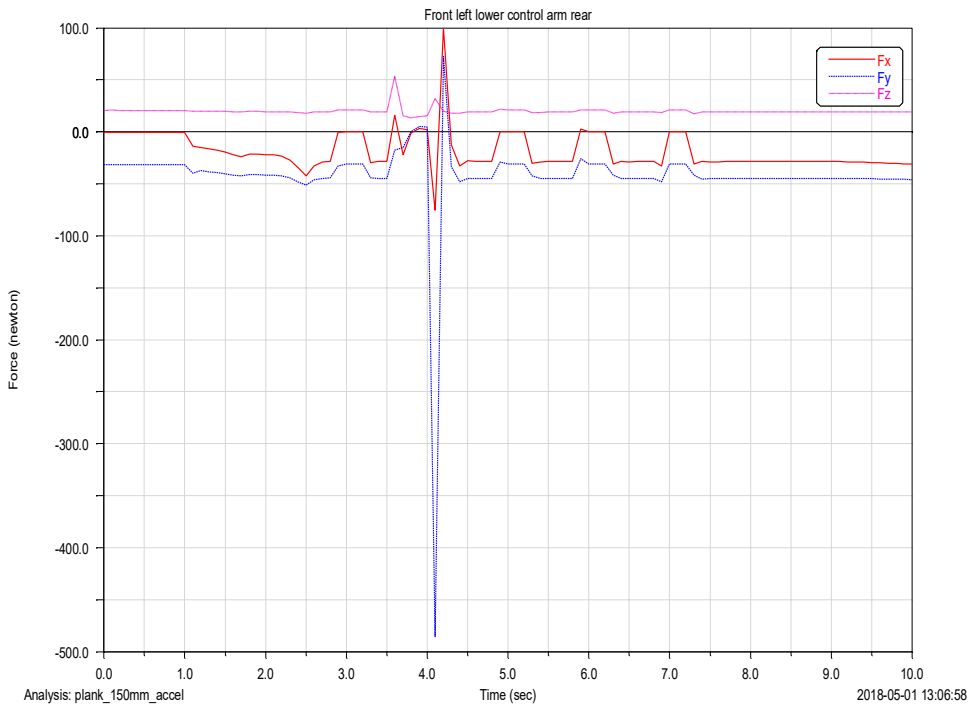
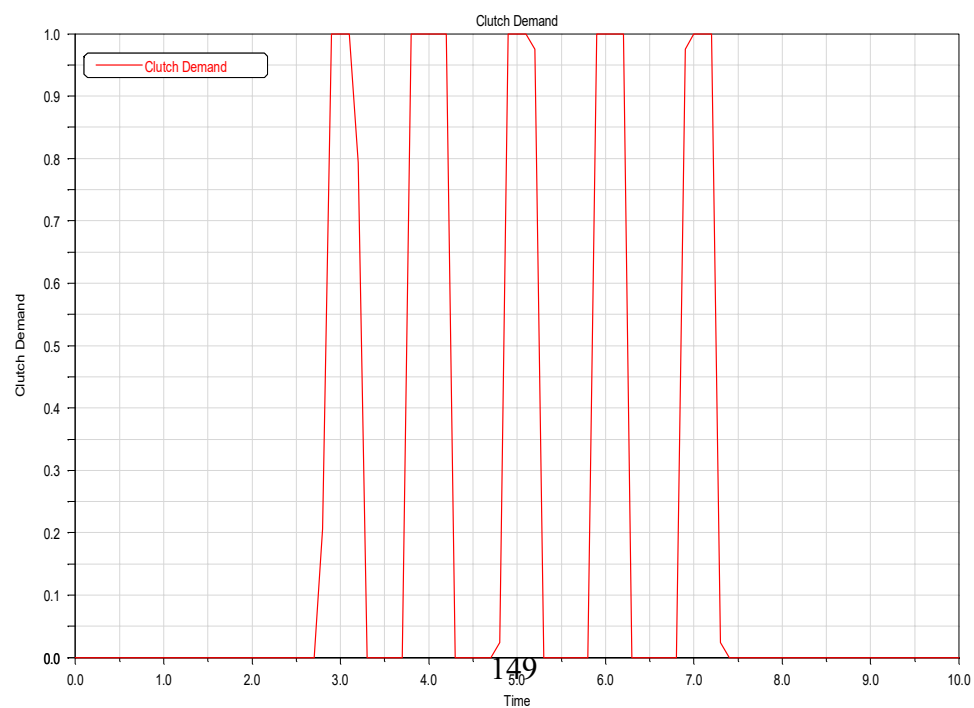
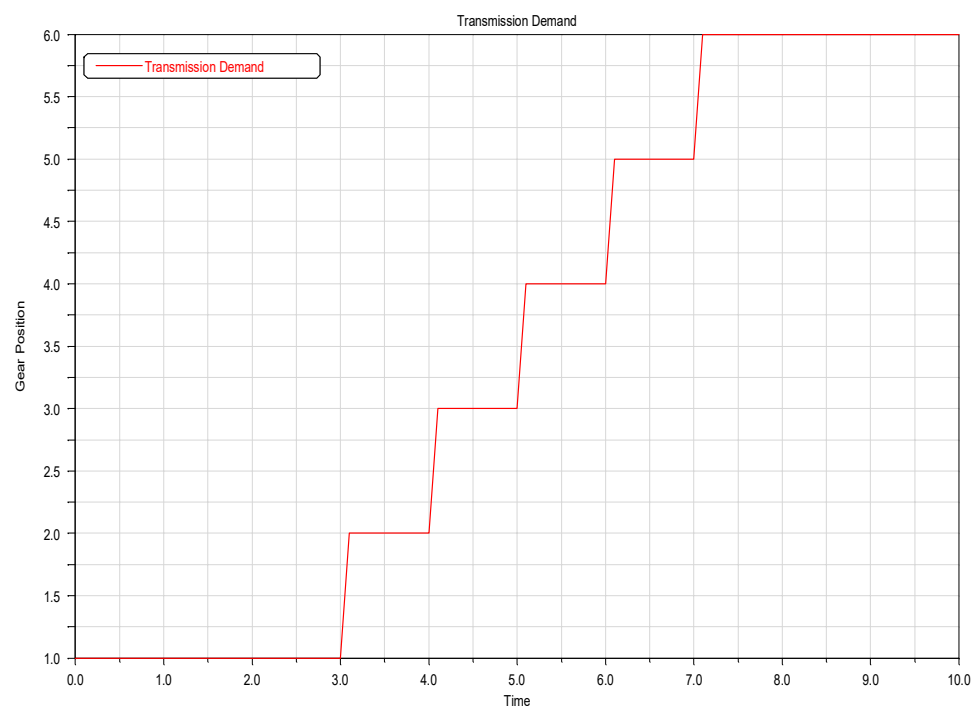
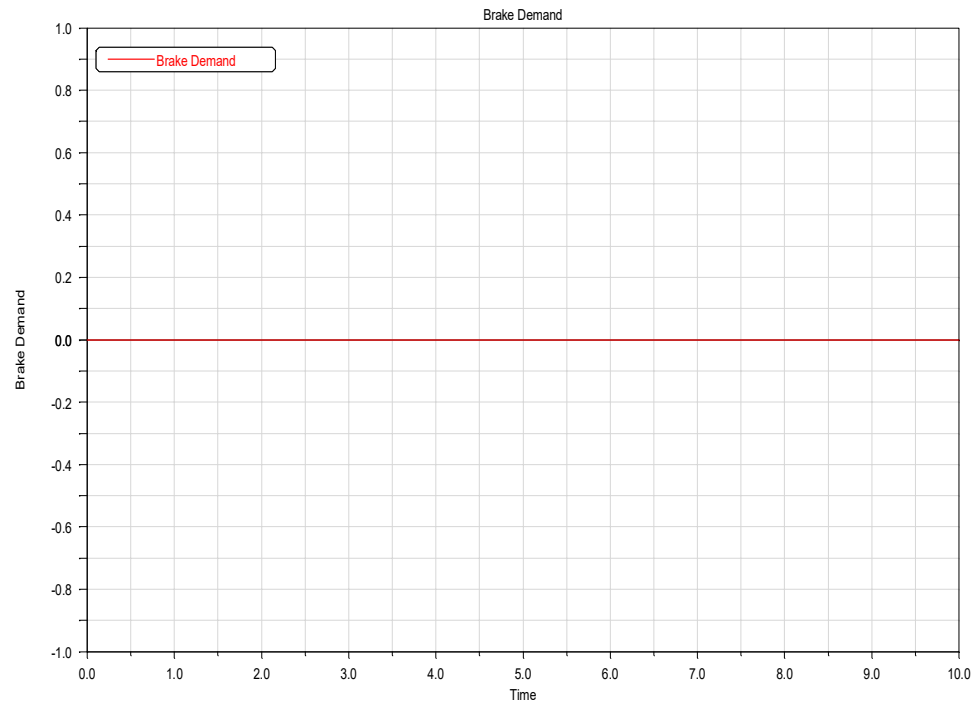
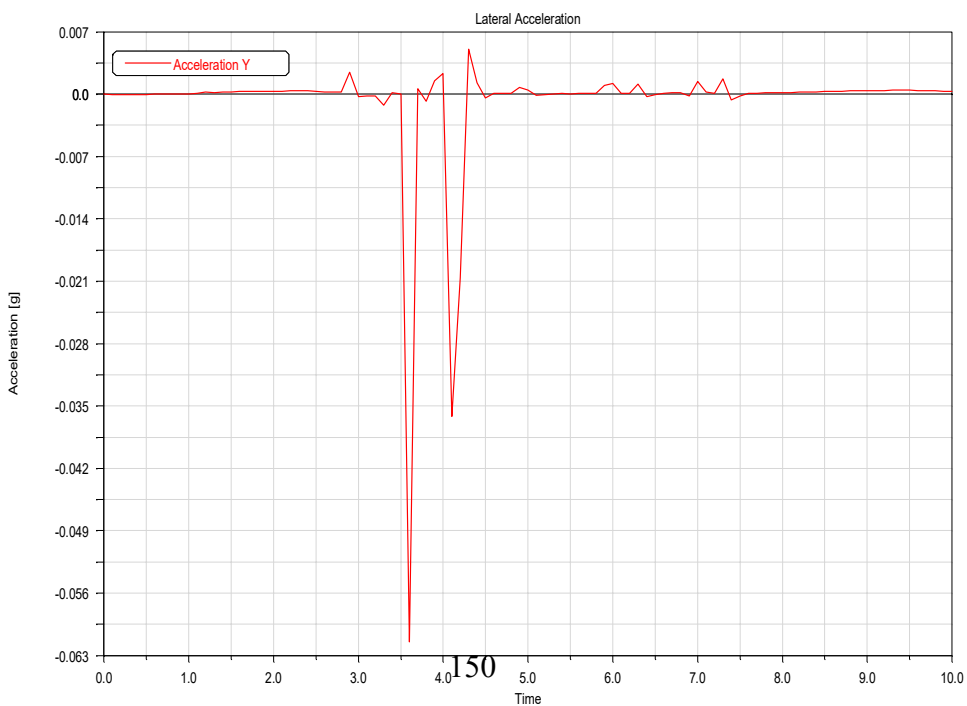
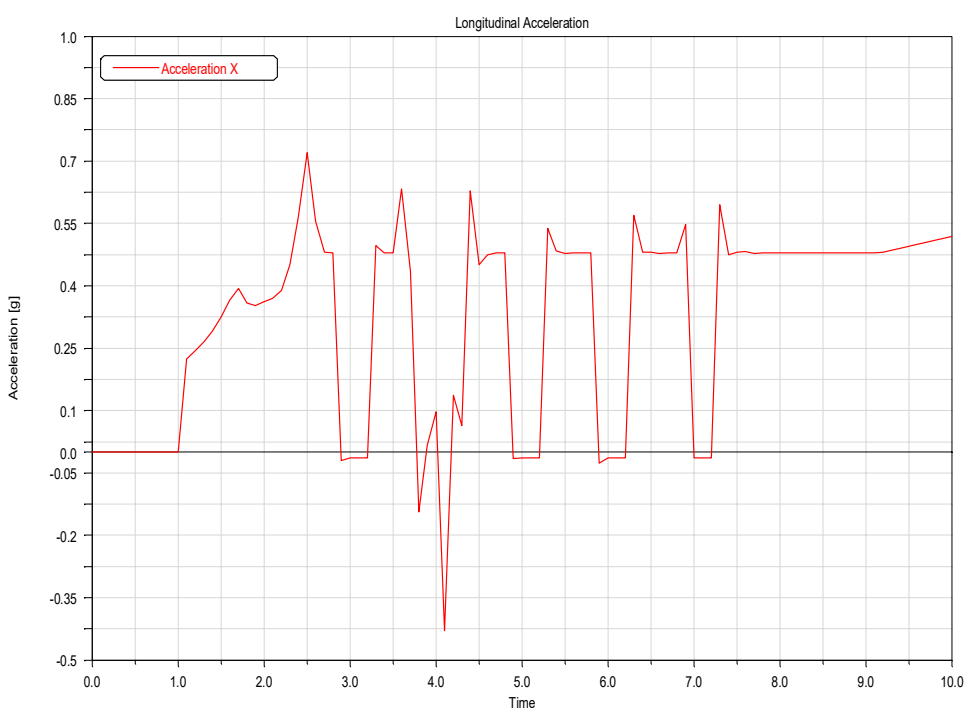
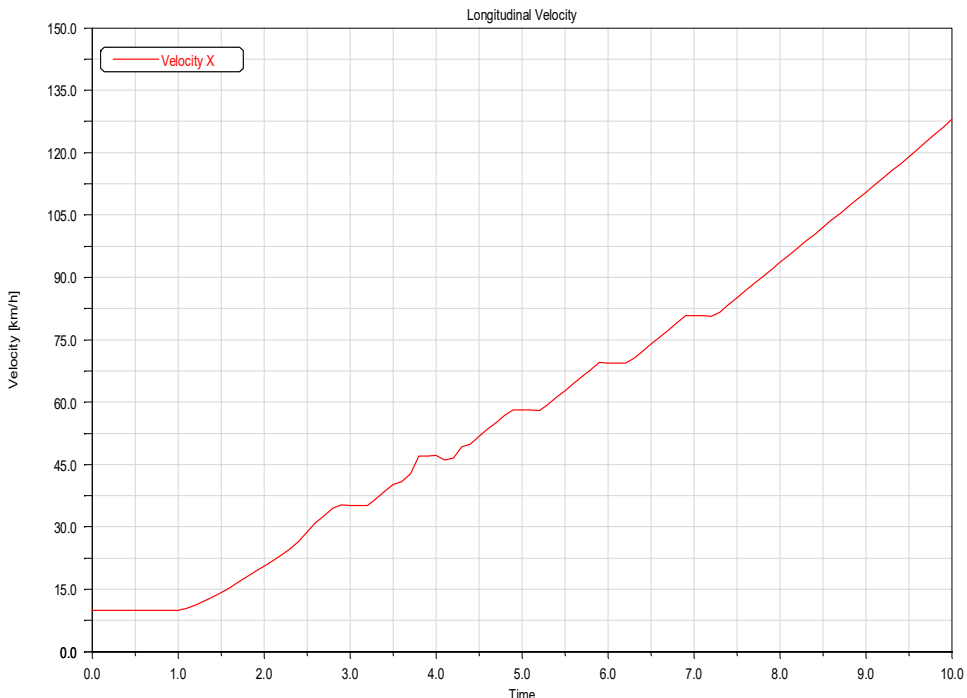
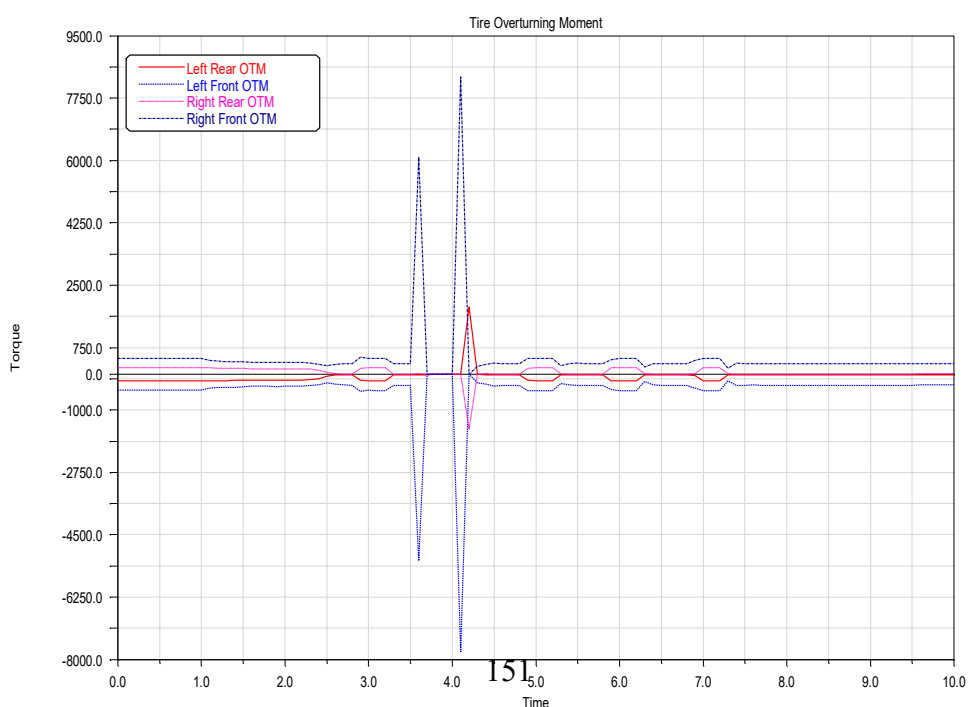
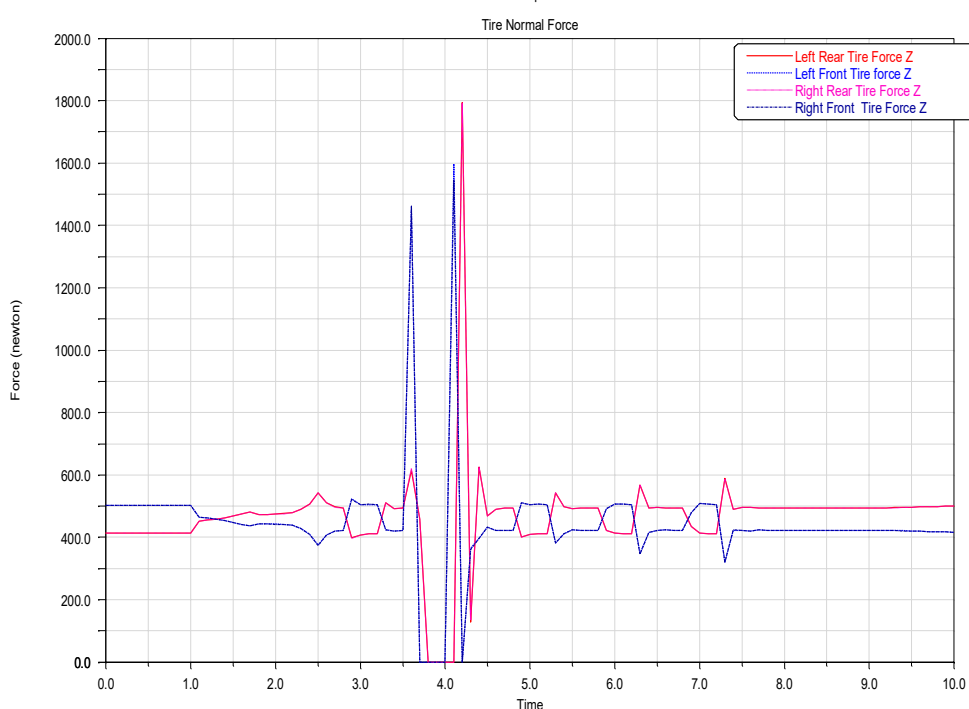
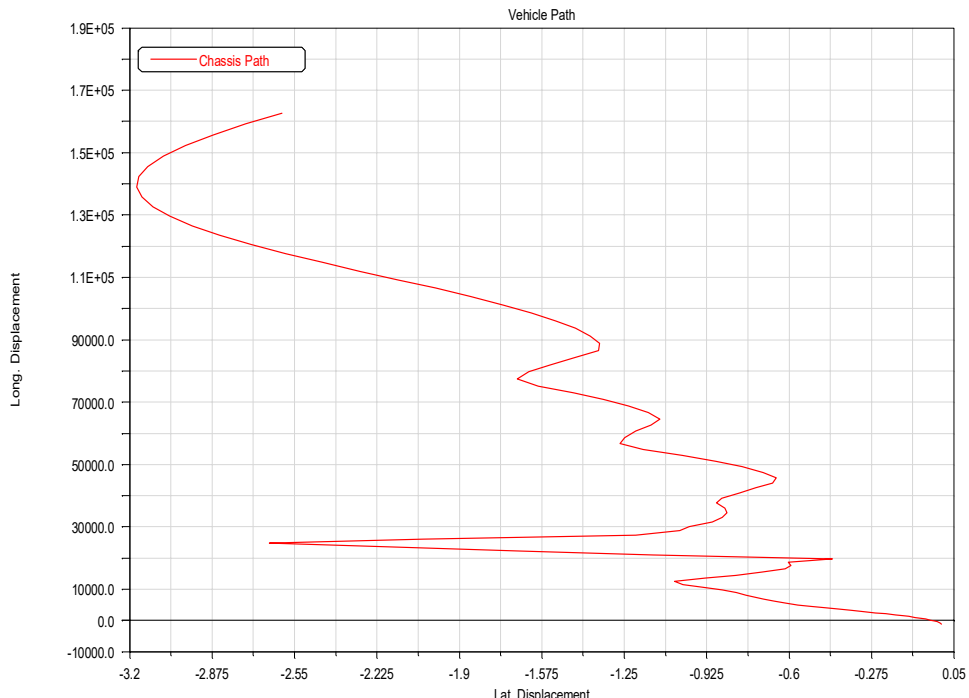


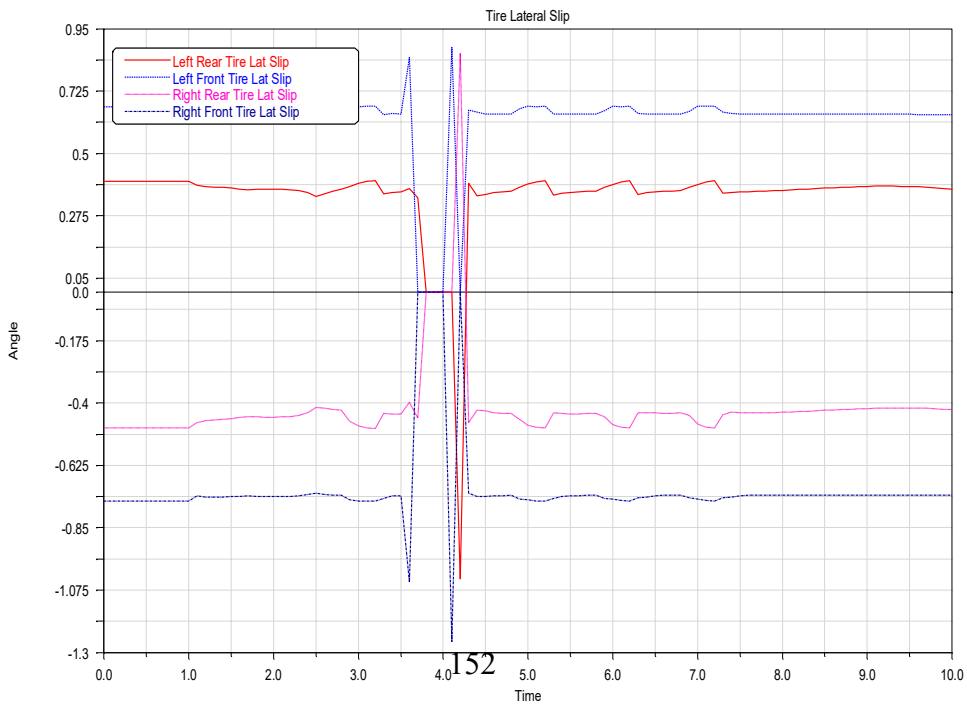
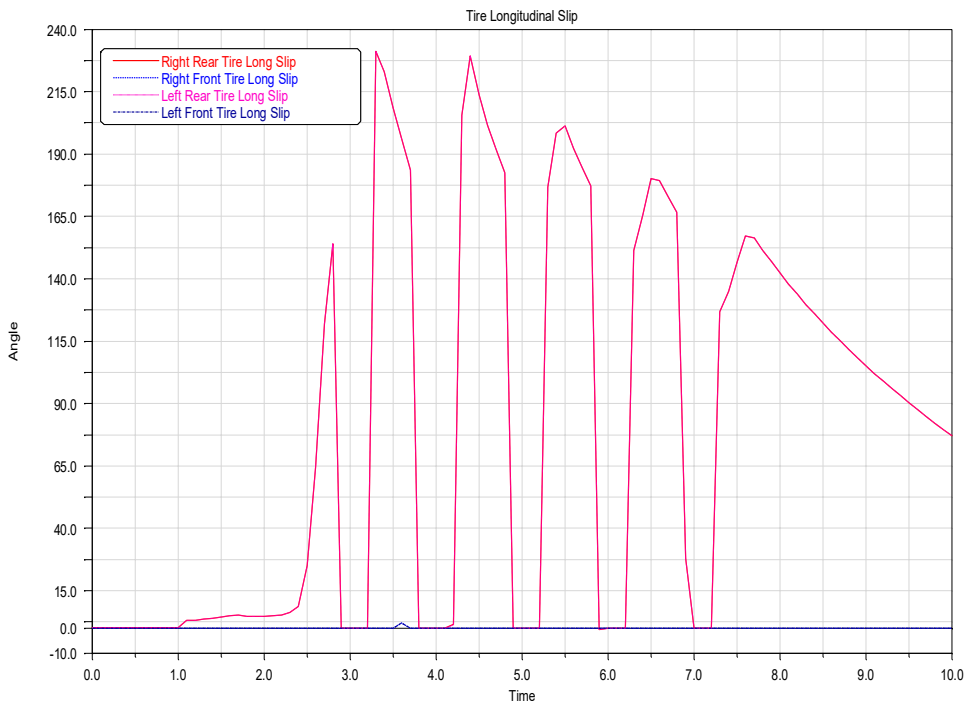
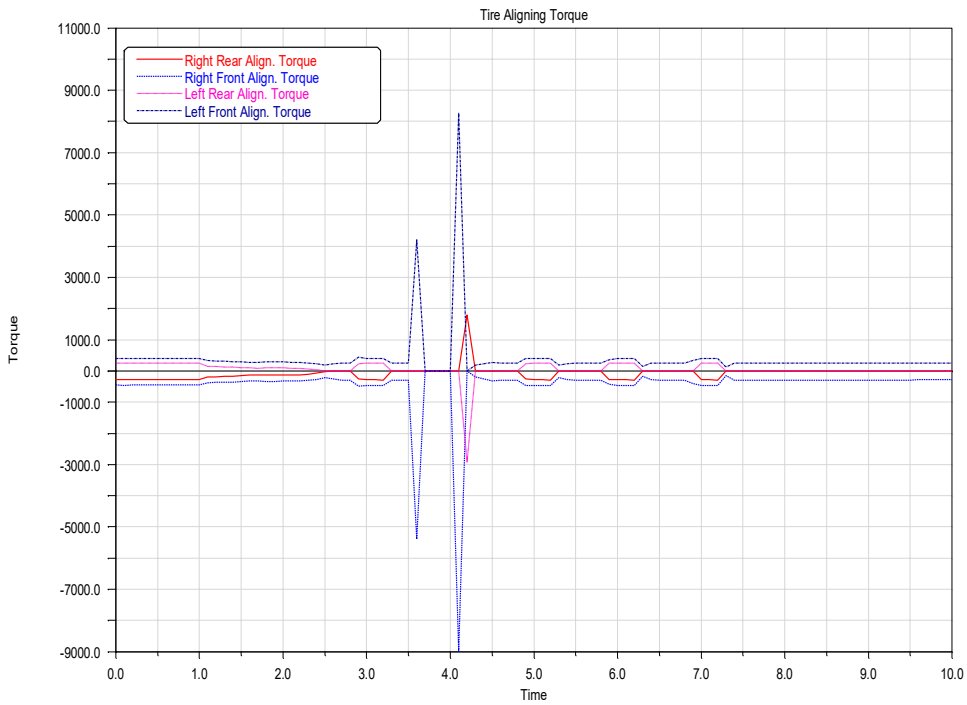
Figure C.2: Adams car [4] plank simulation setup window

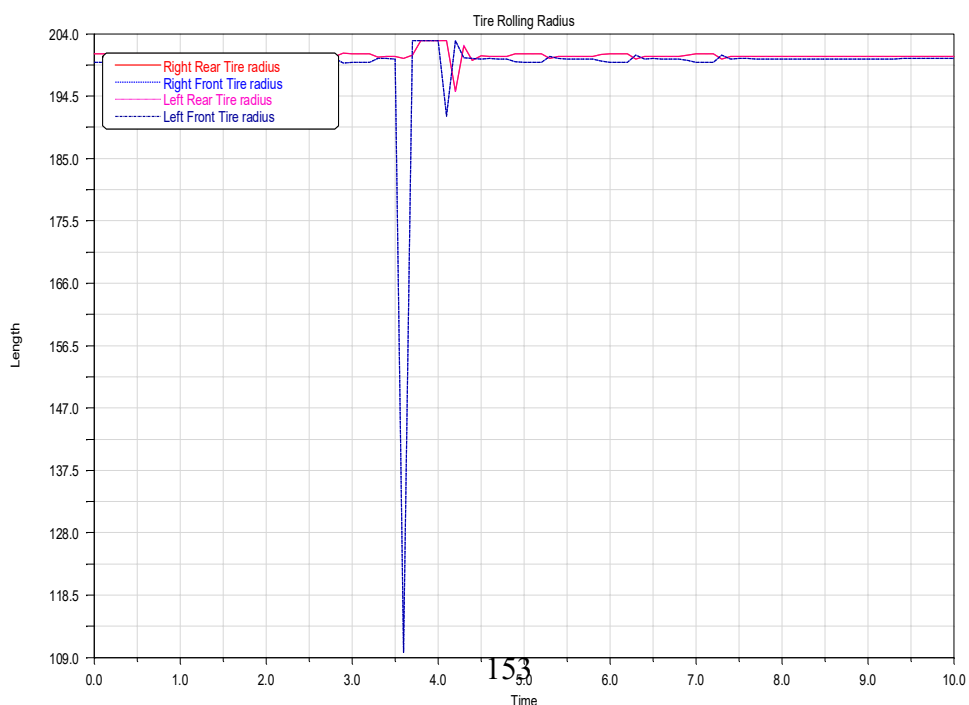
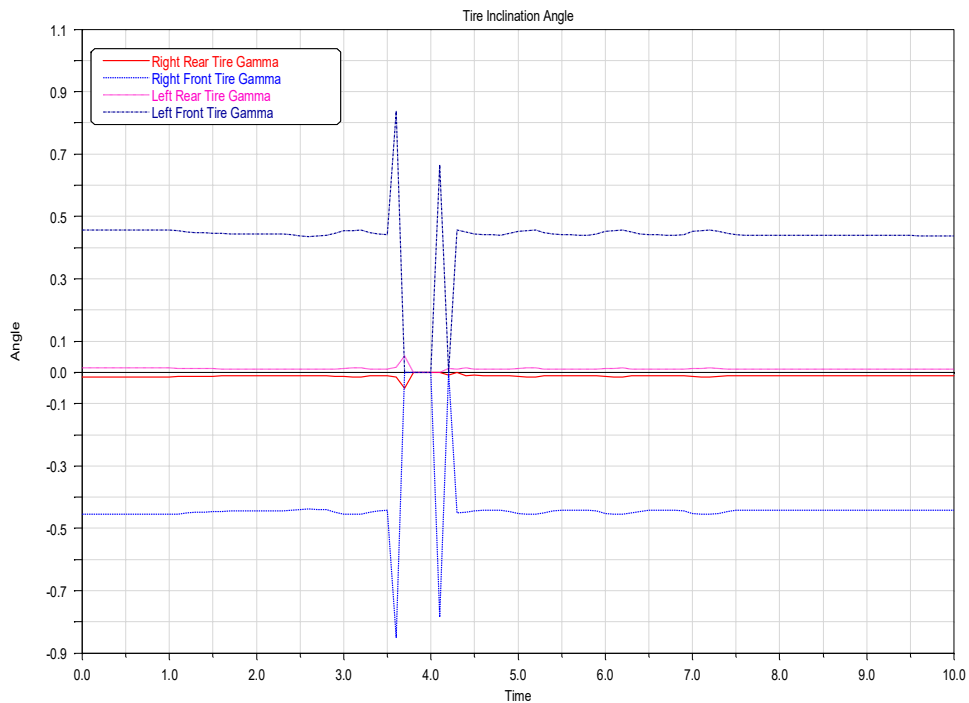
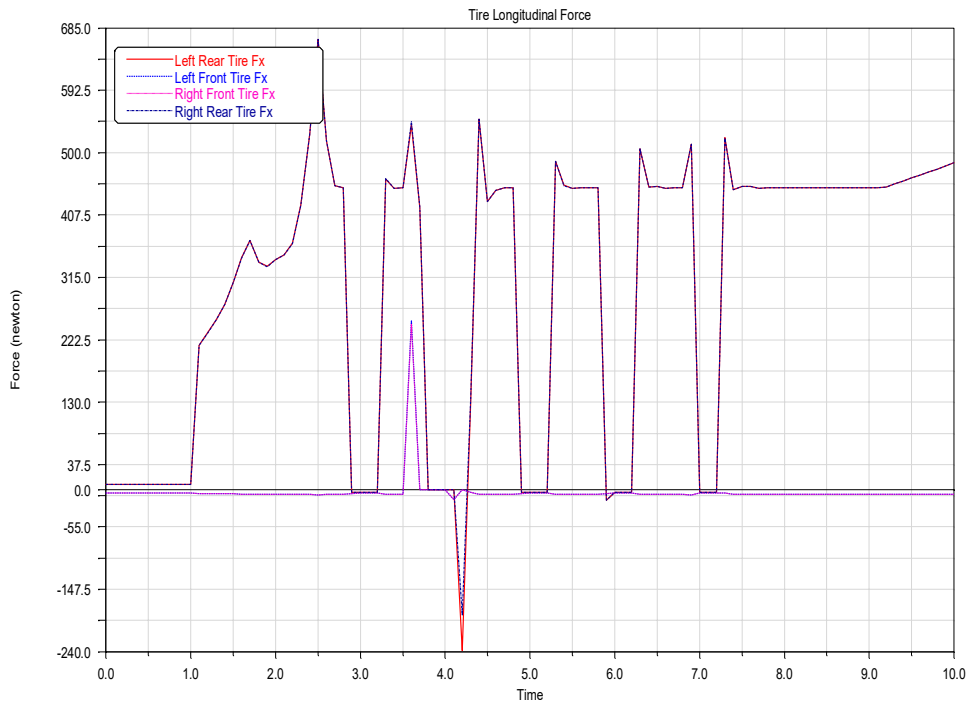


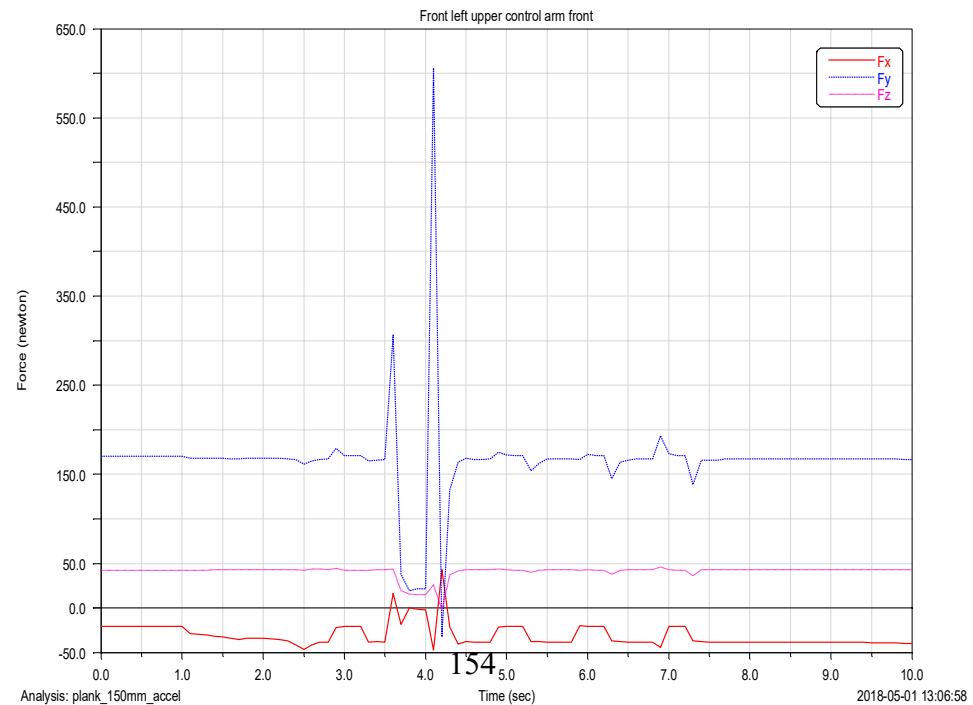
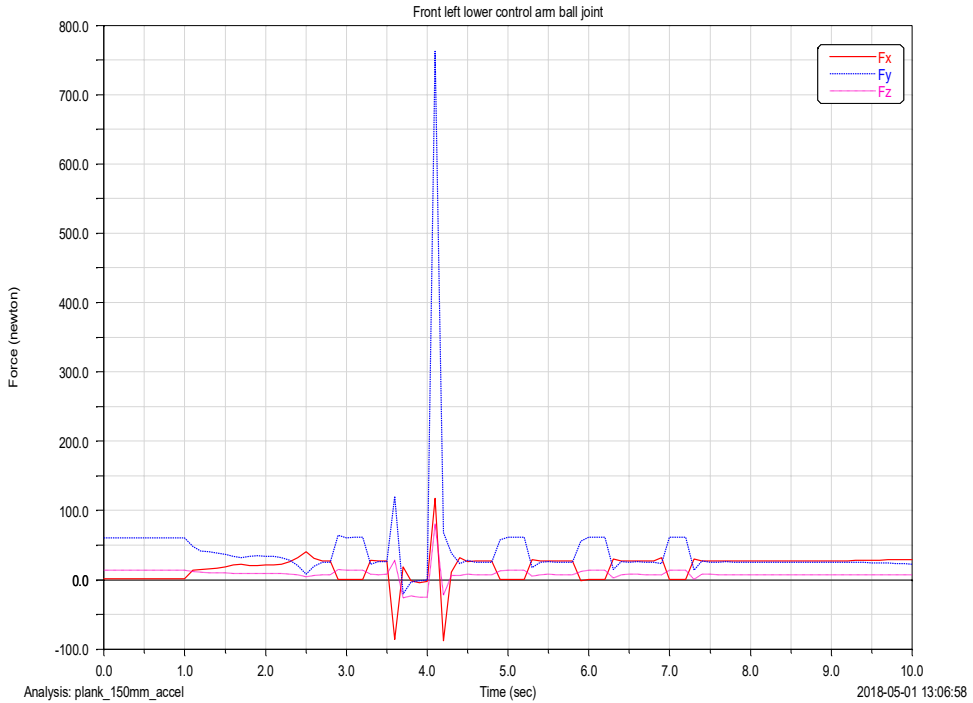
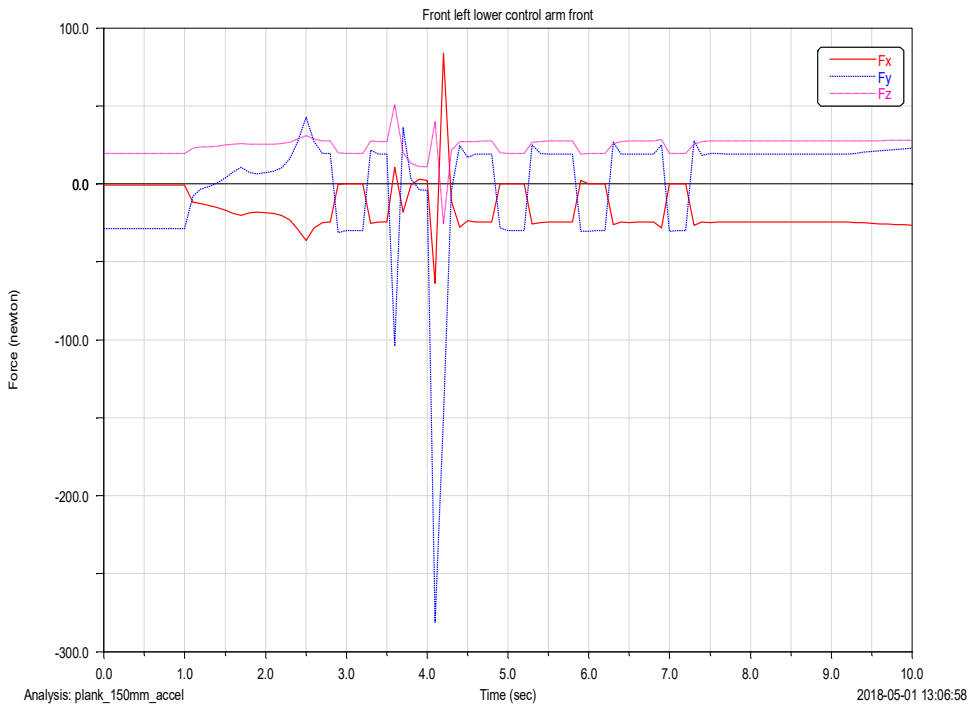


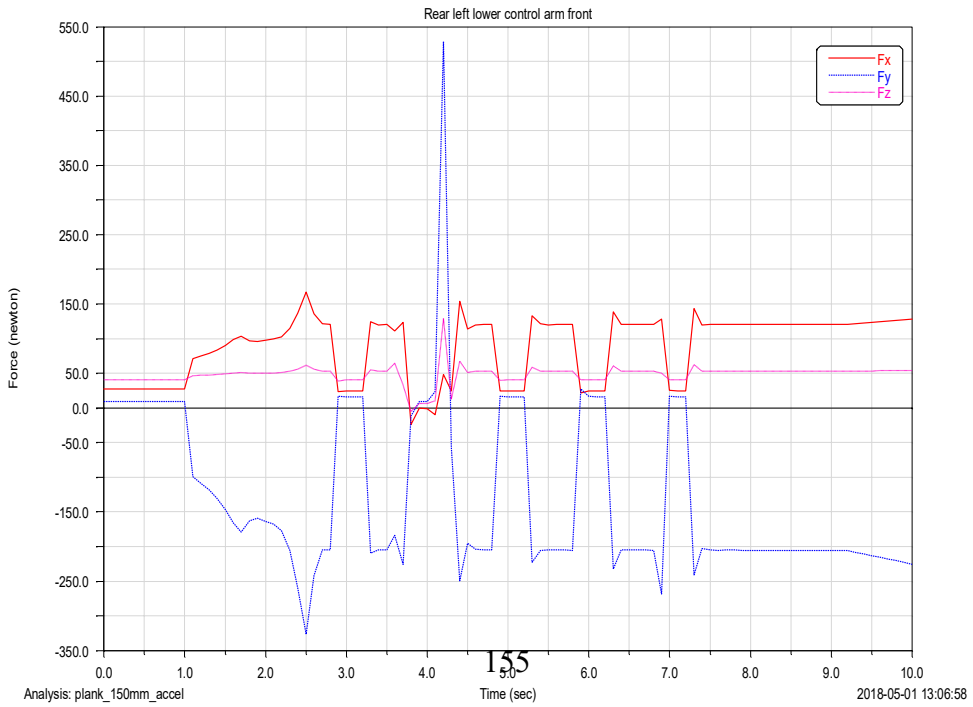
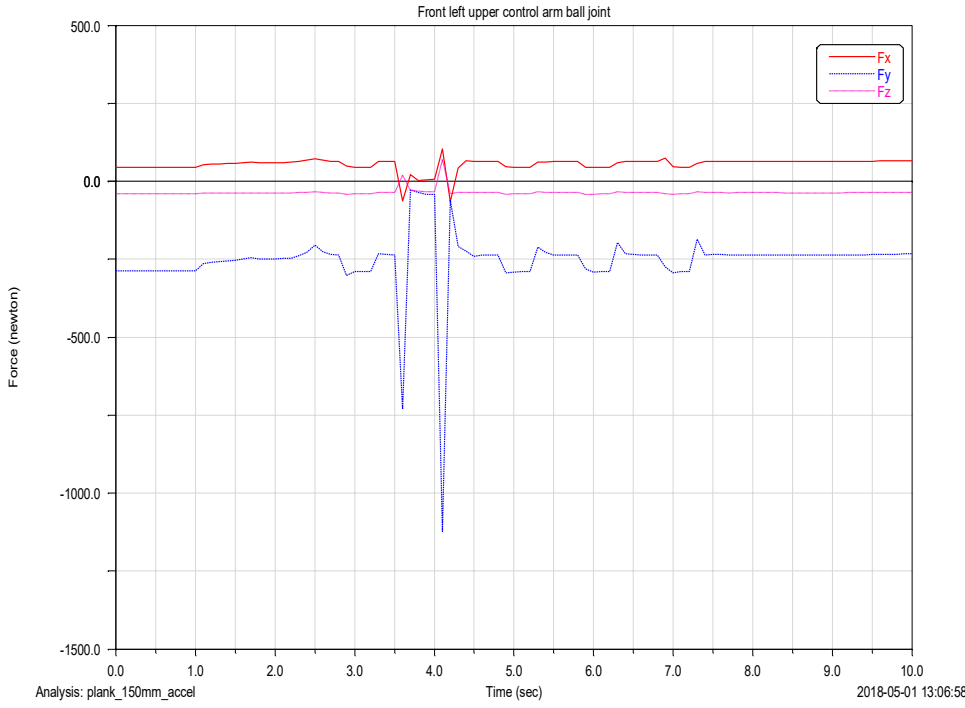
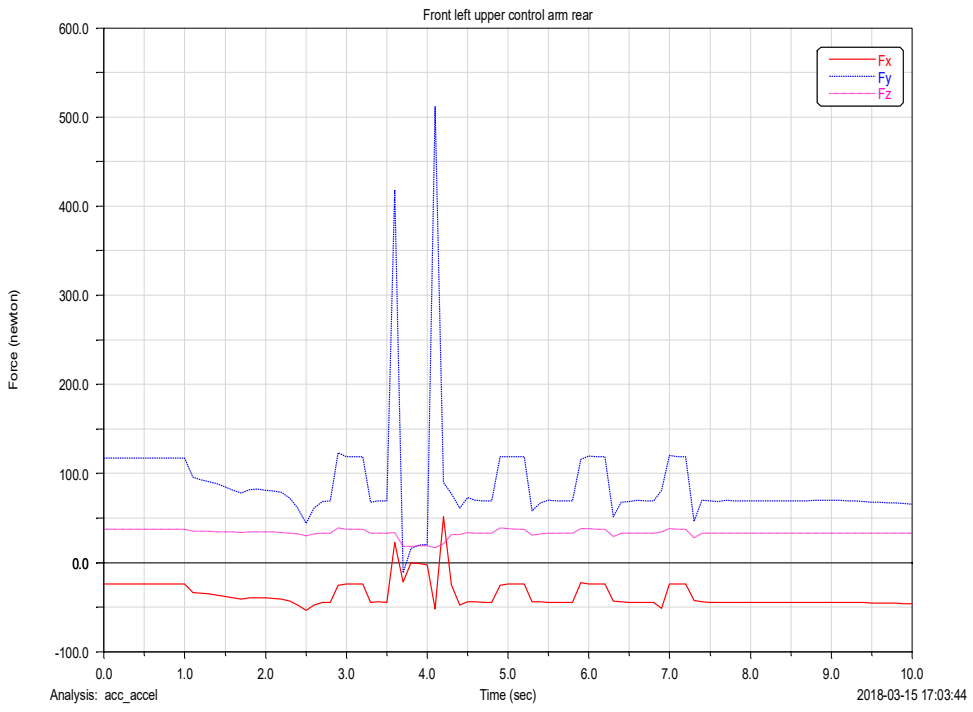


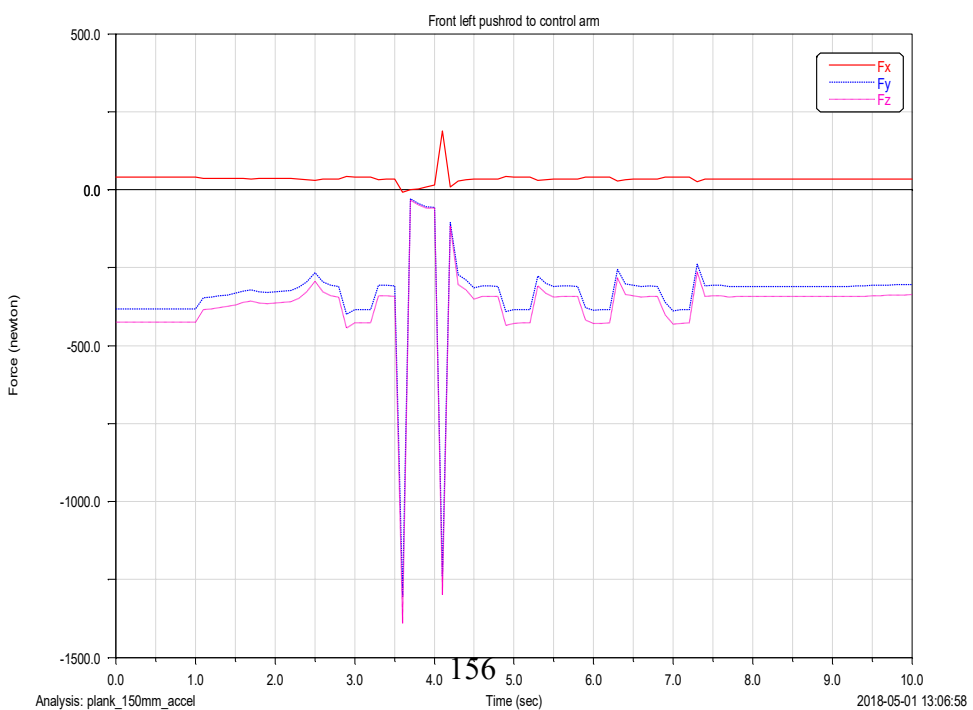
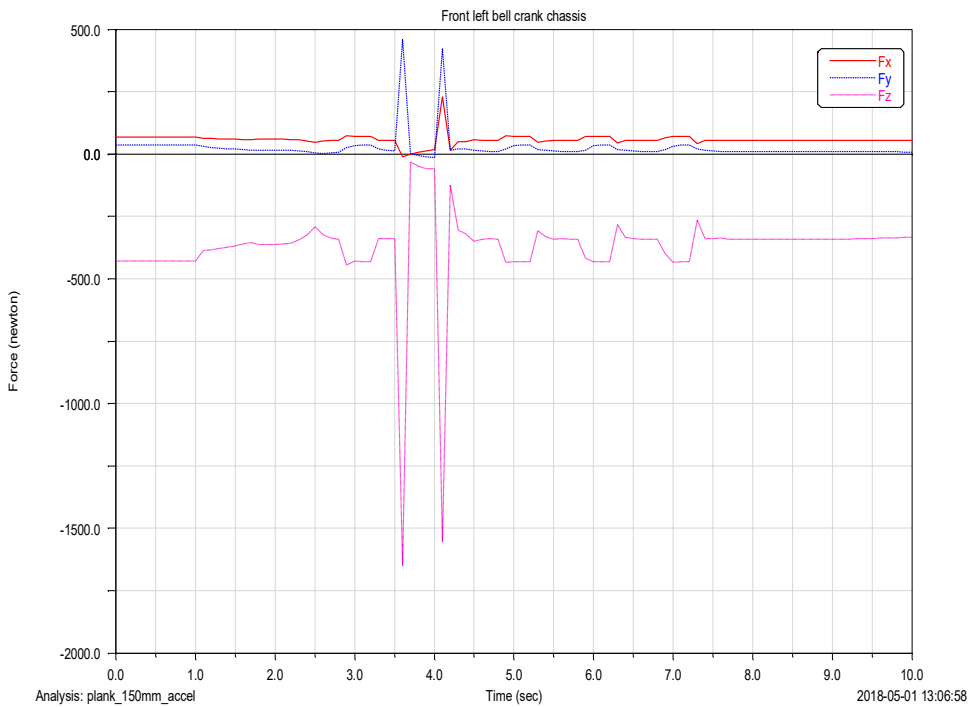
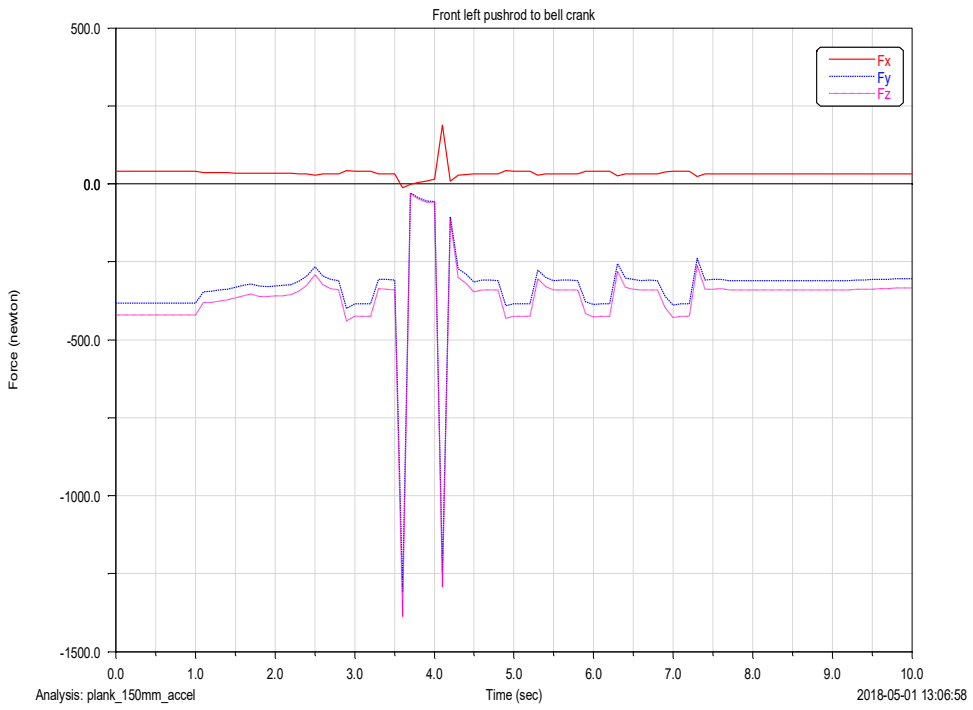


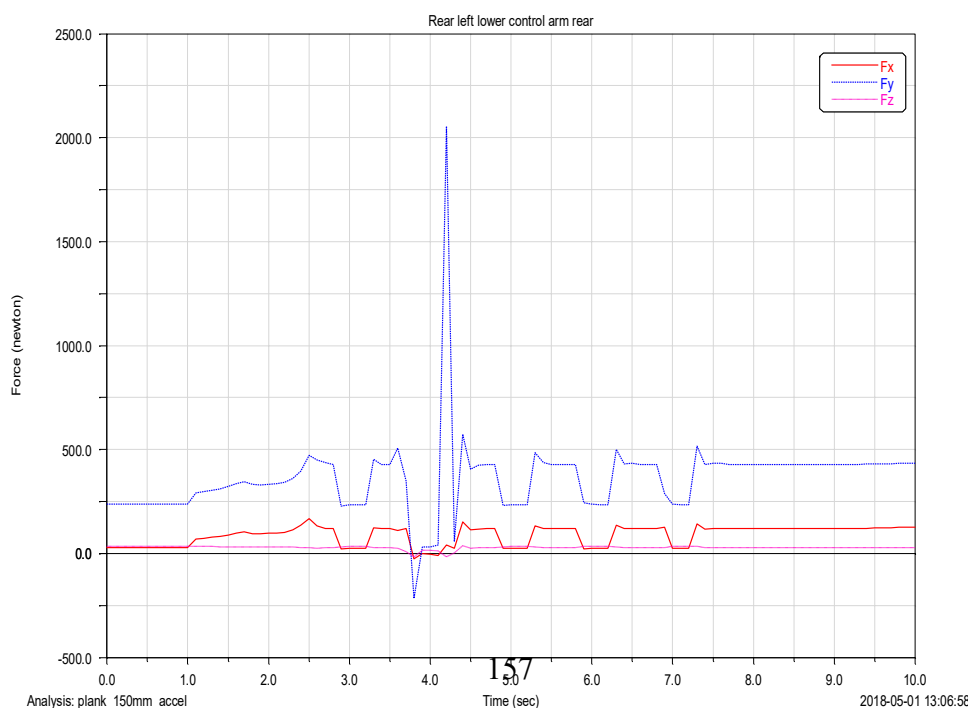
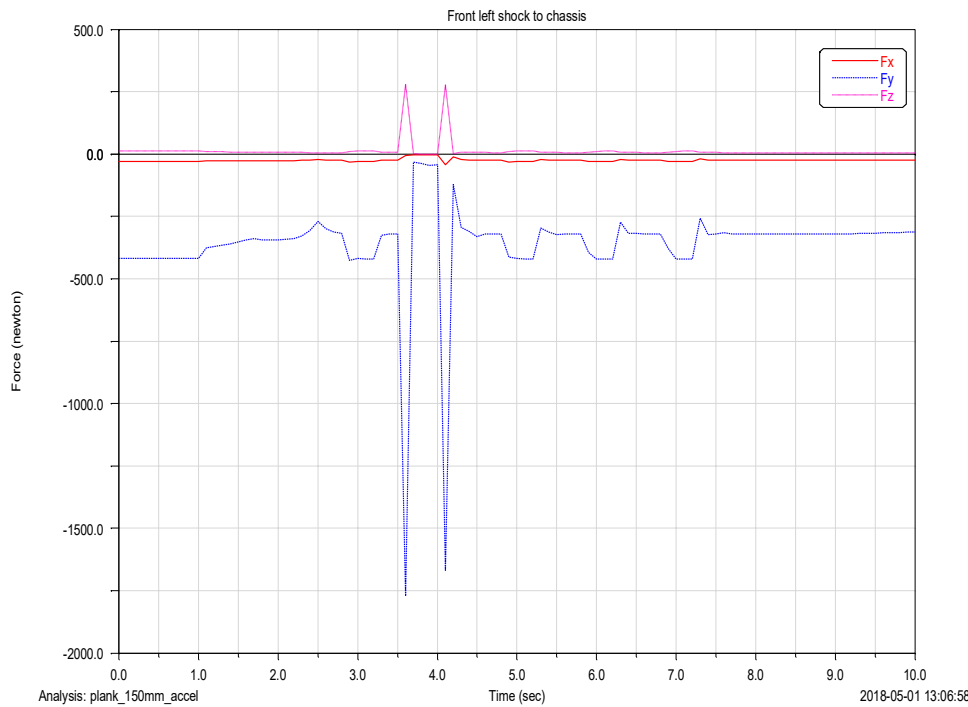
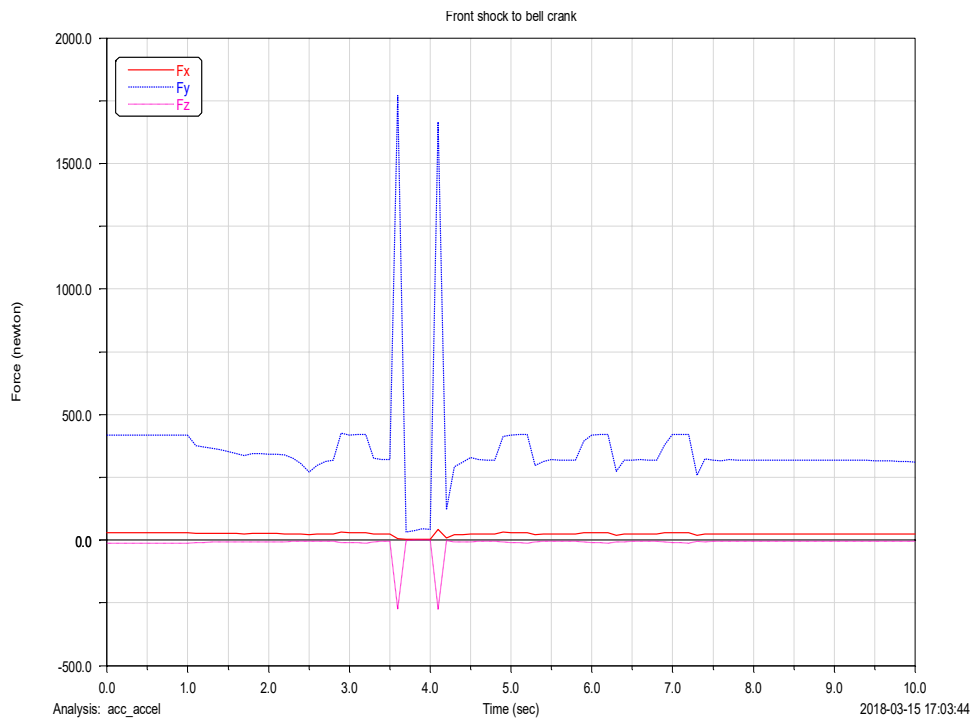


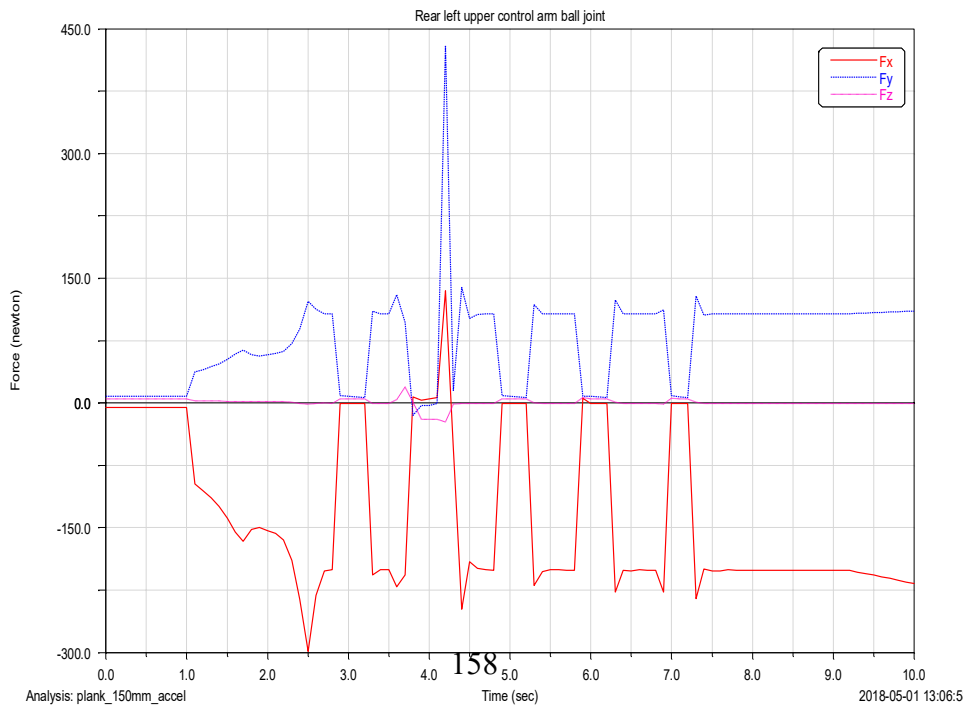
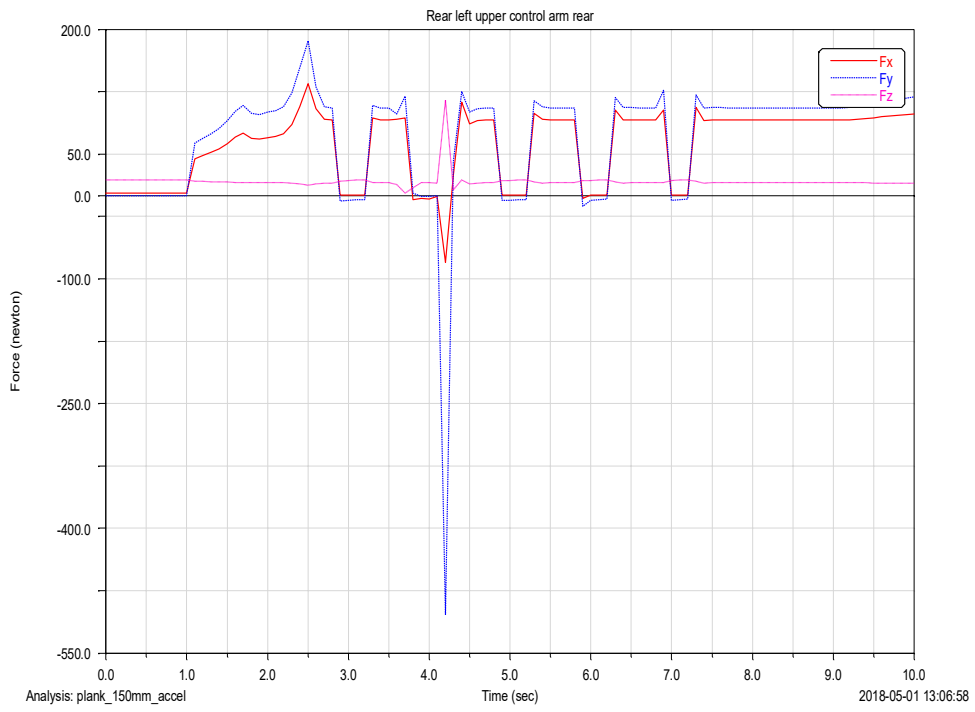
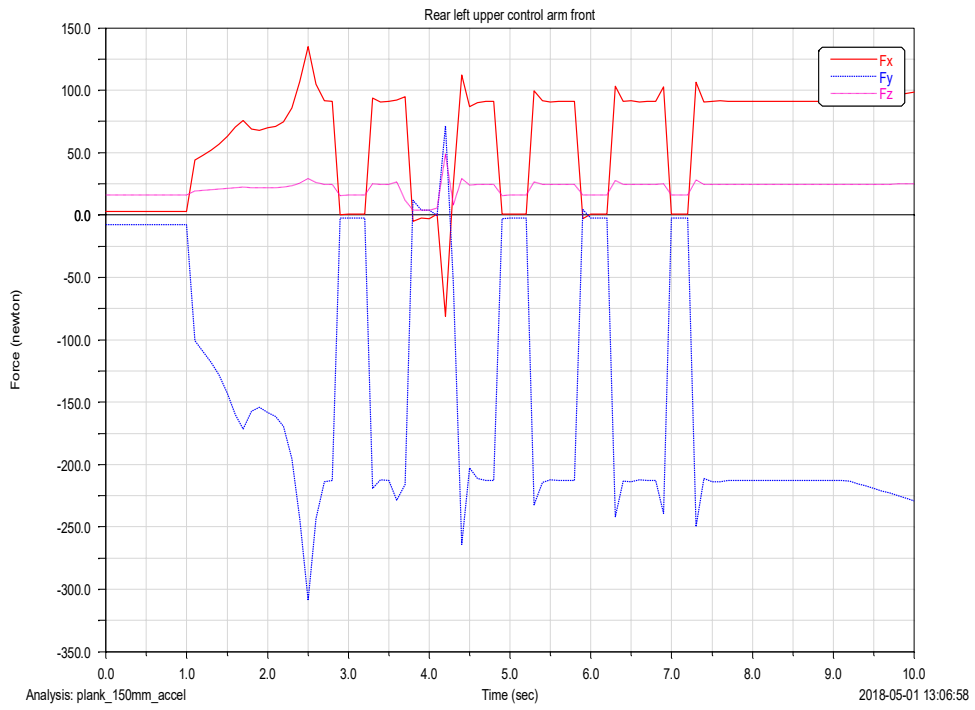


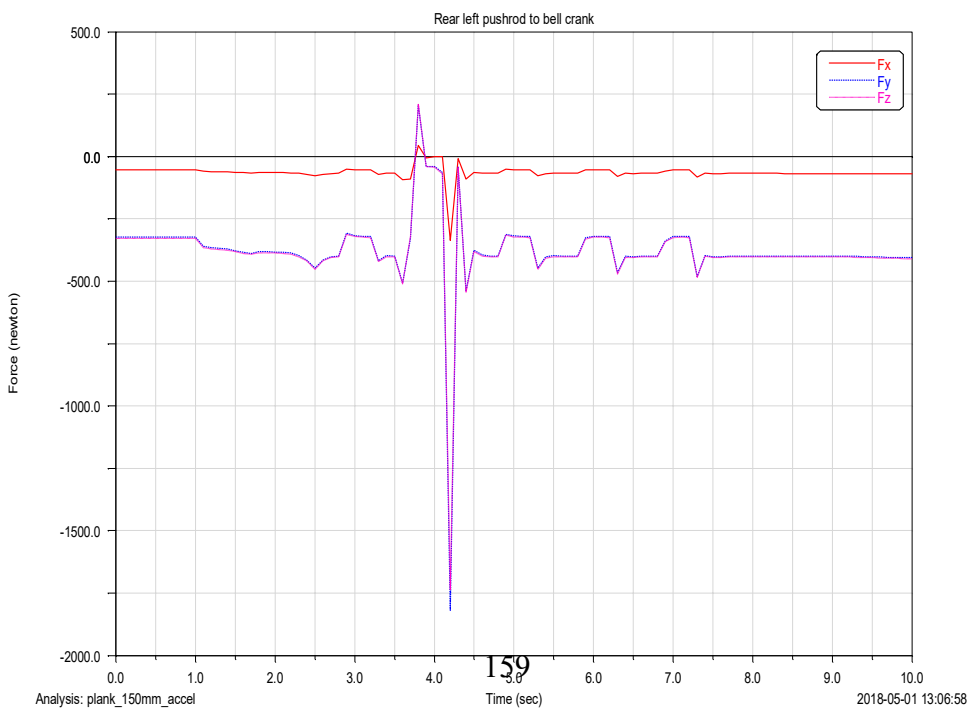
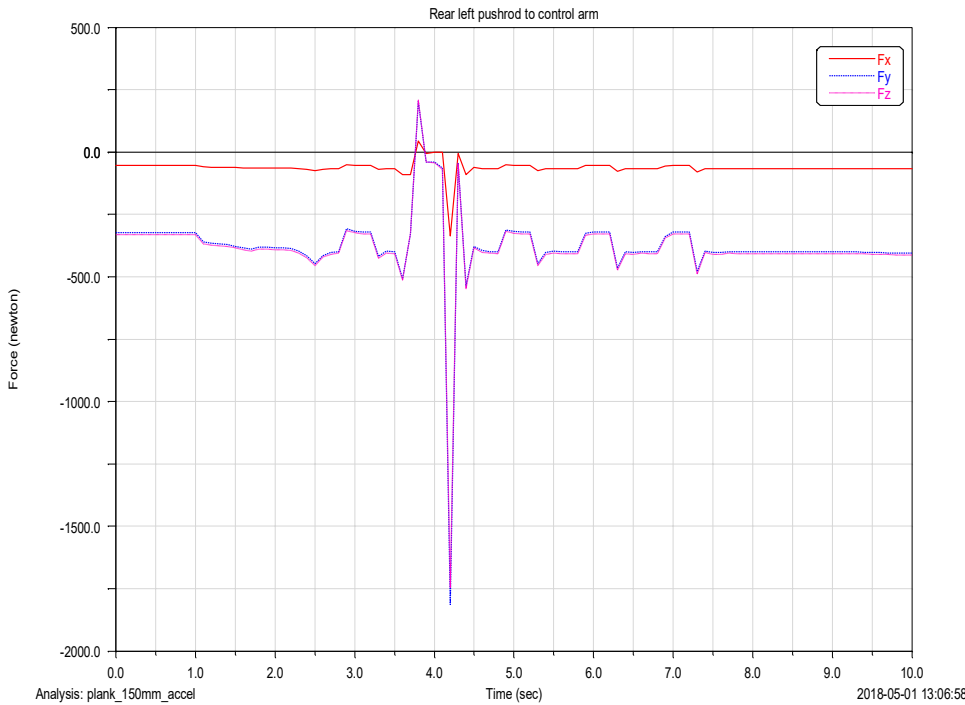
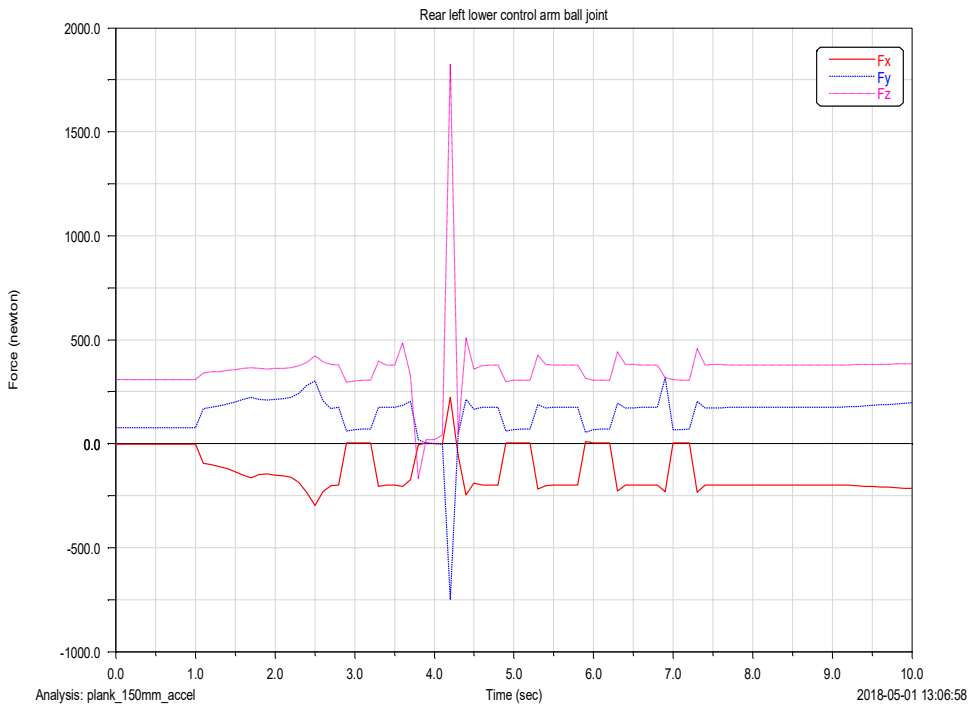


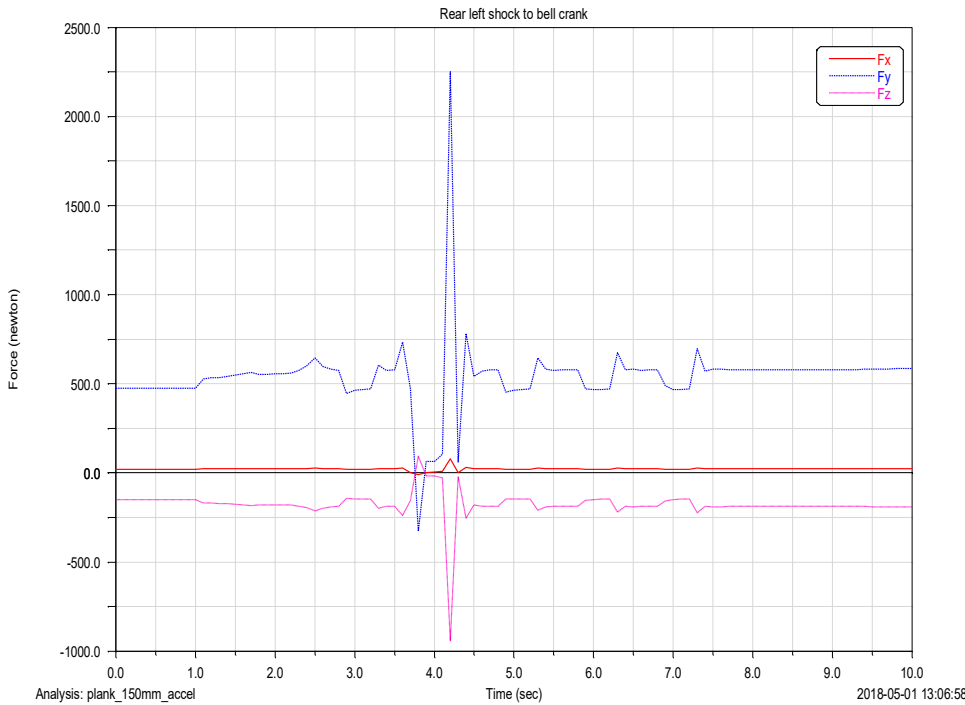
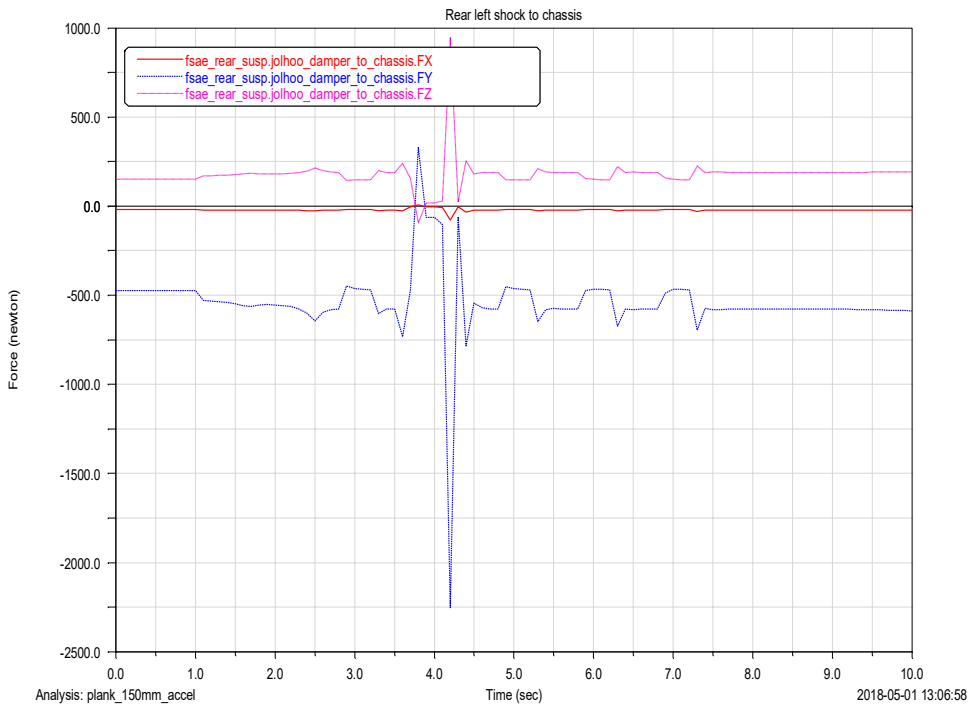












### C.2.4 Constant radius cornering simulation

Full vehicle constant radius cornering simulation driving in a 8 m radius circle during acceleration.

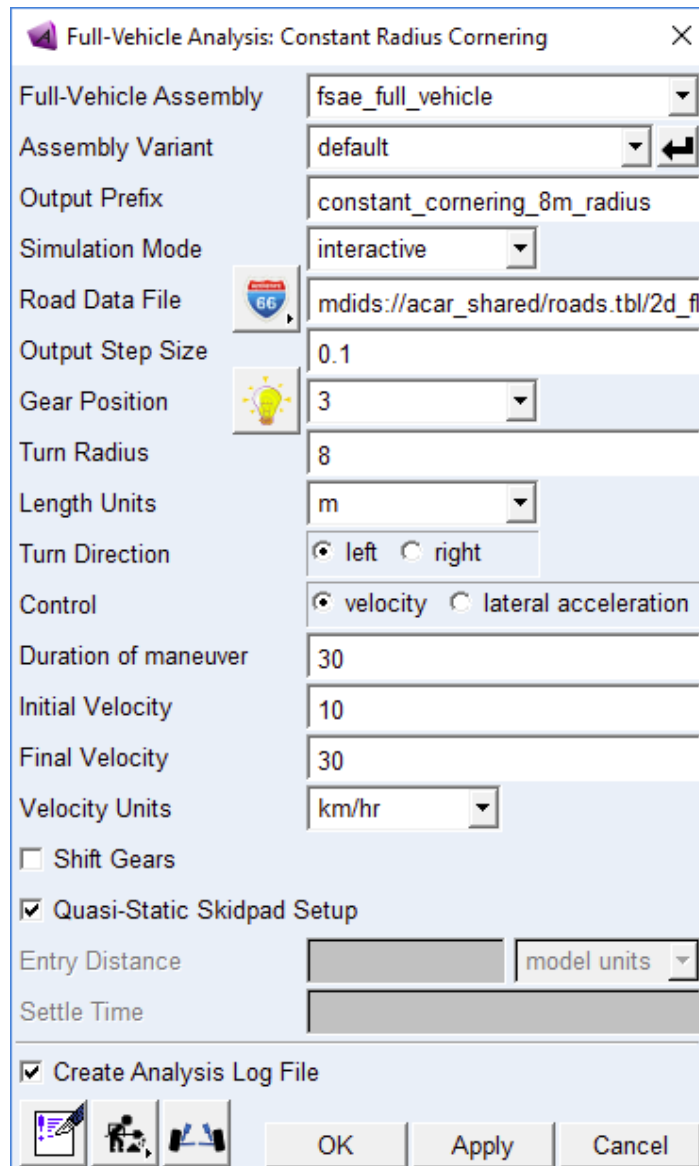
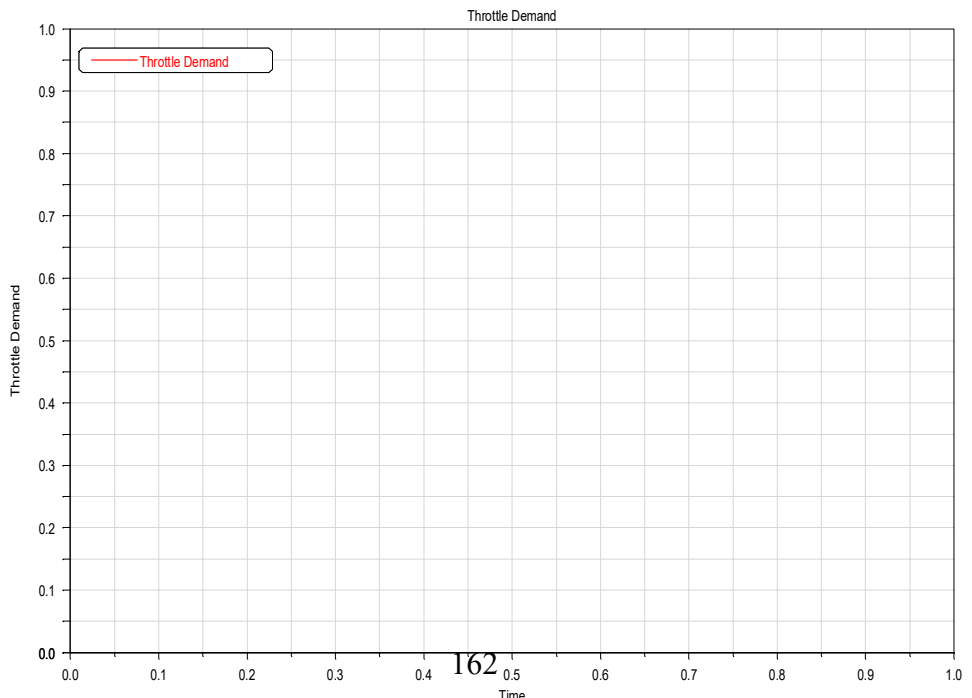
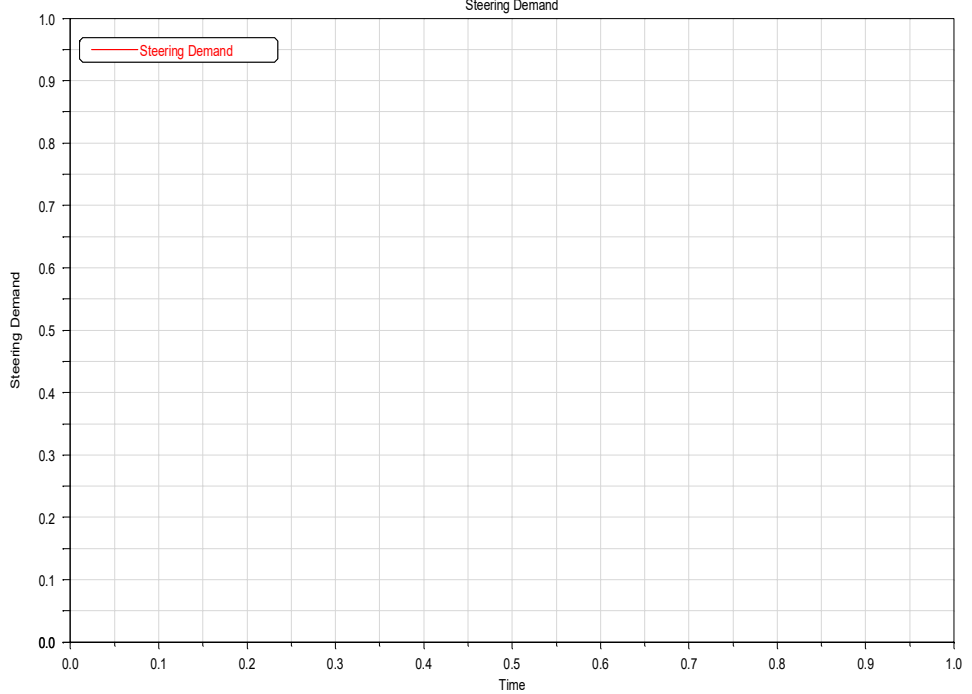
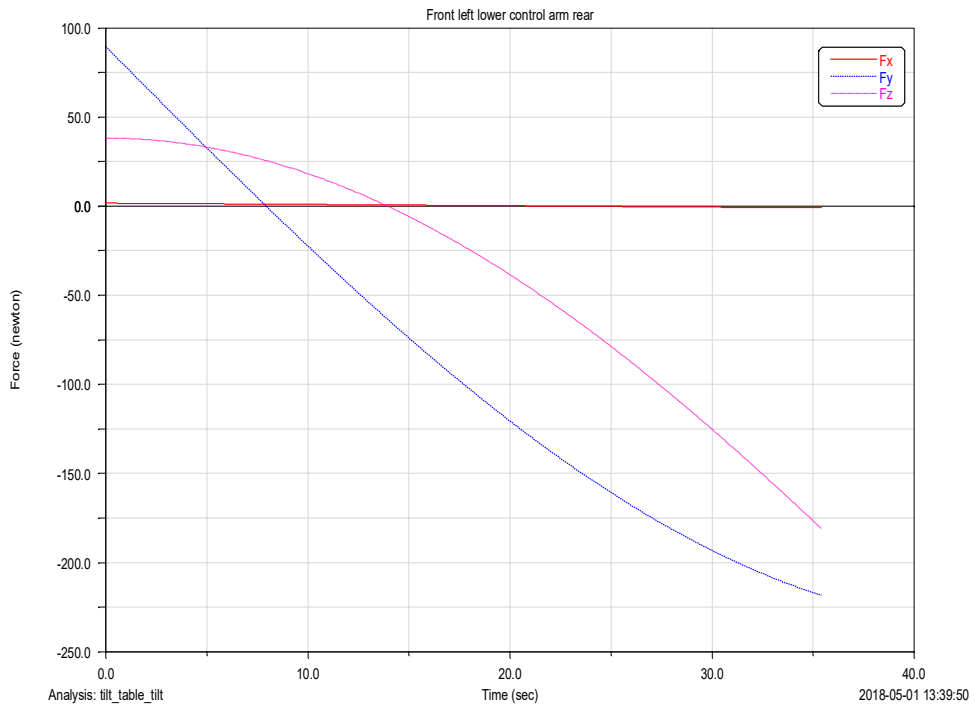
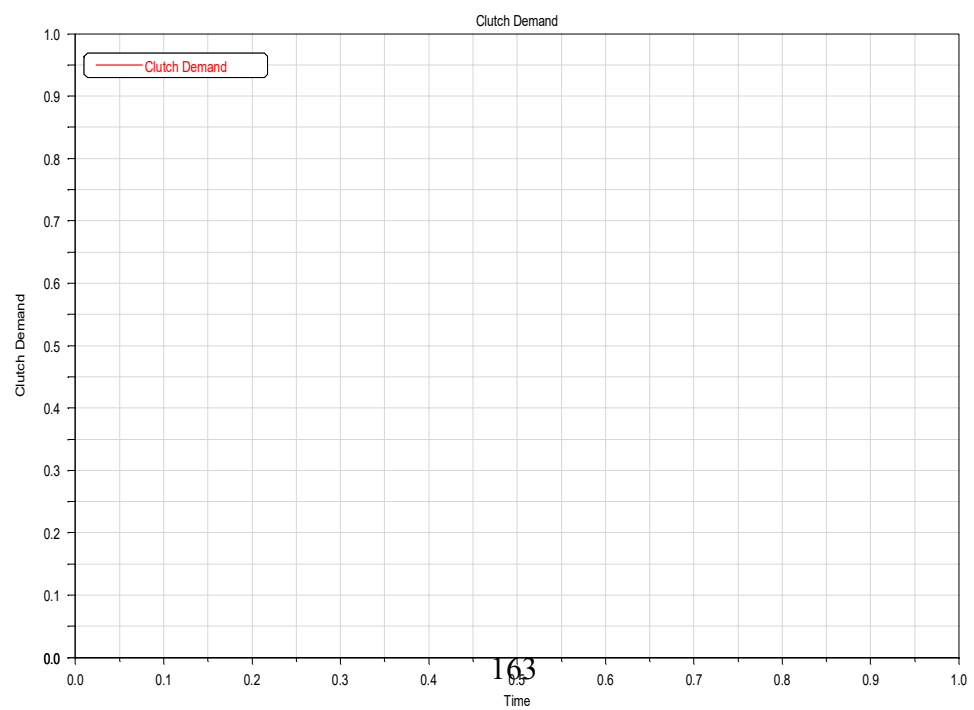
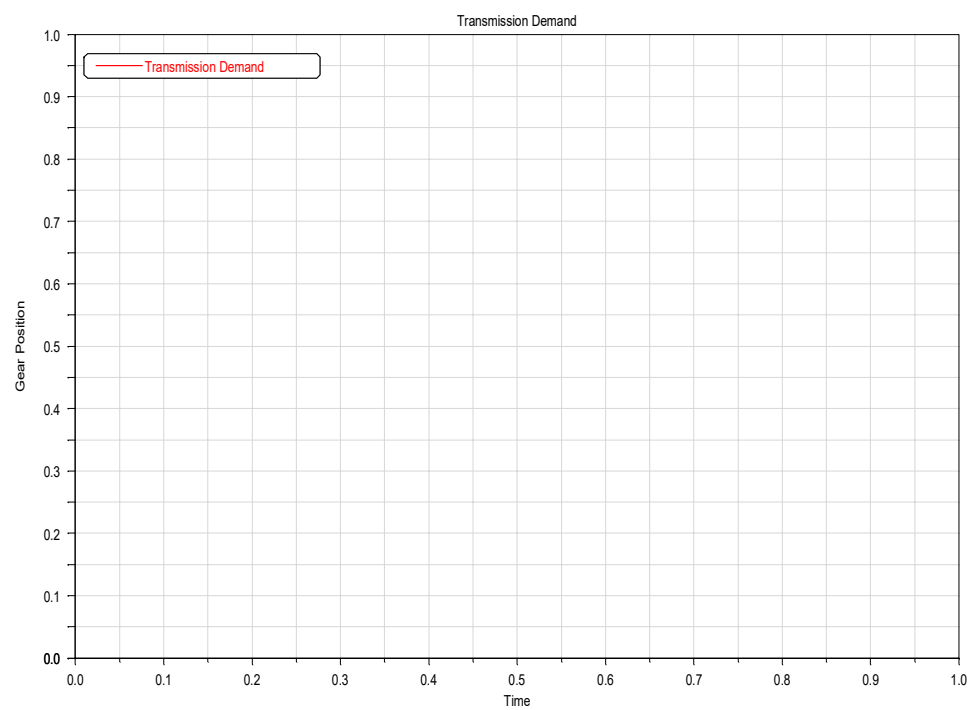
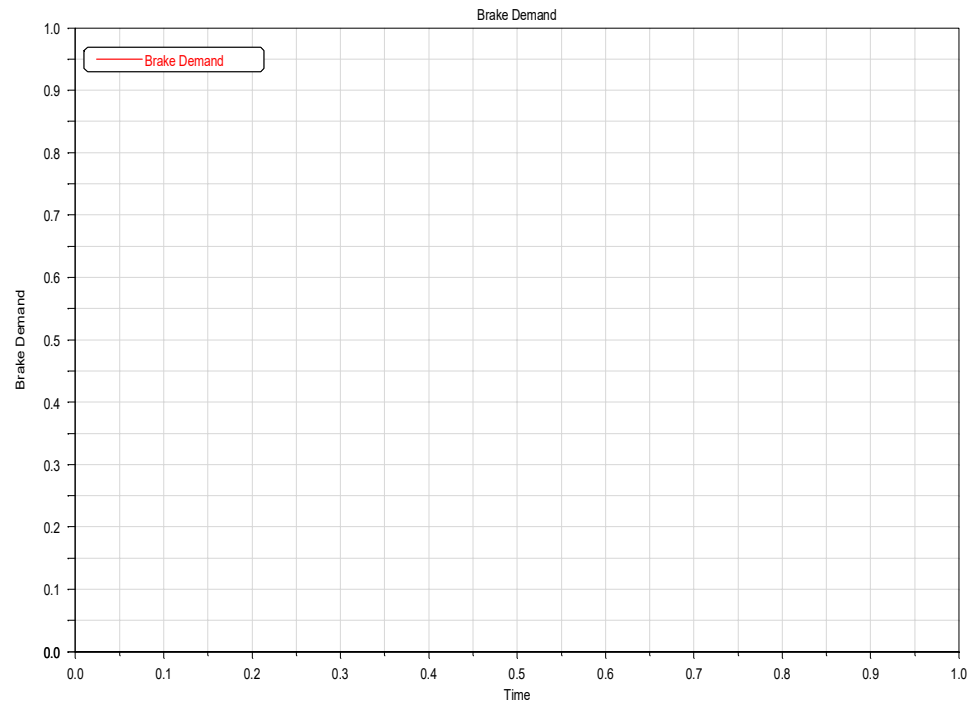
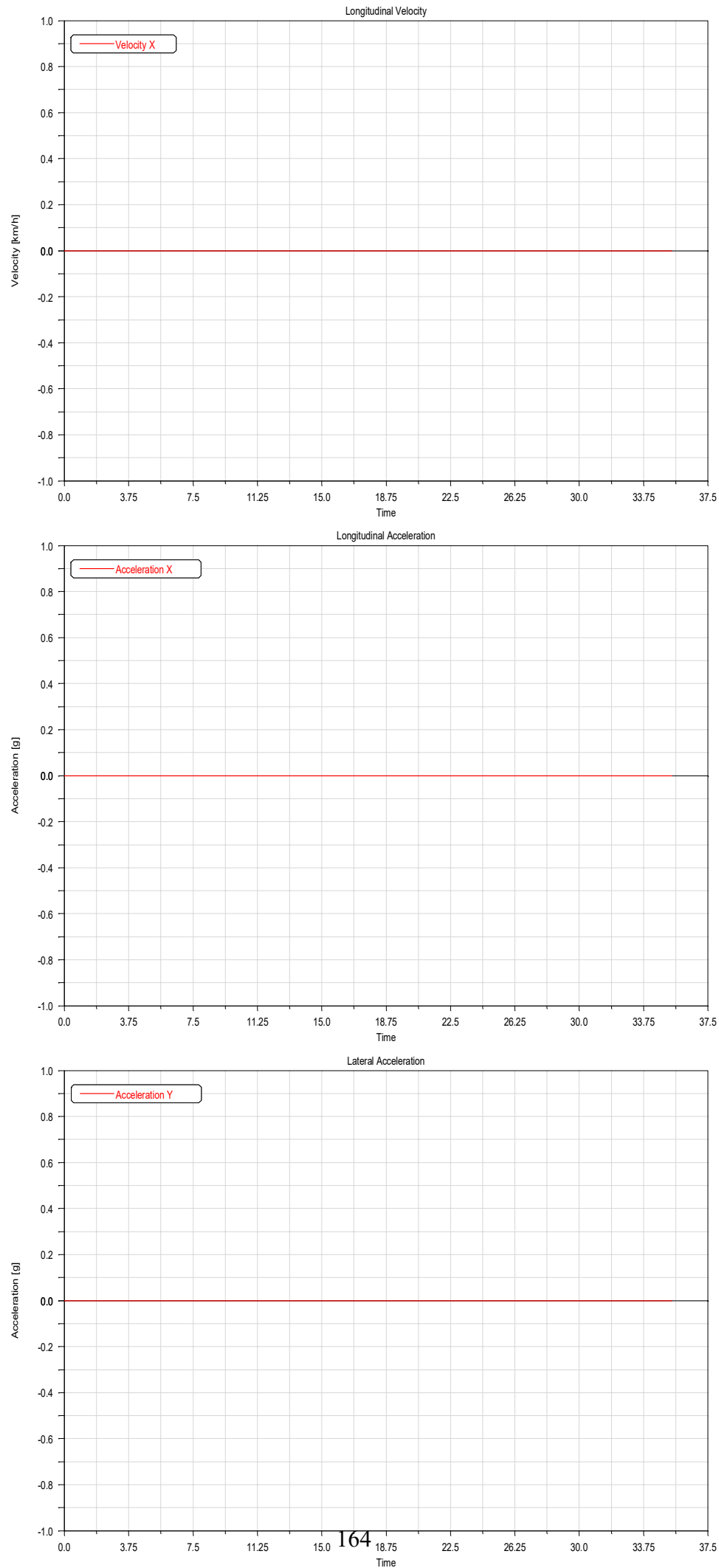
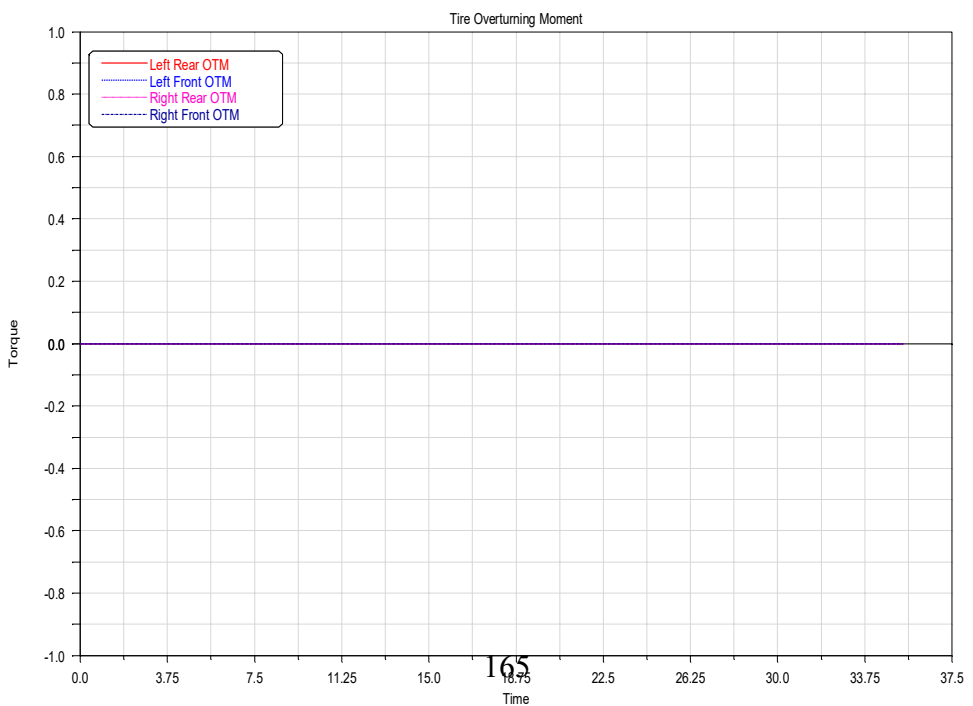
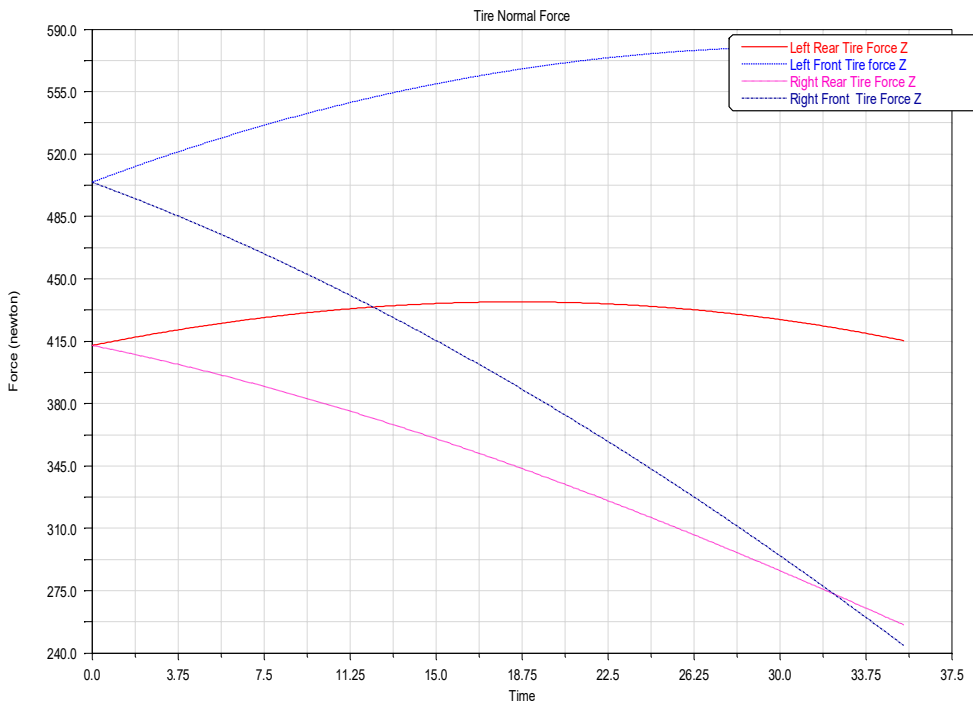
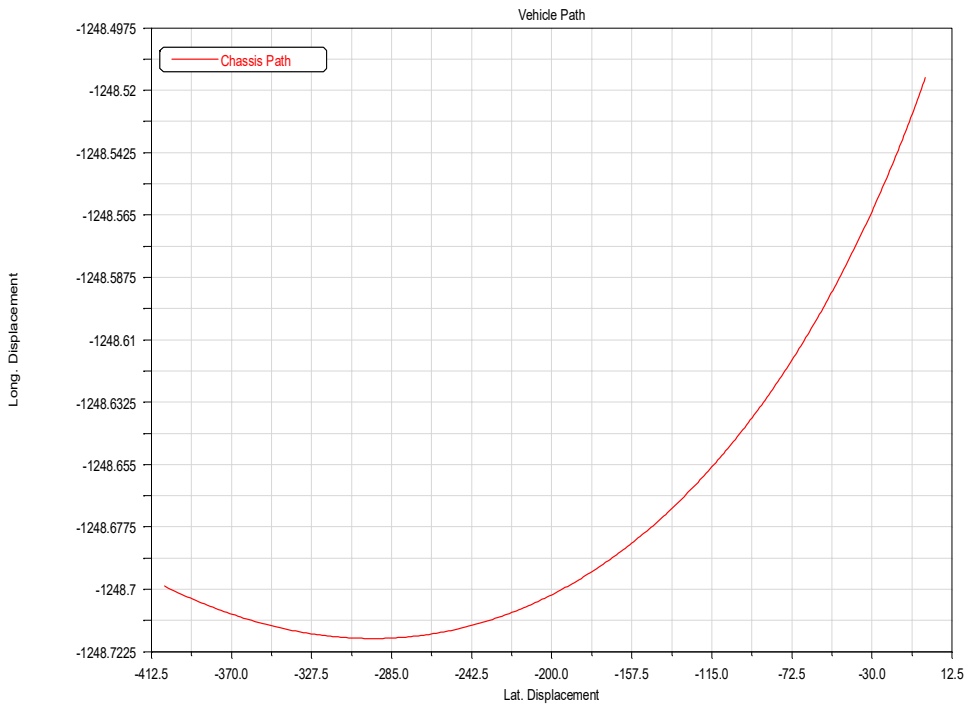


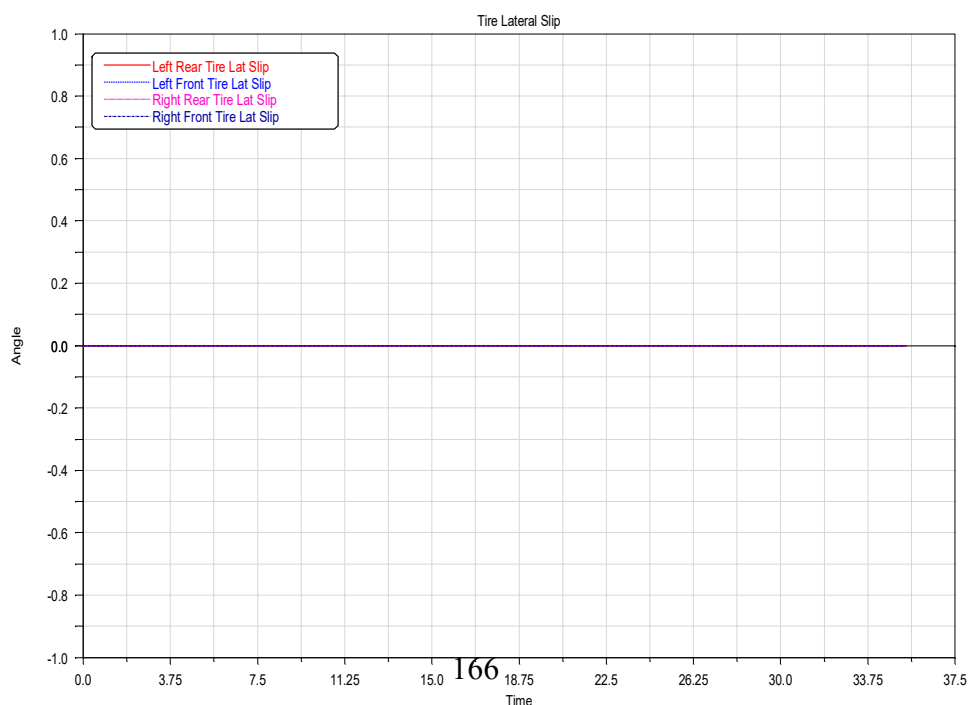
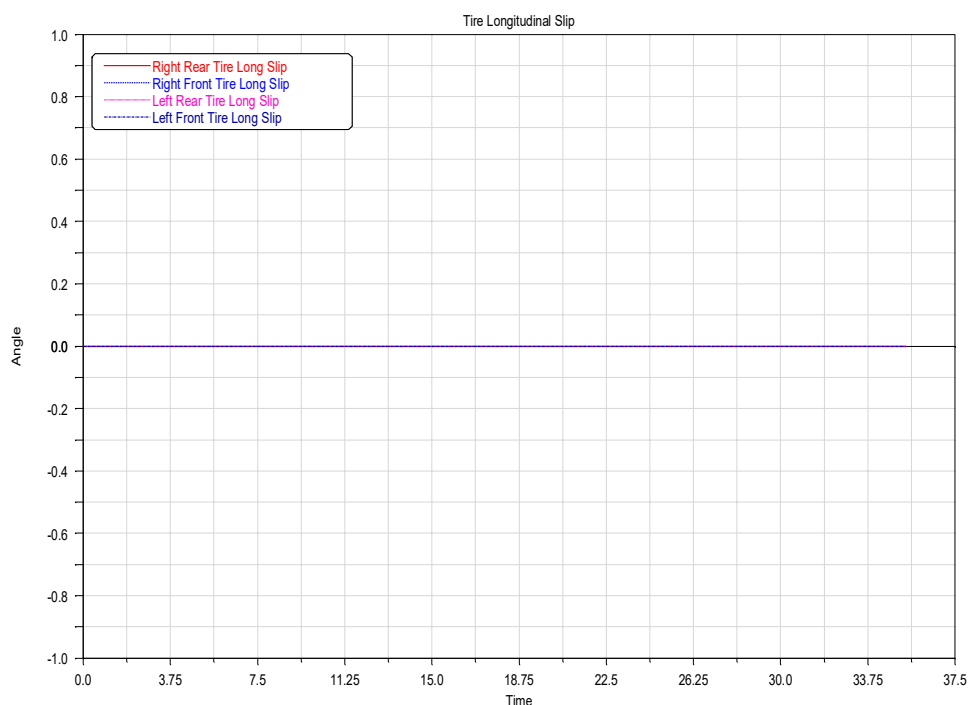
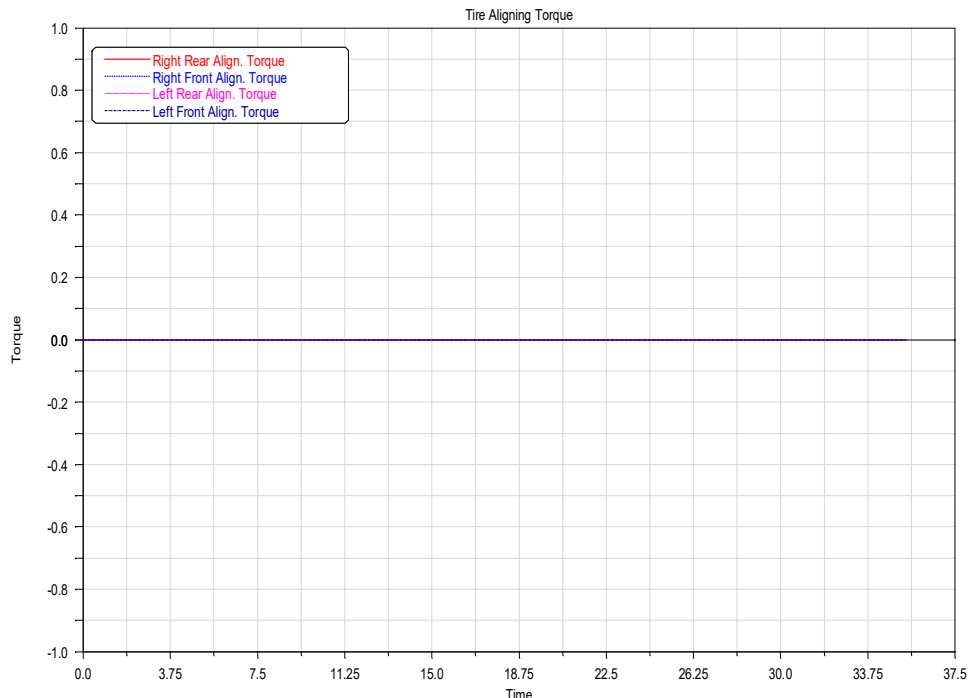
Figure C.3: Adams car [4] constant corner simulation setup window

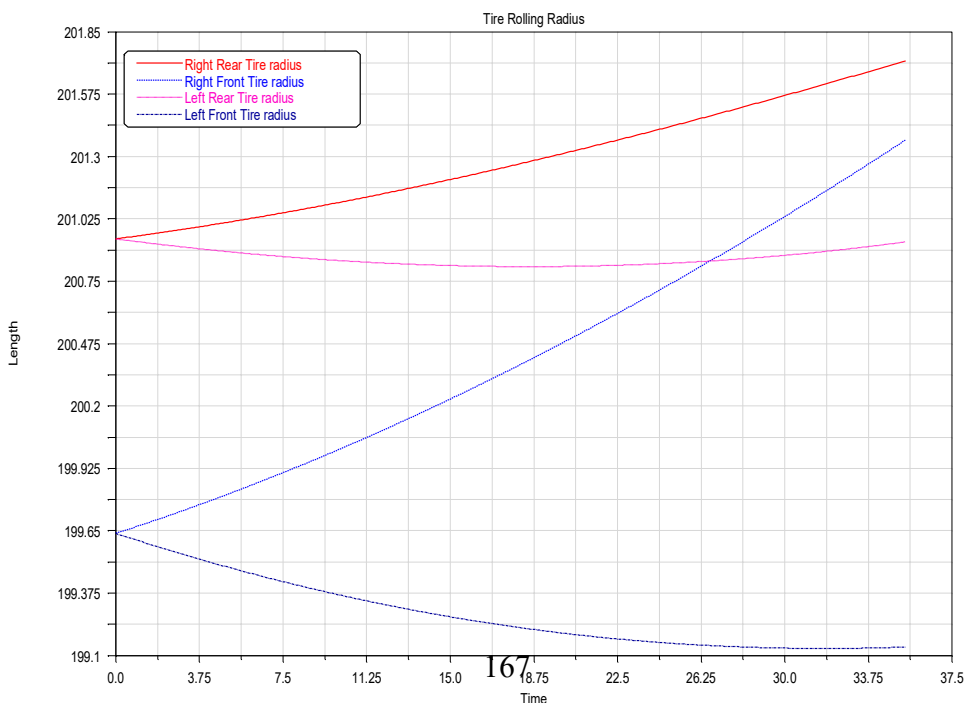
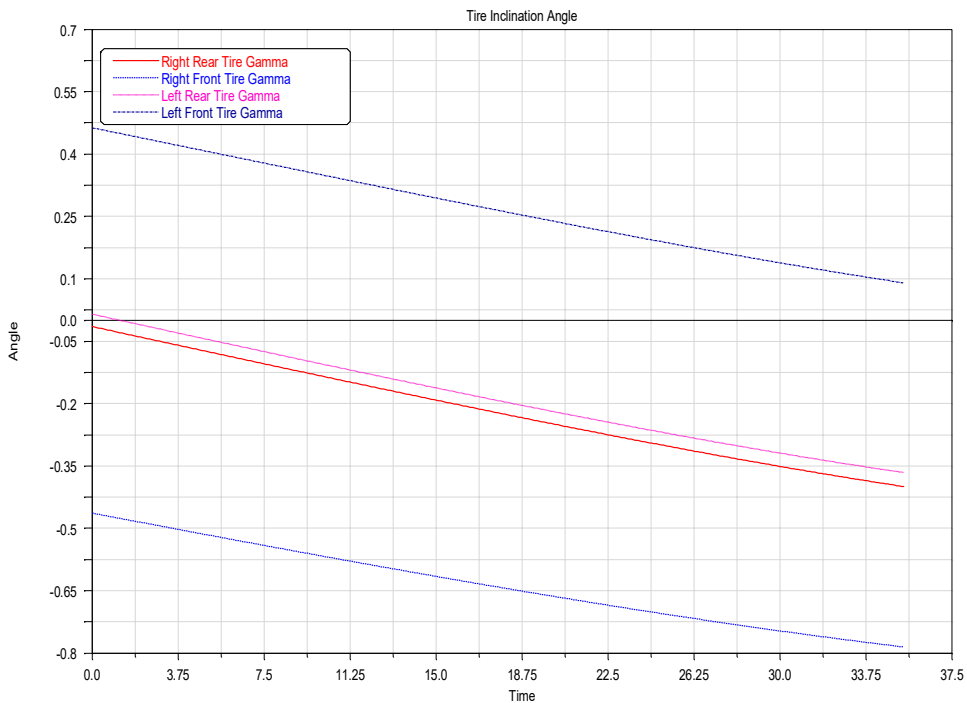
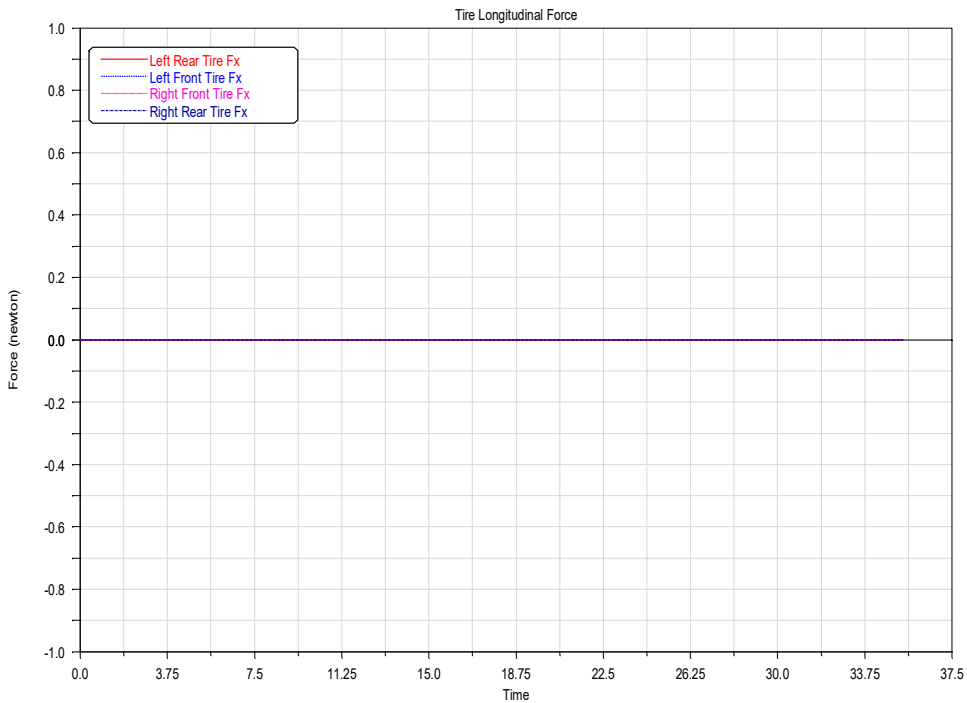


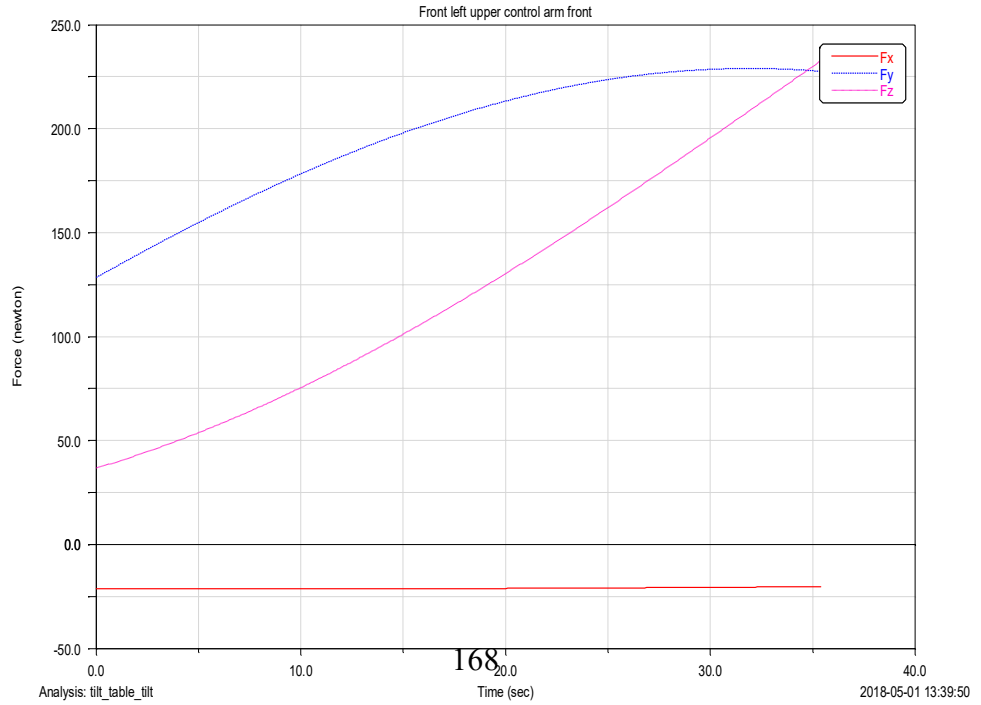
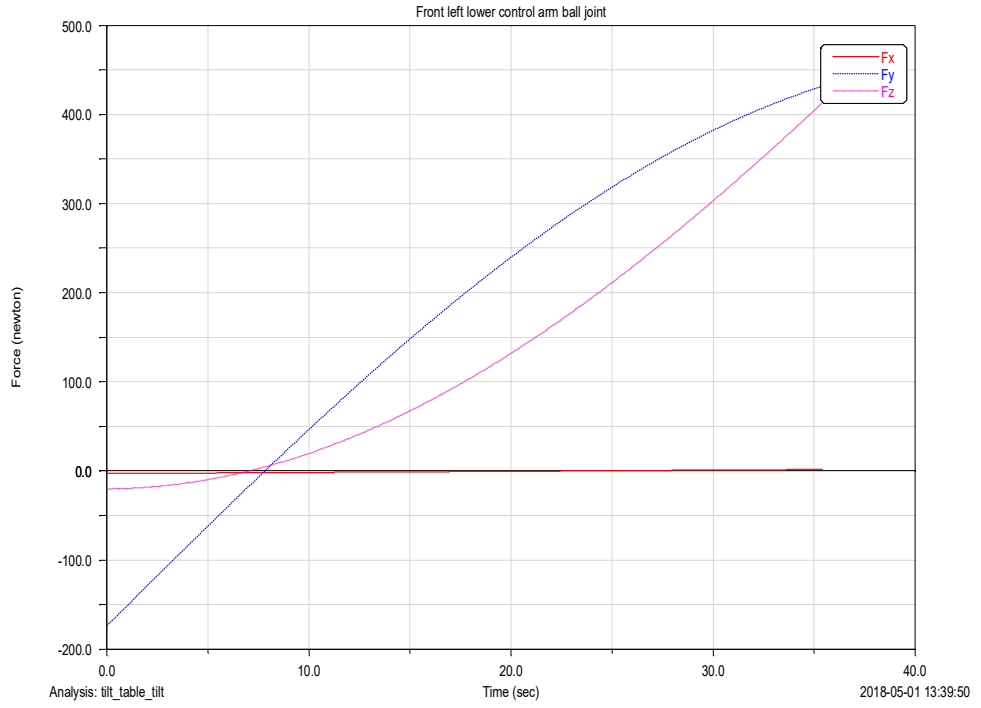
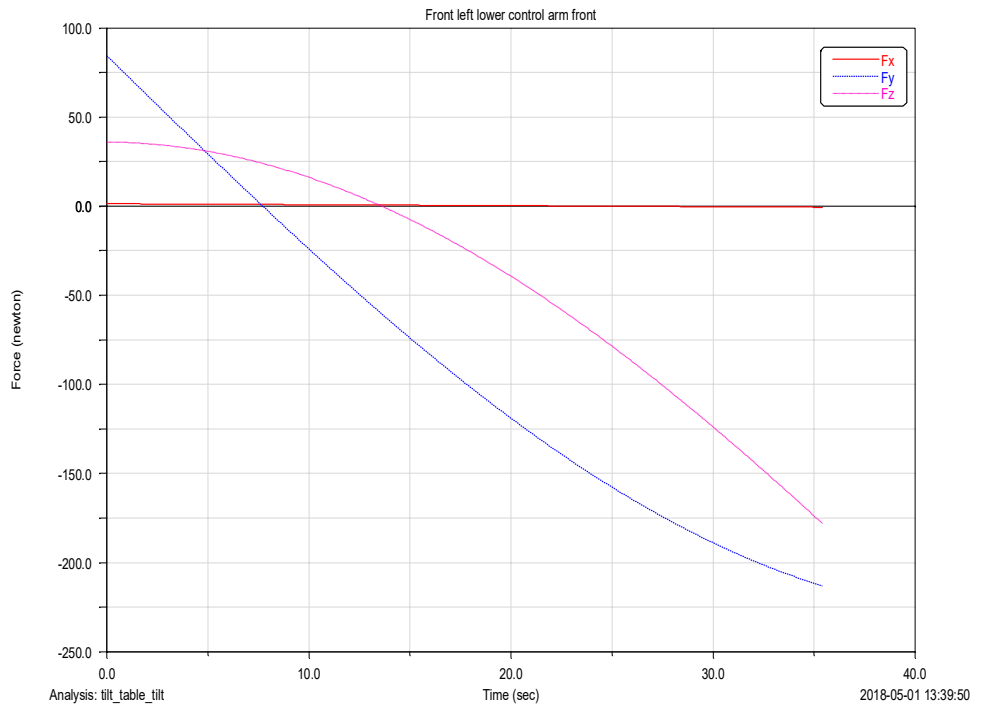


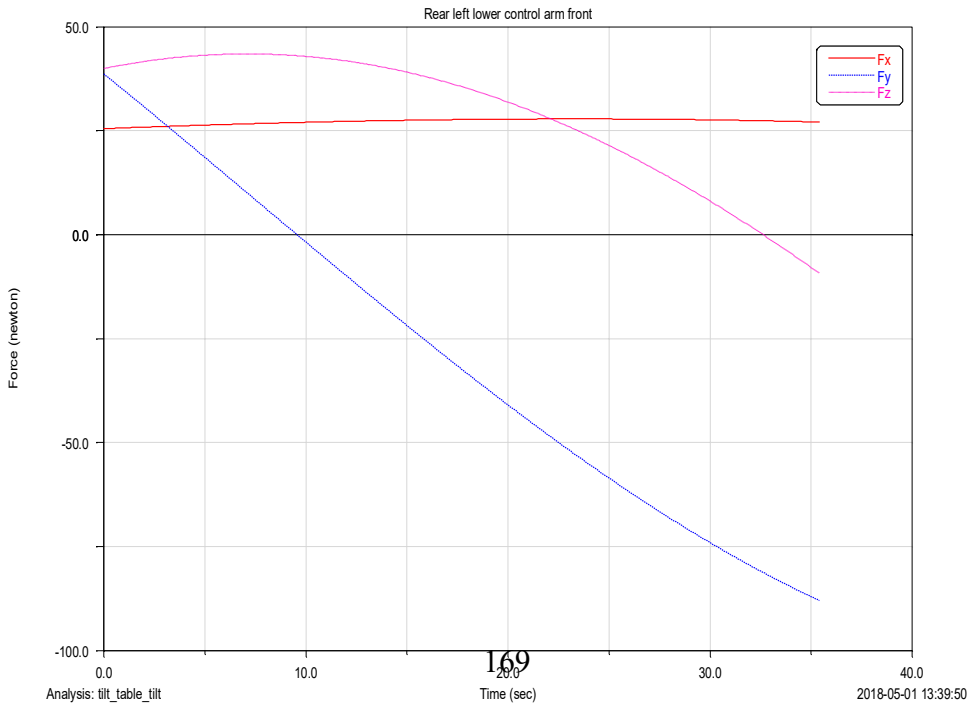
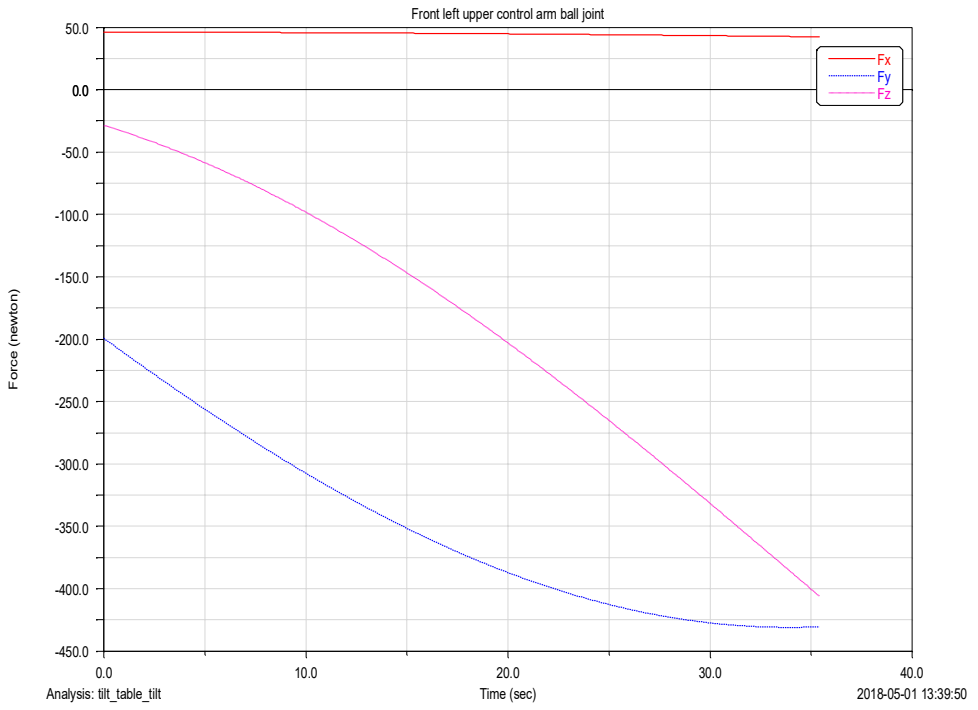
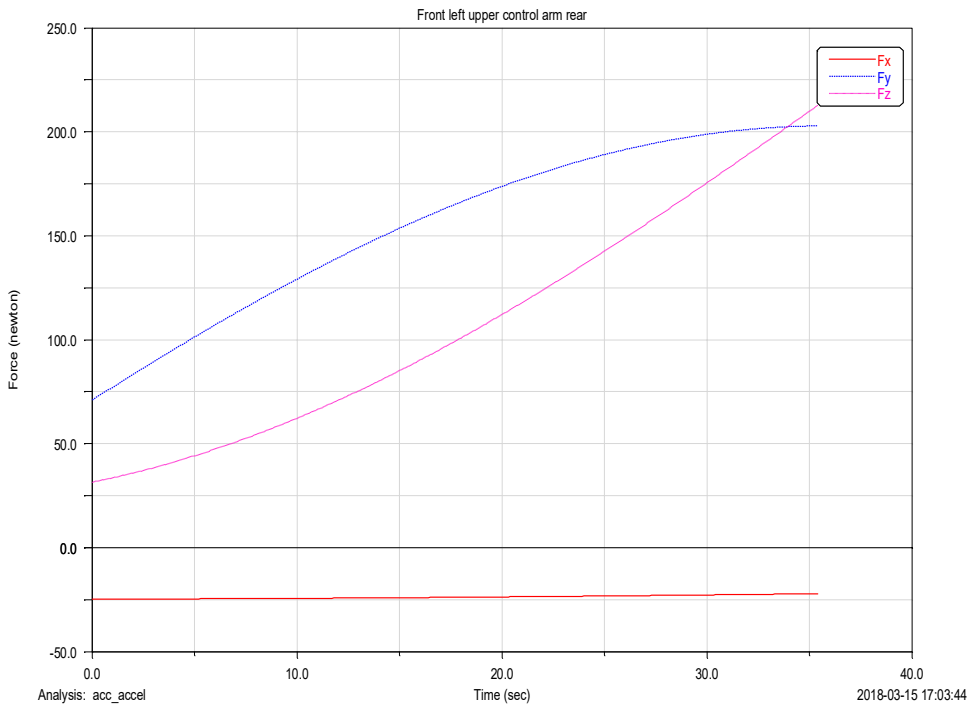


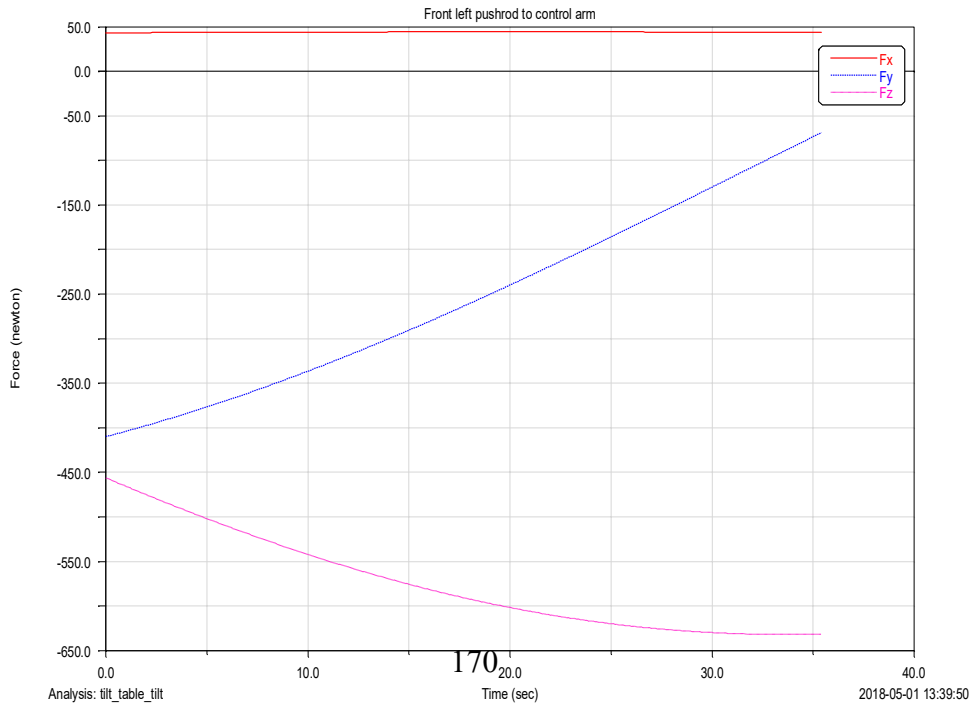
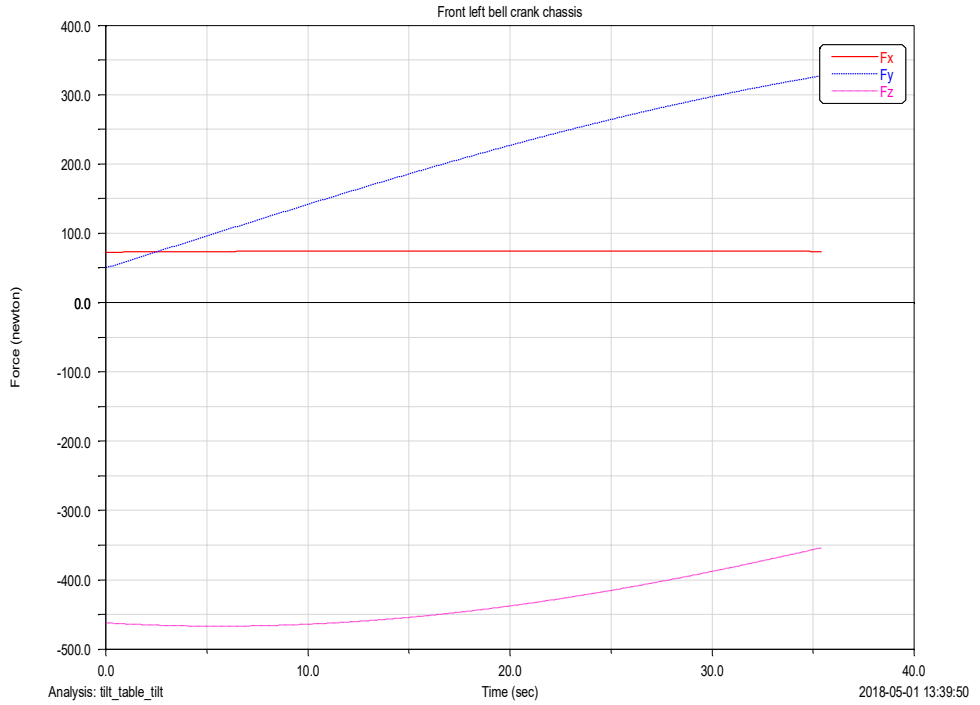
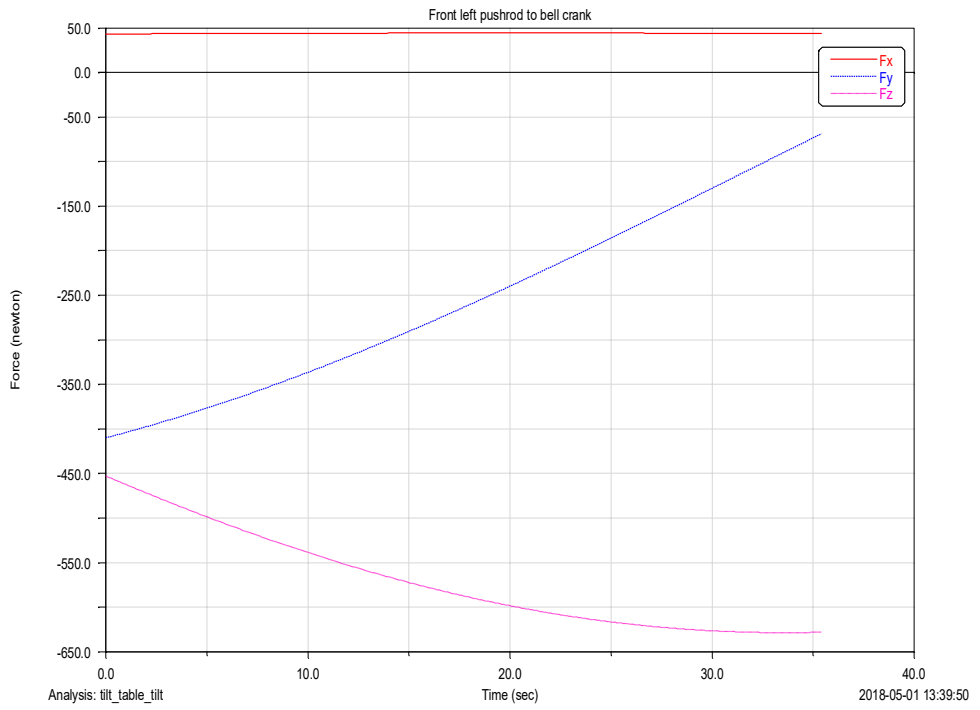


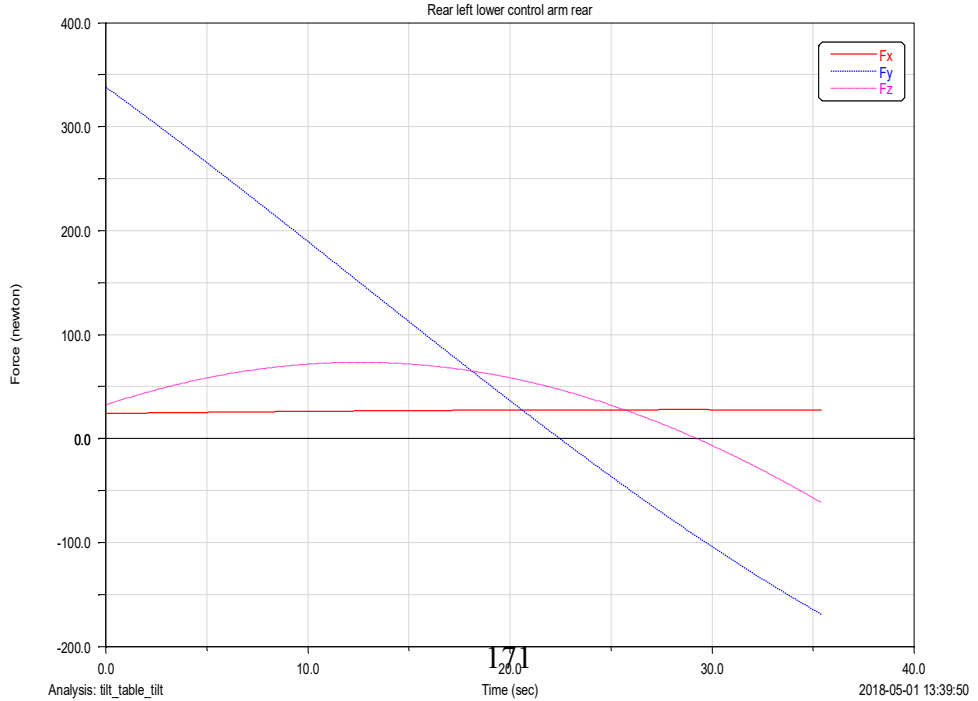
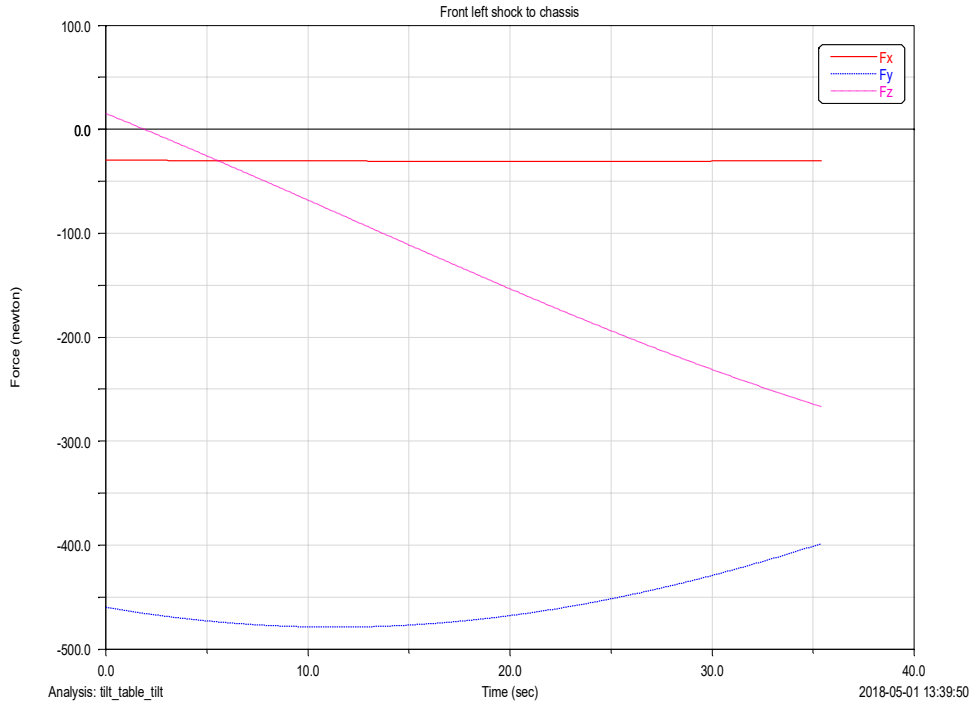
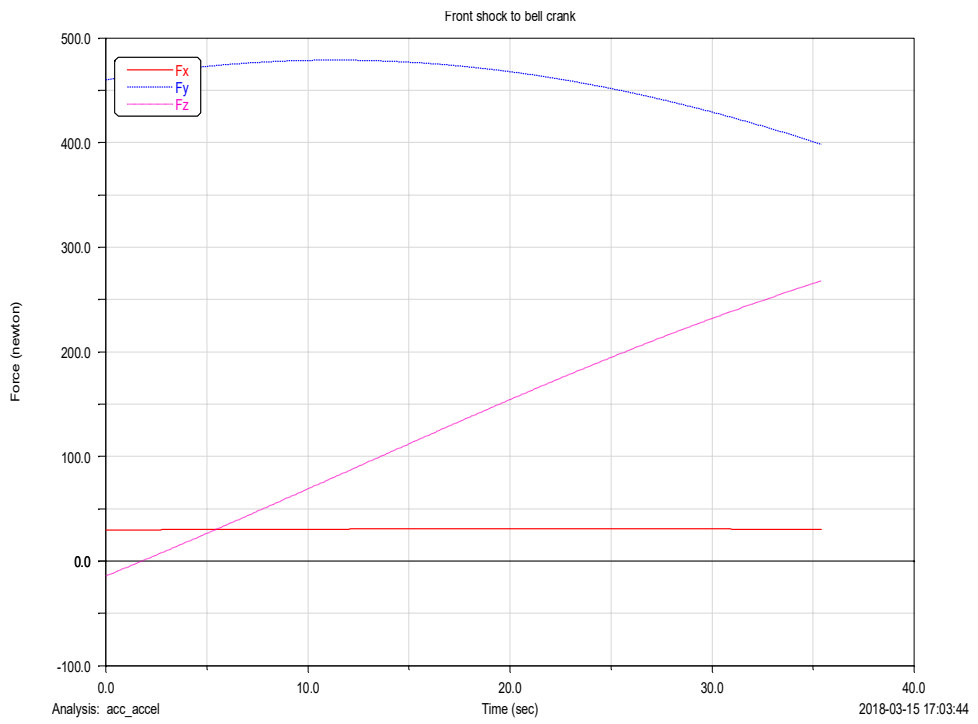


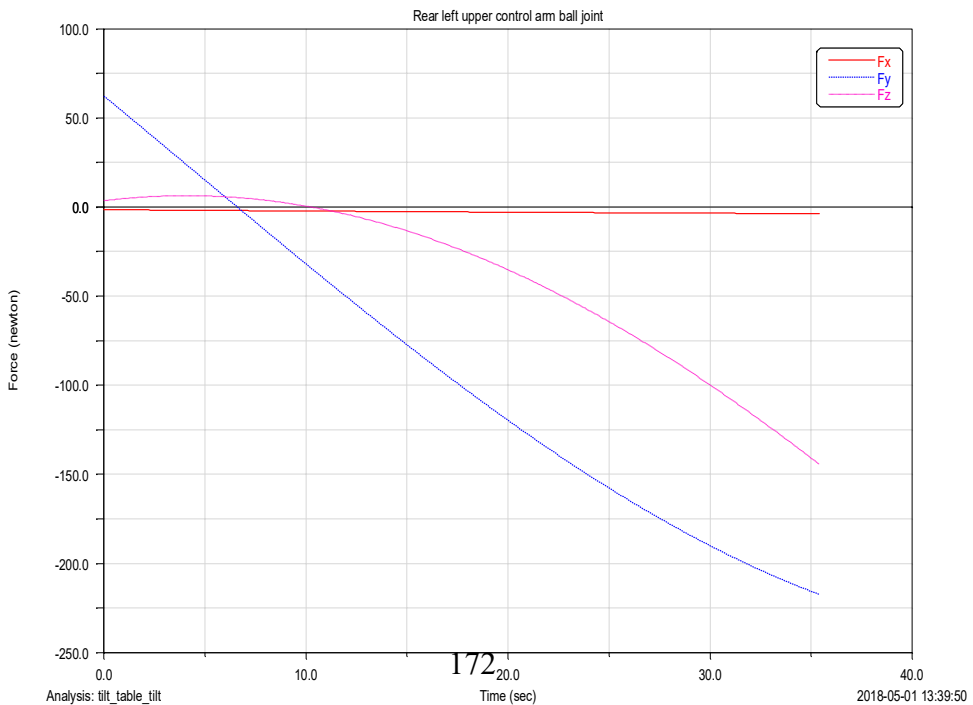
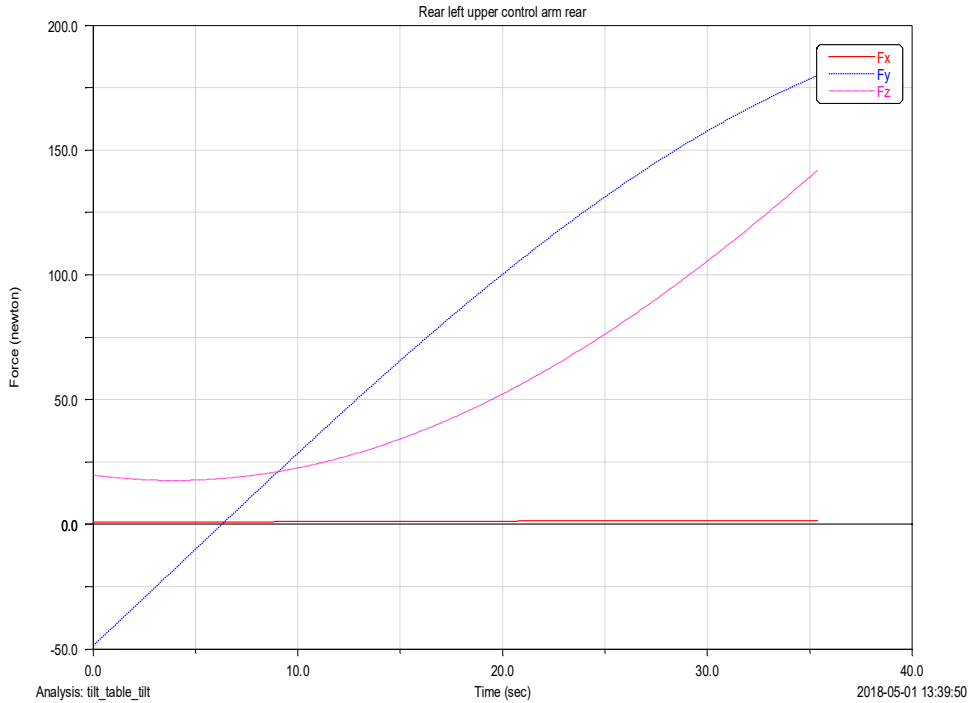
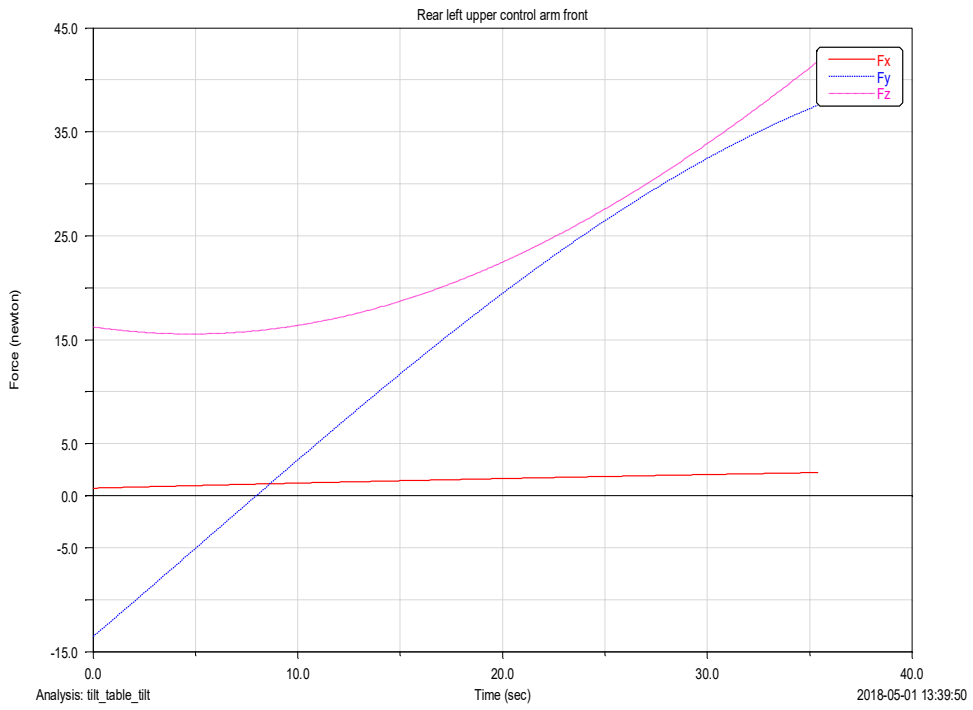


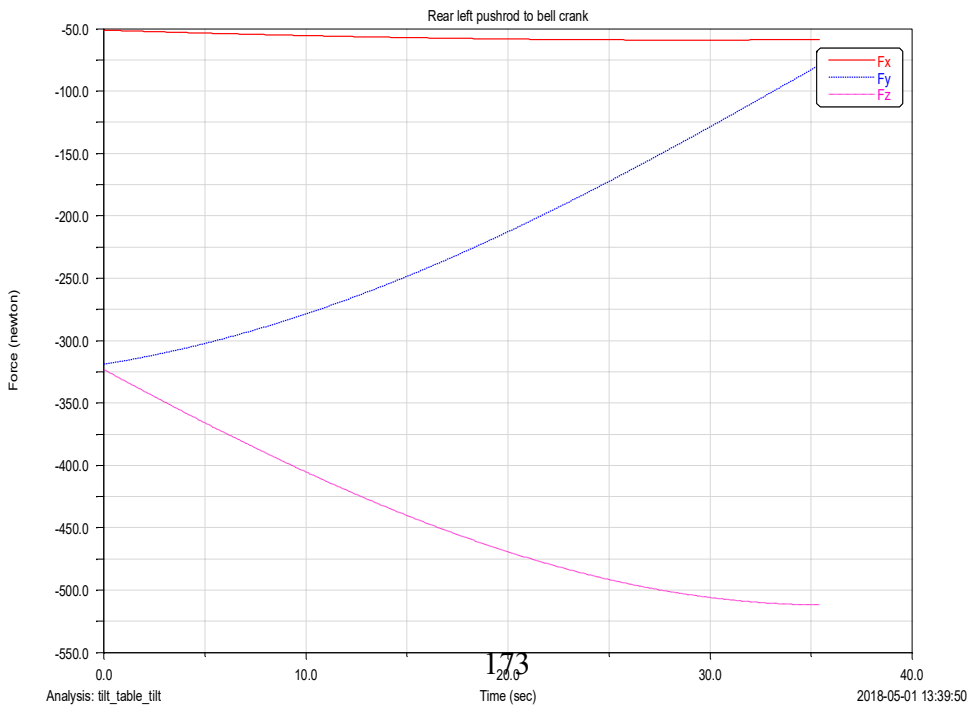
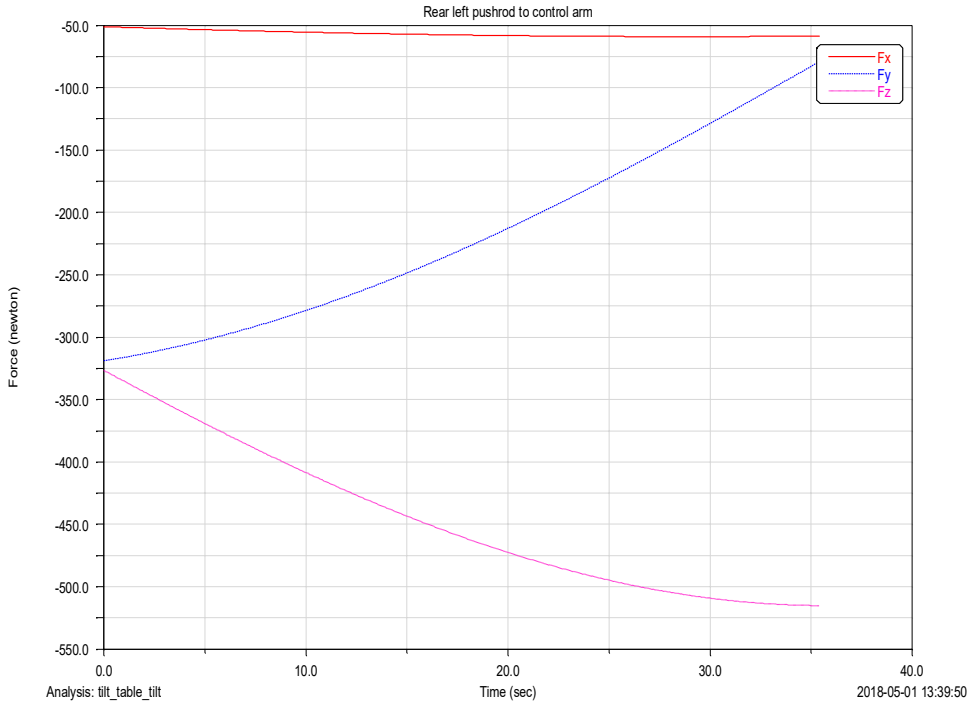
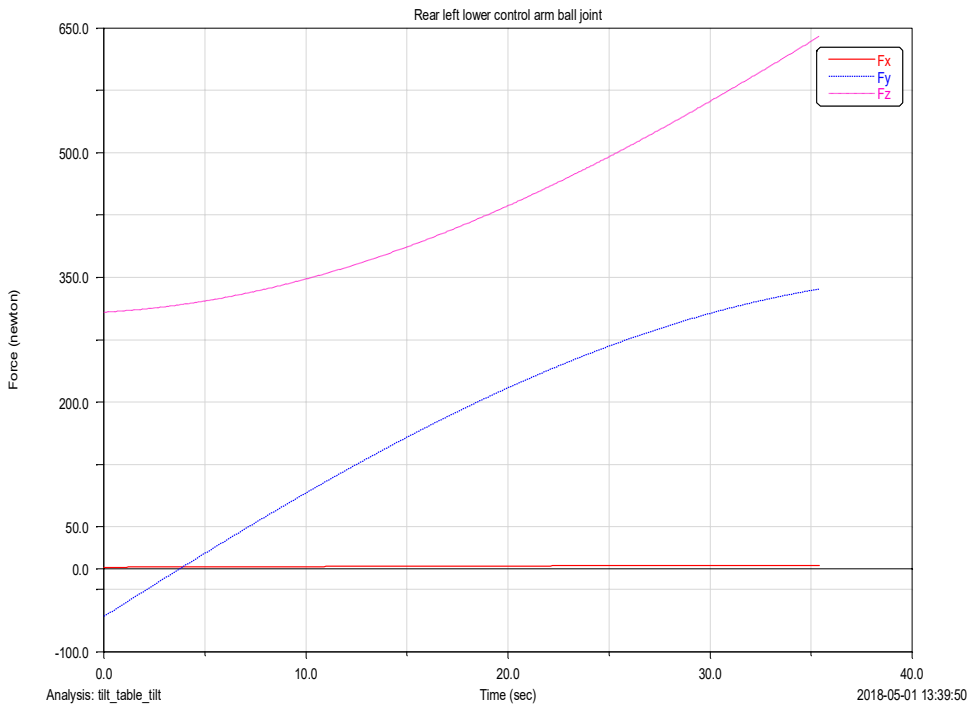


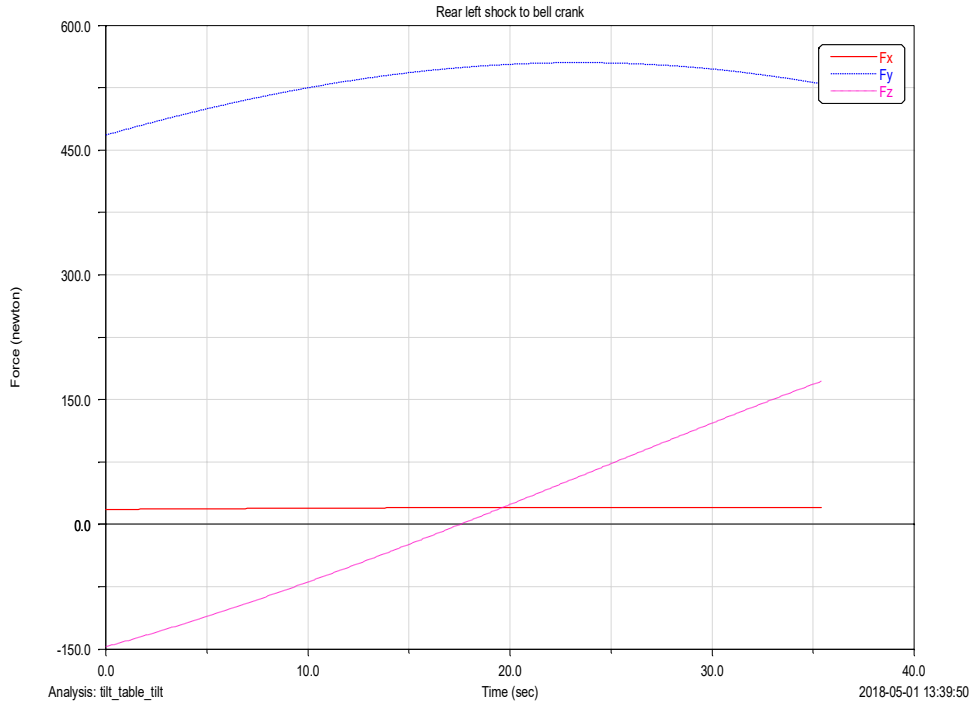
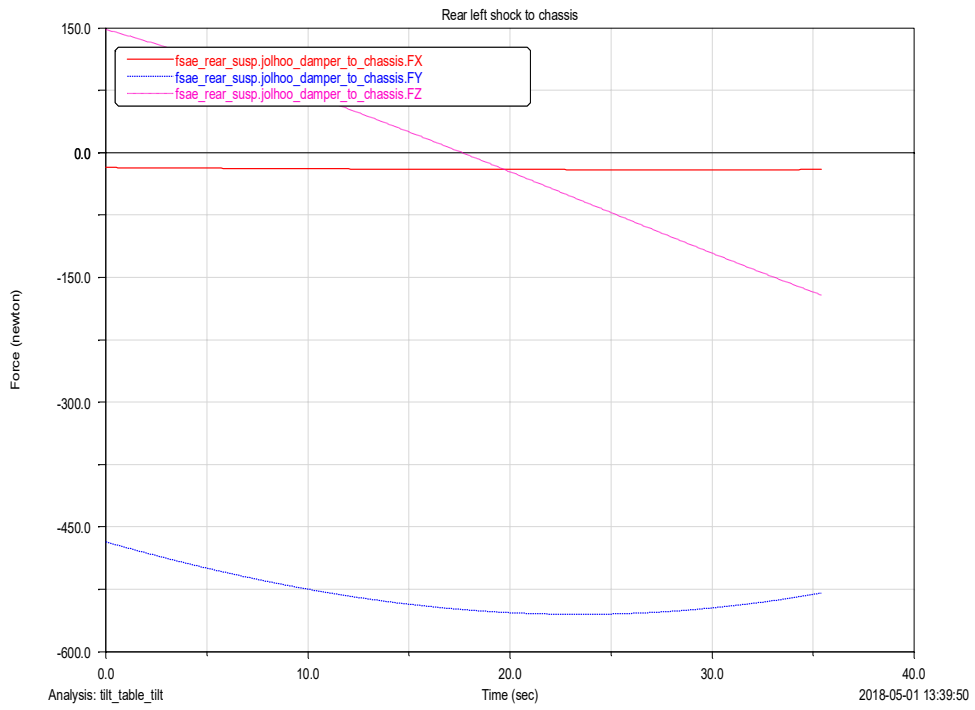












### C.2.5 Tilt simulation

Full vehicle simulation of stationary vehicle tilt to 45°.

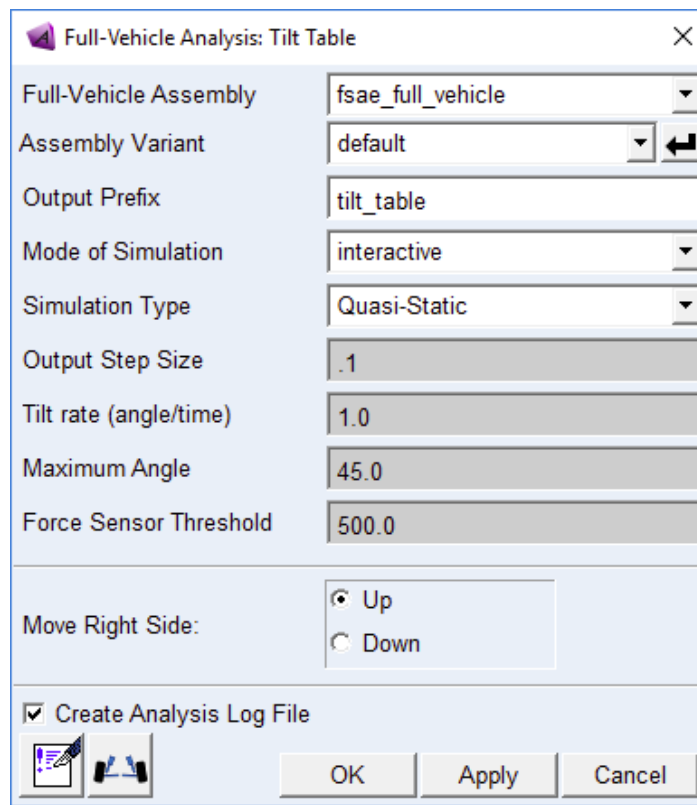
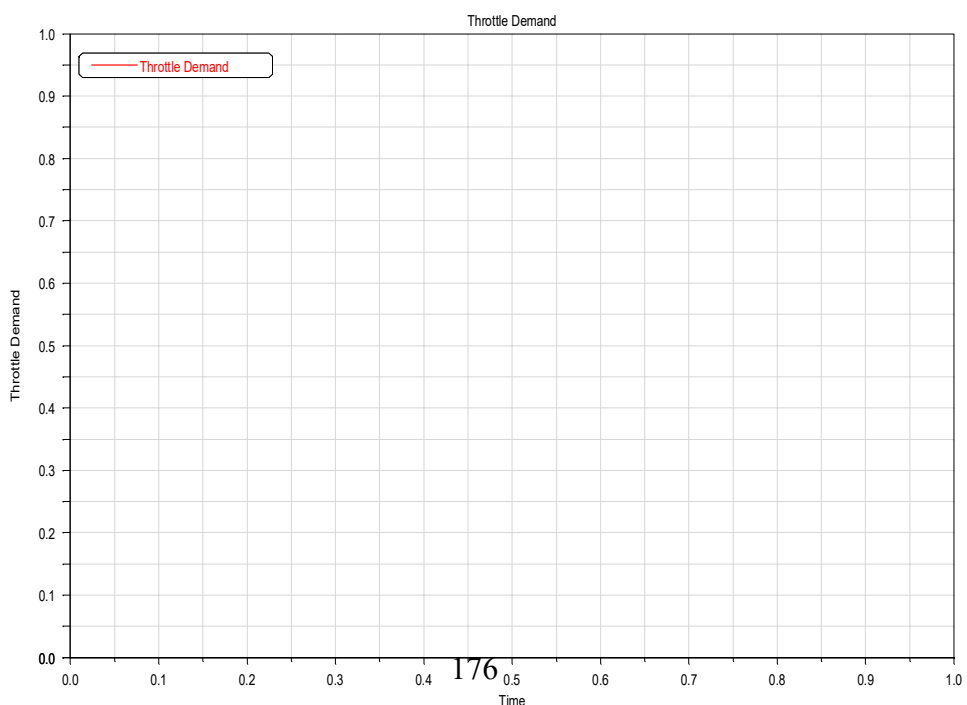
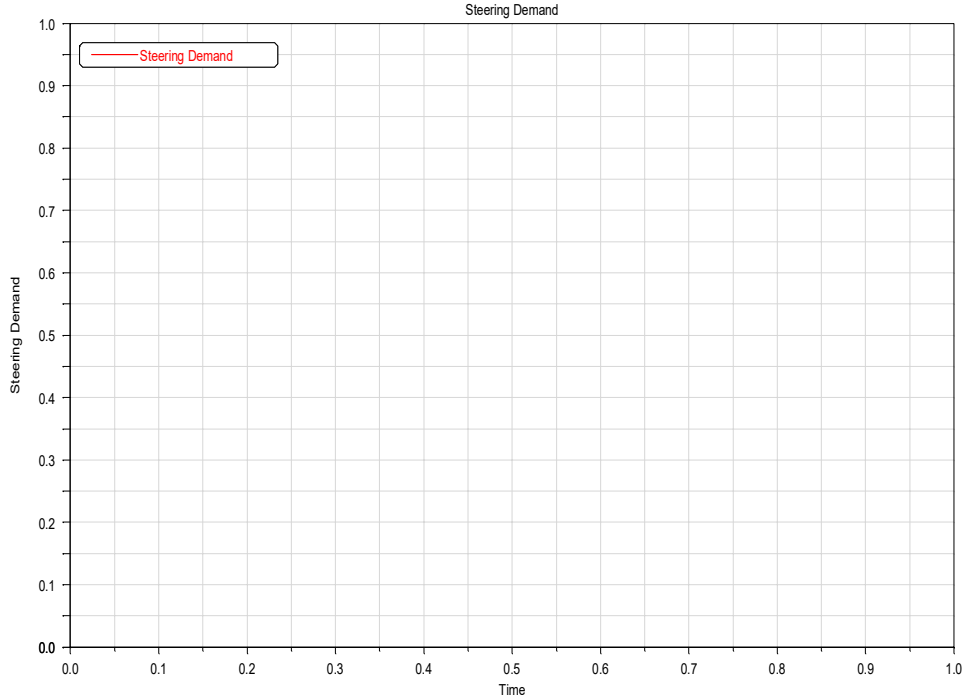
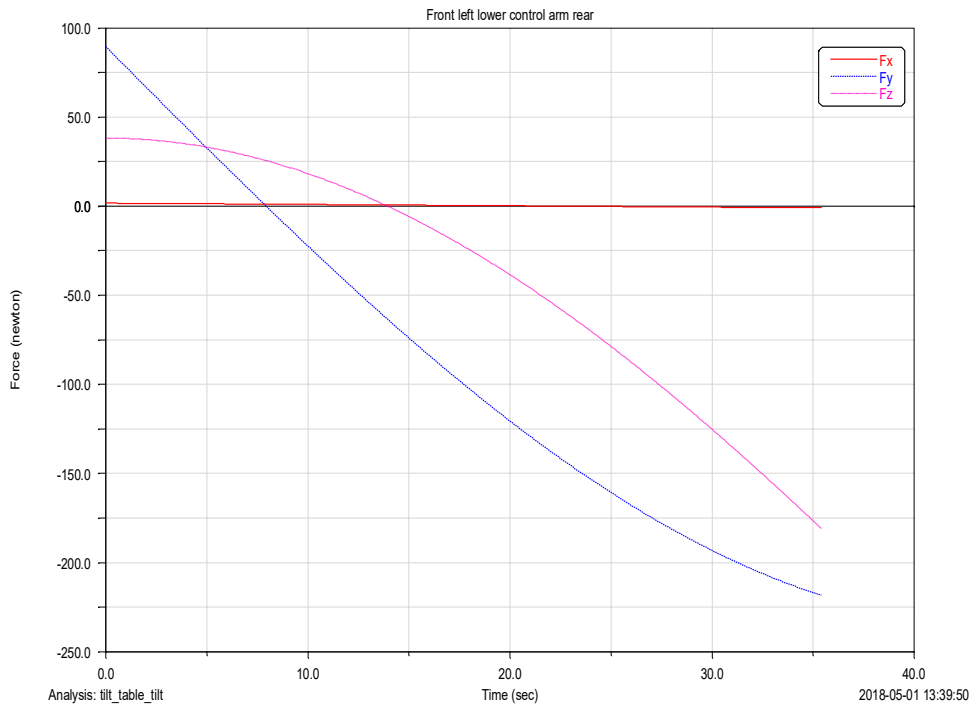
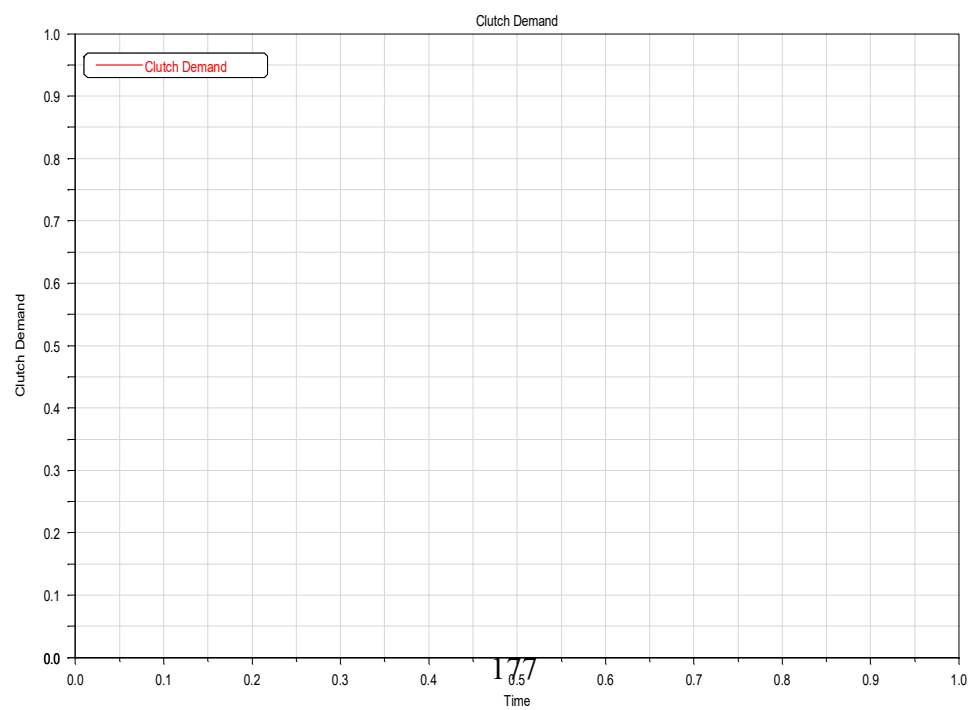
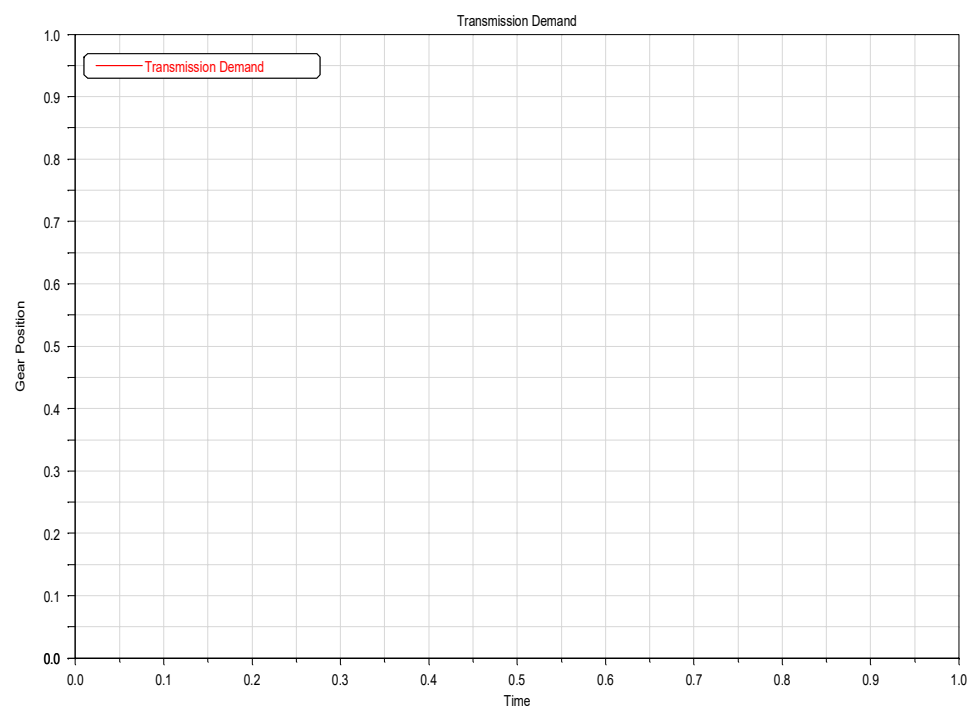
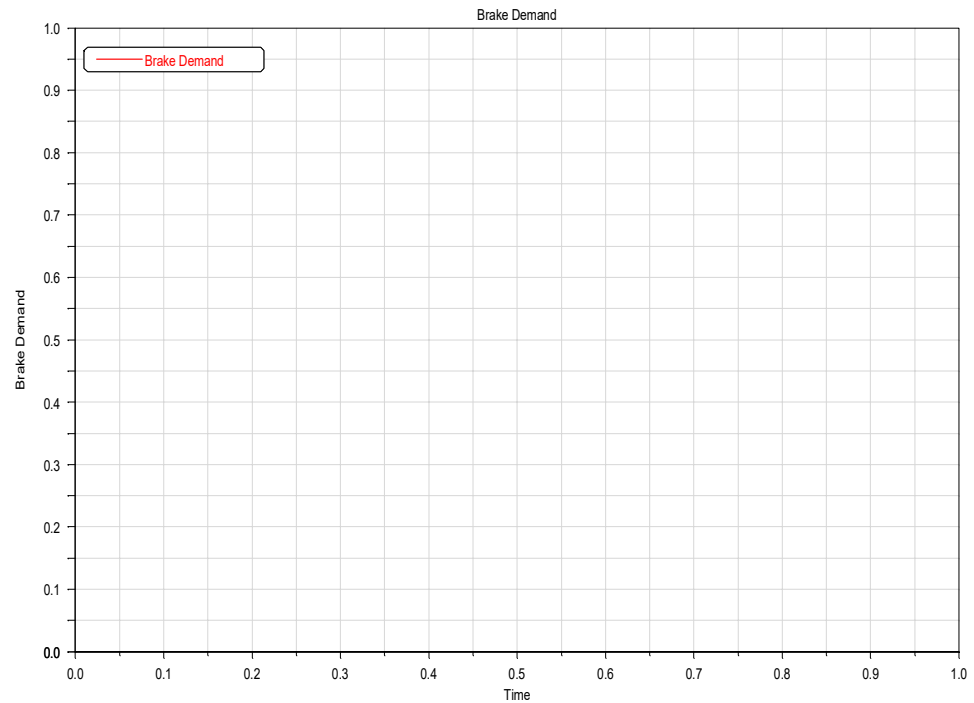
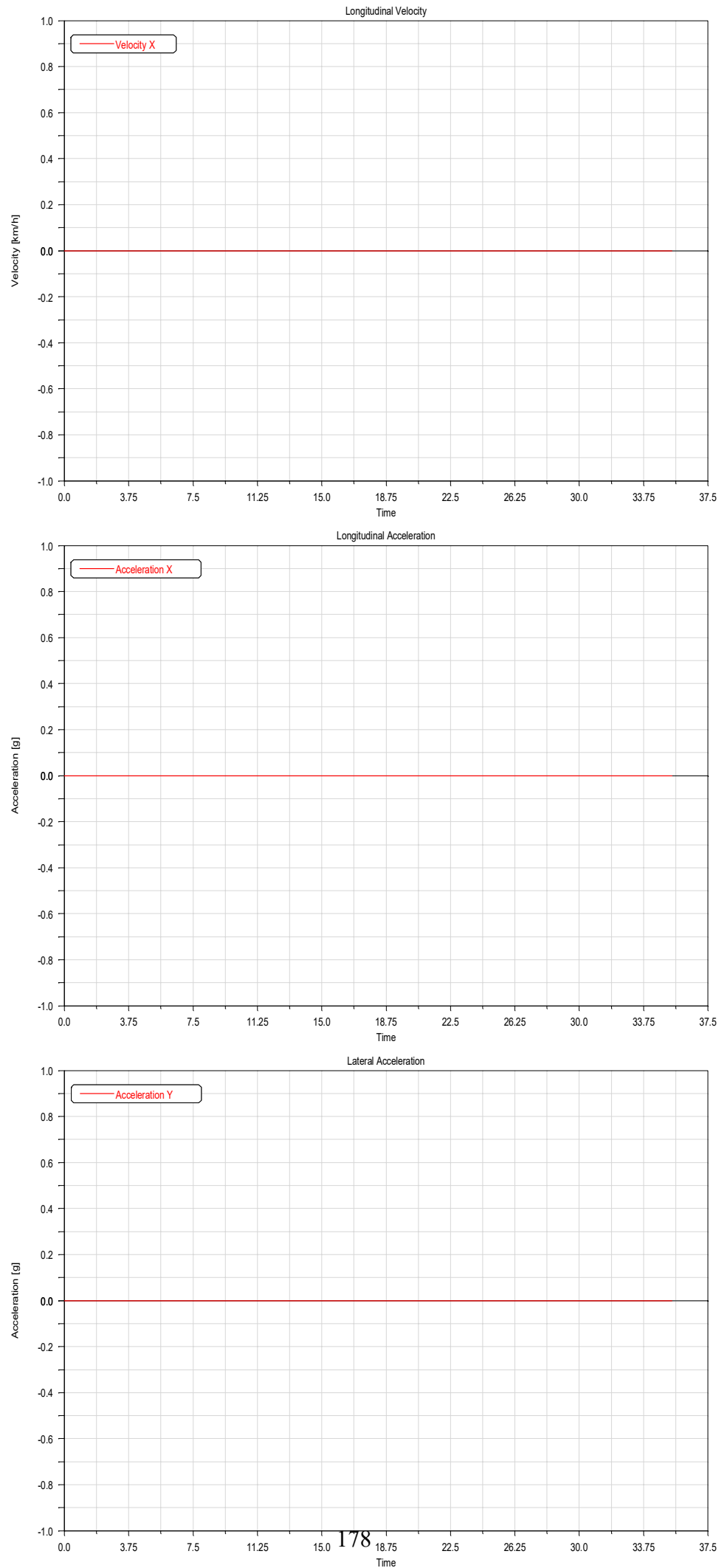
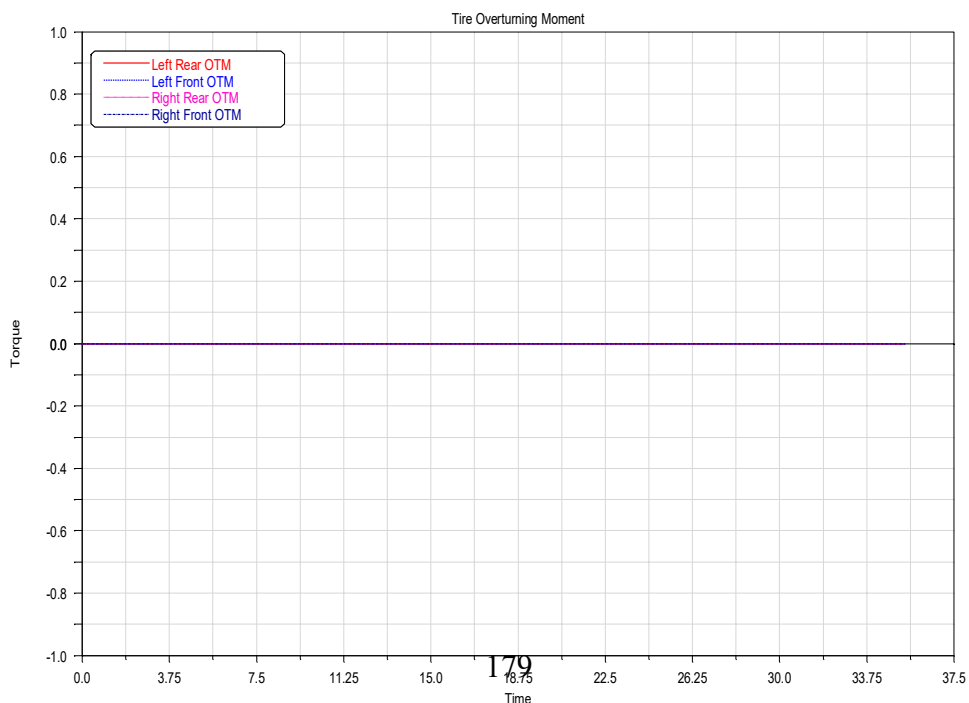
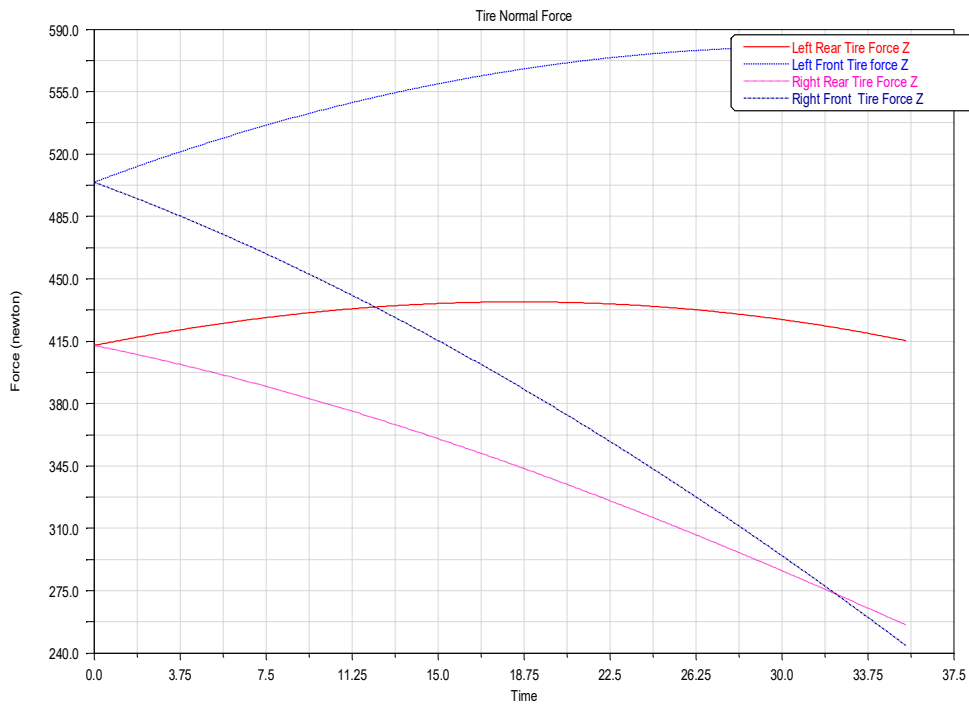
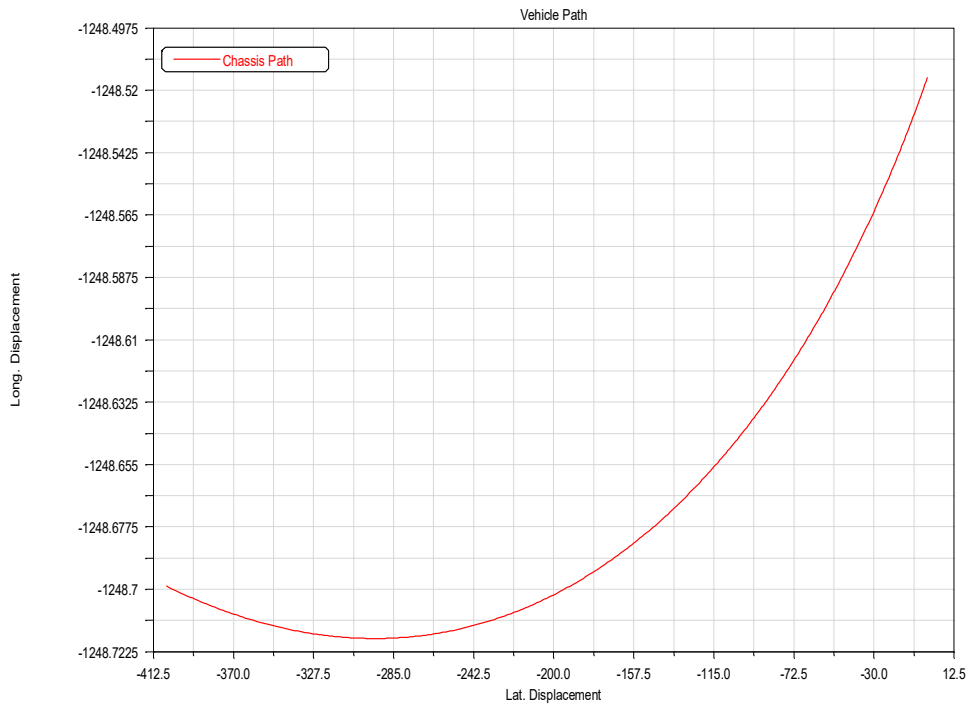


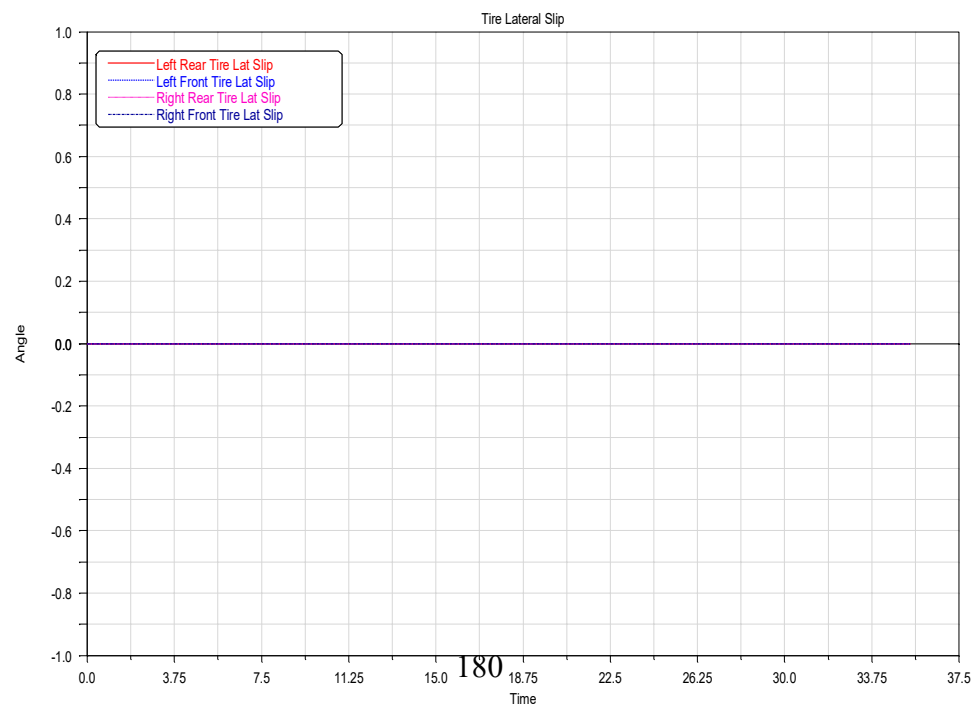
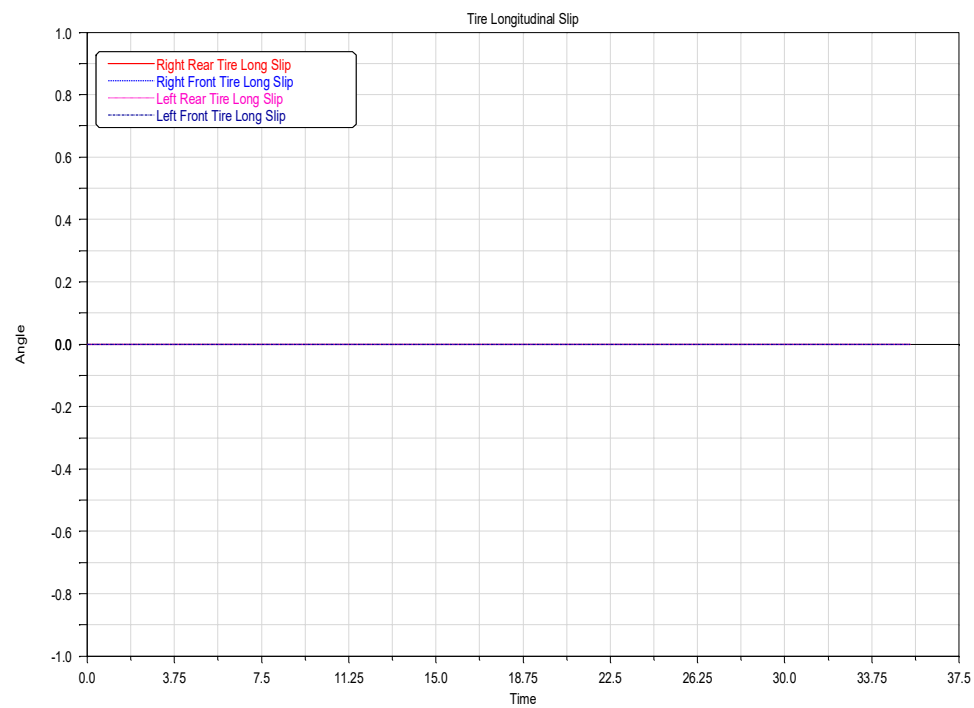
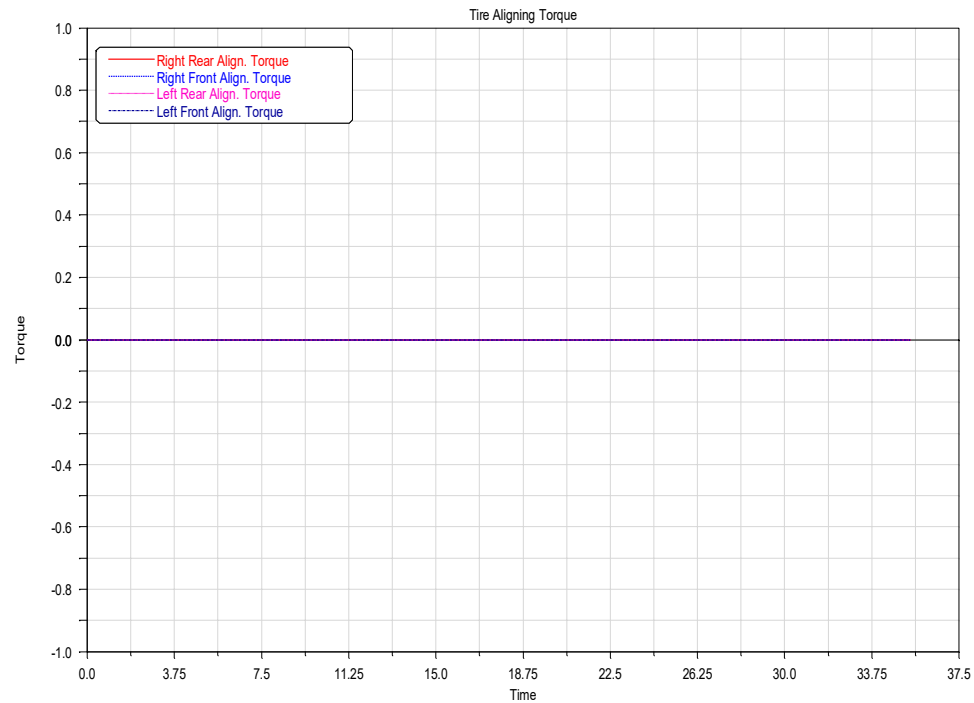
Figure C.4: Adams car [4] tilt table simulation setup window

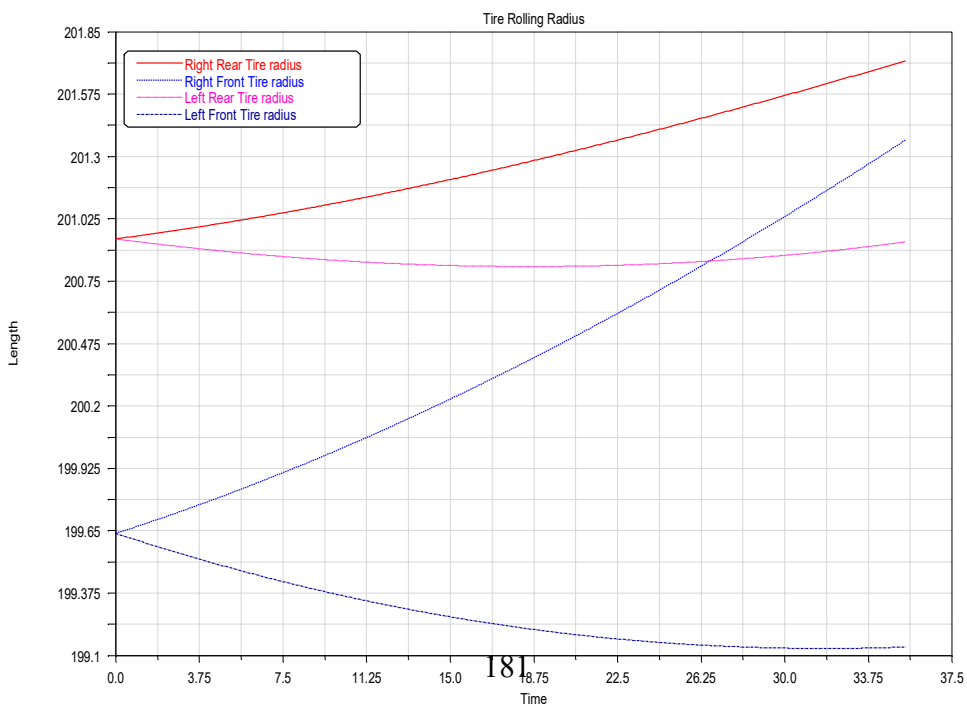
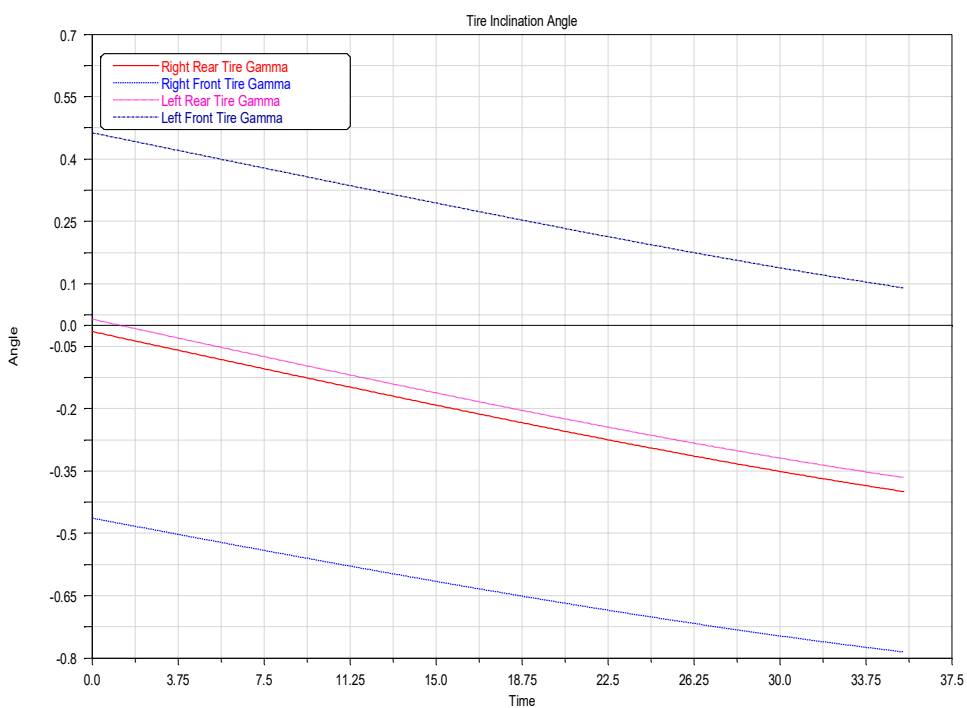
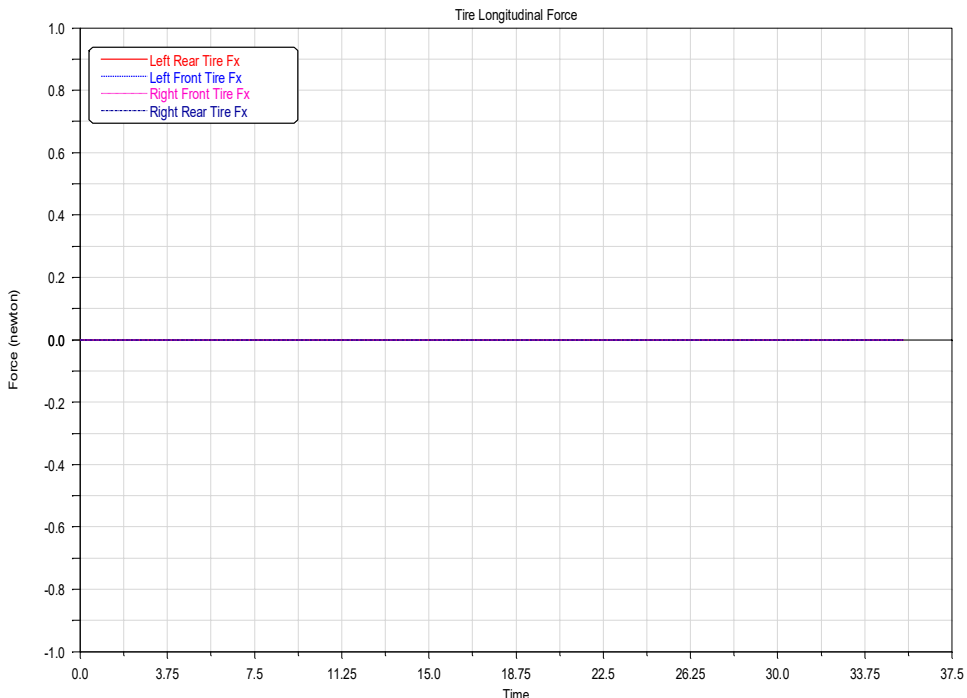


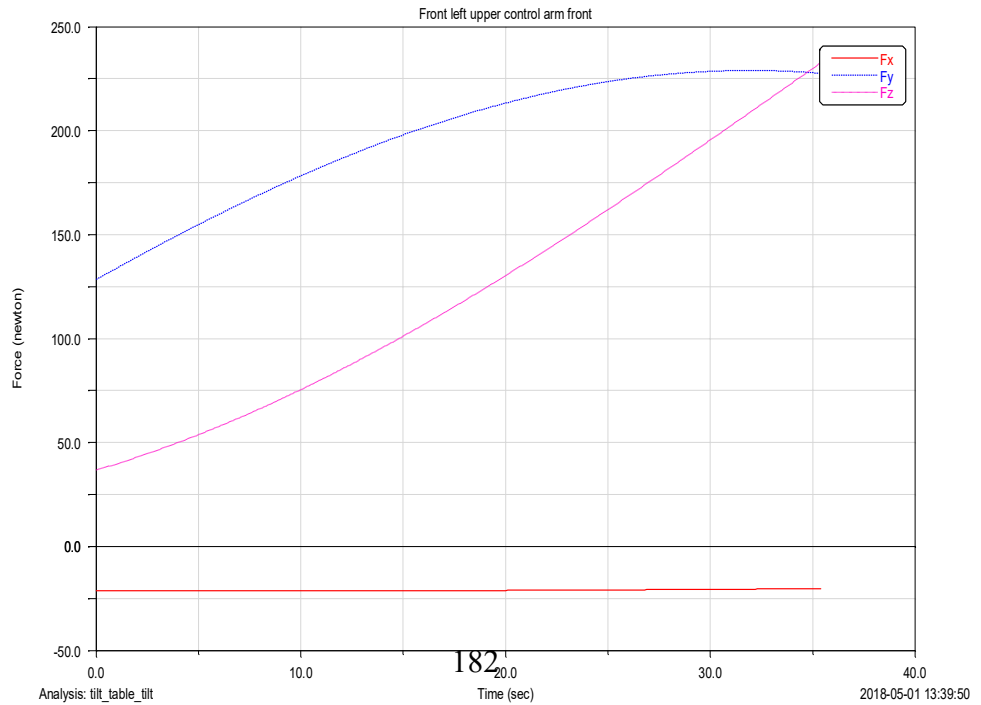
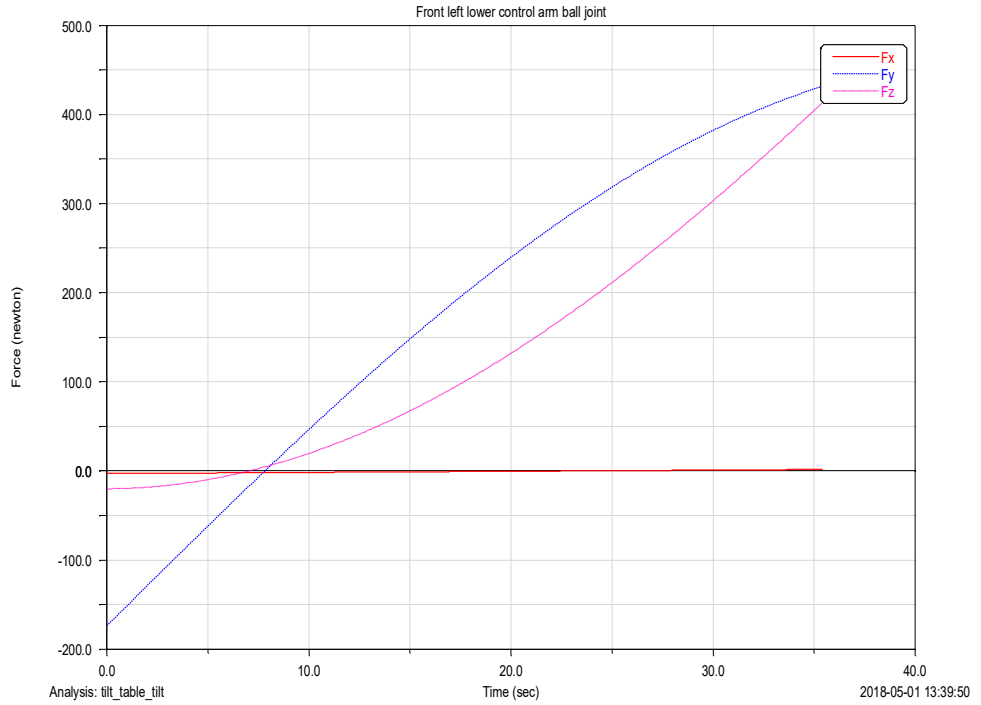
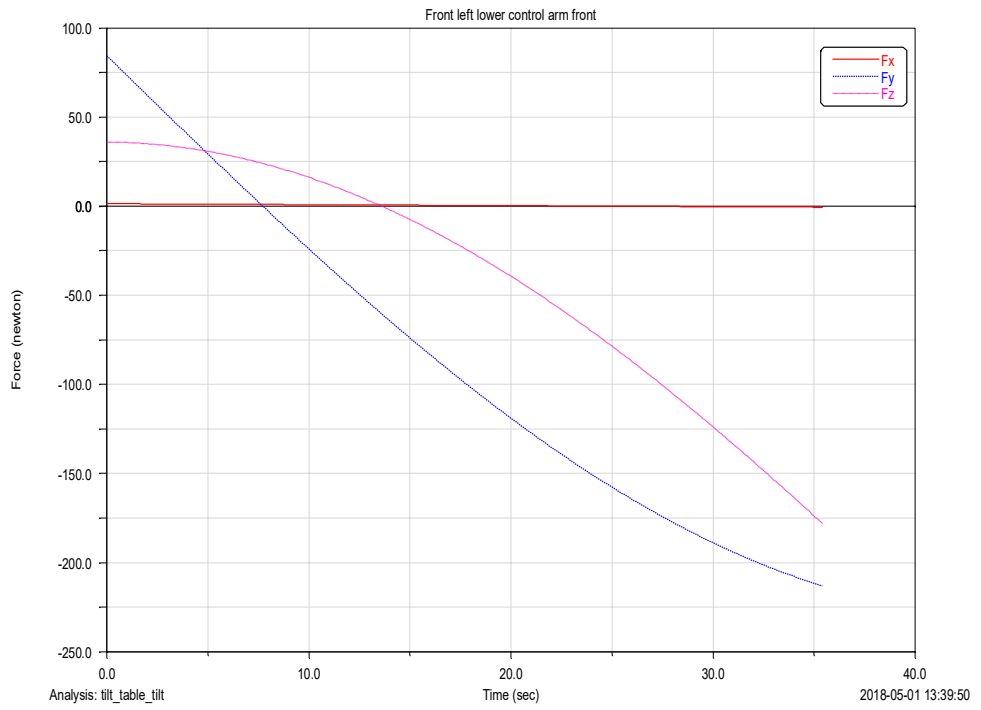


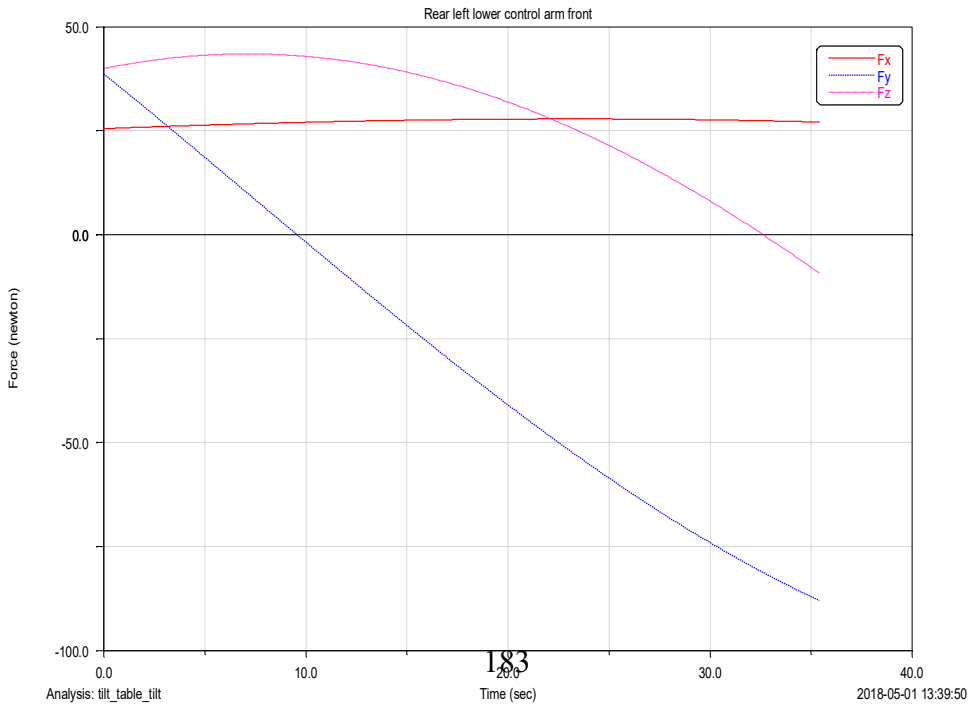
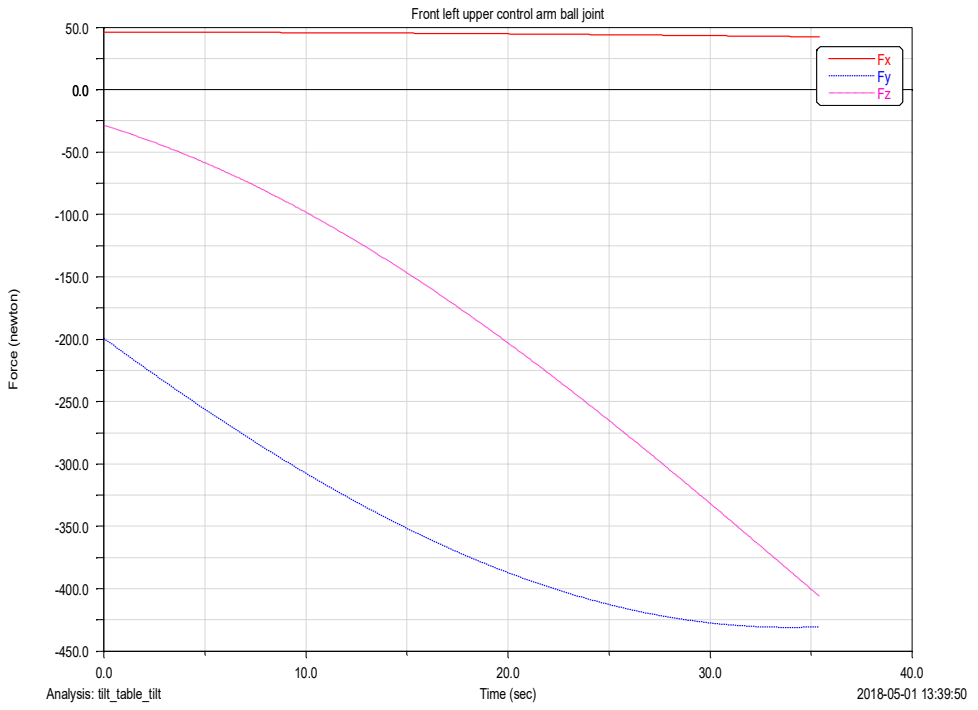
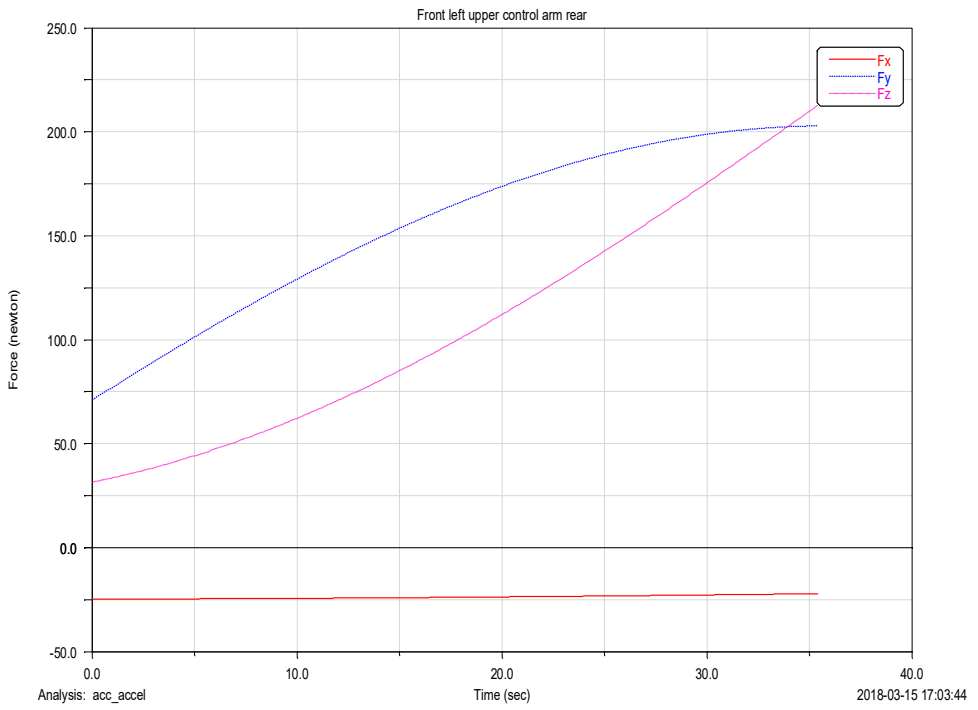


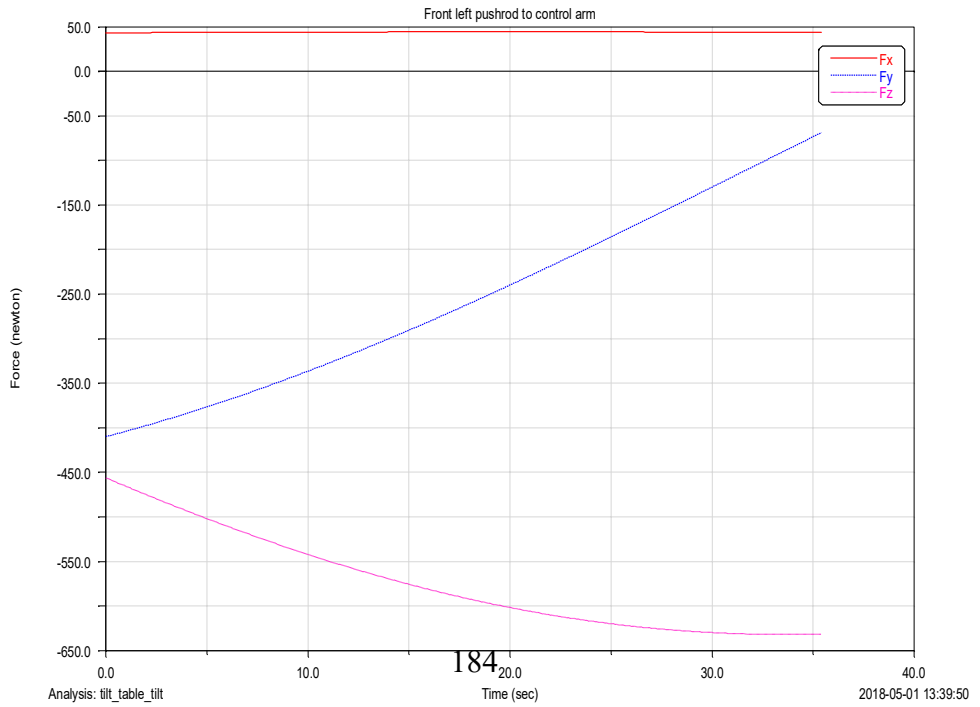
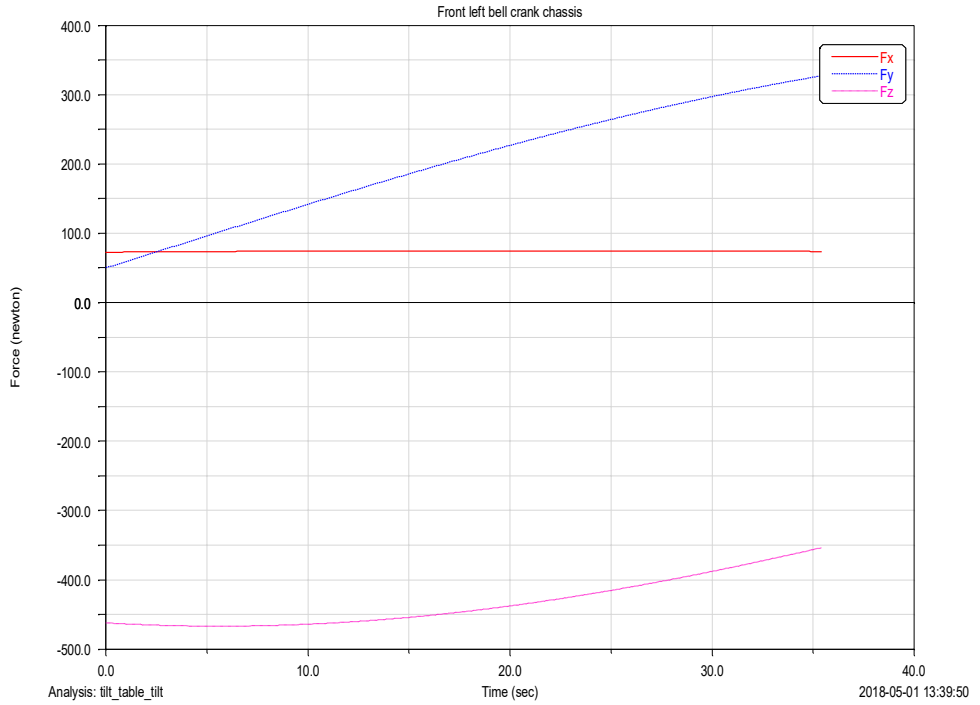
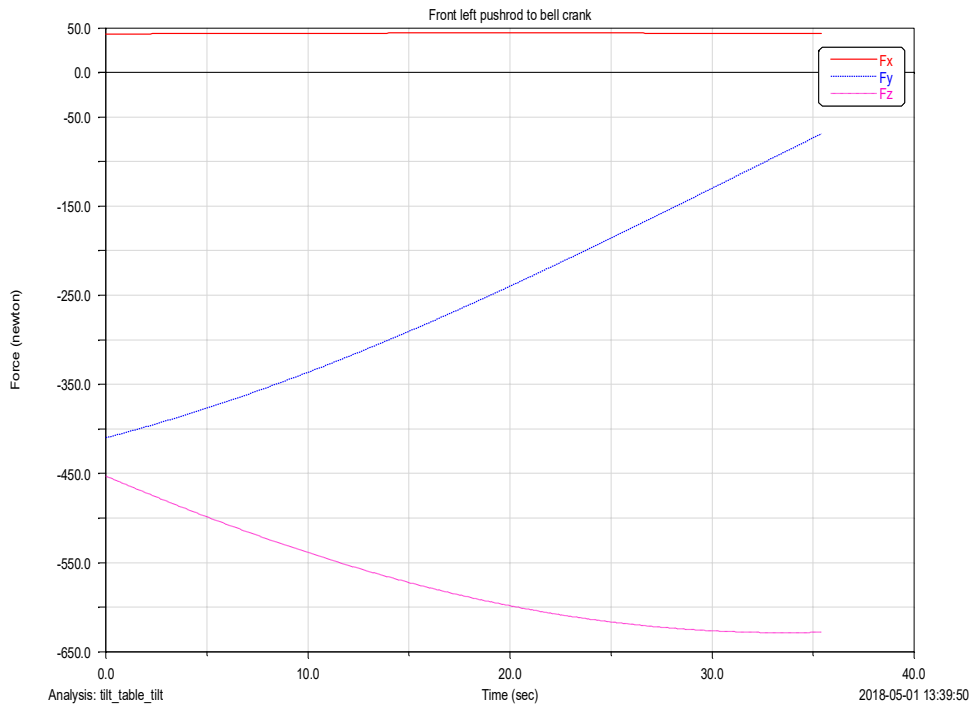


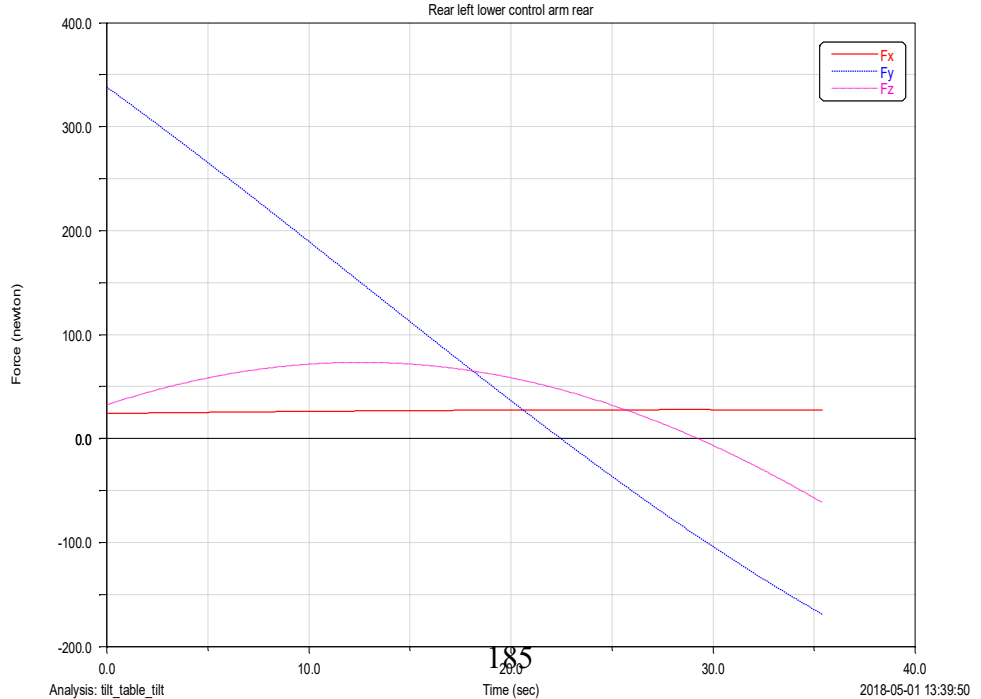
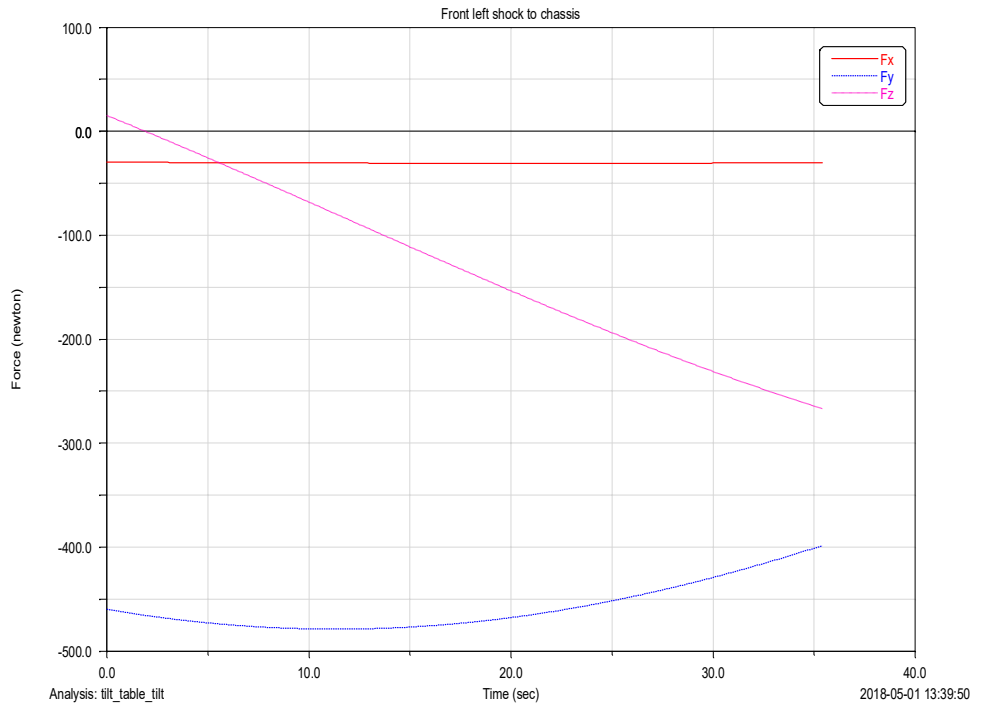
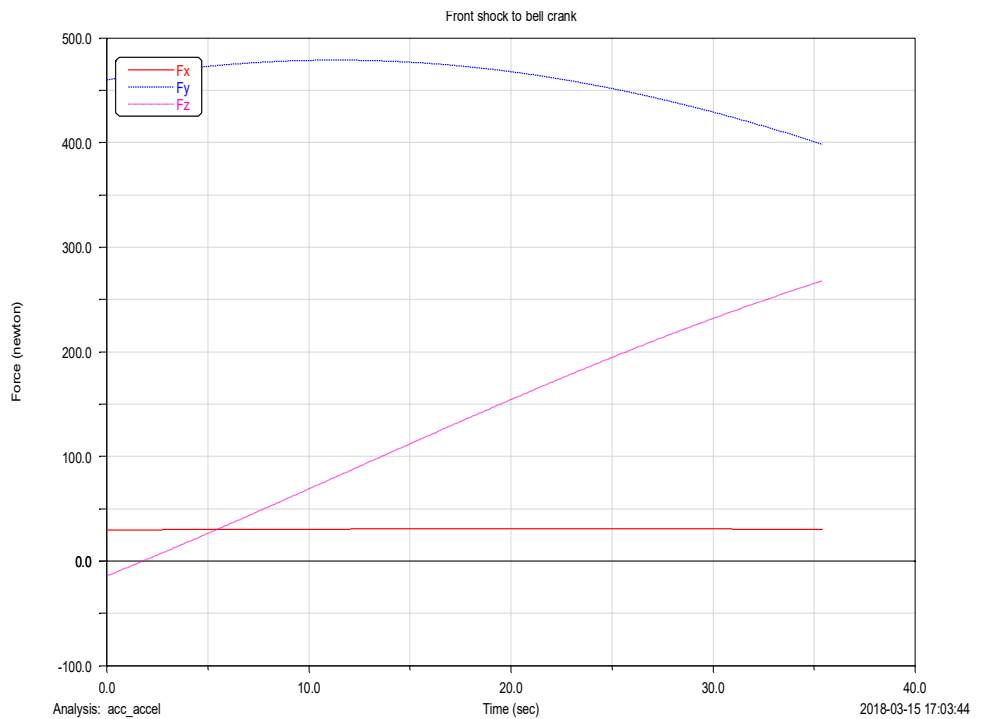


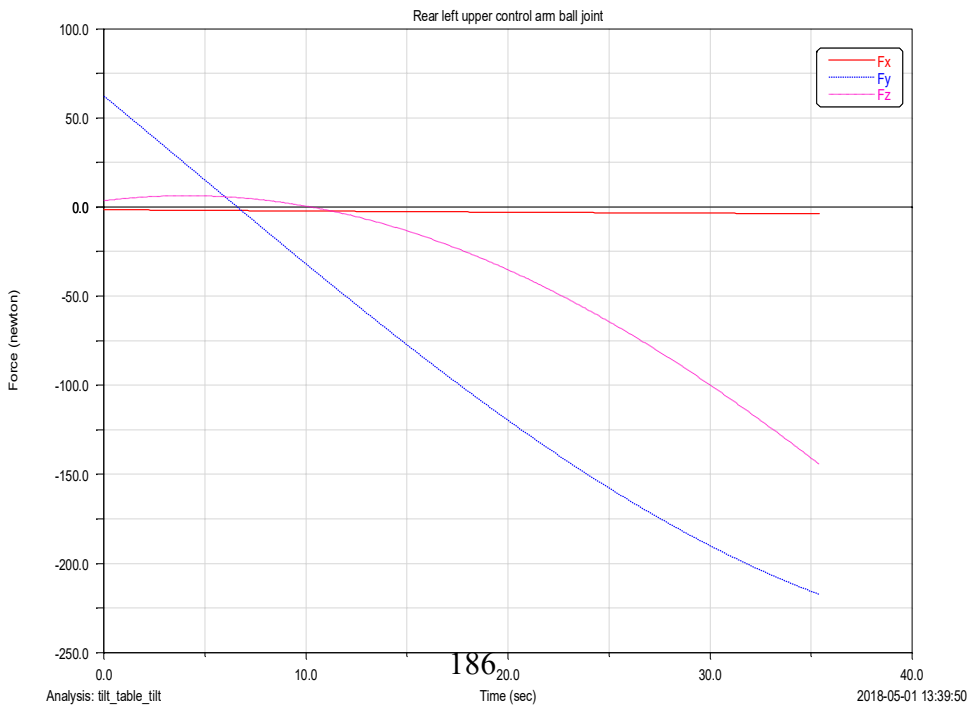
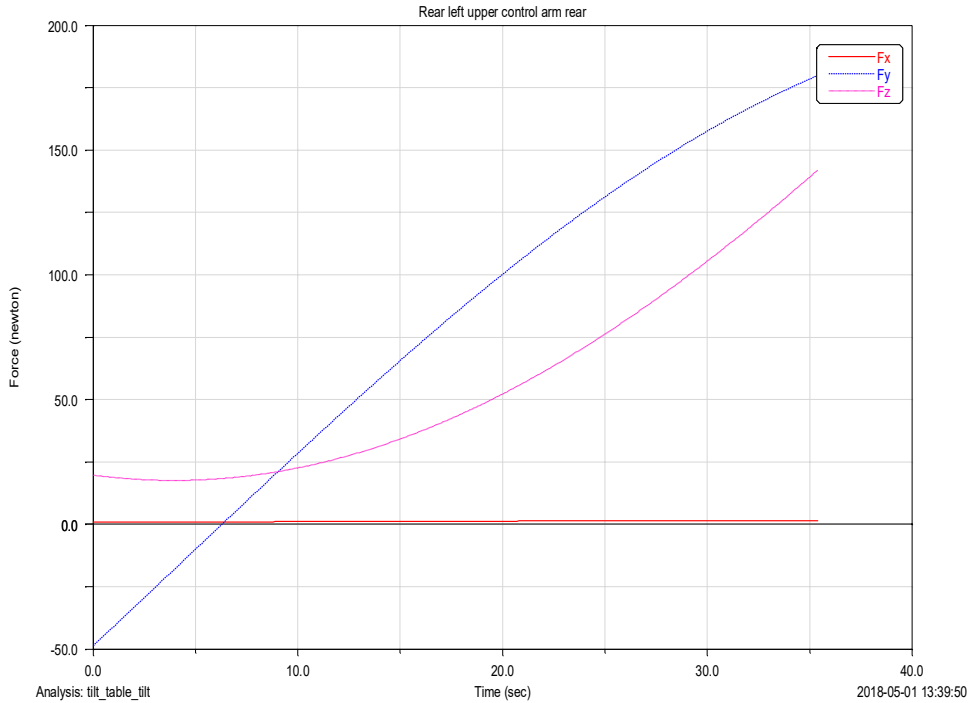
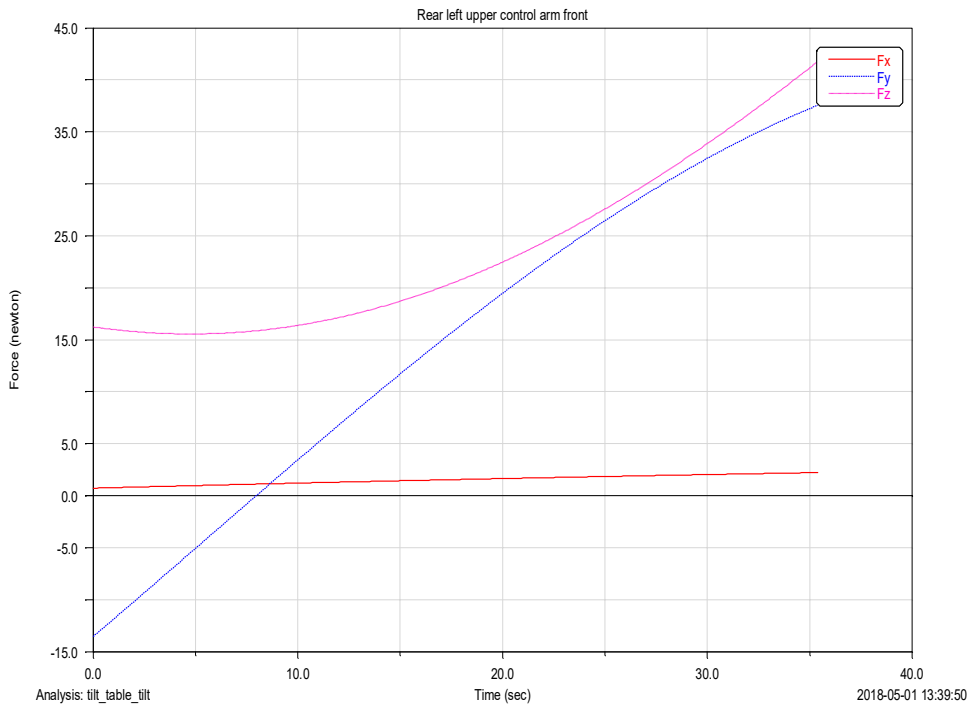


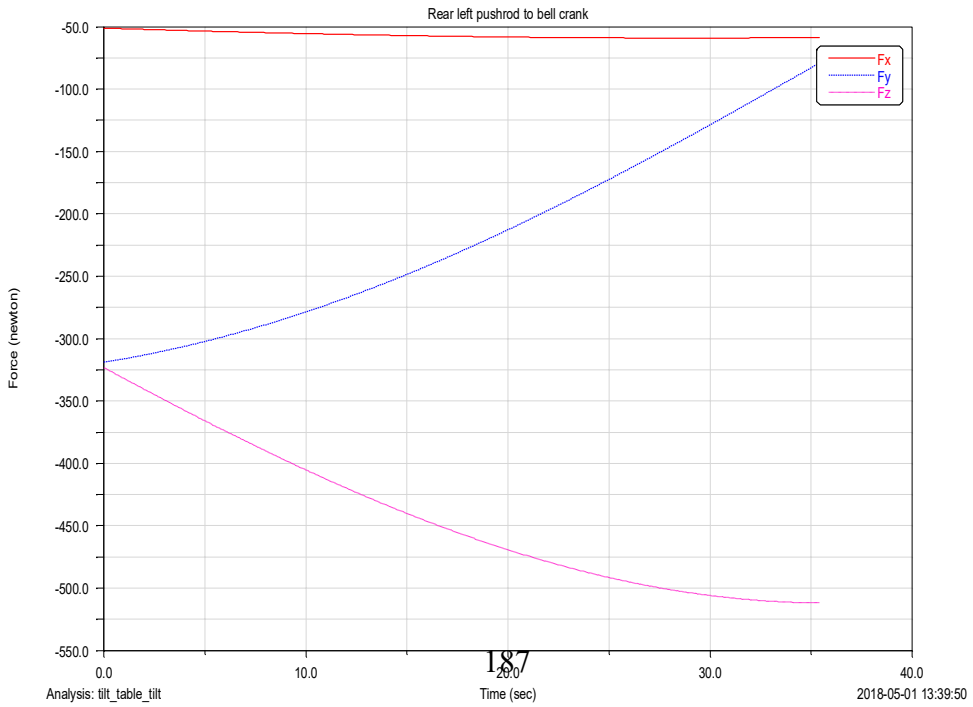
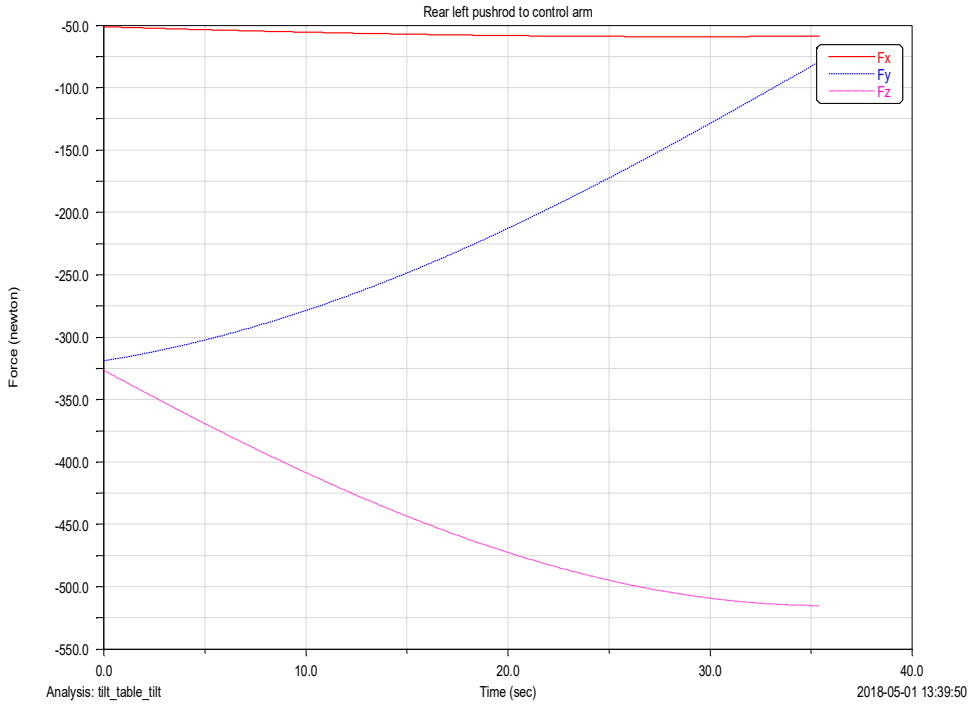
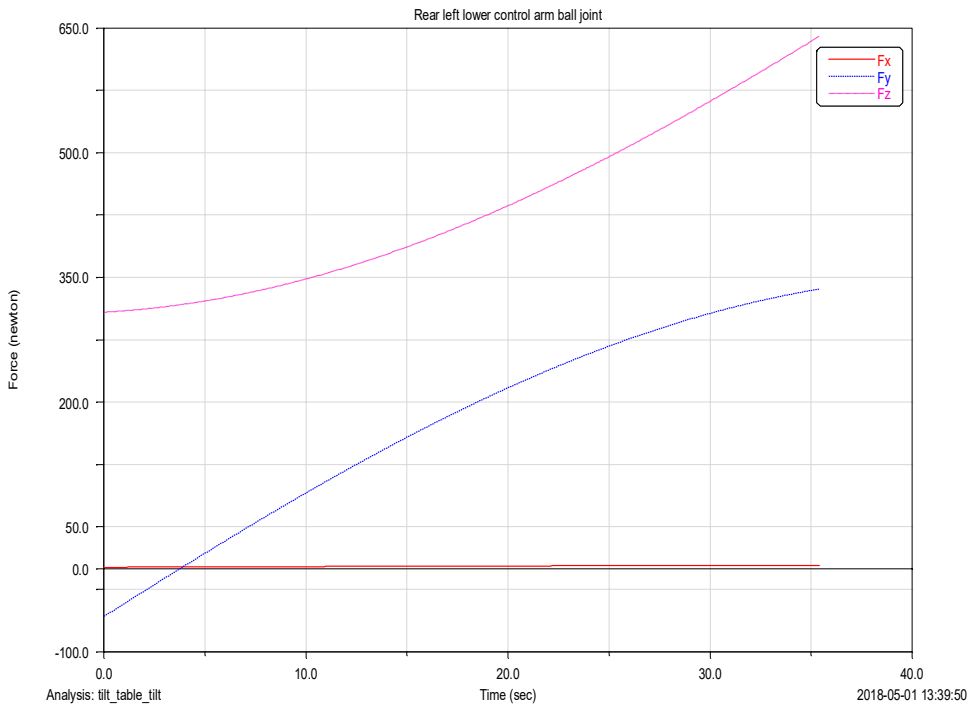


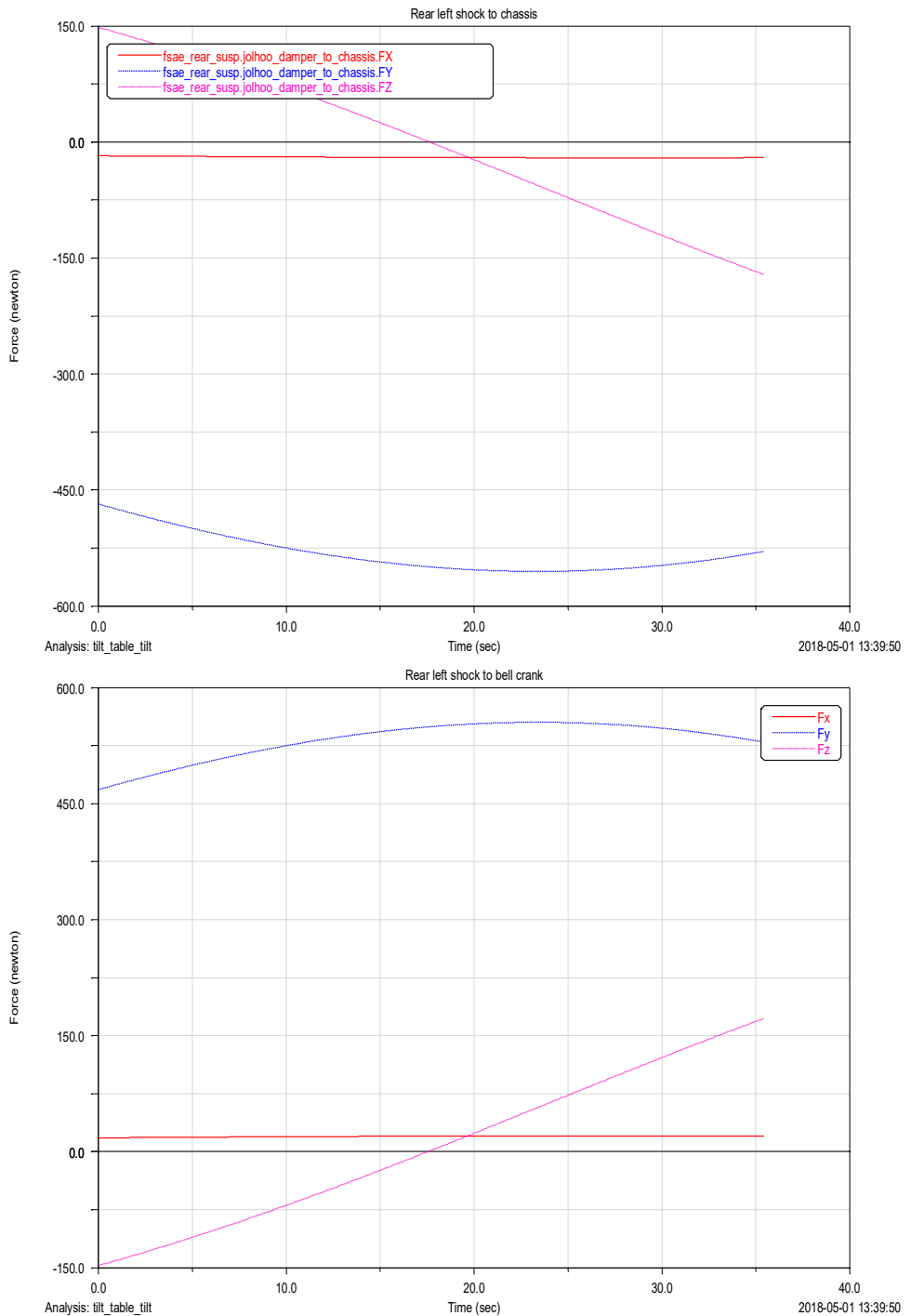












### C.2.6 Front parallel wheel travel simulation

Front suspension assembly parallel wheel travel simulation with 30 mm jounce and 30 mm rebound.

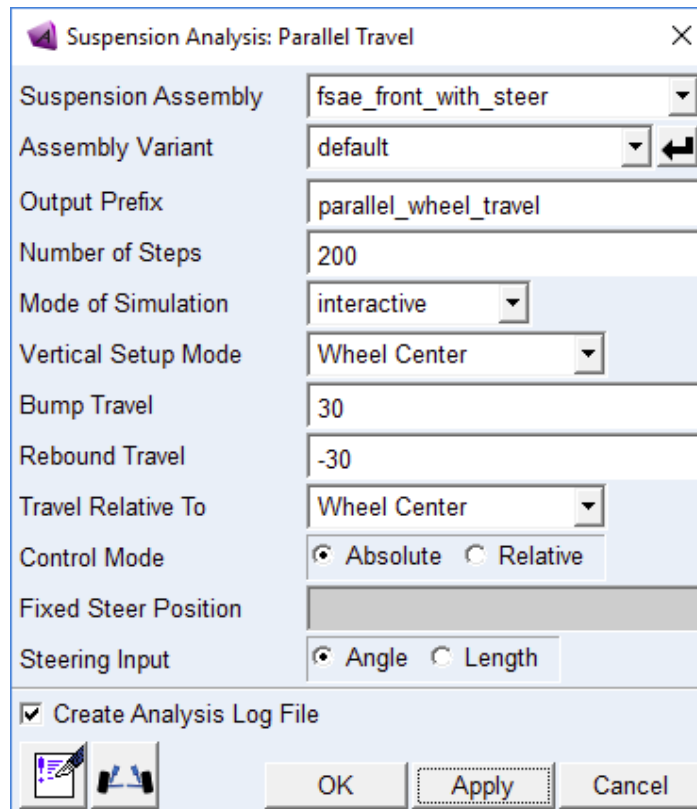
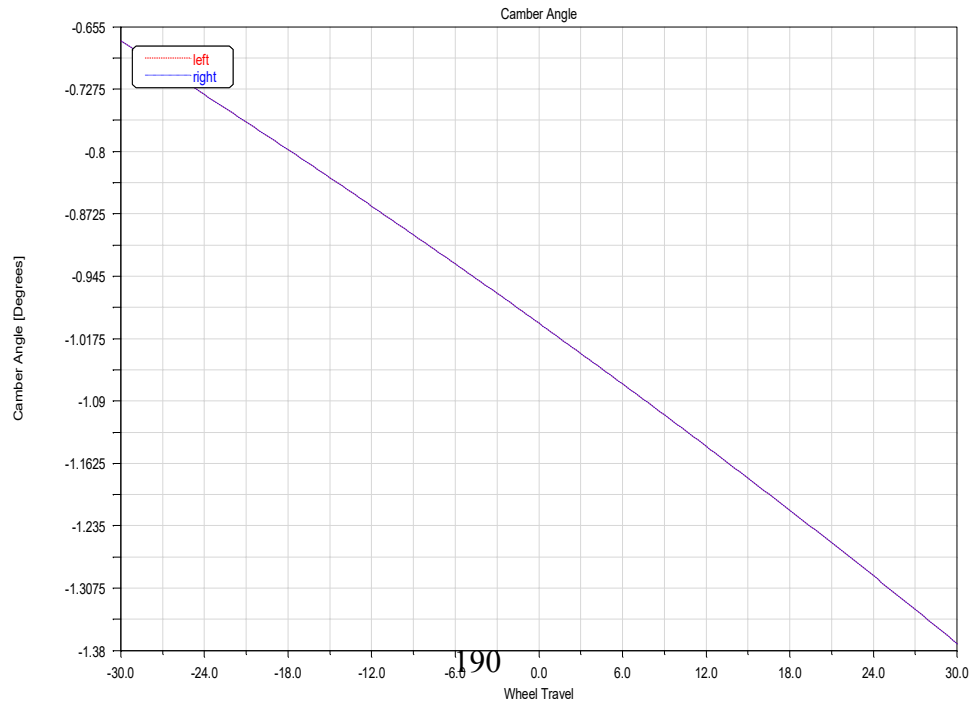
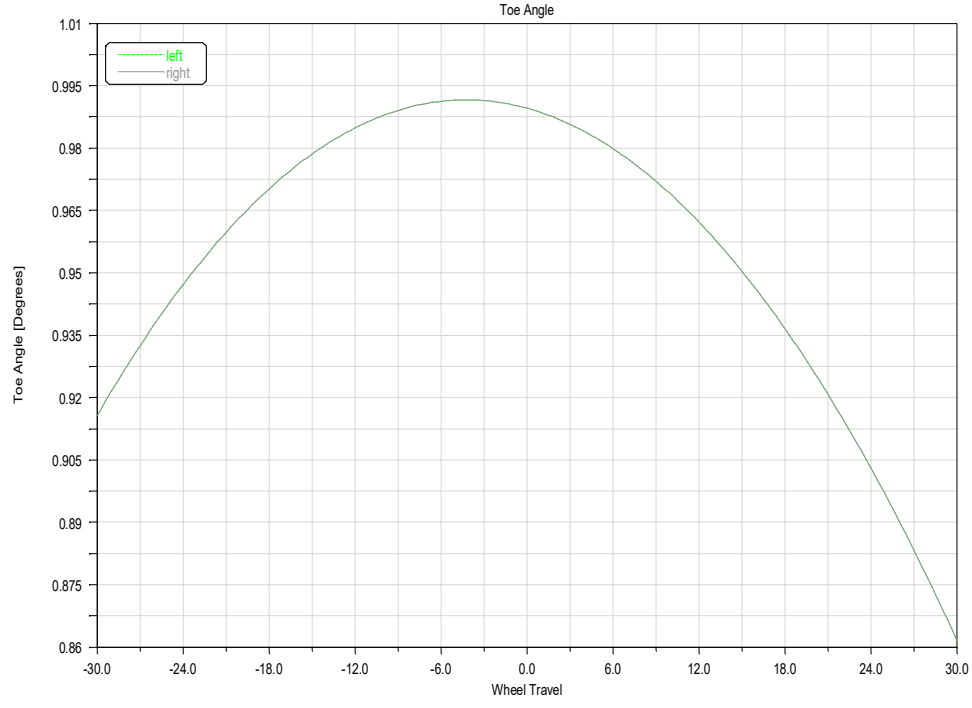
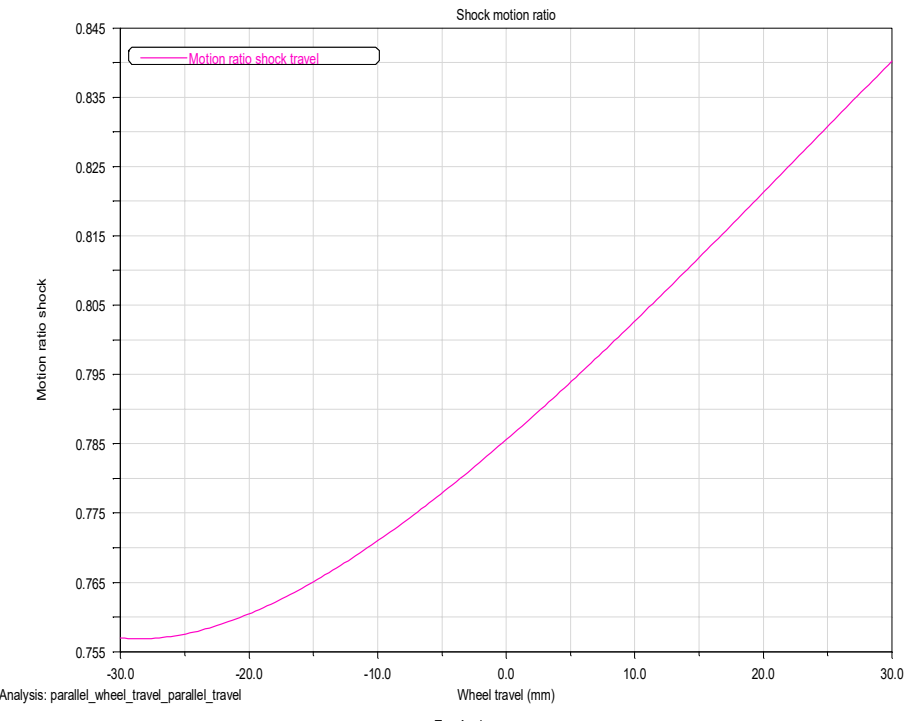
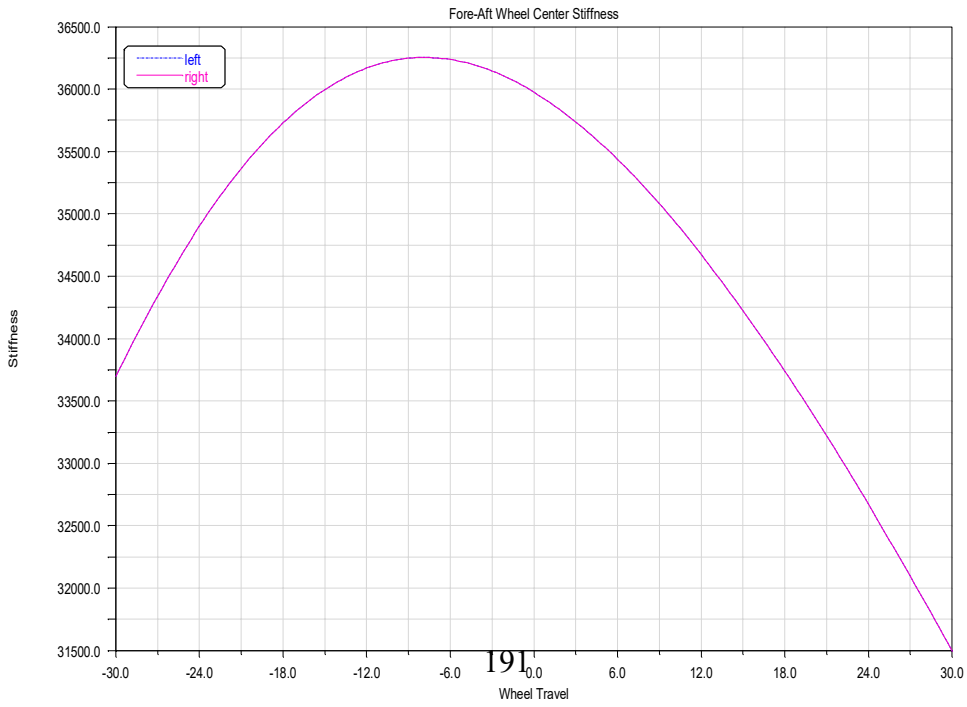
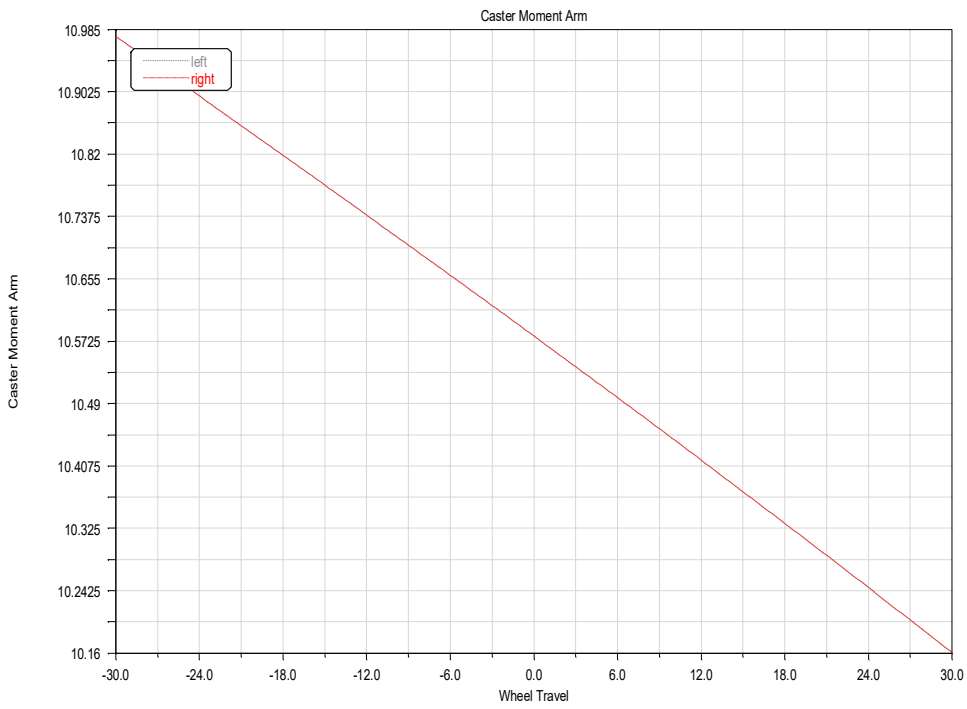
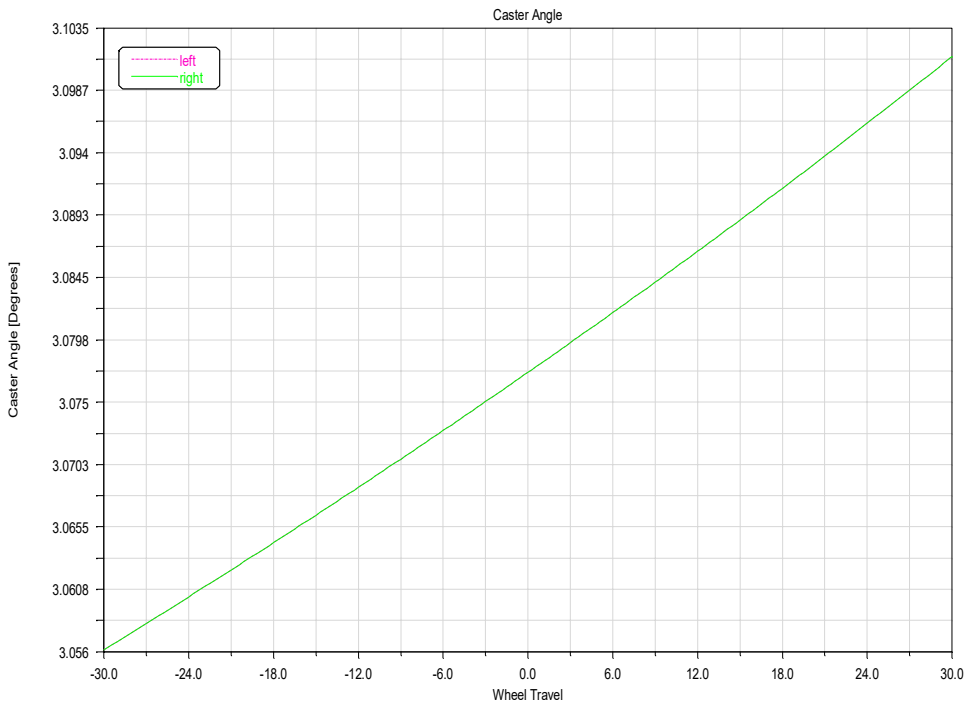
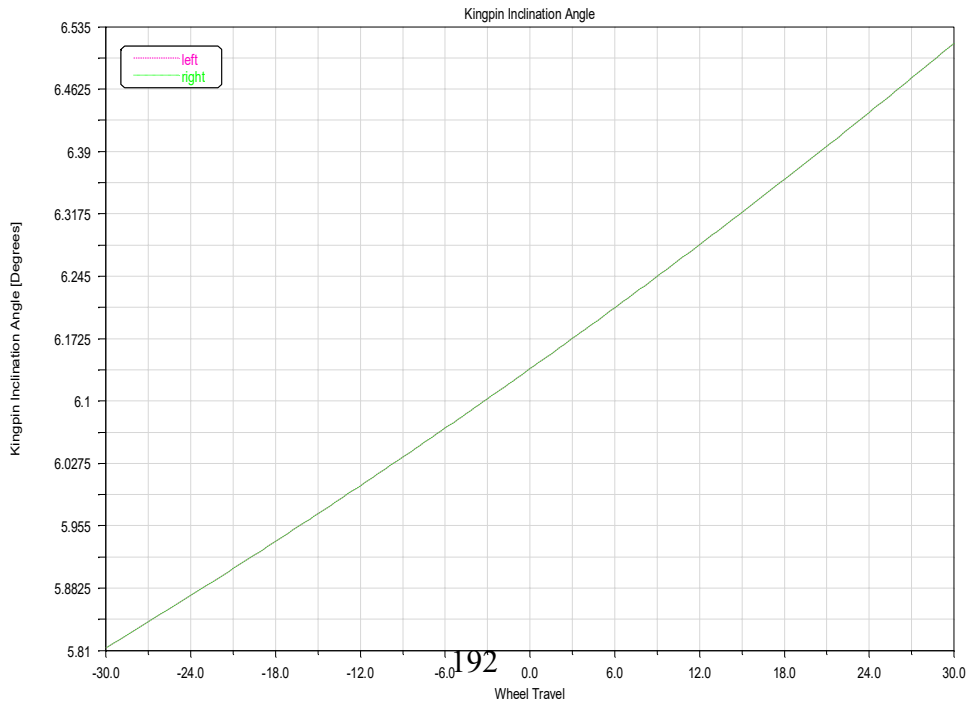
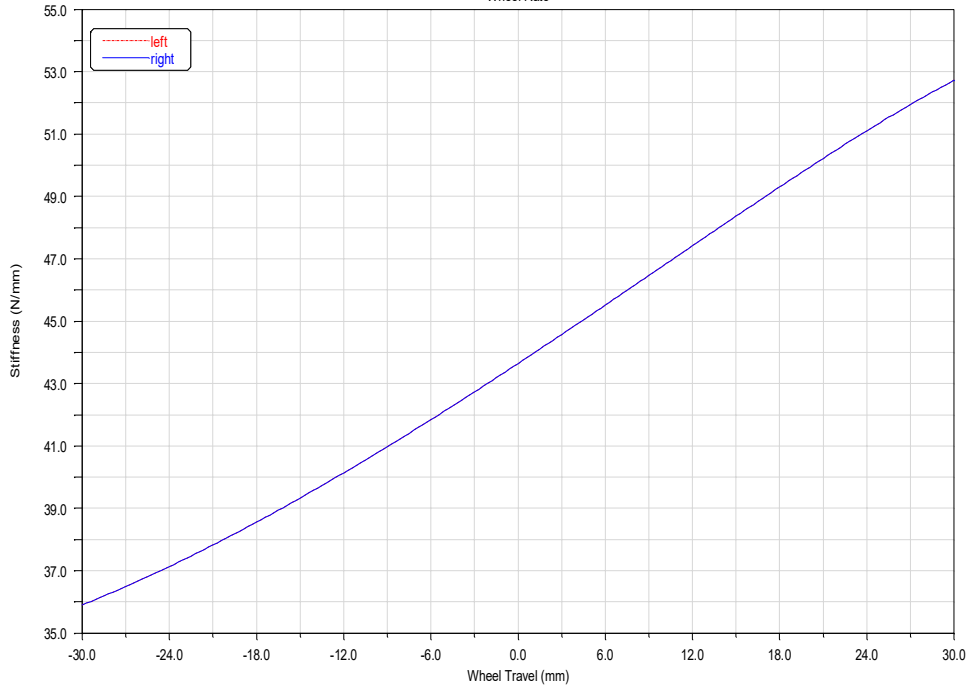
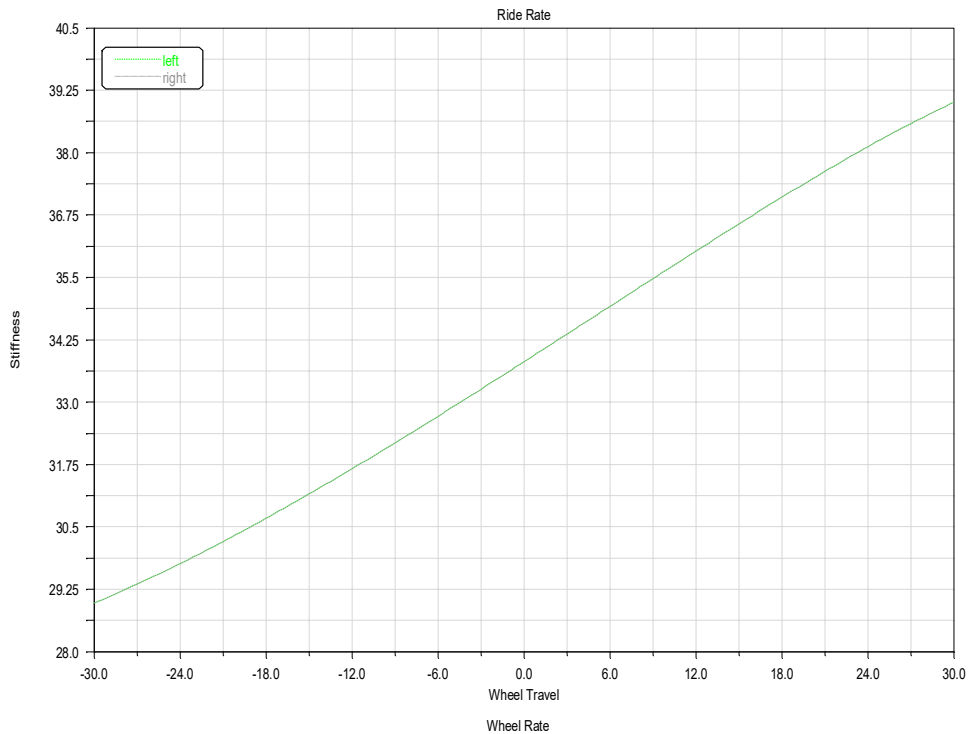
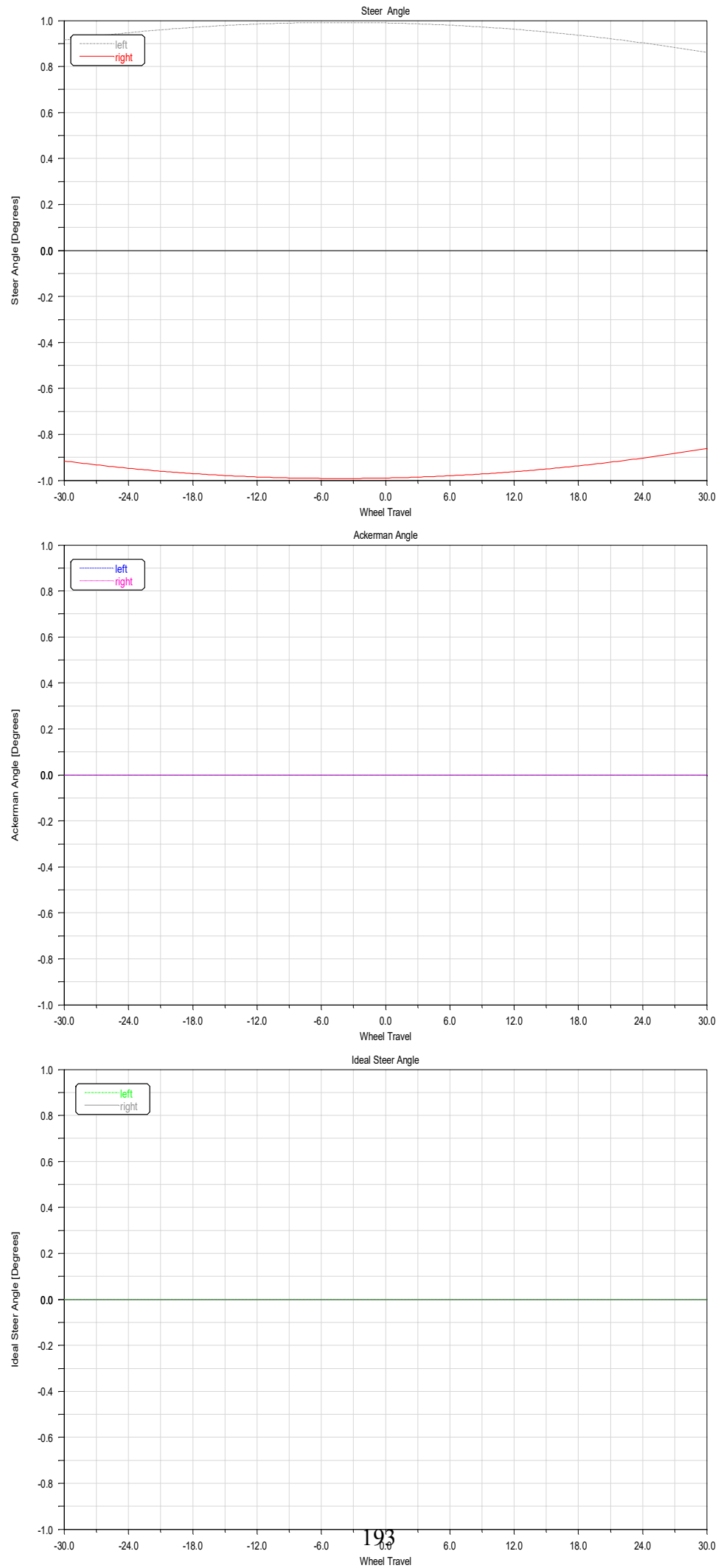


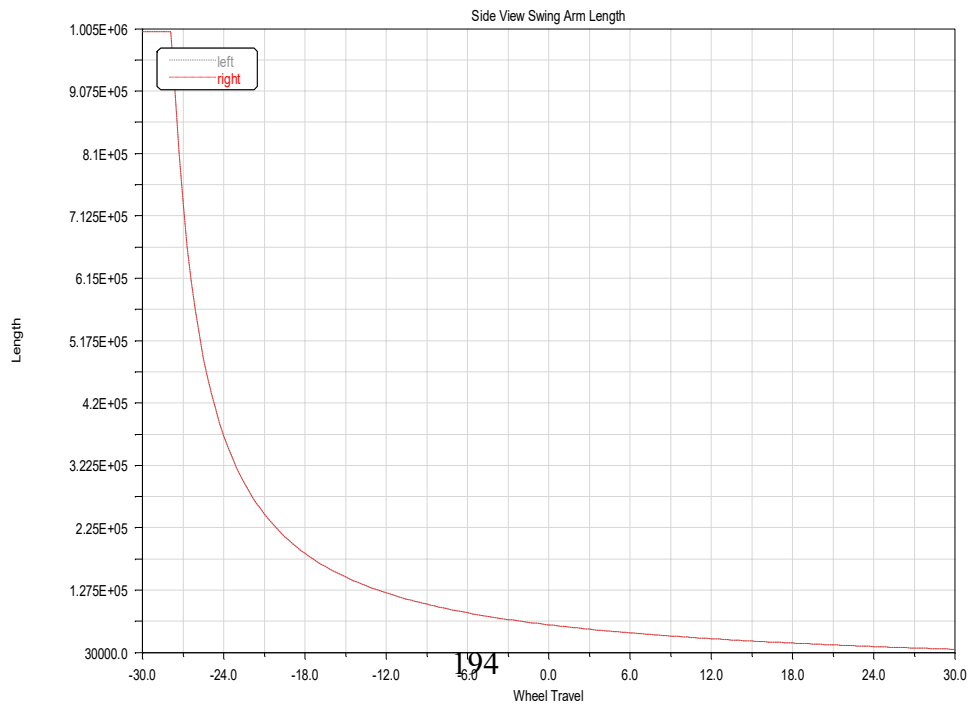
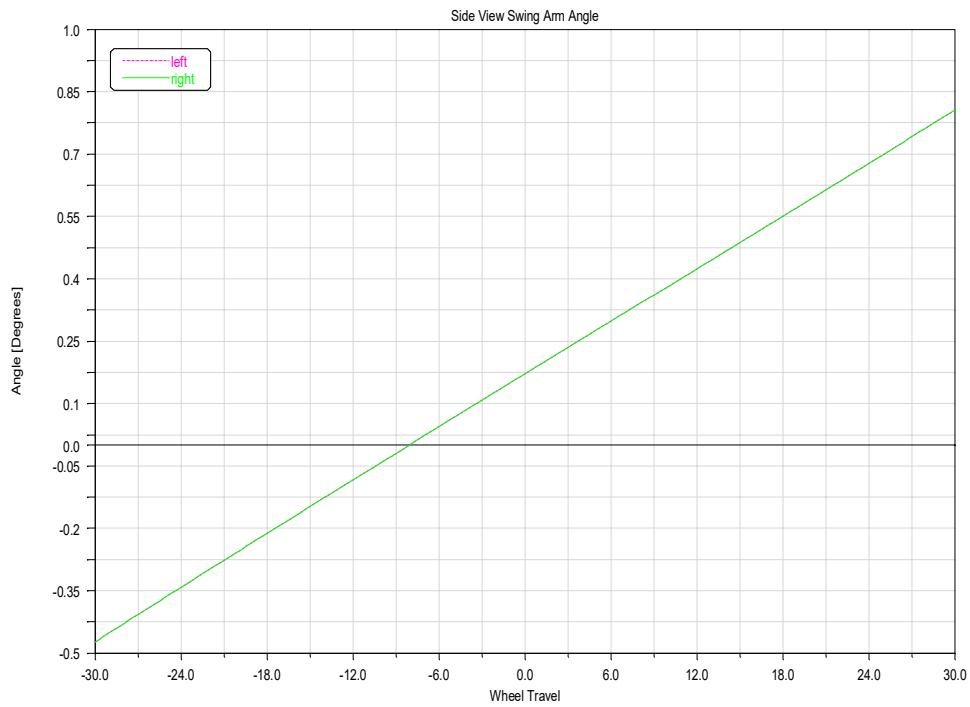
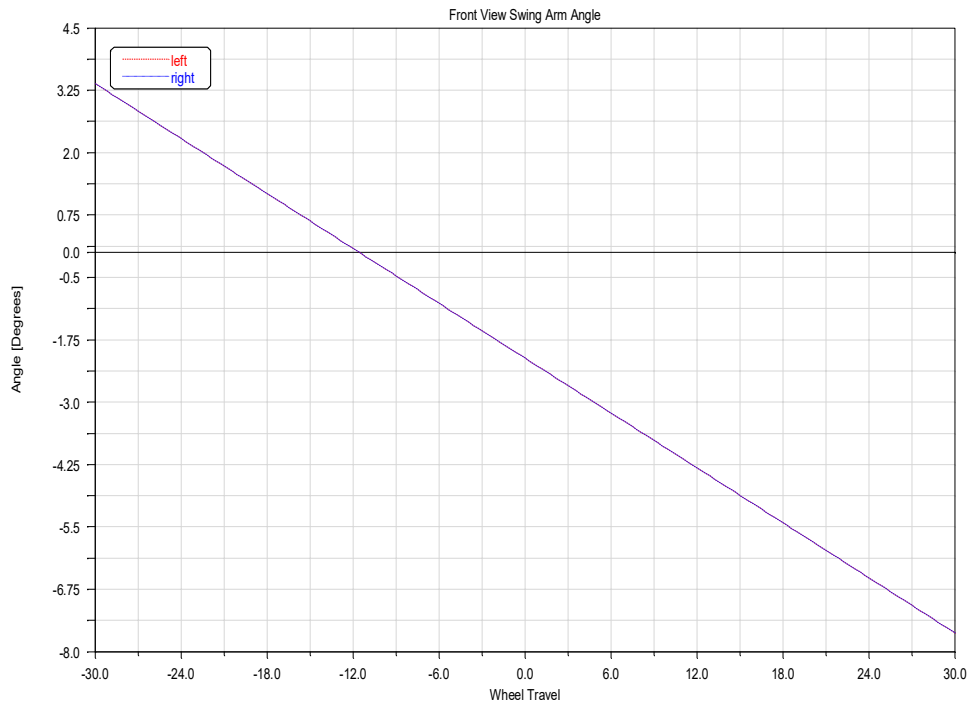
Figure C.5: Adams car [4] parallel wheel travel simulation setup window

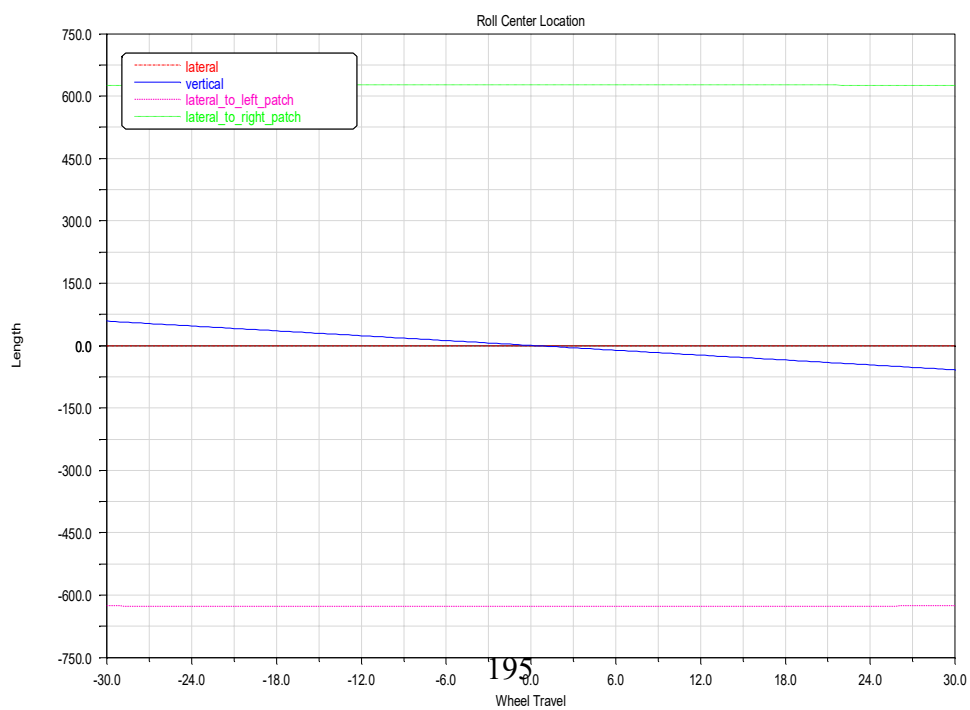
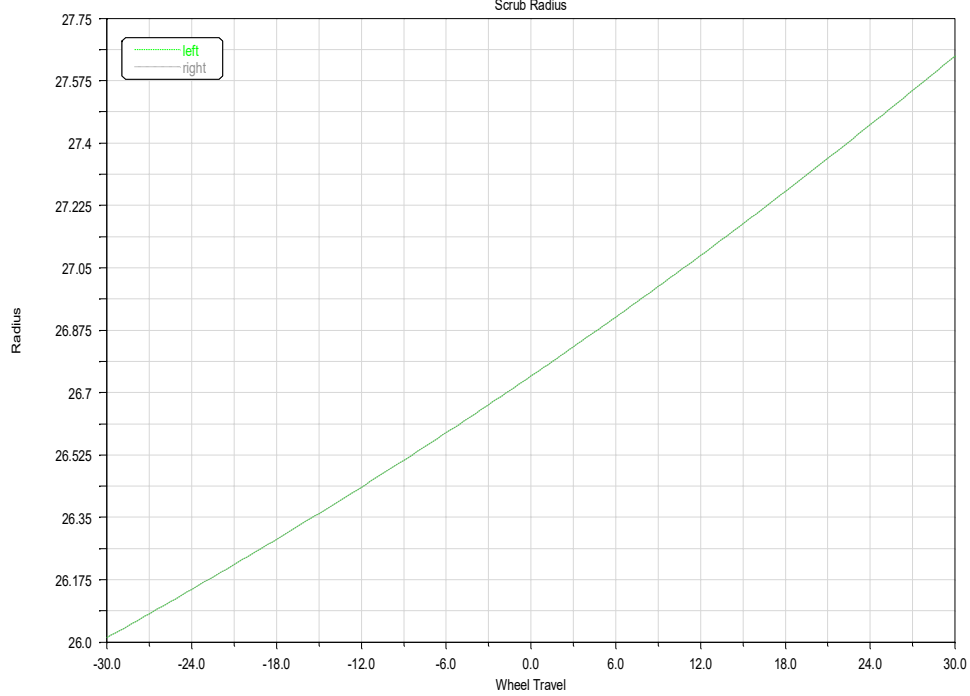
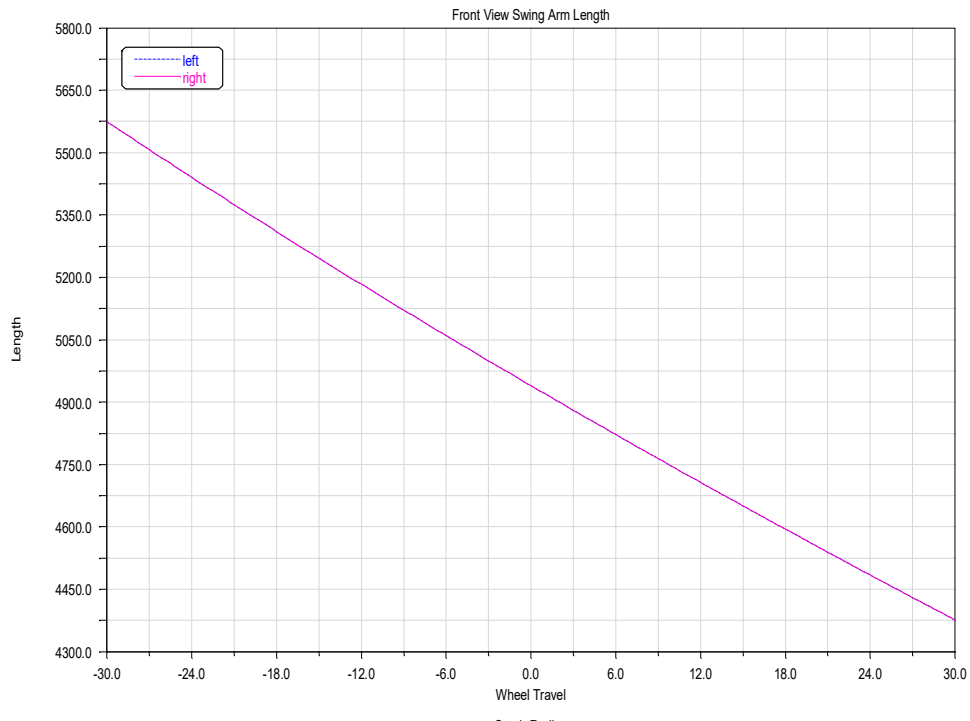


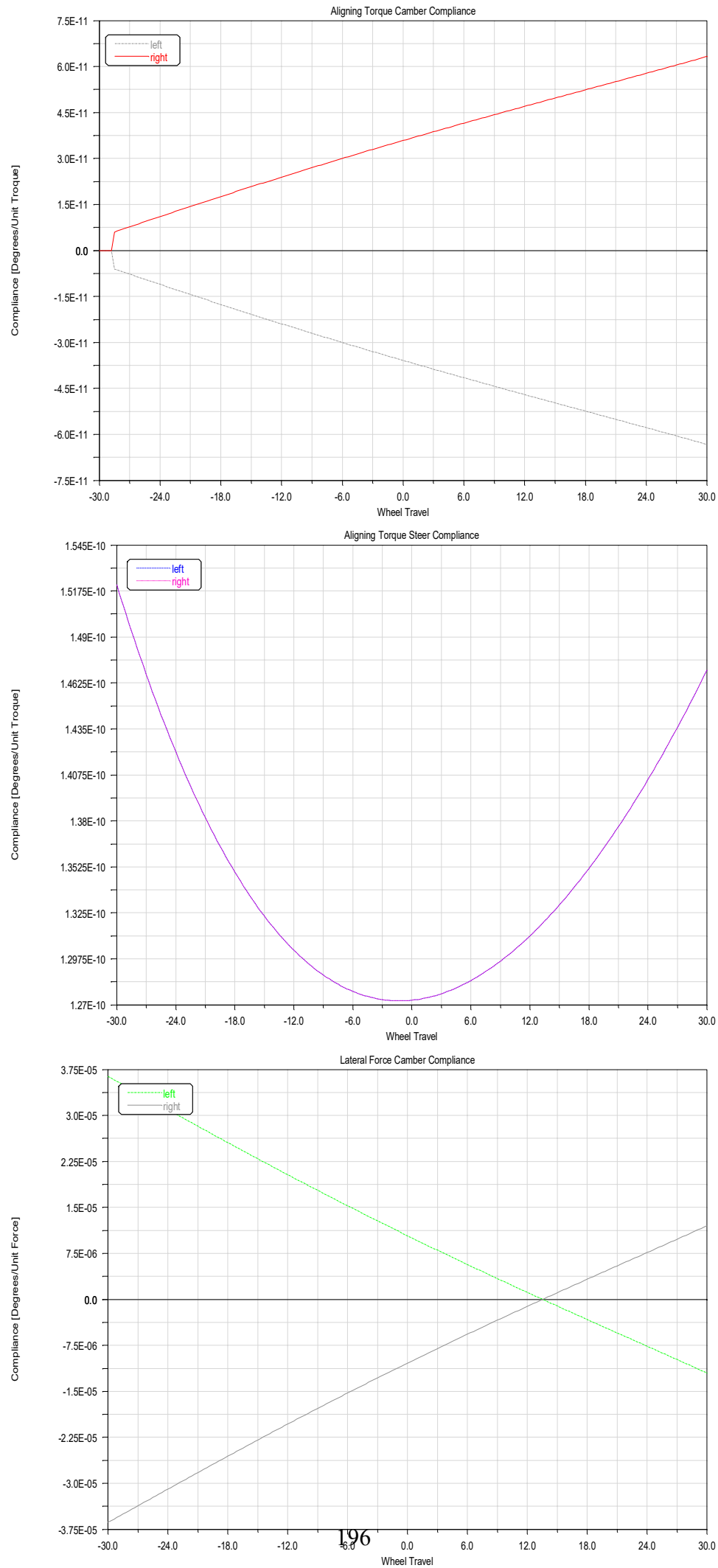


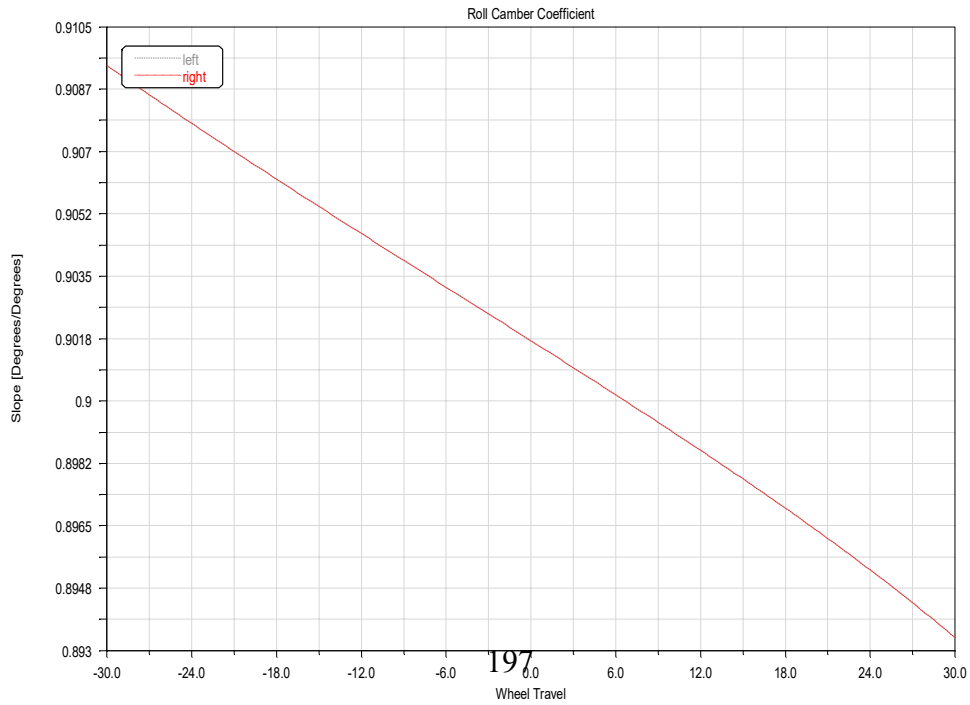
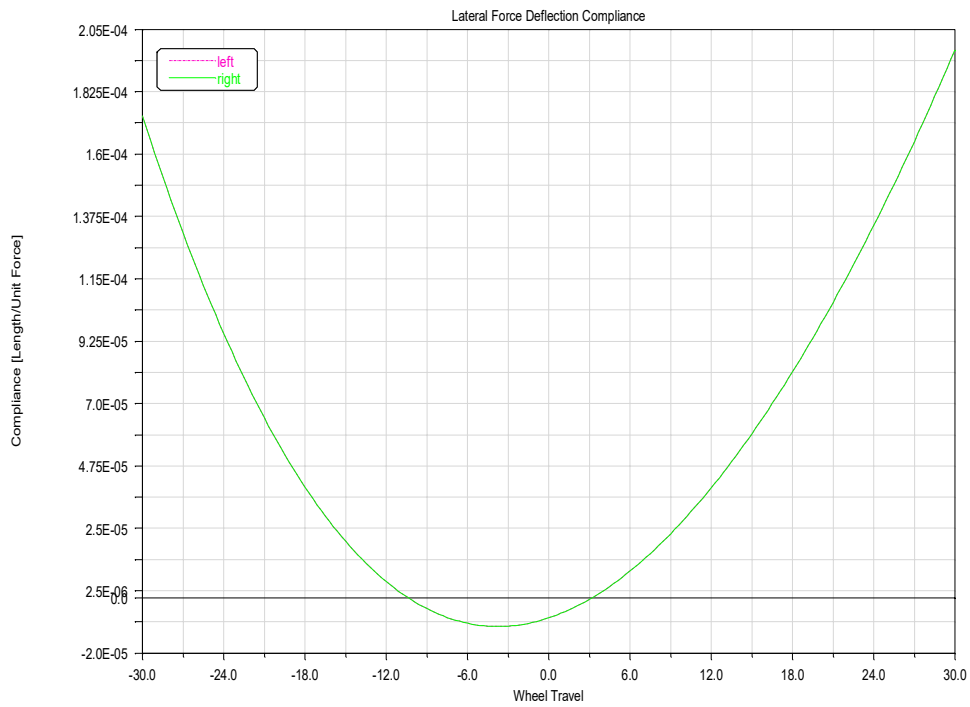
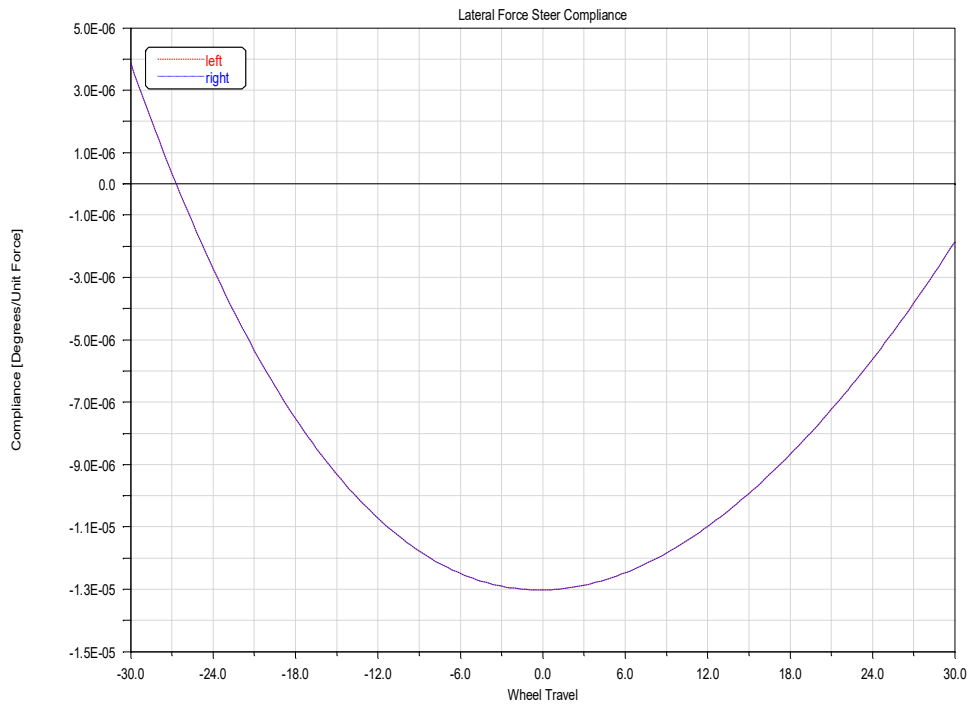


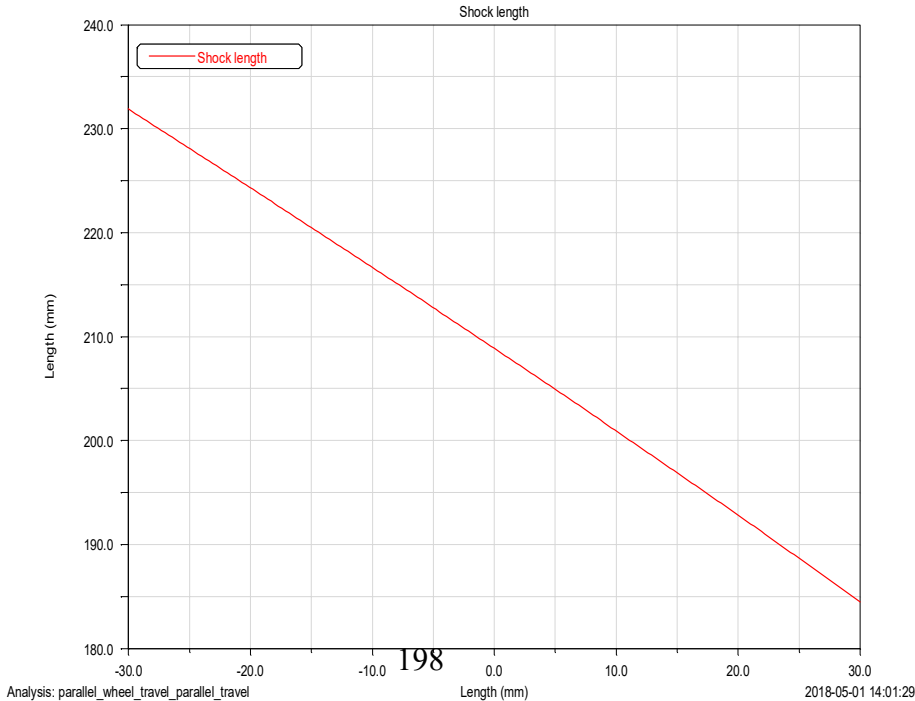
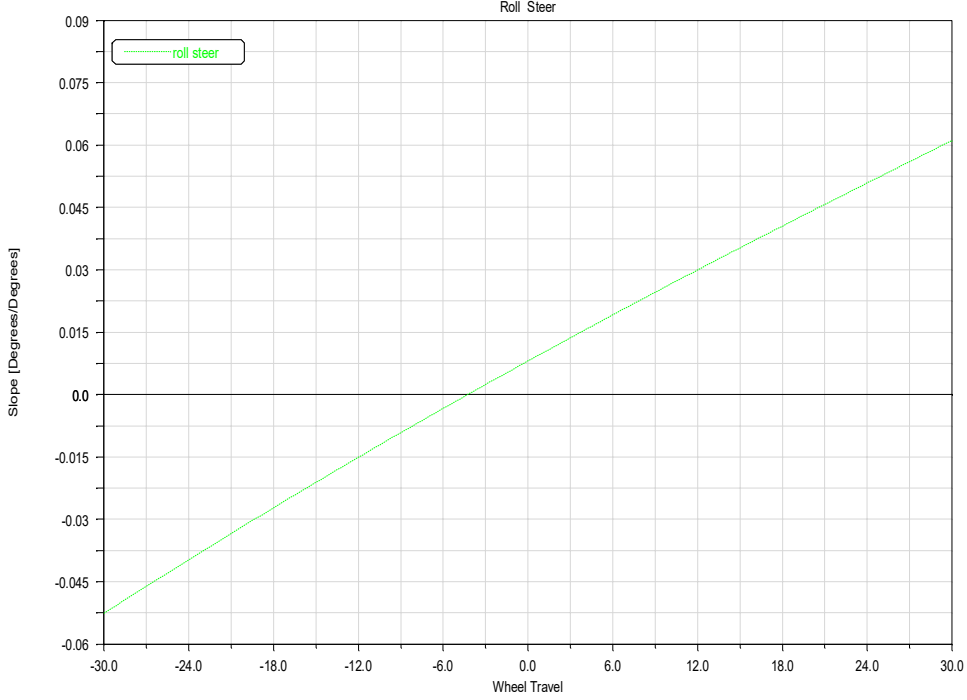
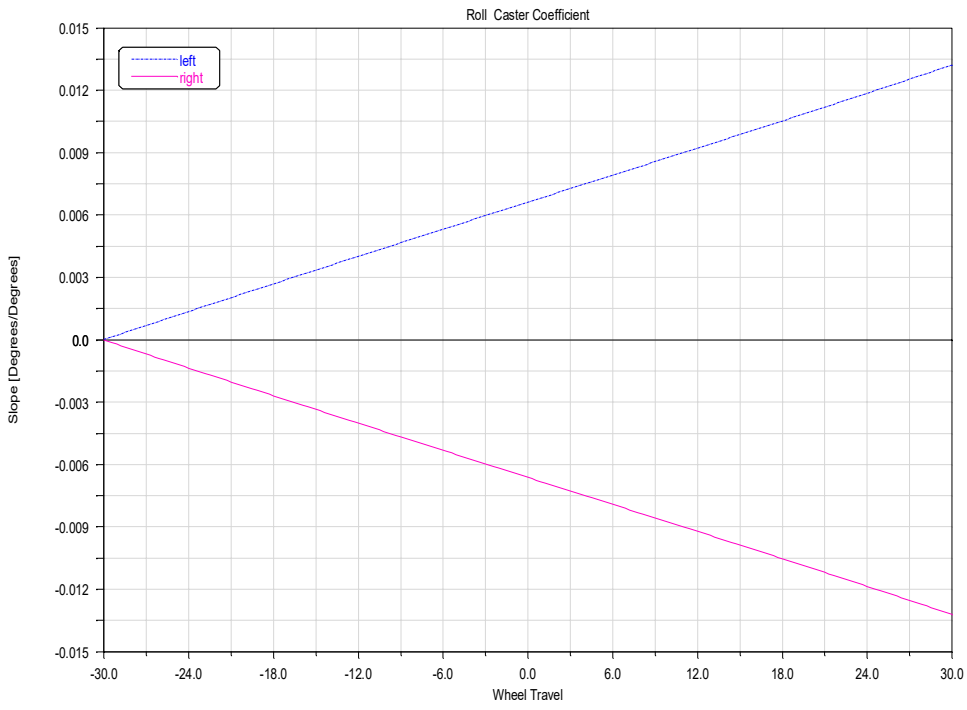












### C.2.7 Rear parallel wheel travel simulation

Rear suspension assembly parallel wheel travel simulation with 30 mm jounce and 30 mm rebound.

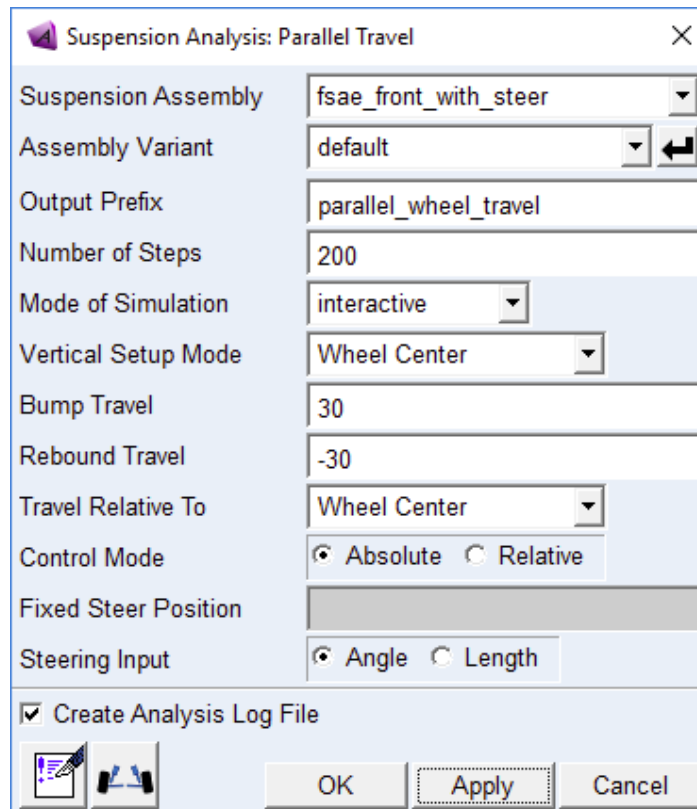


Figure C.6: Adams car [4] parallel wheel travel simulation setup window

